DESIGN OF A MIXED-SPECTRUM LONG-LIVED REACTOR WITH IMPROVED PROLIFERATION RESISTANCE

A Dissertation
Presented to
The Academic Faculty

By

Abdalla Abou Jaoude

In Partial Fulfillment
of the Requirements for the Degree
Doctor of Philosophy in the
School of Nuclear and Radiological Engineering

Georgia Institute of Technology

December 2017

DESIGN OF A MIXED-SPECTRUM LONG-LIVED REACTOR WITH IMPROVED PROLIFERATION RESISTANCE

Approved by:

Dr. Anna Erickson, Advisor
School of Nuclear Engineering
Georgia Institute of Technology

Dr. Bojan Petrovic
School of Nuclear Engineering
Georgia Institute of Technology

Dr. Nolan Hertel
School of Nuclear Engineering
Georgia Institute of Technology

Dr. Adam Stulberg
School of International Affairs
Georgia Institute of Technology

Dr. Nicolas Stauff
Nuclear Engineering
Argonne National Laboratory

-

Date Approved: November 21, 2016

To the memory of my uncle Sami.

ACKNOWLEDGEMENTS

I would like to start by thanking Dr. Erickson for her guidance and support throughout these past four years. I was very fortunate to be given freedom to explore different ideas and think creatively about problems facing the nuclear community. I must also give special thanks to Dr. Nicolas Stauff, who serves on my committee. His technical input and feedback has been incredibly invaluable. The thesis would be severely lacking in rigor were it not for his assistance. I wish to thank the other members of my committee for their help; especially Dr. Stulberg, who encouraging me to consider the broader socio-political context of my research and piqued my interest in the policy field. I owe a great deal of thanks to my colleague and close friend, Evan Redd. He was instrumental in shaping my ideas and always willing to lend an ear, especially during demanding times of my research. I am also very grateful to the Sam Nunn Security Fellowship and the TI:GER program for providing me with financial support during my thesis, and giving me with the opportunity to learn more about business and international affairs.

I owe a great deal of gratitude to my parents for their emotional and financial support throughout my challenging PhD experience. I am especially beholden to my father for his interest in my work, and the long hours we spent discussing different aspects of it. I am also fortunate to have such a wonderful family who has always been there to support me. I am forever grateful to Laura for being such a big part of my life these past two years, always eager to help in any way she can. I am especially indebted to her for all of her moral support during the difficult final months of my PhD. I would like to give special thanks to all my close friends, Georges, Pietro, Giovanni, Joaquin, Stefano, Yann, Lyes, Tony, Ali, Sabine, Tarek, and many others who were always there for me. I single out Georges and Ali for their close friendship and support during my PhD.

Lastly, I want to thank my uncle, who always believed in me, and to whom this thesis is dedicated to.

TABLE OF CONTENTS

LIST OF TABLES

LIST OF FIGURES

SUMMARY

Long-lived fast reactors have been suggested as an effective way of spreading nuclear energy to new countries. These small reactors can be produced at centralized locations, shipped to area of need, then returned to the main hub at the end of their lifetime for decommissioning. Such hub-spoke arrangements disincentivizes states front building sensitive front and back-end technology; however, critics argue they still pose a proliferation risk due to the large quantity of weapon-grade plutonium they produce during their operating lifetime. The dissertation attempts to address this issue by proposing a mixed-spectrum core configuration. A fast neutron zone can increase fissile material production, while a thermalized zone reduces plutonium quality. Moderating material ($ZrH_{1.6}$) is inserted within peripheral assemblies, while the center of the core maintains a fast configuration. Assemblies are then shuffled to ensure all are exposed to the thermalized spectrum. This allows the new design to simultaneously improve proliferation resistance and reduce fast fluence damage, a limiting criterion for long-lived core designs. The objectives are achieved with minimal impact on overall performance. Core lifetime can be maintained at 25 years, without the need for any additional fuel. Inherent passive safety criteria can be met, and power peaking phenomena at the fast/thermal interface was deemed to be manageable. Different design variants that can alleviate power peaking or leverage the ability of thorium-cycle breeding in the epithermal regime, were also investigated. Mixed-spectrum cores pushes the boundaries of what deterministic codes are capable of modeling accuracy. The REBUS suite of codes is modified to provide a more accurate tool to explore the design space. MCNP6 is then used for detailed analysis and safety evaluation of optimal core configurations. The thesis demonstrates the viability of using a mixed-spectrum reactor design to improve proliferation resistance of long-lived cores. The main identified tradeoff was an increase in overall resource consumption, a slightly larger core size, and the reliance on shuffling midway through the core lifetime.

CHAPTER 1
INTRODUCTION AND BACKGROUND

1.1 Nuclear Energy and Fast Reactors

The risks of climate change have driven a global consensus to prioritize carbon-free sources of energy. Nuclear power has received renewed interest, and is being emphasized due to its high reliability and relatively low operating costs. The IAEA predicts that global nuclear energy production will increase by 2% (lower bound) and 56% (upper bound) by 2030.[1] The reality is likely to be somewhere in the middle, with around 100 GW_e of additional capacity produced. This is equivalent to building around 7 new reactor each year until 2030. Under such increasing demand, the nuclear industry has been investing heavily in developing the next generation of nuclear reactors that can more effectively meet the needs across the world.

One such advanced reactor, is known as the fast reactor (shown in Figure 1.1). Ensuring neutrons are maintained at high energies (hence 'fast') within the core, allows these reactors to burn fuel much more efficiently than their counterparts. A typical Light-Water Reactor (LWR) requires a constant feed of uranium fuel, enriched with ^{235}U (at around 5%), an isotope that is depleted to generate electricity. Once the fissile ^{235}U content reaches below a certain level, fresh fuel must be added to the reactor. Fast reactors rely on another nuclear phenomenon to extend fuel burnup. When a fertile isotope (e.g. ^{238}U) absorbs a neutron, it is transmuted into a fissile isotope (in this case ^{239}Pu), which can be subsequently burnt in the reactor. Operating the nuclear reactor on the fast spectrum makes it possible to 'breed' additional fissile material faster than it is depleted. Such fast breeder configurations have been studied since the 1950s, as a means of ensuring nuclear energy would remain abundant in the future.

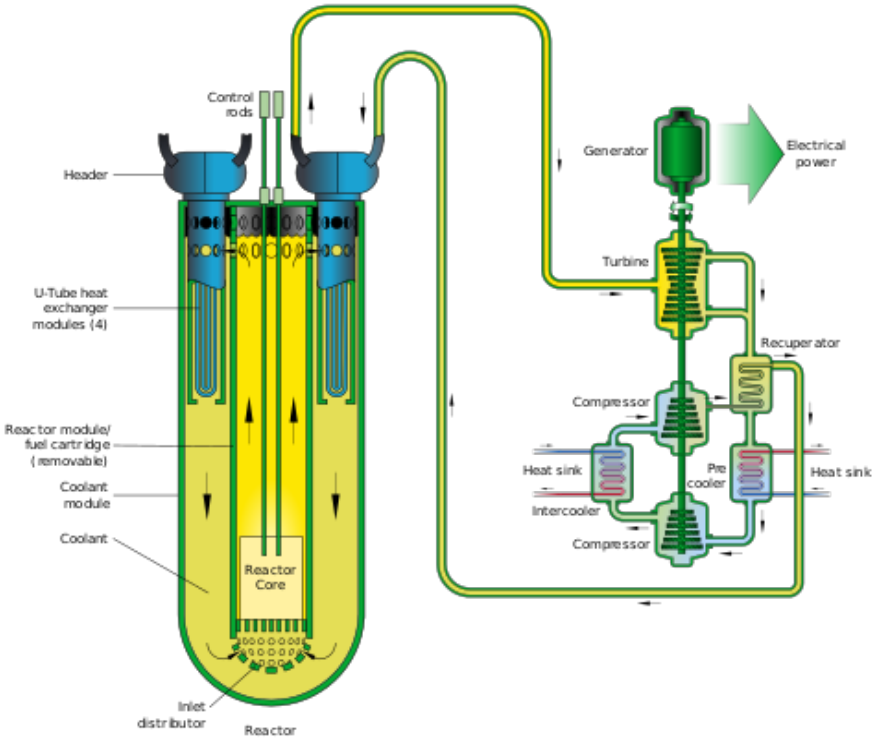

Figure 1.1: Diagram of a liquid-metal cooled, compact, fast reactor. Picture taken from [2].

Originally, the concept was envisaged to be coupled with a reprocessing facility that can recycle the useful isotopes, while eliminating and disposing the unwanted fission products. The approach is beneficial on two fronts: (1) it drastically reduces the volume of radioactive waste to store, as well as its longevity, and (2) it can substantially reduce the total amount of fuel consumed by a nuclear plant. Since only a fraction of the theoretical energy is extracted from uranium at each cycle, this allows plant designers to push the limits of fuel consumption. As a result, a breeder fast reactor is estimated to consume 100-times less mined natural uranium than a typical LWR.[3] The technology is relatively mature with numerous reactor built in the past, as highlighted by Table 1.1. All in all, a total of 350 reactor-years of operation is believed to have been accrued by fast reactors across the world.[3]

Despite their many attractive features, fast reactors have not seen widespread adoption world-wide. The less conventional reactors face multiple challenges that have made them

Table 1.1: Overview of previously-built fast reactors. [4]

Experimental	USA	EBR-II, Fermi, FFTF
	Russia	BOR-60, BR-10
	France	Rapsodie
	Germany	KNK-II
	India	FBTR
	China	CEFR
	Italy	PEC
	Japan	JOYO
	UK	DFR
Demonstration	Russia	BN-600
	France	Phénix
	Germany	SNR-300
	Japan	MONJU
	UK	PFR
	Kazakhstan	BN-350
Commercial	Russia	BN-800
	France	Super-Phénix

less attractive for deployment in the past. A report by the International Panel on Fissile Material (IPFM) cites four main issues: [5]

1. Uranium resources proved to be significantly more abundant than previously estimated; essentially annulling the argument for breeder reactors as a means of reducing strains on fuel resources.
2. Fast breeder reactors have been very costly to build and operate; making it unlikely that in their current form they can become economically competitive with LWRs.
3. Even though they solve many of the safety challenges with LWRs, fast reactors have safety concerns of their own, specifically due to the fact that their coolant can react violently with water or air. This has resulted in frequent fires in these reactors, questioning their reliability.
4. Breeder reactors are a proliferation threat due to the large amount of plutonium that

they produce and the fact that they were designed to operate using plutonium separated in a reprocessing plant.

In part because of the first and fourth highlighted challenge, focus on fast reactor moved away from maximizing the production of fissile material that can spawn enough fuel for other reactors to startup. The main justification for further development shifted to developing self-sustaining reactors operating on closed-cycle, producing very little waste, and not relying on any enriched fuel feed. Rather than breeding more fuel than was burnt (breeding ration, BR, above unity), emphasis was put on generating as much fissile isotopes that are burnt (BR very close to unity). The recycling technology itself was altered in order to avoid reverting to the 'PUREX' process, which is used for extracting plutonium for weapons purposes. US R&D efforts developed pyroprocessing technology instead, where fertile and fissile isotopes are never fully separated, ensuring plutonium is never isolated in a pure form. The development efforts culminated into the Integral Fast Reactor (IFR) program that was shut down in 1994, mainly because of cost and proliferation concerns.

Subsequent and more recent fast reactor R&D efforts have distanced themselves from any type of fuel recycling. Operating on a once-through fuel cycle, research has focused on expanding fuel utilization within reactors. The concepts rely on 'breeding' sufficient amounts of fissile material in fertile zones (depleted or natural uranium) to compensate their depletion in driver regions (containing LEU). These 'breed and burn' concepts were originally proposed in 1958,[6] and have seen multiple variants since, each with different seed-driver configurations. A common feature in proposed designs, is that they do not require any fuel reprocessing, nor any additional enriched fuel. They can maintain criticality without any additional fuel feed, or by simply using natural/depleted uranium as feed material after startup. The larger variants of these cores rely on shuffling or axial blankets to extend burnup. CANDLE-type reactors for instance (e.g. UCFR concept [7]) have elongated fuel with an 'igniter' fissile loading at its bottom, and fertile fuel above it. As fissile material is bred directly above the fissile zone, the active core region travels upwards at a

rate of a few centimeters per year (5 cm/year for the UCFR). Greenspan et al. proposed an alternative configuration that relies on radial rather than axial breeding.[8] By shuffling assemblies containing either depleted uranium or LEU, a 40-fold increase in uranium ore consumption compared to current fuel cycles, without reverting to any fuel recycling.

Alternative high-burnup designs have focused on a more simplistic, 'battery-type' approach. These smaller reactors are designed to last for long periods of time (several decades) without requiring any additional fuel feed or shuffling of the assemblies. While more compact than CANDLE-type core, they still rely on the same basic principle of breeding then burning fissile material in fertile regions in order to increase the core longevity. These 'long-lived' core designs are the main focus of this thesis.

1.2 Long-Lived Reactors

The majority of the future demand for nuclear energy is expected to come from emerging nations; out of the 60 currently reactors under construction worldwide, over 65% are being built in developing nations.[9] A total of 22 countries without nuclear energy (newcomers) have drafted serious plans to acquire this capability as highlighted in Figure 1.2. This has motivated engineers to design and develop nuclear reactor concepts that can effectively cater to their needs. The end result is the proposed 'hub-spoke' fuel cycle concept that relies on long-lived reactors.[10] An illustration of this proposed fuel cycle is shown in Figure 1.3. Because many of the newcomer countries do not possess the required fuel cycle infrastructure to support the construction of a whole front and back-end fuel cycle, such an arrangement can be an attractive alternative. Furthermore, their electricity grids tend to be small, and fuel security tends to be of great concern. Under hub-spoke agreements, a long-lived Small Modular Reactor (SMR) is manufactured at a country with an existing nuclear infrastructure (e.g. US), and 'leased' by a receiving nation. The reactor is shipped to the host nation with enough fuel to operate for up to 30 years, and remains sealed throughout its operating lifetime. The core would not require any additional fuel feed nor any shuffling

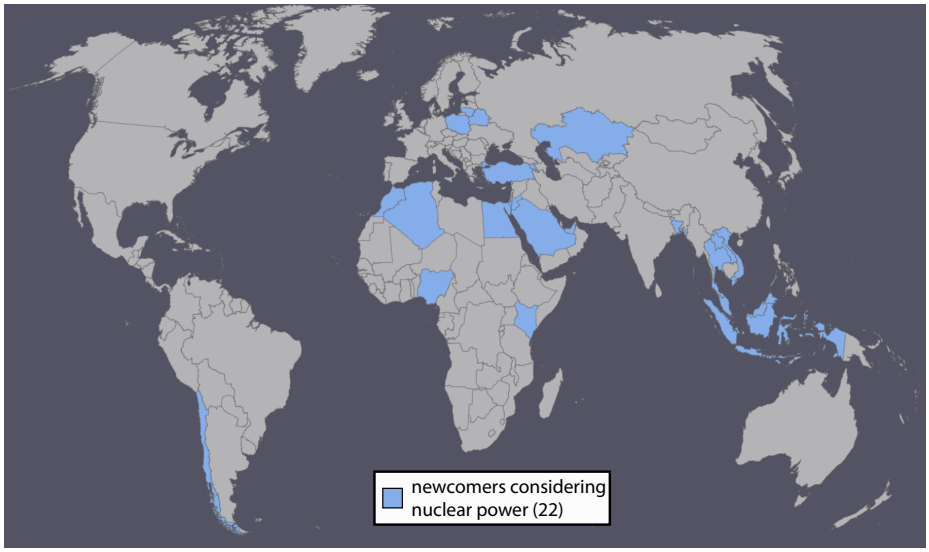

Figure 1.2: Map of newcomer countries considering nuclear power. Data obtained from *World Nuclear Association*.[11]

or fuel handling by the host nation. At the end of its lifetime, the reactor is returned to the original hub-nation that deals with decommissioning and disposal of the radioactive material.

While the concept remains at the theoretical level, many institutions have pushed forward with their own design variants. Indeed, several private companies have been actively developing their own models; this includes Toshiba (4S design), General Atomics (EM^2 design), Oklo (Oklo reactor design), LeadCold (SEALER design), ARC (ARC-100 design), and Gen4 Energy (G4M design). In order to achieve their stated goals, the designs rely on two main characteristics: (1) breeding and subsequently burning additional fissile material (so-called 'deep-burn'), and (2) employing a low power density to extend operating lifetime for the same burnup (so-called 'slow-burn'). The reactors are configured to have different fissile loading throughout the core, with certain zones operating at a high breeding ratio (BR) being driven by regions with higher initial fuel enrichment. Typically, the overall breeding ratio of these cores is close to 0.8, which is why these reactors are characterized as 'burners' as opposed to 'breeders'. This level of breeding is substantially higher than what can be reached in a typical LWR. The power density of long-lived core tends to be

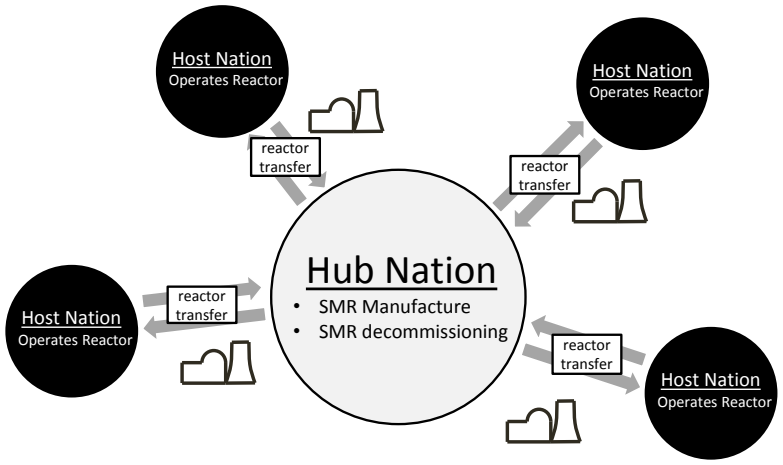

Figure 1.3: Diagram of the hub-spoke nuclear fuel cycle, whereby a whole reactor is 'leased' to a host nation. It is manufactured at the hub country and returned there for decommissioning at the end of its lifetime.

closer to that of a LWR (around 100 kW/l) than that of typical fast reactor (around 250 kW/l) in order to prolong the time until the core becomes sub-critical.

Long-lived core designs have several other advantages that make them ideal for their intended markets. They are compact and transportable; example dimensions are a 12 m height by 3.2 m diameter for the SSTAR reactor developed by Argonne National Lab (ANL).[12] This allows them to be shipped and deployed and in remote locations as well. The reactor modules are relatively simplistic, with minimal piping, valves, or other components. Their size makes them ideal for mass-production at centralized locations, where cost and quality can be better reined on. The reactors are touted to be relatively easy for the operator to control, with near-passive load following capabilities, and minimal burnup reactivity swings. The main challenges facing the deployment of long-lived reactors is their peak fast fluence limits. Cladding material are expected to sustain irradiation damage up a fluence of 6×10^{23} n/cm^2,[13] which is currently beyond the capabilities of tested metals. Fuel burnup limits are also near the observed experimental limits.[14] Another concern is power flattening within the core, which becomes increasingly problematic the longer the reactor operates for. Breeding assemblies see lower power generation initially, but generate more energy

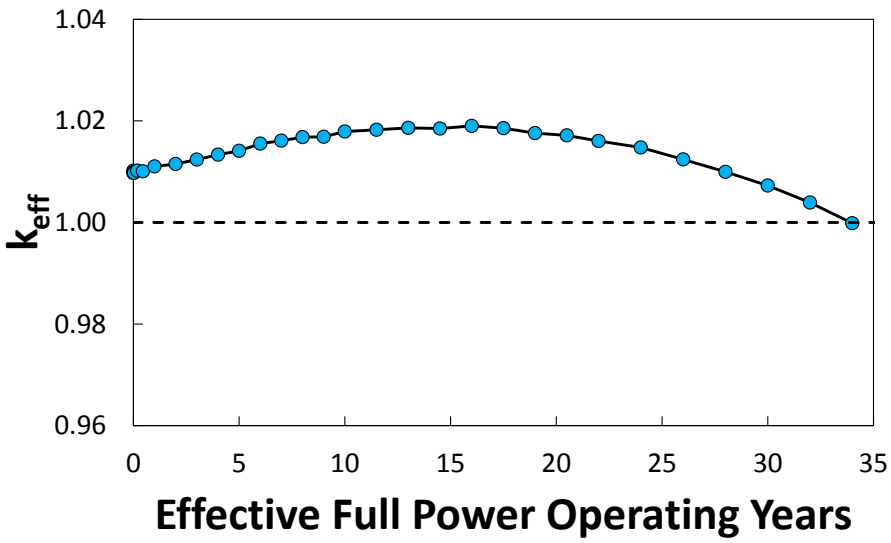

Figure 1.4: Long-lived cores can maintain their eigenvalue above unity for a prolonged period of time, of the order of several decades. The results shown here are for a model that is further discussed in later Chapters.

when they become rich with fissile isotopes. Figure 1.4 shows how the reactivity (k_{eff}) of a typical long-lived core can be maintained above unity for several decades.

Advocates of long-lived reactors argue that they can strengthen the nonproliferation regime since they remove the incentive for a host nation enrich, reprocess or handle nuclear fuel in any way. Critics however, have claimed that such designs bring added proliferation risks.[15] While plutonium is always produced as a by-product of electricity generation, the quality of the plutonium in long-lived cores is much higher than in a typical LWR. Indeed the plutonium remains weapon-grade for the duration of the fuel lifetime in the core, which can be in the order of 30 years, as shown in Figure 1.4. Proliferation characteristics tended to be ignored in the past due to a pseudo-consensus formed on the adequate resistance of LWR designs. Since the vast majority of proposed cores in the past tended to be evolutionary in nature and LWR-based, proliferation resistance has never been of primary importance in the conceptualization phase of reactor designs. It is argued in Chapter 2, that a renewed emphasis on this design characteristic is needed now that advanced non-LWR designs are within the horizon. The main objective of this thesis will be to investigate

Table 1.2: The effect of thermalization in fast and thermal core regions.

	Fast	Thermal
^{239}Pu cross-sections:		
σ_a/σ_f	0.16	1.90
$\sigma_f(b)$	1.75	4.31
End of cycle:		
Pu_{fiss} / Pu_{tot}	95.82%	83.63%
$\text{m}_{Pu-fiss}$ / $\text{m}_{U-initial}$	3.35%	4.82%

potential long-lived core variations that can alleviate proliferation risks without posing a substantial performance penalties. Chapter 3 will discuss different approaches to intrinsically improve the proliferation resistance of these fast reactors. The main path selected for further analysis in this thesis is a mixed-spectrum configuration, whereby a thermalized region breeds lower-quality plutonium and assemblies are shuffled to ensure they are all exposed to the thermalized spectrum.

1.3 Background on Mixed Spectrum Reactors

Mixed spectrum reactors exhibit notable variations in their neutron spectrum between different core regions. Insertion of limited amounts of moderator, in specific locations, allows these cores to reach a wide range of design objectives. In this thesis, the main focus will be on improving proliferation resistance aspects. As shown in Table 1.2 a thermalized spectrum can increase the probability of breeding non-fissile plutonium isotopes. The reactor can improve fuel proliferation resistance in one core region, while maintaining the advantages of a fast configuration (notably higher breeding) in another.

Reactors with dual neutron spectra have been evaluated in the past for a wide variety of applications. The concept of using a mixed-spectrum was first proposed Avery in 1958.[16] The main objective at the time, was to improve the controllability of fast reactors; back when little experience on was accrued on fast systems. In the late 1970s,

Brookhaven National Laboratory (BNL) and MIT developed a more thorough concept, more similar to the 'breed and burn' reactors aforementioned. The main focus was on improving proliferation resistance of an equilibrium core, refueled with natural uranium. BNL focused on a uranium-fueled gas-cooled variant, [17] while MIT studied a sodium-cooled, thorium-fueled concept.[18] In both studies, only blanket regions were thermalized within the core. In the case of BNL, the outer blanket ring was 'sandwiched' between moderating assemblies (referred to as an intra-assembly arrangement), while the MIT design studied heterogenous blanket arrangements with moderators inserted within blanket assemblies (an inter-assembly arrangement).

Subsequent studies investigated the addition of moderating material in a more limited fashion around core peripheries, to burn actinides more efficiently, or denature blanket plutonium. In 2010, Stauff proposed a later model, where blanket assemblies are doped with minor actinides and mixed with $ZrH_{1.6}$ rods to bring their plutonium vector close to that of typical a LWR.[19] Bays investigated using $ZrH_{1.6}$ in axial regions to improve transuranic transmuation.[20] A common feature in all of the previously proposed configurations, is that they only generated small power fractions within thermalized regions. A more recent proposal by Sen, had a near half power split between the fast and thermal regions.[21] The main objective was to obtain a versatile testing facility that could provide both fast and thermal irradiation of samples. Another potential purpose for adding moderators to a fast reactor is to improve some of the reactivity mechanisms. Tsujimoto, showed that the addition of ZrH rods can improve the Doppler and sodium void feedback mechanisms of a sodium-cooled reactor.[22]

The different incarnations of Mixed-Spectrum Reactors (MXR) have had varying designs. An array of materials has been considered, notably BeO, graphite, and ZrH. Different locations for the added moderator was studied, as well as its relative quantity. All of these different considerations will be assessed in Chapter 5. The end goal of the core design optimization efforts will be to reduce overall bred plutonium quality inside a long-lived core

arrangement while maintaining adequate performance and safety characteristics. In order to ensure all of the fuel is exposed to the thermalized spectrum, infrequent shuffling is envisaged (only once) throughout the core lifetime. Chapter 6 will then proceed to evaluate inherent safety criteria of the selected MXR configuration, in order to verify its feasibility. The final chapter will then discuss potential improvements to the design, and perform more in-depth evaluation of performance metrics.

CHAPTER 2

PROLIFERATION RISKS OF LONG-LIVED REACTORS

Upon first look, long-lived reactor exchanged in hub-spoke fuel cycles may seem ideal from a nonproliferation standpoint. They remove the incentive for a state to develop sensitive enrichment or reprocessing technology, that are crucial steps in the development of a weapon. This chapter will discuss how the proposed arrangement creates new proliferation problems as it eliminates others. An overview of nuclear proliferation theory in international affairs circle is provided to discuss how it can relate to long-lived cores. The main finding is that many proliferation concerns are warranted, and should be intrinsically addressed within considered long-lived core designs. Nuclear engineers have historically placed little emphasis on proliferation resistance at the conceptualization stage; and this should be revisited with upcoming non-LWR designs. Ignoring potential concerns raised by the nonproliferation community could lead to a similar demise as the Integral Fast Reactor project in the 1990s.

2.1 Nonproliferation Advantages and Weaknesses of Long-Lived Reactors

One of the main criticism of the Non-Proliferation Treaty (NPT), is that it does little to limit the spread of critical infrastructure that can be used for a weapon; namely enrichment and reprocessing technology. The sticking point resides mainly on the fact these technologies are dual-use in nature and can be plausibly argued to be needed for civilian reasons: enrichment is necessary for the production of nuclear fuel, while reprocessing can be helpful in recycling nuclear waste. As a result, there has been a drive in the nonproliferation community to encourage states to forgo these types of capabilities and rely on other nation's existing infrastructure, rather than building their own indigenous one. From a nonproliferation standpoint, the ideal fuel cycle for developing nation would be one where a state

can benefit from nuclear energy, ensure a fuel supply security, and all the while have no incentive to build sensitive front and back-end technology. As such, the 'hub-spoke' model with a long-lived core appears to be promising upon first look.

The importance of limiting the spread of sensitive technologies was highlighted by the JCPOA agreement with Iran, where the P5+1 states attempted to limit the country's enrichment capabilities. Within the Nuclear Supplier Group (NSG), there is a recent drive towards encouraging 'fuel leasing' options for newcomer nations to the nuclear field. Rather than develop their indigenous uranium mining, enrichment, and fabrication capabilities, states are urged to rely on an external fuel supply while gaining access to state-of-the-art nuclear reactors. This led the US to press the UAE to sign on to the so-called 'Gold Standard' agreement, forfeiting their right to enrich and reprocess fuel.[23] Similarly, Russian vendors have gone even further, and proposed fuel leasing options. Under such an agreement, Russia ensures the provision of enrichment alongside the provided reactor. After irradiation, fuel is returned back to Russia for conditioning and disposal.[24] These arrangement types would, in theory, remove any justification for development of sensitive technologies on the ground of fuel security (Iran) or waste disposal (South Korea). This makes the options very attractive from a nonproliferation standpoint, but may be deemed onerous by some states who fear becoming highly dependent on a single external fuel supplier for continuous operation of their purchased reactor (an argument raised by Iran as justification for pursuing enrichment capability). The IAEA LEU bank in Kazakhstan can help alleviate some of this concern, but would not address fuel manufacturing and disposal. Long-lived reactors are another solution, by virtue of operating for prolonged periods of time without the need for any additional fuel. A host nation would be entitled to decades of nuclear energy without being dependent on an external fuel supply, and without the need to develop any indigenous sensitive technologies. From a broad perspective, such 'hub-spoke' fuel cycle models seem ideal from a nonproliferation standpoint. Long-lived designs have been criticized however, on the basis that they might actually prove to be a more attractive target

to divert nuclear material than a typical PWR.

One study estimates that taken as a whole, these reactors would in fact increase proliferation risks relative to the current PWR by several percentage points (5% increase according to Markov Chain analysis). Glaser points to the fact that resources will have to be spread more thinly to monitor and inspect more facilities for every kW of energy, since these reactors are typically smaller.[15] Additionally, as Figure 2.1 highlights, a single assembly can provide a proliferator with 1 Significant Quantity (SQ) of plutonium (as opposed to two assemblies for a LWR). The plutonium purity also remains at the weapon grade level throughout the core lifetime (as opposed to a few months for an LWR). On the other hand, proponents of such designers are quick to point out that the reactor can be sealed and would remain inaccessible - in theory - to the host nation throughout their operating lifetime. It is argued that this would remove the opportunity for a state to divert material.[25] The are several limitations with relying on core vessel seals however. First, since no reactor can run on a 100% operating capacity, regular maintenance at the core level cannot be disregarded (notably in the case of small cladding ruptures). This could provide a state with an opportunity to divert fuel. Second, it is highly unlikely that when the reactor is sent back to the hub for decommissioning, that fuel will be maintained within it. It would be more prudent, from a safety perspective, to extract the fuel assemblies and place them within separate containers. This would mean that a host state would have at least one opportunity to divert fuel during the operating lifetime (albeit once in 30 years). Lastly, seals are ineffective during breakout scenario where a state can forcefully halt operations and remove plutonium-bearing material.

To better assess the proliferation risks of long-lived reactors, a more holistic review is needed. Tables 2.1 and 2.2 provide a qualitative comparison of different core designs metrics against typical LWR. These reactors are taken as the basis of comparison, despite their proliferation limitations. Gilinski et al. have highlighted some of the proliferation weaknesses of LWR and why they are not as resistant as initially perceived.[26] This mainly

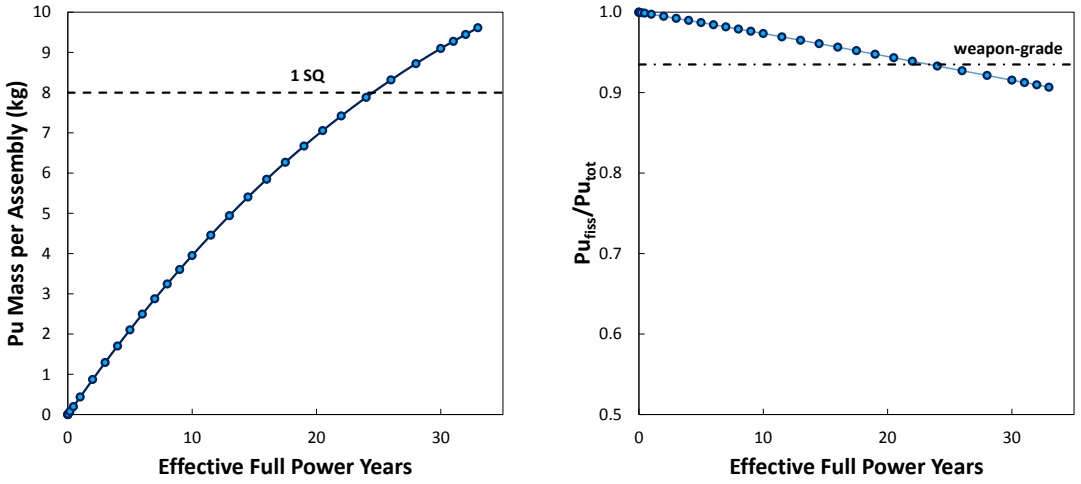

(a) Average mass of Pu per assembly.

(b) Evolution of the plutonium quality in the fuel.

Figure 2.1: Plutonium compositions in a typical long-lived fast reactor. Simulations generated using MCNP6.

comes down to the fact that reactor grade plutonium is still weapon-usable, obtaining enriched fuel is not as challenging as it originally was, and the reactors can be retrofitted to breed weapon-grade plutonium from natural uranium assemblies. Nevertheless, none of these reactors have ever been successfully employed to proliferate in the past, and they are widely deemed 'acceptable' by the nonproliferation community. The GenerationIV International Forum (GIF) stated as one of the goal of future reactor is to be as or more proliferation resistant than the ones they supersede.[27] Therefore, taking LWR as the basis of comparison is a useful approach.

The parameters in Table 2.1 and 2.2 were chosen from a review of the literature on proliferation resistance evaluation methodologies, notably the methods proposed by Sandia National Laboratory.[28] Metrics are grouped between those evaluating the attractiveness of the fissile material (Table 2.1) versus those regarding the general operation of the reactor (Table 2.2). They are also divided depending on their relevance to diversion (D) or breakout (B) scenarios. Both CANDU and long-lived reactors (LLR) are given a qualitative score for each metric based on their performance relative to an LWR. The overview shows how long-lived core perform better that LWRs in terms of intrinsic safeguardability (more '+'

symbols in Table 2.2), but have worse material attractiveness credentials (more '-' symbols in Table 2.1). It can be difficult to assess whether some of strengths outweigh the resulting weaknesses. In order to avoid this dilemma, the thesis will simply assess potential performance cost of improving these highlighted weaknesses, and evaluate how they can be overcome. It is worth highlighting beforehand, in greater detail, why it is important to take this concerns into consideration at the design. Section 2.2 will outline cases where countries have used fast reactor for weapon-use, and Section 2.3 then reviews the historical precedence for attempts to proliferate using any externally provided reactors. Lastly, Section 2.4 will discuss the potential risks of these long-lived reactors from an international relations perspective.

Table 2.1: Comparison material attractiveness parameters for a CANDU and long-lived reactor (LLR) against an LWR. The notation 'D' and 'B' refer to diversion and breakout-scenario respectively. The '+', '-' and '0' sign refer to a performance better, worse or similar to an LWR respectively.

Metric	**Scenario**	**LLR**	**CANDU**
mass of Pu produced in core per year	B	+	0
mass of Pu produced in core per year per unit of power	B	-	0
maximum mass of Pu produced per assembly	D	-	0
average mass of Pu produced per assembly	D	-	0
mass of 1 SQ containing assemblies	D	-	0
volume of 1 SQ containing assemblies	D	-	-
radiation level of material	D	0	0
heat generation of material	D	0	0
average Pu quality in core	D/B	-	0
highest Pu quality in core	D	-	0
amount of Pu/assembly when ^{239}Pu content reaches 90%	D/B	-	-
amount of Pu/assembly when ^{239}Pu content reaches 80%	D/B	-	-

2.2 Proliferation Risks of Fast Breeder Reactors

In order to evaluate the potential risks of an independent fast reactor, it is first important to consider how previous reactors have been repurposed for weapons production. The IPFM report provides a rigorous overview of each country's fast reactor R&D program, notably

Table 2.2: Comparison of operational parameters for a CANDU and long-lived reactor (LLR) against an LWR.

Metric	**Scenario**	**LLR**	**CANDU**
reactor shutdown frequency	D	+	-
online refueling (Y/N)	D	0	-
enrichment of fuel feed	B	0	-
average fuel consumption per year	B	+	-
quantity of irradiated fuel outside core per year	D	+	0
total quantity of irradiated fuel outside core over lifetime	D	+	0
ease of monitoring/accounting material (qualitative)	D	+	-

the French and Indian, both of which were militarized.[5] A brief summary is provided to draw potential parallels with the more novel reactor concepts.

France's R&D program began in 1958 with the design of the Rapsodie experimental facility. The country pushed further with its Phénix reactor, which went online in 1974. Government support for the programs was strengthened in the wake of the 1973 oil shocks; leading to an aggressive expansion of the nuclear fleet. The energy source currently provides arounds 77% of total the electricity produced by France.[9] Following a hike in the price of uranium, fast reactors were seen as a solution to energy security concerns, specifically in terms of long-term nuclear fuel supply. It was in this context that the Superphénix reactor was built in 1985. However, in the aftermath of Chernobyl and the fall in uranium prices, interest in fast reactors started to wane. The IPFM report estimates that the core of this Superphénix reactor contained 5,780 kg of plutonium at super-grade quality. It was the Phénix reactor however, that was the more heavily militarized. Spent fuel from its axial and radial blankets was believed to have been reprocessed at the military UP1 reprocessing plant. Military officials even made open statements that the reactor was intended to be used for weapons production.[5]

Fast breeder reactors were always a key part of India's nuclear program as a response to its small known uranium reserves. The first breeder reactor, FBTR, was constructed with significant assistance from the French fast reactor program. Under the context of separating

fuel for its breeder program, India diverted plutonium from its Trombay reprocessing plant for use in its 'peaceful nuclear explosion' in 1974. The experience highlights how fast reactors and reprocessing facilities can be exploited as cover for a weapons program. This explains why many suspect that India's upcoming fast reactor, PFBR, is being constructed with dual purposes in mind: to produce electricity while also providing plutonium for weapons.[29] These concerns are boosted by the reluctance of the Indian government to place the upcoming reactor under IAEA safeguards.

Nonproliferation issues become increasingly blurred when accounting for reprocessing technology. The most common method of reprocessing is known as PUREX, where plutonium is chemically separated from other elements and subsequently used to manufacture a new fuel. The process has attracted a lot of criticism from the nonproliferation community due to the fact that it can be repurposed, with relative ease, for industrial-scale weapons production. This led chemical engineers to devise alternative schemes that do not isolate plutonium in a pure form. Pyroprocessing and UREX+ were among the proposed means of reutilizing fuel in a fast reactor while keeping the plutonium mixed with uranium and other transuranics. Since plutonium would never be fully separated, the reasoning goes, a proliferator would need to revert back to a separation process (such as PUREX) to develop a weapon.[30]

Critics from the nonproliferation community were quick to point out that the PUREX-alternatives still posed a substantial proliferation risk. The process separates the plutonium from the highly radioactive fission products that are generated in a reactor, making fuel handling easier and further separation much simpler. Researchers pointed out that methods such as pyroprocessing would reduce the radiation barrier surrounding the plutonium mixture to less than 1% of the self-protecting standard as defined by the IAEA.[31] The subsequent plutonium separation for a weapons production would no longer require heavy shielding or remote operations.

These aforementioned issues (alongside economic costs) are what drove the current

U.S. fast reactor development efforts to investigate further 'once-through' reactor cycles, notably using long-lived core designs. However, as previously mentioned, even these reactors are not without risks. While there is a clear consensus in the nonproliferation community that all reprocessing technology (and enrichment) pose a threat, it is unclear to what extent this is also the case for reactors. The next section provides an overview of historical cases where externally-acquired reactors were used (or attempted to use) for proliferation.

2.3 Nuclear Prolifeartion via Externally Acquired Reactors

Two main paths to nuclear proliferation are possible: the uranium or the plutonium route. Ultimately, a state needs to develop one of two capabilities, either enrichment (uranium route) or reprocessing (plutonium route). Security experts have often argued about which path constitutes the weakest link, and therefore requires the most focus in term of safeguarding. If a country were to proliferate without any pre-existing infrastructure, some experts have argued that gas centrifuges are the most effective option.[32] Others believe that a lab-scale reprocessing facility coupled with a crude, small, graphite reactor is the simplest path.[33] The dynamic changes however, if a country already possesses some level of existing infrastructure that it can leverage, notably a civilian or research reactor. This can substantially shorten the plutonium path, effectively removing one roadblock: generating the plutonium. The only remaining task would be to develop a clandestine reprocessing facility, and smuggle irradiated fuel to it. Some international relation theorists argue that due to this reason, any type of sensitive 'nuclear assistance' can increase the risk of a country proliferating (this will be revised in further detail in Section 2.4). This section will provide a review of the historical basis for nuclear proliferation via externally-obtained reactors.

If a country were to attempt to proliferate via an externally provided reactors, two scenarios are possible. In the diversion case, the state diverts sufficient material covertly (significant quantity, or SQ, as defined by the IAEA), while attempting to avoid international scrutiny. In the breakout scenario, the country openly repurposes the considered reactor,

converting it to a weapons production facility. Both approaches have been attempted in the past - albeit with limited success - and must therefore be taken into consideration. Table 2.3 provides an overview of select cases where proliferation was attempted using externally provided reactors. In some cases, countries intended to militarize the facility even before it was acquired, in other, countries attempted to leverage the considered facility as their weapon program progressed. In some cases, it is believed that countries had knowingly provided another with a dedicated production facility (e.g. Pakistan and Israel). In other instances, the transaction was clearly civilian in nature, but the receiving country and concrete plans to leverage the facility for their weapons programs (e.g. Taiwan and North Korea). In many of the remaining instances, original intents are less clear, but the countries subsequently decided to proliferate via the reactors (e.g. India and Argentina). These countries are the most relevant to this thesis and warrant further analysis.

Table 2.3: Overview of states that acquired reactors and were suspected of employing them for weapons program.

Coutry	**Time**	**Reactor**	**Intent**
India	1955	Cirus from Canada-US	peaceful
Israel	1966	Dimona from France	military
Iran	1967	TRR from US	unclear
Argentina	1968	Atuch from FRG	unclear
Taiwan	1969	TRR from Canada	military
Iraq	1970	Osirak from France	unclear
Algeria	1987	Es-Salam from China	unclear
North Korea	1989	IRT from USSR	military
Pakistan	1998	Khusahb from China	military

While India obtained a production reactor in 1955, it was not until 1964 that even theoretical work on a bomb was allowed.[34] Evidently, obtaining the reactor itself was not a deciding factor, but its availability increased the confidence of key proponents of a nuclear program who pressured the decision-makers.[35] The Indian case also highlights the fundamental importance of safeguards. At the time, India was only required to provide 'peaceful assurances' of its use of the reactor. Unsurprisingly, this was far from enough to

deter decision-makers, once the decision to proliferate was made. No similar incident was observed after the NPT entered into force, stressing the importance of safeguards. A second relevant case is Argentina. The country obtained a commercial, non-research reactor, and subsequently diverted some fuel from it to separate 1 kg of plutonium.[34] This illustrates that diversion of fuel from a power-producing facility is not as far-fetched as it may seem. On the other hand, instances where countries obtained dedicated production facilities are less directly related to this study, but are still relevant. They illustrate what state actors have tended to prefer when proliferating.

Scenarios where original intent was unclear highlight how the acquisition of ' production-usable' reactor facility can affect the dynamics of a decision to pursue the bomb. It is therefore important to understand the reactor characteristics that make them more attractive to proliferators, in order to take them into account during the design conceptualization stage. Looking closer into the reactor characteristics themselves, patterns regarding proliferation attractiveness emerge as highlighted in Table 2.4. Heavy Water Reactors (HWR) have been the historically preferred option for proliferating. One explaining hypothesis is that they do not depend on an external fuel feed to operate. Indeed, the reactors are able to operate on natural uranium that a country can usually acquire indigenous. This is a shared characteristic with long-lived cores, which do not depend on external fuel supplies. A second common aspect with long-lived reactors is that these reactors tended to be of the smaller variant (around 50 MW_t) usually. A potential explanation for this is that states may have opted for smaller design to obtain a 'minimum viable product' able to produce material for a bomb. Another reason may be that converting larger electricity-producing facilities may result in a substantial energy disruption. A third pattern that emerges, is that most cores could only produce small quantities of plutonium per year; on the order of 10 kg/year, just enough for a single bomb per year. It appears that this amount of fissile material was deemed sufficient for most proliferators. This highlights the risk that diversion scenarios pose for long-lived cores, where a single assembly can contain more than that amount of

plutonium. Lastly, in most of the cases, proliferators preferred to divert or obtain weapon-grade plutonium, from low-burnup fuel. This is common with the long-live cores where plutonium quality stays in the weapon-grade limit throughout the core lifetime. Overall, it seems that the attractiveness of the material, the ease of access to it, and the ease of converting a civilian facility to a military one, all factor into the decision-making process to proliferate. The next section will review political science theory relating to a state's decision to acquire nuclear weapons, with the aim of distilling conclusions that apply to long-lived reactors.

Table 2.4: Specifications of externally-provided reactors that were involved in proliferation attempts. Note that the plutonium production rate values are only approximations. Fuel types are natural uranium (Nat. U), high-enriched uranium (HEU), and low-enriched uranium (LEU). The majority of the data was obtained from the *Nuclear Threat Initiative* (www.nti.org) unless otherwise stated.

Case	**Type**	**Size (MWt)**	**Fuel**	**kg of Pu/year**
India	HWR	40	Nat.U	10
Israel	HWR	70-150	Nat.U	14-17
Iran	LWR	5	HEU/LEU	0.6
Argentina	HWR	1200	Nat.U+LEU	$<$100
Taiwan	HWR	40	Nat.U	10 [36]
Iraq	LWR	40	HEU	2 [37]
Algeria	HWR	50	Nat.U	10-13 [38]
North Korea	LWR	8	LEU/HEU	$<$1
Pakistan	HWR	50	Nat.U	10-20 [39]

2.4 Nuclear Proliferation, Supply-Side Theory

Nuclear proliferation theorists have long argued about the fundamental reasons driving a state to proliferate. They generally tend to fall into two main school of thought: supply-side and the demand-side theorists. The former believes that the technology imperative pushes states from latency to a weapon by reducing the costs associated with doing so and making it a more attractive venture for a state. Demand-side theorists argue that a wide range of factors (political, military, prestige etc.) are the major drivers of such decisions.

Until recently, demand-side theories were predominant. In *The Dynamics of Proliferation*, Meyer reviews both sides of the debate and reaches the conclusion that there is stronger evidence for the 'motivational hypothesis' (i.e. demand-side) rather than 'technology determinism' (supply-side).[33] He did not find clear distinctions between a country that goes or doesn't decide to 'go nuclear' with relations to its existing capabilities. Later on, Sagan broadened the spectrum of definition to what constitutes 'motivation' for a state to acquire nuclear weapons. He included in it, security concerns (e.g. China), internal politics (e.g. India) and norms (e.g. France).[35] According to the motivational hypothesis, technical capability is an important condition for a state to proliferate, but not a necessary one. Countries are viewed as being continuously influenced by incentives vs. disincentives to proliferate, and aids vs. restraints from external parties.

Lately however, supply-side theory has regained traction by showing that the debate is more nuanced than first thought. The theory can be generally referred to as the technology imperative: once a state acquires the capability to build a weapon (latent capability), it is only a matter of time that it does so. Contrary to the motivational theory, this theory believes that the main factor driving a nation to 'go nuclear' is the technology itself. Under this lens, fast reactors and any type of nuclear-related technology is viewed as a potential threat. They lower the cost for a state to pursue a nuclear weapon and encourage it to do so. There are many different variants of this technological determinism, but they all essentially place more emphasis on technological momentum rather than a state's options and choices with regards to a weapons program. Many in the modern literature emphasize that technology has a probabilistic, not a deterministic effect on proliferation, in order to account for cases such as Libya and Iraq.

Fuhrman's work has questioned Meyer's claim that states with existing capabilities are no more likely to develop a weapon. His analysis shows that states that receive help are more likely to start a weapons program than states that didn't. The former has a 0.43% likelihood of proliferating against 0.1% for the latter.[40] This represents 4-fold increase,

but is still of low probability. This can be explained by the fact that obtaining sensitive facilities may lower barriers for a state, increase their perceived confidence in their ability to do a 'dash for the bomb', and therefore encourage them to proliferate. Fuhrman also assesses why states provide atomic assistance to others, and came to the conclusion that they do not take proliferation concerns into major consideration. The main reasons, he found, were to enhance political influence by reinforcing alliances, partnering with enemies of enemies, strengthening other democracies or to barter nuclear energy for other important commodities. Kroenig also points out that states that receive sensitive nuclear technology are better able to leapfrog designs stages, benefit from tacit knowledge, lower weapon-development cost, and avoid international scrutiny.[41] He argues that providing a state with a nuclear reactor may contribute to 'exporting the bomb' by making it easier for the country to proliferate if it chooses to do so. Section 2.3 showed that specific types of reactors have been favored over others by proliferators throughout history.

Following the supply-side point of view, technology transfers must be subjected to careful scrutiny by the international community. Any type of technology received can be used to some extent in overcoming common obstacles encountered when developing a weapon. This reasoning would conclude that a fast reactor breeding large quantities of high quality plutonium could lead to breakthroughs for a nation that can reduce the expected cost of a program, reduce technical uncertainties, and empower bureaucracies advocating for weapons. Since states can always draw from dual-use technologies, any technology transfer can be seen to be increasing risks of proliferation to some extent. That being the case, it is near impossible to envisage a complete ban on all types of nuclear technology transfer. The real solution would be to persuade states to take proliferation issues more heavily into consideration when they engage in any kind of nuclear transaction.

The aforementioned issues become all the more important when discussing nuclear latency. Jo and Gartzke have quantifiably shown that states can be heavily influenced by latent capabilities, and the diffusion of nuclear knowledge, when pursuing a weapons pro-

gram.[42] Interestingly, they showed that while latent capability can increase the probability of state having a weapons program, it has a lesser effect on the actual decision to produce a bomb. They also predict that regional and middle powers will be the most likely to proliferate in the future, many of which are actively seeking nuclear energy programs. Early efforts by the nonproliferation community were heavily focused on stopping states from testing weapons. Nowadays, attention has shifted to keeping states away from latent capabilities, elongating a state's breakout time, and limiting its production of fissile material. This was the case for the so-called 'Iran Nuclear Deal' of 2015, which may set a precedence for future proliferators. It is foreseeable that states are likely to try and get as close as possible to threshold capacity, by acquiring external technology that can be repurposed for weapons production. There have been many cases in the past, where weapons program were built based on pre-existing latent capacity. The first cases were the UK, France and China; they were soon followed by countries such as Israel and South Africa. A few countries (e.g. Argentina and South Korea) possessed latent capabilities, but did not end up developing a weapon. Lastly, many countries acquired or attempted to acquire the bomb without latent capabilities (e.g. Pakistan, Libya and Iraq).

An increase in the number of so-called 'threshold states' can pose a threat to the nonproliferation regime. In theory, this could be exacerbated by the spread of sensitive reactor technologies, for instance long-live core designs, that could bring states closer to a weapon. Risks are increased when considering a transfer of fast reactor technology to a nuclear newcomer state. Here the issue of 'temptation' comes into play: a state provided with high quality plutonium generating reactor might be more tempted to proliferate than if it were simply provided with a LWR. It is important to mention however, that virtually any plutonium quality can be used in the manufacture of a weapon. The task is rendered easier and more assured if using weapon-grade plutonium that is produced in a typical LEU-fueled long-lived fast reactor. It is therefore warranted to examine how this design weakness can be alleviated to improve the proliferation resistance of these new concepts.

2.5 Chapter Conclusion: A Nonprolifeartion-by-Design Approach

This chapter has highlighted why proliferation resistance is of concern for long-lived fast reactors. Fast reactors themselves have been weaponized in the past, and can pose a risk even when operating in a once-through cycle. Multiple instances exist where countries attempted to proliferate using externally-acquired reactors with attractive features similar to those of long-lived cores. Plutonium quality remains high in these reactors, and a single assembly contains sufficient fissile material for a weapon. There should therefore be a prerogative for reactor engineers to take these concerns into considerations early on the design process.

Safety is always of the utmost importance to a reactor designers, but nonproliferation concerns should be factored in as well. A lot of parallels can be drawn between the two: they both have security impacts, both cannot be reached in an absolute sense (a reactor can never be completely safe nor proliferation resistant), and can be intrinsically or extrinsically incorporated into the design. Extrinsic considerations in safety are usually referred to as active features, in the proliferation world, they are essentially safeguards. Intrinsic features can be 'built-in' to the design and need no external intervention to be enforced. From a safety perspective, this includes relying on passive features that ensure core cooling in an emergency scenario. In nonproliferation, this would involve limiting the accessibility or the usability of the fissile material contained within the core. A good example would be to remove the blanket region of a fast reactor in order to avoid breeding super-grade plutonium. Intrinsic nonproliferation features are the main focus of this thesis. The objective is to use a nonproliferation-by-design approach to reduce potential risks of long-lived reactors. The following chapter will outline potential options for improving proliferation resistance of long-lived cores and discuss the merits and limitations of each approach. Ultimately, a design modification relying on a mixed-spectrum configuration was opted for further analysis in this thesis.

CHAPTER 3
ADDRESSING PLUTONIUM BREEDING IN FAST REACTORS

Ensuring a long reactor lifetime competes directly with proliferation resistance characteristics. To elongate lifetime and increase burnup, a fast reactor must maximize plutonium production, and ensure it is as pure as possible (in ^{239}Pu content). The opposite is true for proliferation matters, a reactor design must minimize both quantity and quality of bred plutonium to reduce its attractiveness to a potential proliferator. Reconciling these competing design objectives is the main challenge of the thesis. In this section, an overview of various means of reducing plutonium attractiveness is provided with a discussion of their setbacks and limitations. Ultimately, a mixed-spectrum configuration is selected for further analysis to reach the desired end goal.

3.1 Fissile Material Production in the Fast Spectrum

Fissile material is always generated within a nuclear reactor (regardless of type). As long as fertile isotopes (^{238}U or ^{232}Th) are present, they can absorb a neutron and generate fissile isotopes (typically ^{239}Pu or ^{233}U) as shown in Figure 3.1. The amount of fertile material that can be converted to fissile material depends on the magnitude of the reproduction factor, $\eta = \nu(\sigma_f/\sigma_a)$. The ratio provides a useful tool to estimate how much neutrons are available in a system for breeding; the higher the value, the easier it is for a core to breed fissile material and stay critical. The η value is neutron energy dependent as highlighted in Table 3.1. It increases in the fast spectrum for all isotopes, despite the fact that cross-sectional values are lower. With more neutrons available per fission reaction, breeding within fertile isotopes can be increased.

A reactor is termed 'breeder' if its breeding ratio (or conversion ratio), defined in Equation 3.1, is above unity. This means that it is able to create fissile fuel faster than it depletes

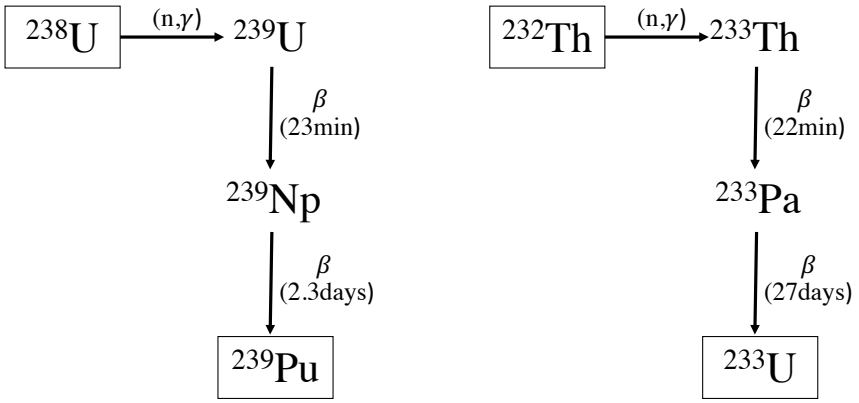

(a) Uranium-plutonium production chain. (b) Thorium-uranium production chain.

Figure 3.1: The conversion of fertile isotopes (top) to fissile isotopes (bottom) for uranium and thorium.

Table 3.1: Reproduction factor η for different fissile isotopes at different neutron spectra. Values obtained from Waltar.[43]

	Thermal Spectrum	**Fast Spectrum**
^{235}U	2.07	2.30
^{239}Pu	2.11	2.70
^{233}U	2.30	2.45

it. As such, it is very attractive for a long-lived reactor to have a BR value as close to unity as possible. Figure 3.2(a) compares the amount of plutonium produced per initial heavy metal inventory in a fast and thermal system. It illustrates how a fast system is substantially more efficient than a thermal one at breeding additional plutonium.

$$BR = \frac{\text{fissile atom production}}{\text{fissile atom destruction}} \tag{3.1}$$

The plutonium purity is also dependent on the neutron energy of a system. This is due to variations in the cross-sections of specific isotopes with incident neutron energy. The plutonium quality is mainly driven by the ^{239}Pu absorption to fission cross-section ratio. Table 3.2 highlights how this ratio differs substantially between a fast and thermal system. As a result, ^{239}Pu is around 30% more likely to breed ^{240}Pu via capture in the thermal

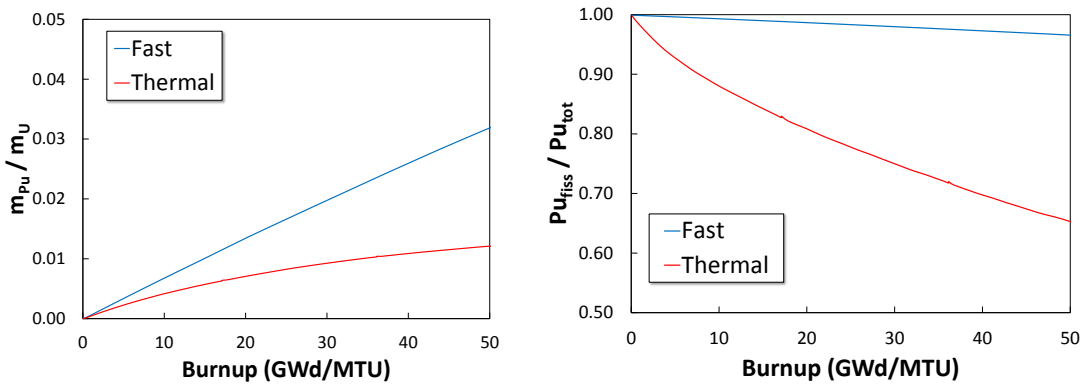

(a) Normalized plutonium production against initial heavy metal inventory.

(b) Ratio of fissile plutonium isotopes over total.

Figure 3.2: Comparison of plutonium production and quality evolution in a thermal and fast system. Pin-level depletion simulations were generated using MCNP6.

spectrum than in the fast spectrum. At high neutron energies, fission reactions become much more dominant than in the thermal spectrum. On the other hand, the fission cross-section value is lower by several orders of magnitudes in the fast spectrum, meaning that a much higher initial fissile inventory to reach criticality compared to a thermal system. Figure 3.2 illustrates the effect of cross-sectional ratios on plutonium quality. The purity in the fast system remains near 100% throughout burnup, while it drops relatively quickly in a thermal one.

Table 3.2: Capture and fission cross-section of ^{239}Pu in the thermal and fast spectrum.

	Thermal Spectrum	**Fast Spectrum**
σ_a (b)	274	0.26
σ_f (b)	741	1.61
σ_a/σ_f	0.37	0.16

3.2 Reducing Plutonium Quantity

Fast spectrum reactors breed larger quantities of plutonium than their thermal counterparts as previously illustrated in Figure 3.2(a). Reducing total plutonium production in a core is a misleading target, since the reactor could simply be made smaller. Proliferation resis-

tance is considered improved if plutonium production per unit of power or per assembly is decreased to match that of conventional light-water reactors. In a diversion scenario, a potential proliferator will favor a reactor with more plutonium per assembly. Needing to divert more assemblies, in order to acquire more material for a weapon, increases the risks of being caught. This is especially problematic for fast reactor assemblies, which tend to already contain 1 Significant Quantity (SQ) of plutonium (defined as 8 kg by the IAEA [44]). In a conventional reactor, two assemblies would need to be diverted to obtain 1 SQ. In a breakout scenario, the amount per assembly is less problematic, but a proliferator would want to maximize the amount of plutonium produced per unit of power generated. Again, fast breeder reactors are ideally suited for such a task.

A simple approach to reducing plutonium production per assembly is to simply reduce the assembly pitch (i.e. make the assembly smaller) or lower the fuel volume fraction. Both method lead to a smaller concentration of fissile material within the core. To counter this, a larger core volume would be required to maintain criticality (and maintain total heavy metal inventory). A larger fraction of non-actinide mass in the core volume could also lead to a reduction in performance characteristics (notably, maximum lifetime). Another simplistic approach would be to reduce overall fuel burnup since plutonium production is directly correlated with overall power produced by the fuel. This is directly counter to the main purpose of a long-lived core design and will not be investigated in this thesis.

An alternative solution is to increase ^{235}U enrichment. This would ensure less ^{238}U would be present in the core to breed plutonium. Figure 3.3 shows the effect of increased enrichment on plutonium production. A benefit of this approach is that core criticality is maintained (even increased) and there tends to be little effect on maximum core lifetime. The main drawbacks of such an approach are economic and proliferation related. The cost of increased enrichment is non-negligible even if no additional fuel is used in the core. Furthermore, the maximum enrichment limit for ^{235}U is set to 20% by the IAEA for proliferation concerns. Anything above that quantity is, in theory, weapon-usable, and

relatively easier for further enriching to the weapon-grade limit of around 90%.[45] Any increases in fuel enrichment essentially makes the task easier for a proliferator to divert fresh fuel and enrich it for use in a weapon.

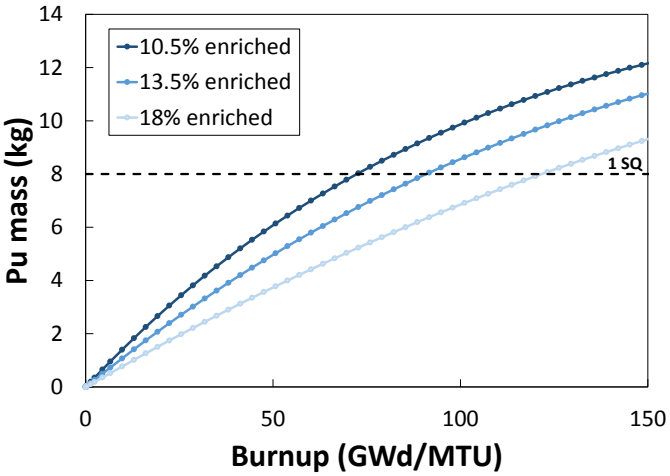

Figure 3.3: Effect of increased assembly enrichment on plutonium production. Assembly-lattice depletion simulations were generated using MCNP6.

Another approach is to rely to both the uranium and thorium production chains highlighted in Figure 3.1. Reducing the overall quantity of ^{238}U proportionally decreases the amount of plutonium generated (as is the case with increased enrichment). At the same time, another fissile isotope is produced from thorium absorption (^{233}U) to extend burnup. Figure 3.4(a) shows the result of adding thorium to the fuel. The plutonium production rate is noticeably reduced. Care must be taken however to account for slight differences in neutronic properties between ^{233}U and ^{239}Pu. This could have effects on overall core performance. Another limitation is the total amount of ^{233}U generated. The isotope can be equally attractive for use in a weapon. Ensuring it is diluted within a starting uranium composition, can ensure proliferation resistance, as long as the quantity falls below the limit set by Forsberg in Equation 3.2.[46] Figure 3.4(b), shows how the fuel remains below the 12w% required limit for the case considered.

$$\frac{m_{U-233} + 0.6m_{U-235}}{m_{U-tot}} < 12\% \tag{3.2}$$

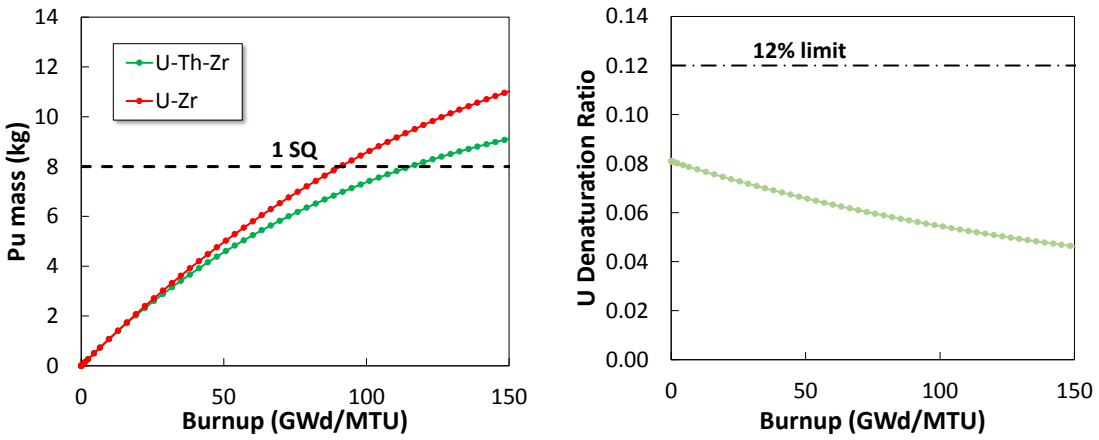

(a) Plutonium production with and without thorium addition.

(b) Denaturation ratio for mixed thorium-uranium fueled assembly.

Figure 3.4: Effect of using mixed U-Th (72w% U, 18w% Th, 10w% Zr) fuel on plutonium production. Denaturation ratio is obtained via Equation 3.2.

3.3 Reducing Plutonium Quality

Alongside reducing overall bread plutonium quantity, reducing its quality is equally important from a nonproliferation standpoint. It should be noted however, that there is little consensus over what constitute 'proliferation resistant' plutonium quality. ^{239}Pu and ^{241}Pu are the main two plutonium isotopes that are fissile, and therefore useful for a weapon. Plutonium breeding in a reactor produces several other isotopes that can complicate the development of a weapon. The main two other isotopes, as highlighted in Table 3.3, are ^{238}Pu and ^{240}Pu. The latter is problematic due to its high rate of spontaneous fissioning, resulting in a continuous release of neutrons. A large presence of ^{240}Pu can result in a 'fizzle', or a preinitiated detonation without the desired yield. ^{238}Pu can also spontaneously fission, and is a high heat emitter (via α-decay). A high content of this isotope would necessitate complex active cooling of a weapon to ensure operability.[47] As such, minimizing the overall proportion of fissile plutonium isotopes is a priority from a nonporliferation standpoint.

There exist different classifications of plutonium depending on the concentration of non-fissile isotope. Generally, the quality is divided into four groupings: super-grade,

Table 3.3: Plutonium isotope properties.[48]

	Half-Life (years)	**Bare critical mass** (kg)	**Spontaneous fission neutrons** $(g.s)^{-1}$	**Decay heat** (W/kg)
^{238}Pu	87	10	2.6×10^{3}	560.0
^{239}Pu	24,100	10	2.2×10^{-2}	1.9
^{240}Pu	6,560	40	9.1×10^{2}	6.8
^{241}Pu	14	10	4.9×10^{-2}	4.2
^{242}Pu	376,000	100	1.7×10^{3}	0.1

weapon-grade, weapon-usable, and reactor-grade. Although there is no standard for determining the composition for each bounds, Table 3.4 shows a typically used classification based on ^{240}Pu concentration. Despite the added difficulties stemming from the non-fissile plutonium isotopes, many experts believe that virtually any plutonium grade can be used in a weapon.[48] Indeed, a 1962 underground test conducted at the Nevada Test Site is claimed to have originated from reactor-grade plutonium.[49] However, it is believed that the plutonium in that test had a ^{240}Pu below the 18% limit, so it would be termed 'fuel-grade' in current standards.[50, 51]

Table 3.4: Plutonium mixtures of different grades.[50]

	^{240}Pu concentration	**Weapon usability**
Super-grade	<3%	Best quality
Weapon-grade	3-7%	Standard quality
Fuel-grade	7-18%	Practically usable
Reactor-grade	18-30%	Conceivably usable

Some researchers have proposed different classifications of plutonium grade based on the ^{238}Pu content, rather than ^{240}Pu.[47] Others, such as Bathke et. al, have proposed Figure of Merits (FOM) that attempt to quantity the attractiveness of different isotopic compositions for weapons production.[52] For the purpose of this thesis, each plutonium grade is deemed more 'proliferation-resistant' than the previous one. Plutonium at the 'reactor-grade' level is considered sufficiently proliferation resistant, on the basis that it widely existing in all PWR plants. Since all of the non-fissile plutonium isotopes are neutron

emitters, the thesis will consider all of their respective concentration when analyzing the plutonium grade (as stated in Table 3.3). As such, the ratio of Pu_{fiss}/Pu_{tot} is used as an indication of how attractive the material is for use in a weapon. The weapon grade limit is defined for a ratio above 93%, and reactor grade is reached when the value drops below 82%. When needed, quantitative comparisons using the Bathke FOM are conducted to gain a more concrete measure of plutonium attractiveness.

In an equilibrium fast reactor (i.e. with recycling), the plutonium composition reaches the reactor grade limit as highlighted in Table 3.5. This is not the case however for once-through fast reactors. Figure 3.5 shows the evolution of the plutonium quality in a typical LWR fuel pin, versus that of long-lived fast reactor. The plutonium composition stays above the weapon grade limit throughout the long-lived reactor operating life, while it becomes reactor-grade in the LWR at around 20-25 GWd/MTU. This is due to the aforementioned reasons in Section 3.1, the cross-sectional ratios result in smaller relative quantities of ^{240}Pu produced with burnup than in a thermal spectrum. In a cycle with plutonium-recycling - as was the case in the proposed IFR design [53] - once an equilibrium composition is reached, the plutonium has already been cycled through the reactor multiple times and accumulated a larger amount of non-fissile isotopes. This is not the case in a once-through design. Addressing this concern is more challenging that reducing plutonium quantity and will form the main focus of this thesis. An overview of different potential approaches is provided in the next sub-sections.

Table 3.5: Discharage plutonium vector for equilibrium systems (fast + thermal) and a non-equilibirium, once-through fast system (e.g. long-lived reactor). Fast equilibrium data obtained from Wade et al.[53], other data obtained from MCNP6 simulations.

	Equilibrium		**Once-Through**
	Thermal	**Fast**	**Fast**
^{238}Pu	8.1%	0.9%	0.6%
^{239}Pu	45.1%	68.8%	91.0%
^{240}Pu	20.6%	25.2%	8.0%
^{241}Pu	18.6%	3.1%	0.4%
^{242}Pu	7.6%	1.9%	0.0%

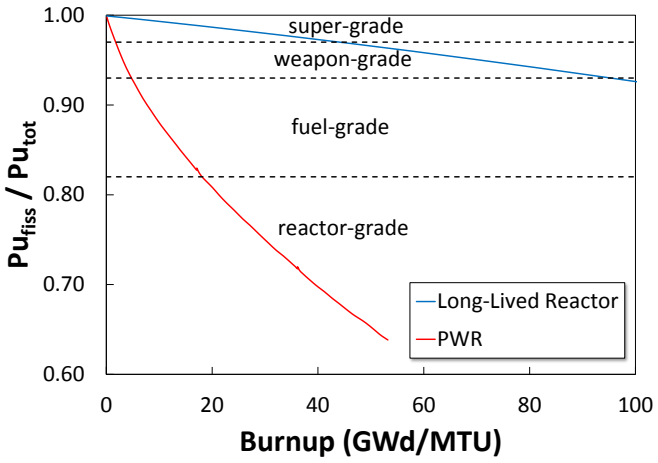

Figure 3.5: Evolution of ^{240}Pu concentration in a LWR versus a Long-lived reactor. The latter fuel is able to reach twice the burnup of the former. Dashed lines mark the boundaries between different plutonium grades. Simulations were generated using MCNP6.

3.3.1 Fuel doping

The most commonly proposed way of improving nonproliferation characteristics of fast reactor fuel has been fuel doping. A first option is to start with an initial plutonium composition that is reactor-grade; for instance, from reprocessed LWR spent fuel. While the proportion of non-fissile plutonium isotopes always increases with burnup in any reactor, it increases much more slowly in the fast spectrum. Starting with a composition that is already of low quality - such as the plutonium vector shown in Table 3.6 - can ensure a plutonium quality above the reactor grade limit throughout the core lifetime. Figure 3.6 shows how the resulting fissile concentration is affected by the addition of LWR plutonium. While this approach is attractive from a quality perspective, it increases the total amount of plutonium contained within each assembly (since the composition has a nonzero initial plutonium mass). The resulting time to reach 1 SQ in an assembly would therefore be shortened, making this effort to improve proliferation resistant somewhat counterproductive.

Another option is to dope the fuel with minor actinides (MA), who naturally decay or decay after neutron absorption into non-fissile plutonium isotopes (e.g. in Figure 3.8(a)).

Table 3.6: Transuranics vector obtained from a pin-level MCNP6 depletion simulation. Compositions are shown for 1 cycle (17.1 GWd/MTU) and 3 cycle (53.2 GWd/MTU) spent fuel.

	1 cycle	**3 cycles**
Pu-Np-Am-Cm	97-3-0.3-0.02%	90-6-2-1%
^{238}Pu	0.4%	2.8%
^{239}Pu	75.1%	48.8%
^{240}Pu	15.7%	25.3%
^{241}Pu	7.9%	15.0%
^{242}Pu	1.0%	8.1%
^{237}Np	100%	85.6%
^{238}Np	0%	14.1%
^{241}Am	67.6%	17.4%
^{243}Am	32.2%	82.5%
^{242}Cm	53.3%	17.4%
^{244}Cm	44.7%	74.9%
^{245}Cm	1.3%	6.4%

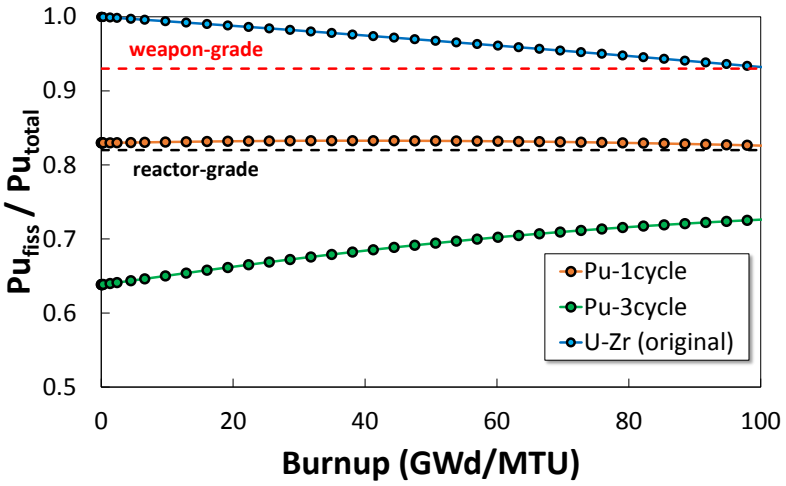

Figure 3.6: Effect of plutonium doping on isotopic quality evolution. Plutonium was set for both 1 and 3 cycle cases at 6w% heavy-metal. Simulations were generated using MCNP6.

A variety of options have been explored in the past: (1) reprocess MA with plutonium from LWR spent fuel and use it as feed for fast reactors,[53] (2) dope fuel with a MA vector without plutonium,[54] or (3) only use specific MA isotopes such as ^{237}Np or ^{242}Am to dope the fuel.[47] Figure 3.7 illustrates the effect of different MA doping schemes on the plutonium quality evolution. The addition of minor actinide with plutonium has a

smaller effect on the final composition by comparison with plutonium-doping in Figure 3.6. Similarly, it appears that doping with only neptunium is as effective as doping with all the other minor actinides. It should be noted that doping with small quantities of minor actinides tends to have little effect on overall fuel performance. The main drawback is the difficulty and complexity associated with extracting these isotopes, and fabricating fuel doped with them.

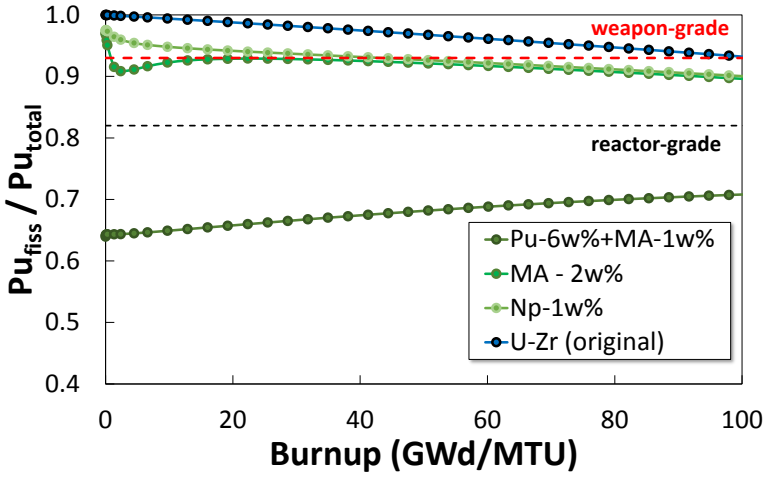

Figure 3.7: Effect of minor actinide doping on plutonium quality. The highlighted weight percentages are relative to heavy metal mass. Simulations were generated using MCNP6.

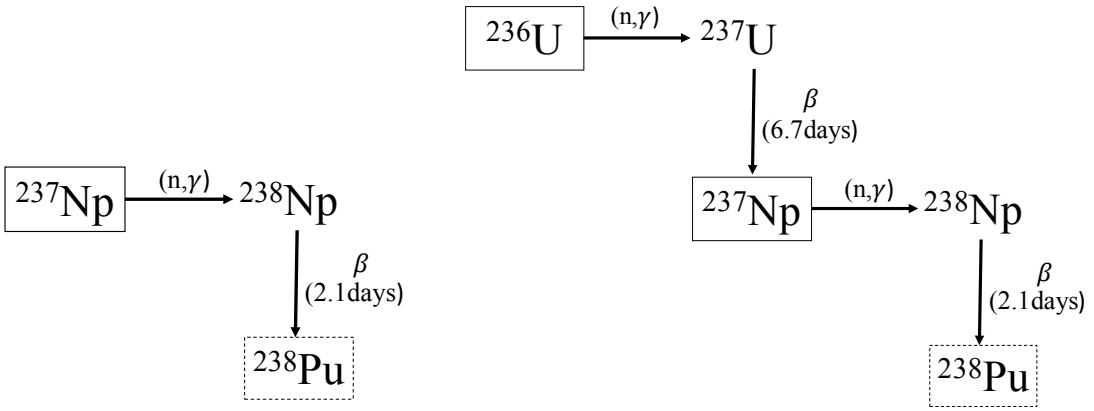

(a) ^{238}Pu-^{237}Np production chain. (b) ^{238}Pu-^{236}U production chain.

Figure 3.8: Examples of production chains generating non-fissile plutonium isotopes.

Kessler proposed to bypass some of these hurdles by relying instead on re-enriched

recycled uranium (RRU).[47] At the end of an LWR operating cycle, the uranium within the fuel is richer in ^{236}U. This isotope can be transmuted into ^{237}Np via neutron absorption, and subsequently breed ^{238}Pu as shown in the decay chain of Figure 3.8(b). Enriching spent uranium will increase the ^{236}U proportion in the fuel alongside ^{235}U, and minimize the need for additional uranium to be mined. Figure 3.9 shows how the plutonium quality in RRU is reduced faster than is typical in fast reactor fuel, but less efficiently than other doping schemes. This is due to the fact that the ^{238}Pu production chain relies on two neutron absorption as opposed to just one in minor actinide chains.

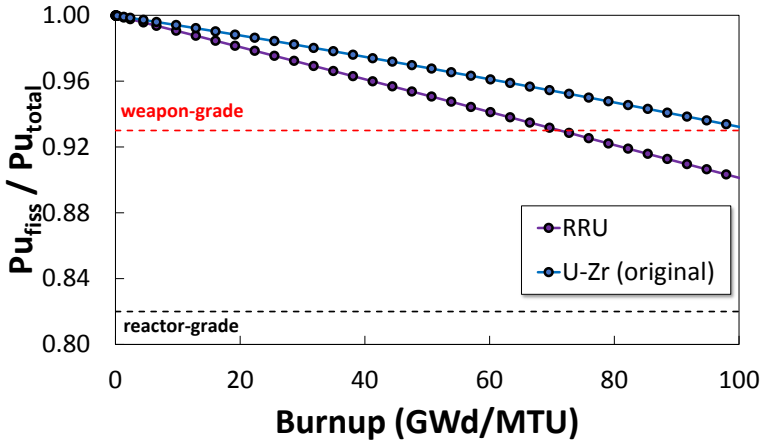

Figure 3.9: Evolution of plutonium isotopic composition for re-enriched recycled uranium (RRU). Simulations were generated using MCNP6.

Ultimately, the main drawback of all these proposed options is that they rely on reprocessing. The process is controversial, expensive, and can delay the deployment time of a solution. More importantly however, reprocessing poses an added proliferation risk as highlighted in Chapter 2. This may be less problematic if doping is conducted at a centralized hub, similarly to the proposed IAEA LEU fuel bank discussed in Chapter 2. However, less demanding alternatives from a feasibility standpoint, to reduce plutonium quality do exist. One such approach is via spectral softening; this will form the main focus of this thesis.

3.3.2 Spectral softening

As discussed in Section 3.1, the fast spectrum is ideal for breeding fissile material in a reactor, while the thermal spectrum generates plutonium at a more proliferation-resistant isotopic composition. The amount of ^{240}Pu production depends on the ratio of capture to fission cross-sections of its precursor, ^{239}Pu. As highlighted in Figure 3.10 this ratio varies greatly with different incident neutron energies, it is particularly low in the fast spectrum and is very elevated within the resonance region.

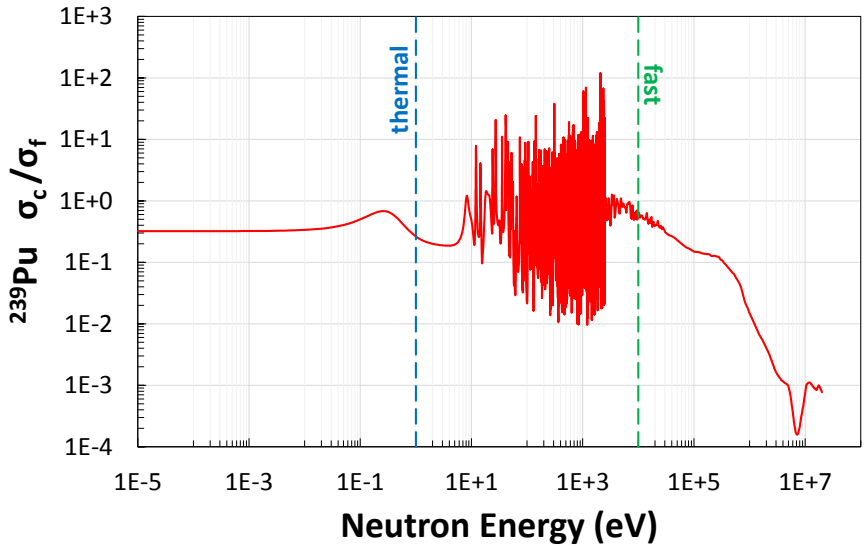

Figure 3.10: Ratio of capture (n,γ) over fission (n,f) cross-sections for ^{239}Pu. ENDF-VII data obtained via KAERI.

Ideally, a compromise must be met to maximize breeding and non-fissile isotope concentration. Two options are therefore possible: (1) either operate the reactor in the epithermal spectrum (in between fast-thermal), (2) use a mix of different spectra in specific core regions. The first option has been investigated by designs such as the Reduced Moderation Boiling Water Reactor (RBMK),[55] and the Transatomic molten salt reactor.[56] In both cases, the design philosophy is the reverse of the one in this thesis: these designs were originally thermal reactors whose neutron moderation was reduced in order to increase breeding. Mixed spectrum configurations on the other hand, have been investigated in pre-

vious work as highlighted in Chapter 1. In this thesis, a combination of both approaches is evaluated. One core region is maintained in the fast spectrum to breed fuel, while another is in the epithermal regime to denature plutonium. In order to achieve spectral softening, moderating material is inserted in localized regions of a previously fast core configuration.

Typical fast, thermal, and epithermal spectra (shown in Figure 3.11) have correspondingly different isotopic cross-sections. This alters the resulting breeding ratio of the proposed configuration, as well as the ^{239}Pu capture to fission ratio. Sample results are shown in Table 3.7. They highlight the characteristics of the outer core region of the core before and after the addition of moderating material. The values were generated using models that will be detailed in later chapters. The epithermal configuration results in a noticeable reduction in plutonium quality within that region. Despite the larger σ_f value for ^{239}Pu (meaning higher fissile material destruction), the total amount of fissile isotopes is relatively unchanged when normalized to the initial heavy metal inventory. This is due to the higher burnup that can be reached in moderated regions. The breeding ratio is still expected to be lower than the original fast spectrum configuration, which may impact the core longevity. Further analysis will be needed to derive a suitable core configuration.

Table 3.7: The effect of thermalizing the outer core region at the Middle of Cycle (MoC).

	Original	**Thermalized**
^{239}Pu: $(\sigma_c)/(\sigma_f)$	0.16	1.90
^{239}Pu: $\sigma_f(b)$	1.75	4.31
(Pu_{fiss}) / (Pu_{tot})	95.82%	83.63%
($\mathrm{m}_{Pu-fiss}$) / (m_{HM})	3.35%	4.82%

3.4 Chapter Conclusion: Improving Proliferation Resistance without Reprocessing

While there exist various ways of improving proliferation resistance of long-lived core design, the thesis will focus on methods that do not rely on any form of fuel reprocessing. Doping the fuel with reactor-grade plutonium or minor actinides was shown to reduce the bread material quality to below the weapon-grade limit. The added proliferation risks of a

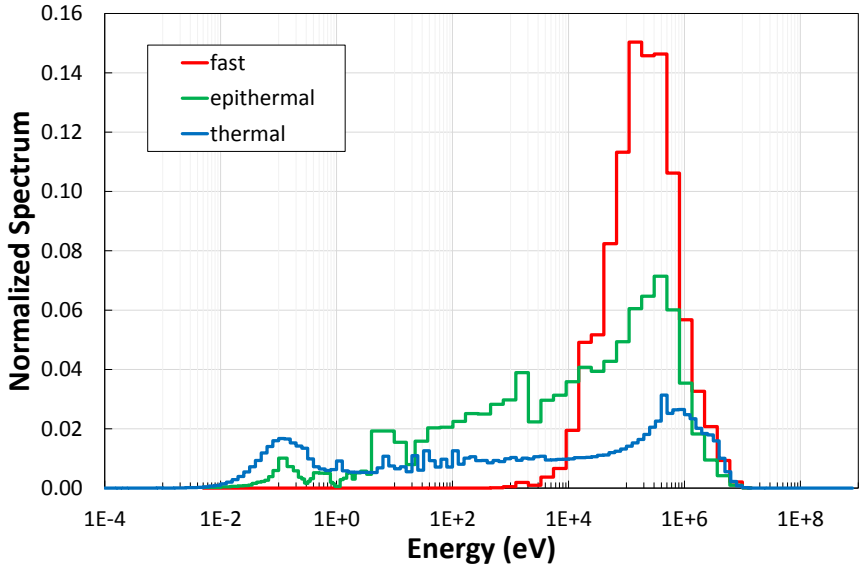

Figure 3.11: Probability distribution of fast, thermal and epithermal spectra. Note that epithermal spectra tend to vary greatly between designs and this particular spectrum is not necessarily used in later analyses.

reprocessing facility however, are deemed counterproductive (even if reprocessing is conducted in the hub nation). Reducing plutonium quantity can be achieved a wide range of options, such as reducing fuel volume fraction and mixed U-Th fuel. These will be investigated in later chapters, but with secondary emphasis. The primary goal will be to design a Mixed Spectrum Reactor (MXR) with reduced plutonium quality. Mixed configurations have been the subject of limited prior research, and none focused on once-through cycles. Modeling this type of reactor can be particularly challenging. Deterministic codes are typically used for this type of core cycle evaluation and design optimization. They cannot be readily used for the MXR due to breakdown of fundamental assumptions in the underlying code. On the other hand, stochastic codes can reach higher levels of accuracy, but are prohibitively expensive from a computation standpoint for iterative depletion analysis. The next chapter will go into greater detail about these modeling difficulties and discuss potential workarounds. Ultimately, the MXR concept will be combined with other approaches to simultaneously reduce bread plutonium quantity per assembly and its quality.

CHAPTER 4

MODELING AND SIMULATION OF MIXED SPECTRUM REACTORS

Evaluating the behavior of a nuclear reactor core consists of modeling the neutron transport equation, shown in Equation 4.1. It describes the loss (via absorption or leakage), gain (via fission) and movement (via scatter) of neutrons within a system. Analytically solving the transport equation is not feasible in complex geometry. Instead, nuclear engineers rely on different types of approximations. The two main approaches are stochastic and deterministic codes. Stochastic codes rely on random sampling of particles and the 'law of large numbers' to evaluate specific core parameters. They can model very complex geometries without simplifications, and are often considered to be the 'gold standard' for neutron transport simulations. Their main drawback, however, is that they tend to be very computationally expensive, especially when a wide range of different parameters need to be resolved. Alternatively, deterministic codes simplify and discretize Equation 4.1 in order to solve it. Energy groups are segmented into bins, and geometries are truncated into cells. These assumptions inherently resolve a wide array of core parameters (e.g. flux distribution throughout core). They tend to significantly reduce computational needs, but are considered to be less versatile than stochastic codes when it comes to accuracy. These tradeoffs between the two code types are the main subject of this chapter. The next section will go into more detail on the two types of modeling approaches, while following sections will discuss their implementation for mixed-spectrum reactor analysis.

4.1 Overview of Deterministic and Stochastic Codes

Equation 4.1 is the mathematical expression describing neutron transport within a system. In it, ψ is the neutron angular flux, v the neutron speed, $\hat{\Omega}$ the solid angle, E the neutron energy, and σ, σ_s, σ_f denote the total, scattering, and fission cross-sections respectively.

The prime symbol is used in the scattering and fission terms to denote incident neutron energies (E') or angle ($\hat{\Omega}'$).

$$\frac{1}{v}\frac{\partial\psi}{\partial t} + \hat{\Omega}.\bigtriangledown\psi + \sigma\psi = s + \int_0^\infty dE' \int_{4\pi} d\hat{\Omega}'\sigma_s(E', \hat{\Omega}' \rightarrow E, \hat{\Omega})\psi(E', \hat{\Omega}') + \int_0^\infty dE' \int_{4\pi} d\hat{\Omega}'\nu(E')\sigma_f(E', \hat{\Omega}' \rightarrow E, \hat{\Omega})\psi(E', \hat{\Omega}') \tag{4.1}$$

As previously mentioned, two main approaches exist for attempting to obtain a solution for this equation inside a complicated system. The first employs a stochastic approach to randomly sample events and infer an aggregate neutronic behavior. The main stochastic code employed in this thesis is MCNP (Monte Carlo N-Particle code); a general-purpose, continuous-energy, generalized-geometry neutron transport code that is widely used in the nuclear industry.[57] The code employs Monte Carlo probabilistic methods to track neutron particle interactions. Instead of using differential methods to solve the transport equation above, stochastic codes resolve the neutron transport equation by simulating individual particles and recording some aspects (tallies) of their average behavior. The general behavior of the neutrons in the physical system can then be inferred from the averaged behavior of the simulated particles. The code essentially transports particles between probabilistic events that are separated in space and time and simulates each event in a process sequentially. The probability distributions governing these events are statistically sampled in a random fashion to describe the total phenomenon. A particle is followed from its source point throughout its life to its death (e.g. by absorption or leakage). Monte Carlo transport methods are very well suited to model complicated three-dimensional problem, and allow detailed representation of all aspects of the physical data. They are especially efficient at eigenvalue calculations, and tend to reach high levels of accuracy. Because they rely less on specific approximations, stochastic codes, like MCNP, can be more versatile, and used for a wide variety of core models. Ensuring adequate levels of accuracy tends to rely on ensuring a sufficient number of source particles to track, in addition to good convergence

in the fission source distribution.

Alternatively, some deterministic codes make use of some approximations to Equation 4.1 that are valid in specific systems (such as fast ones), and have become very established for these applications. They solve approximated formulations of the transport equation to deduce average particle behavior. The approximations include a multigroup energy distribution, discretized nodal geometry, as well as simplifications to neutron scattering phenomena. Two main variants of the approximated transport equation exist. The first one referred to as the S_N method, is shown in Equation 4.2 in the simplified steady-state, 1-D form. It relies on n discrete angular ordinates (i.e. segmented angular neutron directions) to account for scattering within systems. The second one, the P_N method, is shown in Equation 4.3, also for 1-D steady state. This method relies on the Legendre expansion to model different m angular harmonics that are solved individually. In each case, a set of equations must be solved for each discretized cell volume and for each discretized energy group.

$$\mu_n \frac{\partial \psi_n}{\partial z} + \sigma \psi_n = \frac{\sigma_s}{2} \sum_{i=1}^{N} w_i \psi(\mu_i) + s_n \tag{4.2}$$

$$\frac{m+1}{2m+1} \frac{\partial \psi_{m+1}}{\partial z} + \frac{m}{2m+1} \frac{\partial \psi_{m-1}}{\partial z} + (\sigma - \sigma_{sm}) \psi_m = s_m \tag{4.3}$$

While Monte Carlo codes only supply targeted information when prompted by the user, deterministic models inherently provide a more complete set of information (e.g. the neutron flux distribution) throughout the phase space of the problem. Deterministic codes can be more complicated to set up in order to ensure simplifications and assumptions are valid. Fine tuning is required for many parameters, such as polynomial orders, iteration numbers, mesh sizes, scattering angle discretization, etc. One deterministic code package that has become well established for fast reactor modeling was developed at Argonne National Laboratory (ANL).[58] The REBUS package employs four main sub-codes: (1) MC^2 is a multi-group cross-section processing tool that collapses data from the ENDF libraries; (2)

TWODANT is a 2D S_N flux solver, that is used to flux weight the cross-section collapsing in MC^2; (3) DIF3D/VARIANT is a nodal, 3D, P_N flux solver that estimates the neutron flux throughout the core using the cross-sections generated in MC^2; and (4) REBUS uses the flux computed by DIF3D to deplete the isotopic composition. The different stages of a simulation are highlighted in Figure 4.1. The computations are normally divided into two main parts: cross-section generation and depletion analysis. The main output from the first stage is an ISOTXS file containing all the cross-sectional data. TWODANT and MC^2 are coupled to flux-weight and group-collapse cross-sections in a two-stage approach. First, an ultrafine-group structure is generated; then, it is flux-weighted to obtain coarse group cross-sections (typically 33 or 73 groups). In step 1, a simplified 2-D cylindrical core geometry with different r-z regions is used. Care must be taken to ensure volume of the approximated rings and the original core assemblies is maintained. In step 2, the core geometry is discretized into individual assembly nodes with a spatial polynomial expansion of the flux terms used to model inter-assembly flux variations. DIF3D generates a flux distribution throughout the whole core, which is then used by REBUS to deplete isotopes and generate an update core composition. Incremental iteration between the two modules is performed until the final specified timestep is reached. More detailed information of the calculations and settings at each step is provided in Appendix B.

Computational requirements for depletion analysis vary greatly between MCNP and REBUS. Despite the fact that REBUS may seem more complex and is not parallelizeable, it is several orders of magnitude faster for this type of analysis than its counterpart. This is due to the inherent feature of deterministic codes that automatically evaluates the flux distribution throughout which can then be used to obtain the composition distribution throughout individual assemblies even. Tracking the composition within several regions of each individual assemblies can be prohibitively expensive using a code such as MCNP. As a result, REBUS was originally preferred for the analysis, but MCNP was weighted on more heavily later on, when accuracy limitations of REBUS became apparent when modeling

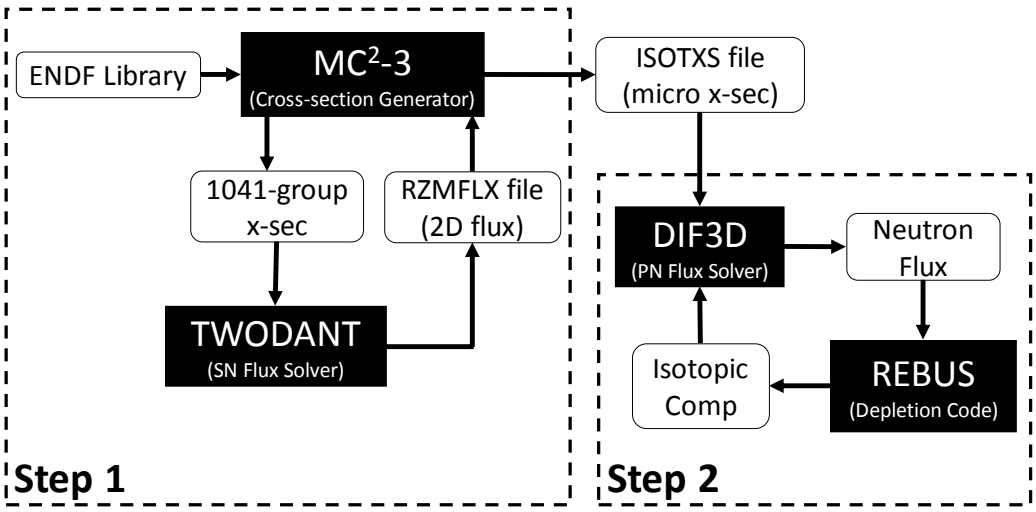

Figure 4.1: Layout of the different REBUS modules for depletion analysis. Black boxes represent code modules and white boxes represent specific outputs at each steps. A two step iteration is needed in step 1, while step 2 iterates between the different modules until the final specified timestep is reached.

mixed-spectrum reactors. These will be discussed in greater detail in Section 4.3.

4.2 Design Specifications and Base Model

The base design for the analysis is referred to as the Long-Lived fast Reactor (LLR). Its geometry and characteristics are based on the AFR-100 developed at ANL,[13] which is itself based on the established SPRISM design.[59] The design was selected because it was judged to be one of the most realistic long-lived designs in the open literature, and relies heavily on established sodium fast reactor knowledge. Table 4.1 summarizes the main relevant design specifications of the LLR. The sodium-cooled metal-fueled reactor touts a reactor lifetime of up to 25 years without needed any refueling or reshuffling. The design ensures its lifetime is not limited by neutronics, but rather by material damage limitations. Peak fast fluence (ψ) in the cladding becomes the main restraint. Experimental data has been acquired up to a fluence of up to 4×10^{23} n/cm^2,[14] as such, most long-lived core design hinge on the future availability of advanced clad material that can reach higher irradiation damage limits.[13] This limitation will be investigated further as part of the

MXR design proposal. For the purpose of the LLR, the same fluence limit as the AFR-100, 6×10^{23} n/cm^2 is taken to be the end-of-life (EOL).

Table 4.1: Main characteristics of the proposed LLR. (Note: EFPY is Effective Full Power Years).

Parameter	**Value**
Fuel type	U-10Zr
Power	250 MW_{th}
T_{in}/T_{out}	395/550°C
EFPY @ k_{eff}=1.0	34 years
EFPY @ $\Psi = 6 \times 10^{23}$	25 years
Active core height	110 cm
Av. power density	58.3 kW/l
Fuel vol. fraction	43.9%
Av. enrichment	13.5%
Av. discharge burnup	92 GWd/MTU

In order to ensure high-burnup without relying on reprocessing, the design employs a relatively high enrichment (13.5%), which is maintained below the 20% limit . The core has an 'onion layout' whereby the enrichment is varied both axially and radially (Figure 4.2). Zones further away from the center have higher enrichment levels, while the enrichment is also higher at the upper and lower edges of each assembly than its center. This compensates for the high level of neutron leakage in the peripheral zones. The innermost region then acts as a 'seed', breeding plutonium that is depleted later during the core lifetime. The operating life of the reactor is further extended by significantly reducing the power density (58 kW/l versus 200 kW/l for a typical sodium fast reactor). This ensures that for the same average burnup as a typical fast reactor, the LLR can operate continuously for several decades, as opposed to 1-2 years. Operating at a low power density can bring additional safety benefits and alleviate some design limitations, such as using larger fuel rod diameters in driver regions.

The geometry specifications for the base design are summarized in Table 4.2. HT9 steel was used for the cladding and the bottom reflector material. The outlet temperature is slightly higher than a typical sodium-cooled reactor, but it was deemed feasible in light

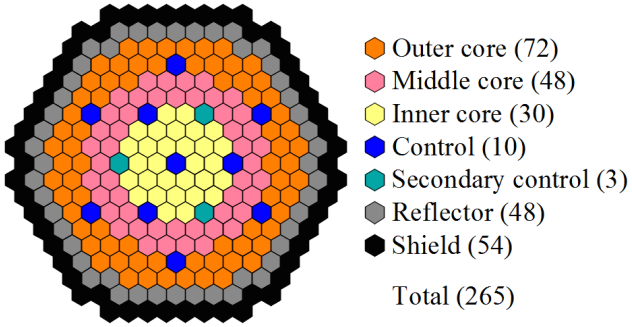

(a) Radial core assembly configuration.

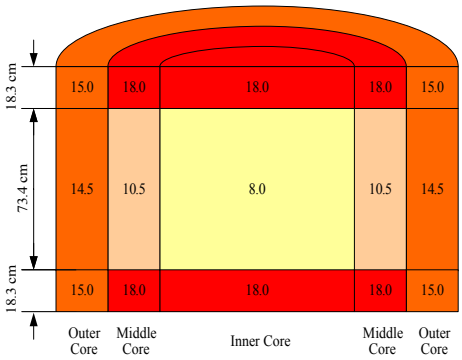

(b) Variation in axial and radial fuel enrichment.

Figure 4.2: LLR core configuration. Based on the AFR-100 model [13].

of the lower power density in the core. An average core temperature of 472.5°C is used throughout the core volume for simplicity. Thermal expansion and axial fuel swelling are accounted for in the simulated model. All of these geometric effects are explained in greater detail in Appendix A. The inner rod volume consists 25% of Na and 75% U-Zr to account for irradiation swelling of the metallic fuel. Because this phenomena peaks after a small burnup is accumulated, the core is modeled with the fully expanded configuration. The U-Zr slugs are in contact with the inner clad wall throughout the simulated lifetime, and the sodium bond is pushed to the upper rod plenum region (originally filled with only gas). Axial and radial thermal expansion of HT9 are also taken into account in the simulation. Figure 4.3 shows a visualization of the built models using MCNP6, along with the resulting evolution in k-eff over time. Subsequent modifications to the base model to generate an MXR configuration are outlined in Chapter 5. For the purpose of benchmarking in this chapter, configurations with ZrH inserted within outer assemblies are used to compare MCNP and REBUS.

4.3 Improving Deterministic Codes Modeling Capabilities

Many assumptions of the REBUS suite of codes are only valid for fast spectrum systems. They can break down when modeling thermal or mixed fast-thermal systems. The main

Table 4.2: Main characteristics of the proposed LLR (at room temperature). Based on the AFR-100 model.[13]

	Fuel Assemblies
Number of pins	21
Assembly pitch (cm)	16.5
Duct thickness (cm)	0.3
Active height (cm)	110.0
Rod diameter (cm)	1.49
Clad thickness (cm)	0.05
Wire wrap diameter (cm)	0.107
Pitch-Diameter ratio	1.075
Fuel vol. fraction	43%
Structure vol. fraction	16.1%
Coolant vol. fraction	25.3%
bond vol. fraction	14.6%

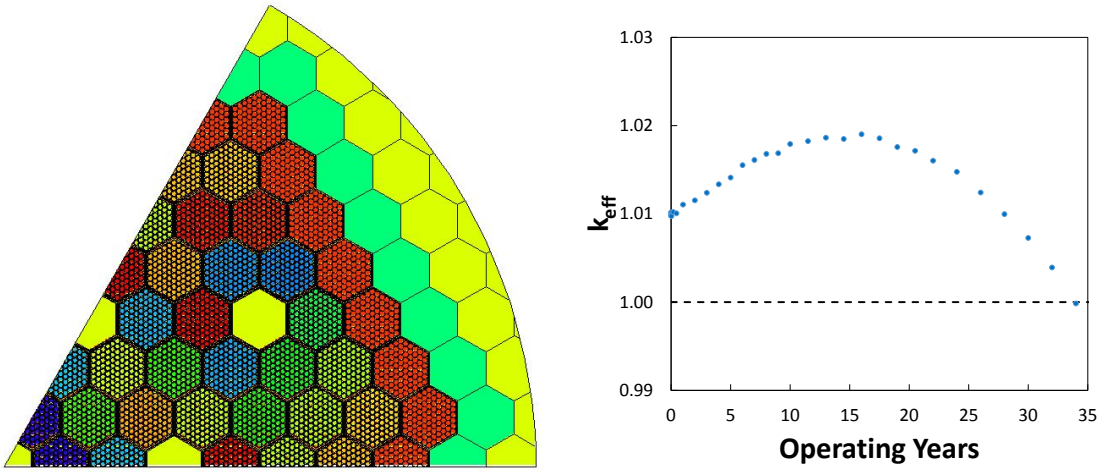

(a) $1/6^{th}$ MCNP model of the LLR.

(b) AFR k-eff evolution.

Figure 4.3: MCNP model based on the LLR design specifications. Visualization was generated using the VISED tool. The internal geometry of the shield assemblies (turquoise) was homogenized. Each assembly has a different color gradient because their material compositions are tracked separately.

limitations are:

1. Using a coarse group structure at lower energy bounds is no longer adequate when more thermalized neutrons are present in the system.
2. Homogenizing the assembly is a less valid assumption, since spatial shielding effects are no longer negligible (this is a valid simplification in fast systems since the average

neutron mean free path is greater than an assembly pitch).

3. Spatial polynomial expansions can struggle to capture the flux distribution at low-energy groups in mixed fast-thermal systems. The sharp gradients at those boundaries can cause numerical convergence issues with negative values appearing in some regions.
4. Fission products have a higher neutron importance than in fast systems. They can no longer be lumped together (as is common in REBUS) and must be updated more frequently with burnup (typically a middle-of-cycle composition is generated and never updated).

These different challenges are discussed in greater detail in following subsections. Implicit and explicit modifications to the REBUS suite are outlined, along with the results of benchmark calculations with MCNP6. The stochastic code is taken as a reference due to the absence of inherent limitations with modeling mixed-spectrum or epithermal systems. While the objective is not to necessarily reach same levels of accuracy as stochastic codes, results must at least be sensible to be able to draw conclusions during comparative analyses. As a wide range of models were considered in the optimization process, benchmarks tended to focus on sample models that were deemed representative and conservative. Discrepancies with the original REBUS code were more pronounced the higher the fraction of moderating content was inserted into the system. A $1/3^{rd}$ core symmetry is used by REBUS, with a P_3 scattering order. TWODANT flux weighting used a setting of S_{12}. Appendix B goes into more detail about the simulation settings used in the models.

4.3.1 Low-energy group structures

MC^2-3 was designed specifically for fast reactor applications. In such systems, the neutron flux is near zero in the epithermal and thermal energy levels. Due to this reason, group structures were designed to be fine at higher energy groups and coarser at lower ones. The code lumps all neutron energies below 4.17×10^{-1} eV in one single, last group. Since

up-scattering is nearly nonexistent in the high energy range, it is ignored by the code. These approximations result in large deviance between thermalized systems when comparing against MCNP, as highlighted in Figure 4.4. The results are for a relatively large $ZrH_{1.6}$ content (40% of fuel rods replaced), and for the two outermost assembly rings (both containing moderating rods). Deviances are apparent for nearly every energy group, which is not the case for innermost assemblies that are maintained in the fast spectrum. A large spike at the last energy group is observed, indicating that finer group structure treatment at the $< 4.17 \times 10^{-1}$ eV level may be required. These deviance result in incorrect cross-sectional collapsing in the thermalized regions, and subsequent flux resolution errors as shown in Table 4.3.

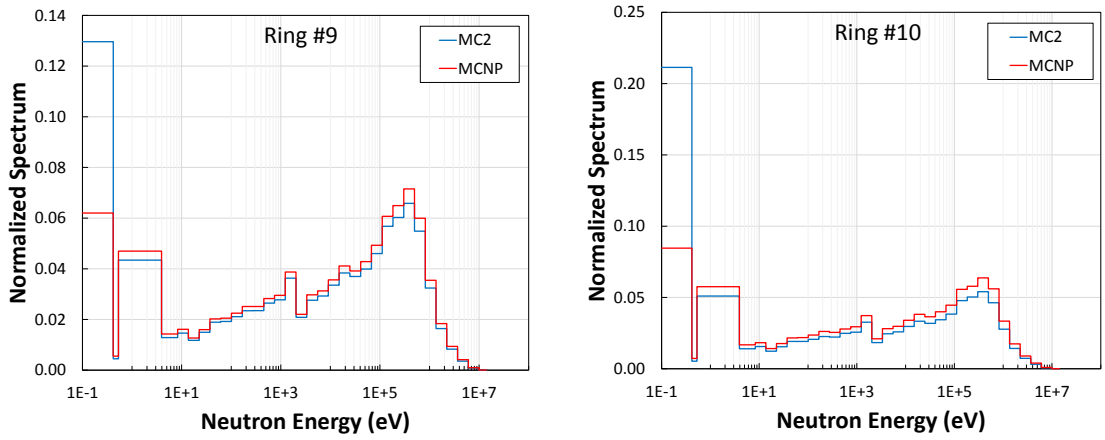

(a) Comparison at the 9^{th} assembly ring.

(b) Comparison at the 10^{th} assembly ring.

Figure 4.4: Comparison of the neutron spectrum at the two outermost rings of a benchmark reactor. Comparison are performed for REBUS with the original MC^2 against MCNP. Both models homogenized the internal assembly geometry. Note that MCNP statistical error bars are too small to appear on the graph and were all of the order of $\pm$ 0.1%.

In an attempt to rectify this issue, a new version of MC^2, henceforth referred to as MC^2-THERM, is currently under development at ANL, but has not been publicly released as of August 2017. The new version is capable of accounting for up-scatter, finer group structures at lower energy levels, and a lower group boundary of 5.0×10^{-3} eV (3 orders of magnitude lower than the original code). Table 4.4 displays the 73 group structure employed with MC^2-THERM as opposed to the original 33 group structure typically used in

Table 4.3: Percentage deviance between MCNP and REBUS without any special treatments. MCNP models had homogenized assemblies. Tallied cross-sections in MCNP had an max error of 0.27%.

	Fast Assembly	**Thermalized Assembly**
^{238}U σ_c	-0.8%	-21.0%
^{239}Pu σ_f	-0.2%	79.8%
ϕ	2.8%	7.8%

MC^2. A different ultrafine group structure is also used when collapsing ENDF libraries using the TWODANT discrete ordinates code. The effects on the neutron spectrum become immediately apparent as shown in Figure 4.5. Substantially greater agreement is reached for the same model when MC^2-THERM is used to generate the ISOTXS file. The average error for all energy bins i, as calculated using Equation 4.4, was 0.0002%, and 0.0001% respectively for each assembly ring. Additionally, the lower energy group boundary eliminates the large spike at the final energy group.

$$\delta^i = \frac{\phi^i_{REBUS} - \phi^i_{MCNP}}{\overline{\phi_{MCNP}}} \tag{4.4}$$

Further parameters were benchmarked to validate MC^2-THERM capabilities. Table 4.5 highlights deviances in microscoping cross-sections (σ) of the ^{238}U and ^{239}Pu isotopes (most important for plutonium breeding). All one-group collapsed cross-sections errors were below 5%, which was deemed acceptable. In the original MC^2-3, errors as high as 20% were observed in the thermalized regions. The total flux in each of these rings also showed good agreement. Figure 4.6 highlights how closely matched the two flux distributions are. Lastly, the eigenvalue deviated between the two codes by 529 pcm, a non-negligible quantity. Deterministic and stochastic tend to deviate by several hundred pcm, but such an elevated value will be investigated further in later modifications.

MC^2-THERM is able to address significant shortcomings of the original REBUS code package, but other requirements are still not met. Upon comparison with heterogeneous

Table 4.4: Comparison of the energy group structure bounds(in eV) in two MC^2 versions.

MC^2-3	1.419E+07	1.000E+07	6.065E+06	3.679E+06	2.231E+06	1.353E+06
	8.209E+05	4.979E+05	3.020E+05	1.832E+05	1.111E+05	6.738E+04
	4.087E+04	2.479E+04	1.503E+04	9.119E+03	5.531E+03	3.355E+03
	2.035E+03	1.234E+03	7.485E+02	4.540E+02	2.754E+02	1.670E+02
	1.013E+02	6.144E+01	3.727E+01	2.260E+01	1.371E+01	8.315E+00
	3.928E+00	5.316E-01	4.175E-01			
MC^2-THERM	1.419E+07	1.000E+07	6.065E+06	3.679E+06	2.231E+06	1.353E+06
	8.209E+05	4.979E+05	3.020E+05	1.832E+05	1.111E+05	6.738E+04
	4.087E+04	2.479E+04	1.503E+04	9.119E+03	5.531E+03	3.355E+03
	2.035E+03	1.234E+03	7.485E+02	4.540E+02	2.754E+02	1.670E+02
	1.013E+02	6.144E+01	3.727E+01	2.260E+01	1.593E+01	9.877E+00
	4.000E+00	3.300E+00	2.600E+00	2.100E+00	1.855E+00	1.500E+00
	1.300E+00	1.150E+00	1.123E+00	1.097E+00	1.071E+00	1.045E+00
	1.020E+00	9.960E-01	9.720E-01	9.500E-01	9.100E-01	8.500E-01
	7.800E-01	6.250E-01	5.000E-01	4.000E-01	3.500E-01	3.200E-01
	3.000E-01	2.800E-01	2.500E-01	2.200E-01	1.800E-01	1.400E-01
	1.000E-01	8.000E-02	6.700E-02	5.800E-02	5.000E-02	4.200E-02
	3.500E-02	3.000E-02	2.500E-02	2.000E-02	1.500E-02	1.000E-02
	5.000E-03					

Table 4.5: Percentage deviance between MCNP and REBUS using MC^2-THERM. Rings 8, 9 and 10 contain moderating material. Tallied cross-sections in MCNP had an average error of 0.16%.

Assembly ring no.:	**2**	**6**	**8**	**9**	**10**
^{238}U σ_c	-0.71%	-1.00%	-4.34%	-0.81%	0.17%
^{239}Pu σ_f	-0.01%	0.01%	1.47%	-0.56%	-2.94%
ϕ	2.42%	-1.82%	-1.82%	0.61%	2.47%

MCNP assembly models, spatial self-shielding effects become noticeable. Figure 4.7(a) highlights the deviance in the REBUS spectrum compared to the MCNP tallied spectrum in the whole assembly, in the fuel, and in the moderating rods. The relative error (calculated using Equation 4.4) in Figure 4.7(b), is shown to be non-negligible. The resulting isotopic cross-sections now see significantly larger disagreements in the thermal zones. With σ_c

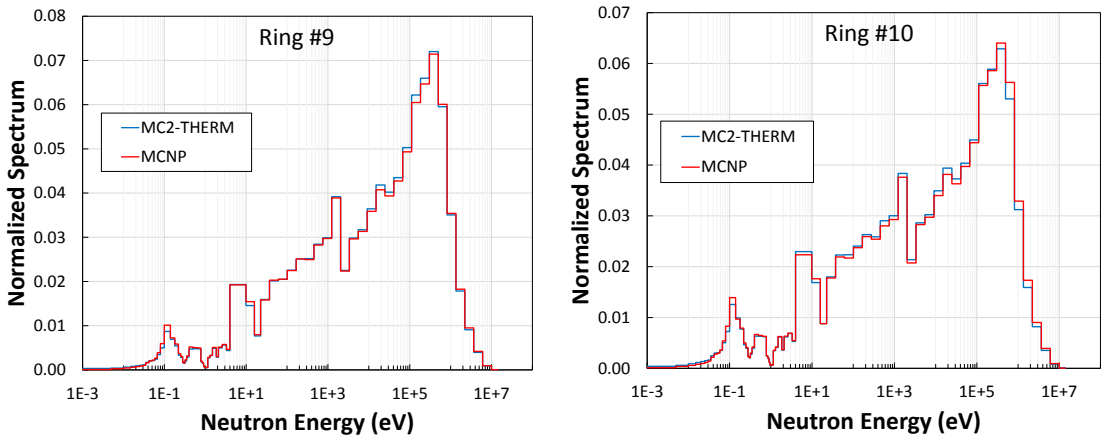

(a) Comparison at the 9^{th} assembly ring.

(b) Comparison at the 10^{th} assembly ring.

Figure 4.5: Comparison of the neutron spectrum at two outer rings of a benchmark reactor. REBUS cross-sections are generated with MC^2-THERM and MCNP tallies employed the same 73 group structure shown in Table 4.4. Both models homogenized the internal assembly geometry. Note that MCNP statistical error bars are too small to appear on the graph and were all of the order of $\pm$ 0.1%.

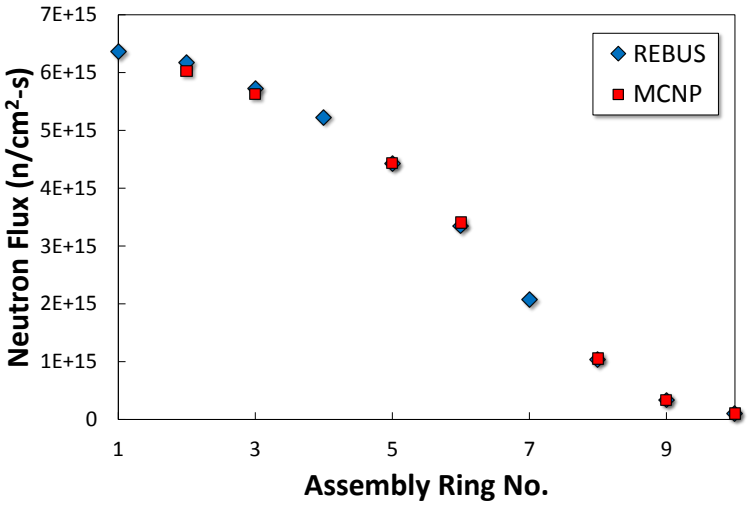

Figure 4.6: Total flux at different fuel assembly rings. REBUS results were obtained using cross-sections generated with MC^2-THERM. Average MCNP relative errors were of 0.09%, error bars are too small to appear on the plot.

for ^{238}U seeing errors as high as 21.2% for the outermost (moderated) assembly ring. The following section will attempt to address the spatial self-shielding effect.

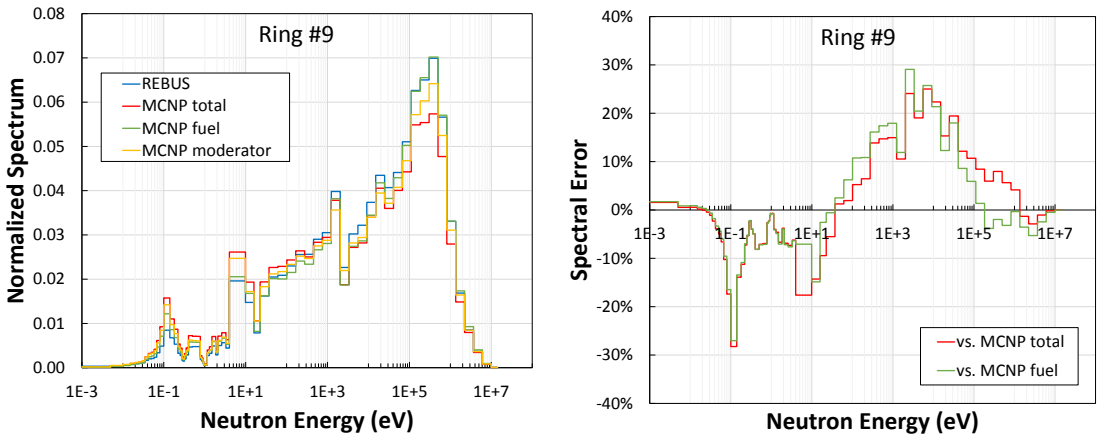

(a) Comparison with heterogeneous MCNP model.

(b) Resulting spectral error.

Figure 4.7: Comparison of the neutron spectrum at ring no. 9 with a heterogeneous MCNP model. Flux values were tallied for the whole MCNP assembly (total, in red), the fuel rods (green) and the moderator (yellow). Spectral errors were then calculated using Equation 4.4. MCNP statistical error bars are too small to appear on the graph and had an average value of $\pm$ 0.1%.

4.3.2 Heterogeneity and spatial self-shielding

This challenge is harder to address since the DIF3D and REBUS modules cannot account for assembly heterogeneity. Assemblies are modeled as hexagonal nodes with a homogenized composition mixture. This is a valid assumption in a fast spectrum system when a neutron mean free path is larger than the assembly pitch. As such, neutrons do not 'see' individual rods within assemblies; using a homogenized mixture while conserving masses tends to be a valid approximation. This was evidently the case in Table 4.5 with the fast assembly rings (no. 2 and 6). However, as highlighted in the previous section, this assumption breaks down when neutrons are moderated. These slower neutrons have shorter optical depths and are affected by spatial heterogeneities within the assembly, which must be accounted for.

A potential workaround to the DIF3D and REBUS limitations is to use implicit functions in MC^2 that correct cross-sections to account for spatial effects. A wide range of methods exist to correct cross-sections and account for spatial shielding effects. They all tend to be based on the equivalence theory outlined by Bondarenko.[60] The basis of this

approach relies on defining background cross-sections that take heterogeneity effects into consideration when resolving resonances. A wide range of approximations can be used to estimate this background cross-section (e.g. using Dancoff and Bell-Levine factors), but MC^2 employed a transport-based approach. The code estimates the background cross-section using the escape probability of an isotope k in region i, P_{ei}^k. The value is estimated using Equation 4.5 for any energy group g; all the terms in the equation have their usual definitions. Obtaining the value of the flux in each region (ϕ_i), and the collision probabilities in region j relative to region i, P_{ij}, is achieved using transport methods. The 1-D Collision Probability Method (CPM) is used, it is another transport equation similar to the S_N and P_N method. It solves the fixed source problem shown in Equation 4.6, for each region in the system. Σ_{pg} is the potential scattering cross-section for each distinct region. The equation is solved to obtain both fluxes in each region, and collision probabilities between different regions. These are then used in Equation 4.5 to estimate escape probabilities and deduce the background cross-sections.[61]

$$P_{ei,g}^k = \sum_{j \neq i} \left(1 - \frac{\Sigma_{tj,g}^k \phi_{jg}}{\Sigma_{ti,g}^k \phi_{ig}}\right) P_{ij,g} \tag{4.5}$$

$$\Omega \nabla \psi_g(r, \Omega) + \Sigma_{tg}(r) \psi_g(r, \Omega) = \Sigma_{pg}(r) \tag{4.6}$$

Since spatial self-shielding can only be accounted for in one dimension in MC^2, the closest approximation to an assembly with a mixture of fuel and moderating rods, is a cylinder as shown in Figure 4.8. The assembly is modeled as concentric rings of coolant, clad, fuel and moderating material with masses of each composition conserved. This correction is performed at the second stage of MC^2 calculation; after the ultrafine group collapsing and the TWODANT flux distribution generation in r-z geometry. This global (whole core) flux distribution outputted by TWODANT is then used for flux spectrum weighting and group collapsing of cross-section (as before).[62] While, CPM is employed for spatial treatment

of cross-section at a local assembly level. The final output is the same ISOTXS data file with a 73 group structure for the case of MC^2-THERM.

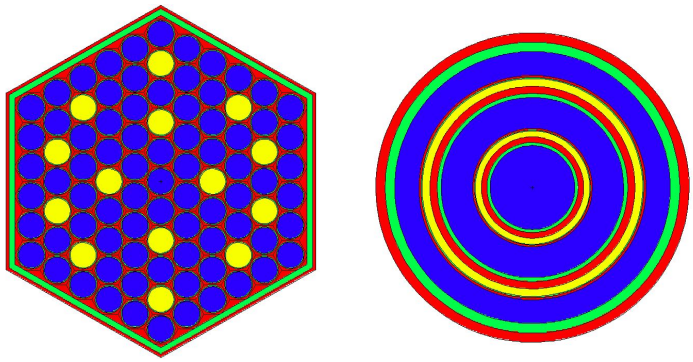

(a) Original model. (b) Approximated cylindrical model.

Figure 4.8: Modeling approximation to the assembly layout performed by the 1D CPM tool in MC^2. Fuel is in blue, moderator in yellow, structural material in green and coolant in red.

Table 4.6 highlights the improvement in cross-sectional accuracy of the system. The results are for the central axial slice of all moderated assemblies in a given core configuration (the configuration was selected to be very similar to that used in later chapters). While errors in the ^{235}U cross-sections see little variation, it is the ^{238}U isotope where the majority of improvement is observed. Correctly estimating σ_c for this isotope is critical for reactors with relatively high breeding ratios. The flux spectrum is compared for this region in both MCNP and REBUS. The distribution in Figure 4.9 is more closely aligned with the flux within the fuel region than was observed in Figure 4.7.

Table 4.6: Percentage deviance in microscoping cross-sections between MCNP vs. REBUS with and without 1-D spatial treatment. Comparison was performed for an axial slices of all moderated assembly rings. Cross-sectional tally standard errors in MCNP were 0.06% and 0.05% for total and fission respectively.

	without CPM	**with CPM**
^{238}U σ_c	10.66%	0.36%
^{235}U σ_f	-1.02%	1.95%
^{235}U σ_c	1.7%	1.92%

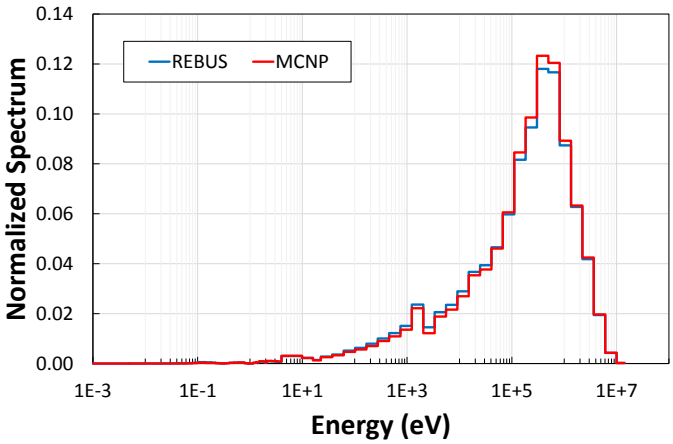

Figure 4.9: Closer agreement in the neutron spectrum when 1-D spatial treatment is applied to cross-sections. The results are averaged for the central axial region for all moderated assemblies. MCNP results were tallied within every fuel rod geometry. The stochastic standard deviation was 0.04% on average.

The improvements discussed thus far have only addressed improving cross-sectional accuracies of the deterministic code. System integration will be taken into account in the following two sections. First, numerical convergence issues that arise when resolving the flux in a mixed-spectrum configuration, will be addressed. Then, benchmarking of depletion calculations will be performed alongside a discussion of potential improvements.

4.3.3 Neutron flux discontinuities

Operating in a mixed-spectrum configuration can limit modeling capabilities of deterministic codes. Neutron transport approximations can break down at sharp boundary gradients, notably at the fast/thermal interface within the core. Lower energy groups can see pronounced jumps from one radial ring to another as shown in Figure 4.10. Due to the absence of moderator in the fast regions, the flux in some groups can be near zero, and increase dramatically at the epithermal zone. In the highlighted case, the ratio between ring 8 and 1 of $\phi \times V$ is 4.53 for group 10, and 5.52×10^6 for group 30. This six order of magnitude jump is essentially a discontinuity that can cause numerical convergence problems with variational nodal codes such as DIF3D. The problem is exacerbated when moderated

assemblies produce a relatively large fraction of the core power and are not employed as blankets.

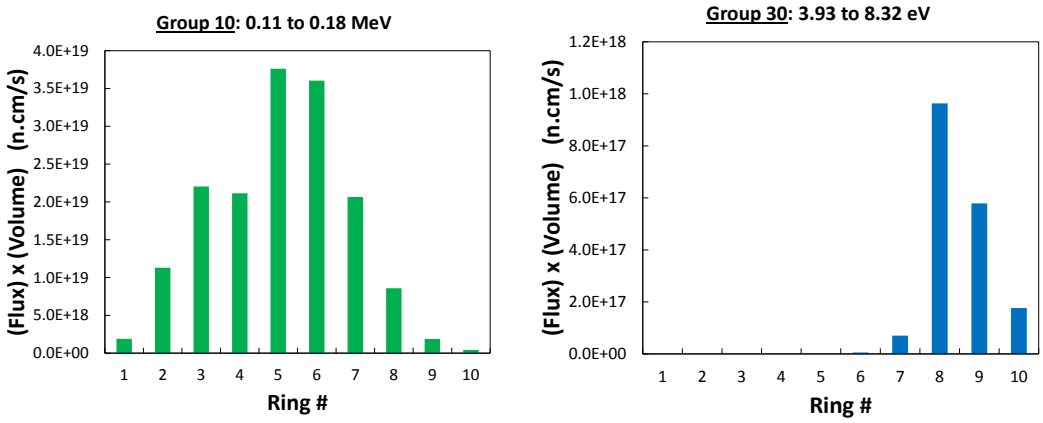

(a) Group 10 radial evolution.

(b) Group 30 radial evolution.

Figure 4.10: Variation of the flux multiplied by the volume ($\phi \times V$) radially, in each assembly ring. A sharp discontinuity can be observed for lower energy groups. In this model, ring 8, 9 and 10 are moderated; they produce only a small fraction of core power.

The flux solver in DIF3D employs the P_N method with spatial polynomial expansions. At each node, the internal flux, the source term (i.e. fission), and the leakage on the surfaces, are all evaluated. Each of these three terms can be spatially expanded using different polynomials, as illustrated in Figure 4.11(a). Since the radial meshes are as small as the assembly itself, this is necessary to account for variations within each assembly. While this is a valid approximation of neutron transport within continuous systems, the assumption can break down when sharp discontinuities appear. As highlighted with Figure 4.11(b), accurately representing a step function (such as the one shown in the figure), requires an ever higher polynomial order. Lower orders can result in unphysical negative values due to oscillations and mathematical convergence problems further away from the interface point. In reality, the value should be approaching zero, but numerical oscillations shown in Figure 4.11(b), can lead to overcorrections in some nodes and subsequent negative values.

Increasing polynomial orders proportionally increases computational requirements, and can help rectify the problem. Other code settings can also help alleviate the concerns. Table

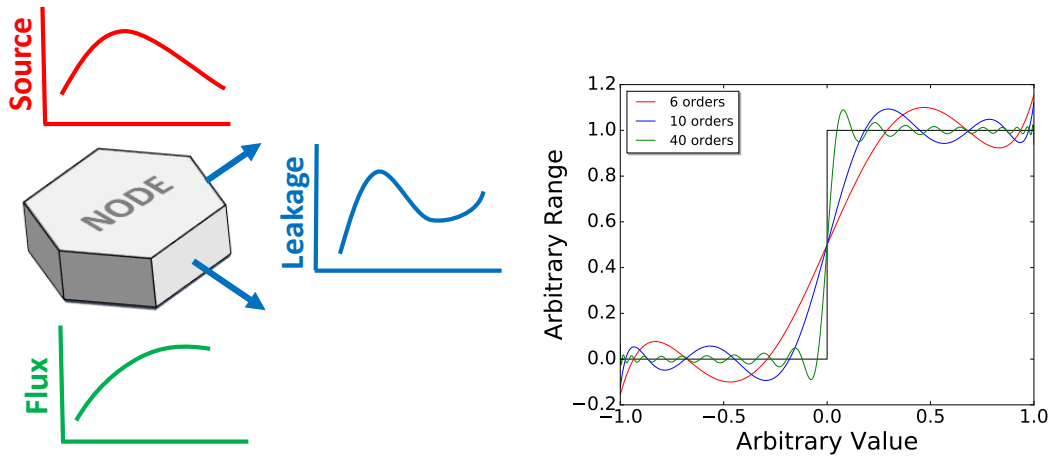

(a) Leakage, source and flux polynomial terms in each node.

(b) Polynomial approximation of the heaviside (step) function.

Figure 4.11: DIF3D/VARIANT model each assembly as a hexagonal node slice. Accounting for discontinuities from one node to another requires extremely large polynomial orders.

4.7 summarizes the different attempts to resolve the negative fluxes in one of the extreme cases encountered during the optimization process in Chapter 5. Sensitivity analysis is conducted on parameters in the following order: angular scattering order, spatial polynomial expansion, number of sweeps per group, convergence criteria, and number of energy groups. As highlighted in the table, increasing the flux or source terms appears to have little effect on the total number of negative groups. Increasing the leakage term however, has the largest impact, but up to a limit. Other parameters, such as the angular scattering order or the number of sweeps appear ineffective, but do show some improvement in the eigenvalue. The convergence criterion shows only limited improvement relative to the resulting increase in computational costs. In this highlighted case, the most effective approach appeared to be lowering the group structure number to 45. However, doing so has its own limitations, as it results in very high deviance in k_{eff}.

Other approaches to alleviate this challenge included removing regions of low neutron importance from the simulated model. Ultimately, no solution was found to be ideal due to inherent mathematical limitations in the REBUS code for this type of analysis. This

Table 4.7: Different settings options in DIF3D/VARIANT to reduce the number of flux groups that see negative values. The term S-F-L refers to the spatial polynomial order of the source, flux, and leakage term respectively. Sweeps refers to the number of partial current sweeps per group, and convergence refers to the average convergence criterion for the eigenvalue and fission source.

Angle	**S-F-L**	**Sweeps**	**Convergence**	**E-Groups**	$\mathbf{k}_{eff}$	**Negative Groups**
P0	4-6-1	2	1E-5	73	1.00725	14
P1	4-6-1	2	1E-5	73	1.01111	14
P3	4-6-1	2	1E-5	73	1.01153	14
P1	4-10-1	2	1E-5	73	1.01136	14
P1	10-10-1	2	1E-5	73	1.01117	14
P1	4-10-2	2	1E-5	73	1.01080	12
P1	4-10-3	2	1E-5	73	1.01071	4
P1	10-10-4	2	1E-5	73	1.01055	4
P1	4-6-2	4	1E-5	73	1.01111	14
P1	4-6-2	6	1E-5	73	1.01111	14
P1	4-10-2	2	1E-6	73	1.01080	12
P1	4-10-2	2	1E-7	73	1.01080	12
P1	4-8-3	5	1E-8	73	1.01062	4
P1	4-10-2	5	1E-8	45	1.10192	0
P1	4-10-2	2	1E-5	45	1.10256	0

meant that the code could only be used for comparative analysis and results will always require cross-validating using stochastic codes. A 4^{th}, 8^{th}, and 1^{st} degree expansion of source, flux, and leakage was settled on, for computational expediency. Care was taken to ensure negative flux values were limited to groups of low neutron importance and that total fluxes in a region remained positive. Further benchmarks of the code with MCNP6 are highlighted in the next section.

4.3.4 Core depletion and fission products

In fast reactor fuel cycle analysis, it is typical to generate a single ISOTXS cross-section file that is used throughout the core depletion. A composition corresponding to what is expected at the middle-of-cycle (MOC) is used by MC^2 and TWODANT to collapse cross-sections. Using the same microscopic cross-sections (macro ones are updated as the iso-

topic composition is depleted in REBUS) tends to be a reasonable assumption as they change by relatively minute amounts with depletion. As shown in Figure 4.12, the neutron spectrum sees little change over time in fast systems; more pronounced differences are observed for the epithermal spectrum however.

A further simplification in fast reactor analysis is lumping fission products together into groups. A collective microscopic cross-section is generated for all the isotopes instead of storing individual ones. This can save on memory and processing times. There tends to be five main lumped groups, one for each of the major fissile/fissionable isotopes: ^{235}U, ^{238}U, ^{239}Pu, ^{240}Pu, and ^{241}Pu. Because of the relatively lower neutron importance of fission products in fast systems (as opposed to thermal reactors), this tends to be an acceptable simplification.

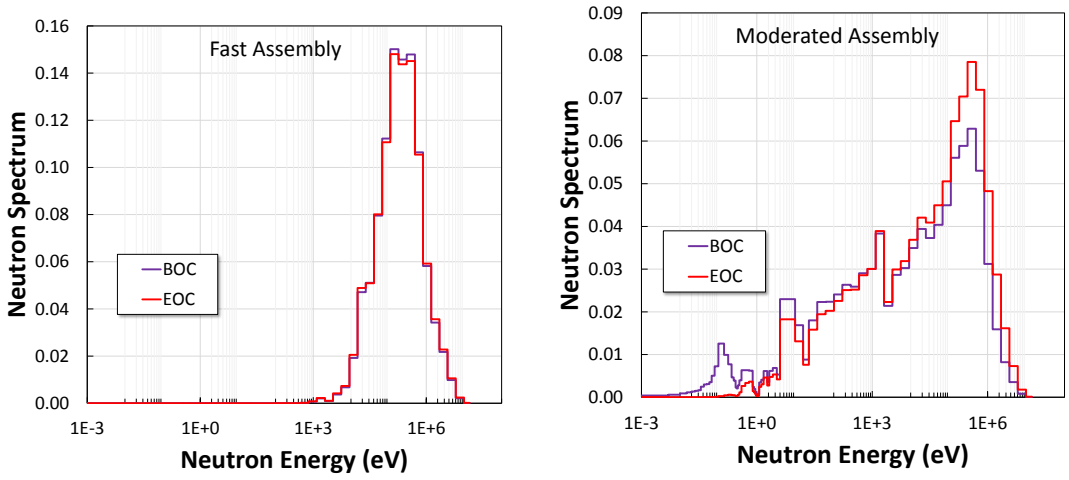

(a) Spectral evolution in fast assembly.

(b) Spectral evolution in moderated assembly.

Figure 4.12: Variation of the neutron spectrum with burnup in a fast and moderated assembly. The results are shown for beginning-of-cycle (BOC) and end-of-cycle (EOC).

These two assumptions break down when moderating material is inserted into the system. Fission product poisoning becomes more prevalent and must be more finely evaluated. Furthermore, spectral variations over time are more pronounced (Figure 4.12(b)) and must be taken into account. To rectify these limitations of the REBUS package, an explicit solution was developed at ANL by Dr. Nicolas Stauff. An external software uses REBUS

to deplete individual timesteps while manually updating the resulting cross-sectional data at every point. Figure 4.13 illustrates the process methodology. Essentially new REBUS and MC^2 inputs are generated for every timestep (the same TWODANT flux weighting is used throughout for simplicity). The software, referred to as '*REBUXS*' (REBus Updated Cross-Sections), can incorporate previously highlighted improvements to cross-sectional treatments, including the use of MC^2-THERM and spatial self-shielding correction factors. *REBUXS* is also capable of explicitly modeling fission product decay chains to more carefully track individual isotopic evolutions, rather than lumping them together (a list of the various isotopes tracked is shown in Appendix B). This is important, notably for xenon production and its effects on core neutronics.

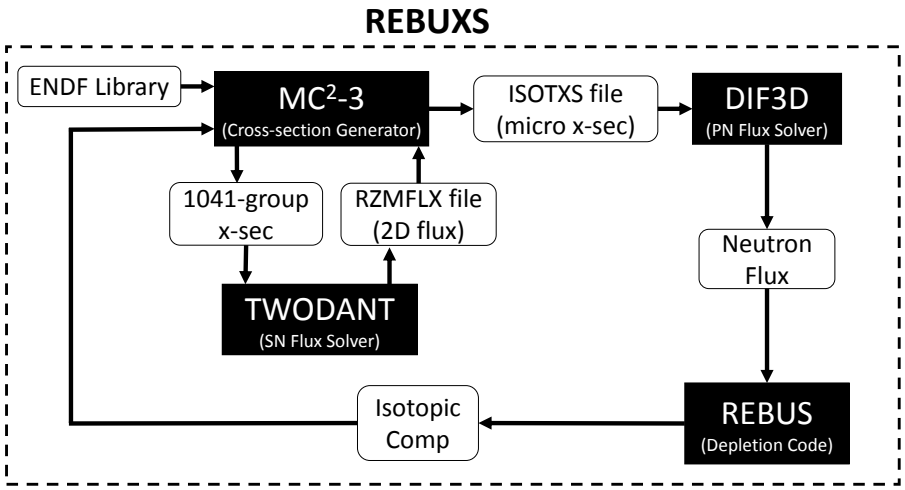

Figure 4.13: Modified layout of code modules using the explicit *REBUXS* script. For every updated isotopic composition at each timestep, a new ISOTXS (cross-section data) file is generated. The process is repeated until the final timestep is reached.

The external software was then used for final benchmarks with MCNP6. Eigenvalue evolution over time is shown in Figure 4.14. An average deviance of 693 pcm was still observed throughout the simulation cycle. The deviance appears systematic, as shown in Figure 4.14(b), and remains relatively constant throughout the simulation. As such the *REBUXS* script can be a useful indicator of k_{eff} trends in different cores. The slight under-estimation provides a conservative estimate for scoping analyses. Table 4.8 com-

pares the final isotopic compositions at end-of-cycle (EOC) for the models. Good agreement is reached here for relevant plutonium metrics, notably the fissile-to-total ratio. The largest mass error observed are for plutonium isotopes that are produced in minute quantities. The results demonstrate that the improved code version can be used for design scoping analysis. Since trends are captured in the model, it can be accurately employed for comparative analysis. Further benchmarks and improvements are needed if the code is to be more heavily relied on. In the long term, more advanced deterministic codes such as PROTEUS,[63] which are capable of capturing complex geometries could be employed to improve modeling capabilities, but at a cost to computational requirements. Analysis with the deterministic code must be limited to k_{eff} and isotopics comparisons, stochastic codes will be employed for more in-depth analysis.

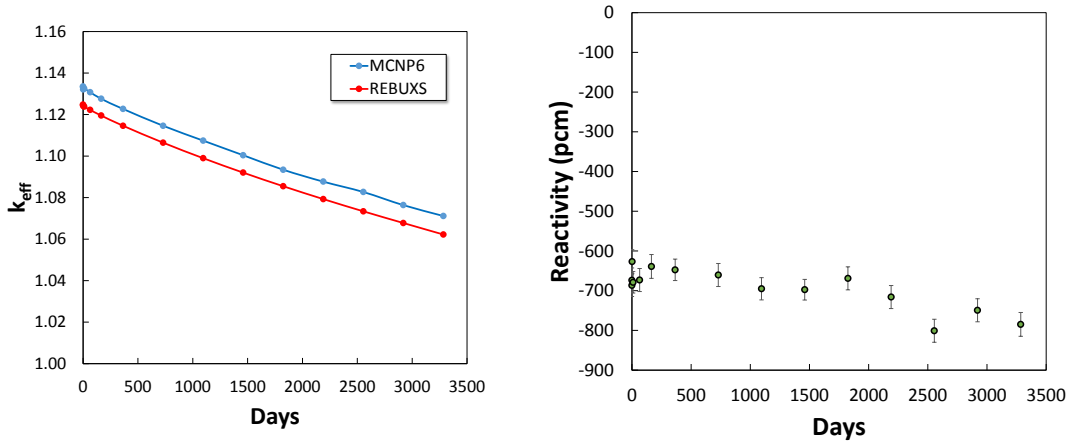

(a) Eigenvalue deviance between the two codes.

(b) Resulting reactivity, $\rho = \frac{k_2 - k_1}{k_2 k_1}$.

Figure 4.14: Eigenvalue benchmarks between MCNP6 and REBUXS. Error bars are too small to appear on the k_{eff} plot, but are shown in the (b).

4.4 Stochastic Modeling of Mixed Spectrum Cores

Due to aforementioned limitations of deterministic codes, stochastic ones were also used in the thesis. Modeling mixed-spectrum reactors with these codes can be challenging, but is not inherently limited due to underlying assumptions, as is the case with the REBUS de-

Table 4.8: Mass deviance between *REBUXS* and MCNP6 at end-of-cycle (EOC). Results are summed for the inner, mid and outer core regions.

	Inner	**Mid**	**Outer**
^{235}U	0.062%	0.510%	-0.110%
^{238}U	-0.002%	0.034%	-0.002%
^{238}Pu	6.643%	1.263%	-4.512%
^{239}Pu	-0.373%	-1.525%	0.239%
^{240}Pu	-1.830%	-3.083%	2.173%
^{241}Pu	0.998%	-7.393%	-12.273%
^{242}Pu	9.789%	-4.785%	-8.566%
Pu_{fiss}/Pu_{tot}	0.023%	0.028%	0.028%

terministic package. Reaching valid conclusions from the simulations relies on two main factors: (1) a sufficient number of virtual particles to ensure good neutron transport statistics, and (2) an accurate representation of the evolution of core material composition with depletion.

The first challenge must be addressed on a case-by-case basis. Standard deviations are outputted by the code and must always be checked to ensure acceptable error levels are reached. Figure 4.15, shows the convergence of the eigenvalue, and a flux tally, with increasing number of particles. As highlighted, increases in accuracy follow the expected $1/\sqrt{N}$ relation (Figure 4.15(c)), where N is the number of particles simulated. This limits the benefit of further increasing number of simulated particles, since it proportionally increased computational costs. A high cycle number is also recommended to ensure good fission source convergence. In the highlighted model, little added accuracy is gained at beyond 5×10^6 particles, and this was chosen to be the baseline for most simulations.

The second limitations is more challenging to address. The particle transport module MCNP was successfully coupled with a depletion module, CINDER90, in version 6. Flux is implicitly tallied at each material specified to be depleted, and is used to solve the Bateman Equation (shown in Equation 4.7). The time variable is discretized into specified

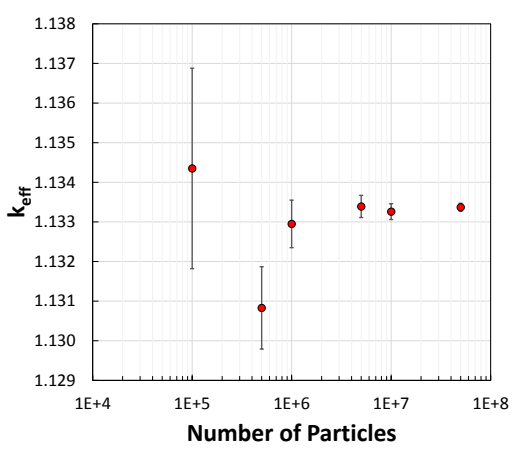

(a) Eignevalue convergence with number of particles.

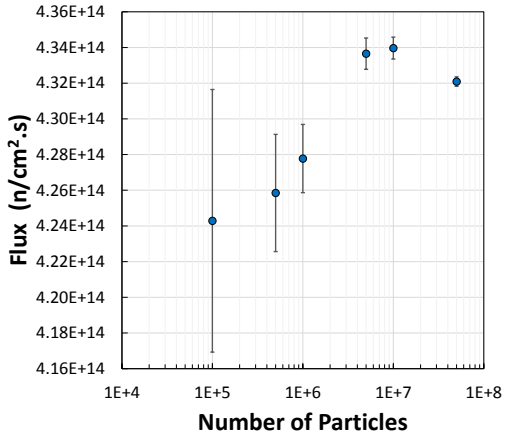

(b) Flux tally convergence with number of particles.

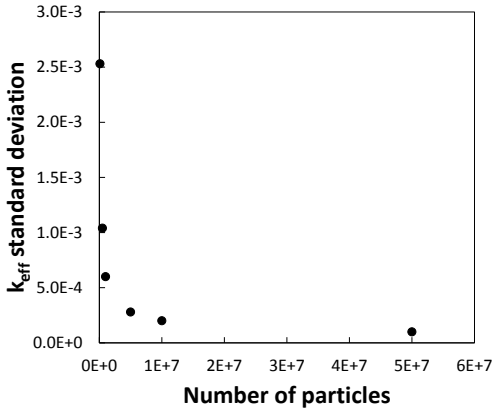

(c) Evolution of k_{eff} error bars, following $1/\sqrt{N}$ trend.

Figure 4.15: Simulation convergence with increasing number of particles. A particle number of 5×10^6 was deemed appropriate for most depletion analysis.

timesteps. MCNP6 performs a predictor calculation at $t_{i+1/2}$ to obtain a flux that is then used to deplete a material from step t_i to t_{i+1} (corrector step).[57] Accurately modeling depletion at a core level requires tracking a large number of materials and depleting them. This scales computational times proportionally, as more regions need to be tallied in order to derive the flux to use in Equation 4.7. Combined with the need to perform two transport calculations for each timestep (predictor and corrector), and the end result is a prohibitively expensive simulation. This is not the case in deterministic codes such as REBUS, where transport calculations are much more efficient, and whole core flux distribution is systemat-

ically derived. A workaround to the computational demands of MCNP6 depletion analysis, is to leverage the parallelizability of the code (not the case in REBUS), and 'brute force' the problem by subdividing to multiple processors. Nevertheless, simplifications to the amount of tracked material are necessary to reach reasonable computational requirements.

$$\frac{dN_i}{dt} = \sum_{j \neq i} \lambda_j N_j + \sum_{k \neq i} (\phi \times \sigma_x^k) N_k - [\lambda_i + (\phi \times \sigma_x^i)] N_i \tag{4.7}$$

One approach to reduce the amount of material to track, without any loss in accuracy, is to rely on core symmetry. While REBUS is only able to model 1/3rd core models (with the exception of finite-difference schemes), the versatility of MCNP allows to take advantage of the 1/6th core symmetry of the LLR (See Figures 4.2(a) and 4.3(a)). This halves the number of regions to track. Reducing the number of materials to deplete any further relies on merging different core regions together. Figure 4.16 shows the eigenvalue evolution when different core regions are grouped in the LLR. At the highest level, three regions are tracked in every single fuel assembly, corresponding to the three axial enrichment zones in Figure 4.2(b). This resulted in a total of 74 tracked individual regions. Since the upper and lower edges of each assembly have the same enrichment level, they were merged in a first order simplification. A total of 50 regions then needed to be tracked, a reduction of 32% relative to the previous case. Lastly, because neutron flux tends to vary little within individual fuel rings, radial merging of neighboring assemblies was evaluated (with two-axial zones in each ring). Only 14 regions then needed to be tracked, an 81% reduction. Figure 4.16(b) shows relatively good agreement between the three cases. The reactiviy deviance stays relatively constant over time, with an average error of 10 and 33 pcm between the first two cases, and between the last and first case. The reactivity standard deviation was estimated using Equation 4.8, with $\rho = \frac{k_2 - k_1}{k_2 k_1}$.

$$\sigma_\rho = |\rho| \sqrt{\left(\frac{\sigma_2^2 + \sigma_1^2}{k_2 - k_1}\right) + \left(\frac{\sigma_1}{k_1}\right)^2 + \left(\frac{\sigma_2}{k_2}\right)^2} \tag{4.8}$$

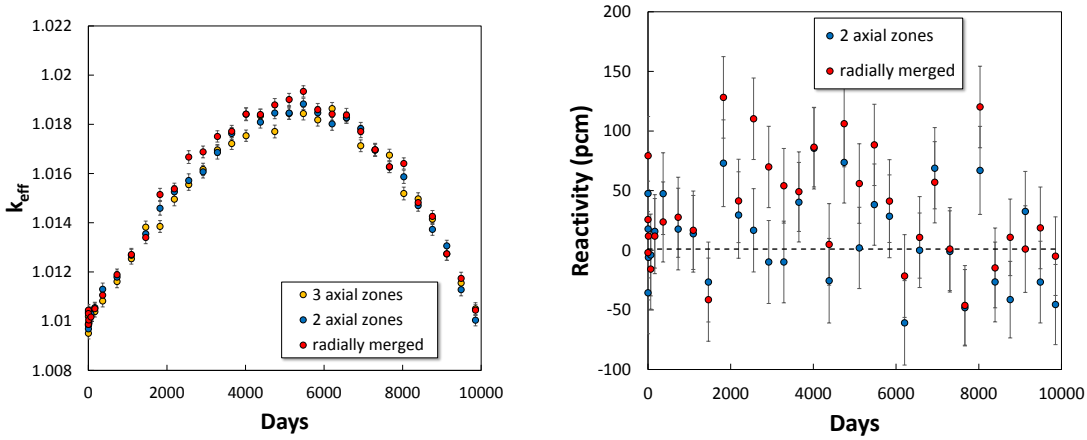

(a) k_{eff} evolution between the three MCNP models. (b) Reactivity deviance with the 3 axial region case.

Figure 4.16: Benchmarks of MCNP models with different number of regions with 3 axial regions per assembly, 2 axial regions per assembly, and radially merged assemblies.

The isotopic composition was tracked for all three cases, to ensure good convergence. Table 4.9 highlights the similarity between the different cases, the radially merged case does see small deviance in some plutonium isotopes. Merging multiple assemblies together conserves the total mass, but fails to capture variations within each assembly. Because assembly shuffling needs to be simulated in later chapters, radial merging of assemblies is not performed. From a nonproliferation standpoint, it is also important to know the exact composition of individual assemblies when assessing the maximum attractiveness for diversion. On the other hand, since the two-axial region per assembly simplification has yielded adequate results, it will be relied on in further MCNP analyses to reduce computational costs (relative to the three region model).

4.5 Chapter Conclusion: Optimization with Deterministic Codes and Evaluation with Stochastic Codes

Two different modeling approaches were considered for the MXR. The first relied on deterministic codes; they are less computationally expensive and systematically output detailed information about the core configuration. The second relied on stochastic codes, which are

Table 4.9: Mass deviance against the 3 axial region MCNP model for assembly number 803. Radially merged results are divided by the number of assemblies.

	2 axial zones	**radially merged**
^{235}U	-0.065%	-0.740%
^{238}U	0.038%	-0.082%
^{238}Pu	0.083%	2.762%
^{239}Pu	0.103%	1.308%
^{240}Pu	0.053%	3.908%
^{241}Pu	0.337%	6.229%
^{242}Pu	-0.313%	7.698%
Pu_{fiss}/Pu_{tot}	0.002%	-0.109%

more versatile and are usually considered to be the 'gold standard' in terms of accuracy. Due to inherent limitations in the REBUS deterministic code with modeling epithermal and mixed-spectrum configuration, improvements were implemented. Some of these were implicit (e.g. higher polynomial orders to account for group discontinuities, and 1-D spatial self-shielding models to account for heterogeneity), and others were explicit (e.g. using MC^2-THERM generated group structures, and manually updating cross-sections at each timestep). The code was not able to reach the same accuracy as MCNP however, but important trends were captured. As a result, deterministic code usage in this thesis was limited to scoping analysis to better understand the design space. With its reduced computational requirements, REBUS can be used to rapidly screen different design options to arrive to important conclusions. Once attractive core configurations are identified, more detailed analyses will be conducted with MCNP. These models form the basis of design evaluations for the proposed MXR configurations.

CHAPTER 5

DESIGN OPTIMIZATION OF MIXED SPECTRUM CORE

With the modeling tools for the Mixed Spectrum Reactor (MXR) established, identifying an optimal core configuration is the next task. The main objective in this chapter will be to derive a core configuration that achieves the two main objectives: (1) long operating lifetime without refueling, and (2) reduced plutonium attractiveness within individual assemblies. To rapidly screen through different core options, the REBUS code package is employed, specifically with the *REBUXS* script. This was used for comparative evaluations in order to identify ideal design characteristics. A systematic approach was used to explore different types of moderators, volume fraction, placements within the core, shuffling mechanism, fuel enrichment, and core dimensions. MCNP6 was relied on for assembly-level screening studies as well as for more in-depth analysis of optimal core configurations.

5.1 Parametric Studies on Core Moderation

The first issue encountered when designing a mixed spectrum configuration is how to introduce moderating material into the system. By virtue of employing a mixed-configuration, shuffling of assemblies (at least once) is inevitable in order to expose all assemblies to the moderated spectrum. As such, at least half the core assemblies must see a more epithermal spectrum during half the core lifetime, and will then be shuffled with those in the fast spectrum. This must be taken into account when deriving a moderating mechanism. Once this is addressed, the moderator type, quantity and arrangement must be considered. These first steps will shed light on the design space and reduce the total amount of core-level REBUS simulations conducted.

5.1.1 Inter and intra-assembly moderation

There are two main approaches to moderate a specific core region while allowing for shuffling. The two methods will be referred as 'inter' and 'intra'-assembly moderation. Inter-moderation relies on mixing fuel rods with moderating ones within individual assemblies. To allow for shuffling, empty channels are needed within all assemblies to insert and remove moderating material. The intra-approach relies on mixing moderator-filled and fuel-filled assemblies. Moderated fuel assemblies can be 'sandwiched' between moderating assemblies to thermalize neutrons. Neutrons are born at fast energies, with mean free paths exceeding that of an assembly pitch. Intra-assembly thermalization relies on neutrons traveling to nearby moderating assemblies, down-scattering after collision with moderating material, and returning to a fuel assembly. In inter-assembly moderation, the down-scattering path is shortened since fuel rods and moderating rods are mixed within the same assembly. The differences between the two approaches is illustrated in Figure 5.1. Previous work on intra-assembly moderation includes the MIT-BNL study of an equilibrium core with shuffling and a 5 batch scheme.[18, 17] Research on inter-assembly design includes a proposal to moderate the blanket assemblies of fast reactors.[19]

Shuffling in intra-assembly configurations is relatively simple since it only involves switching around individual fuel assemblies while keeping moderating assemblies in place. Inter-assembly shuffling is more involved, but not prohibitively so, since shuffling is only expected to occur once in the core lifetime. A mechanism will need to extract moderating material, and place it into fast assemblies before shuffling takes place. A system similar to the 'spider' mechanism for inserting control rods within assemblies in a typical PWR is conceivable. As highlighted in Figure 5.2, all assemblies would contain empty channels in which moderating rods can be inserted. The main limitation in both approaches is that the resulting fuel volume fraction in the core is reduced, which results in a k_{eff} and breeding penalty.

Simulations were conducted using REBUS to compare the two configurations illus-

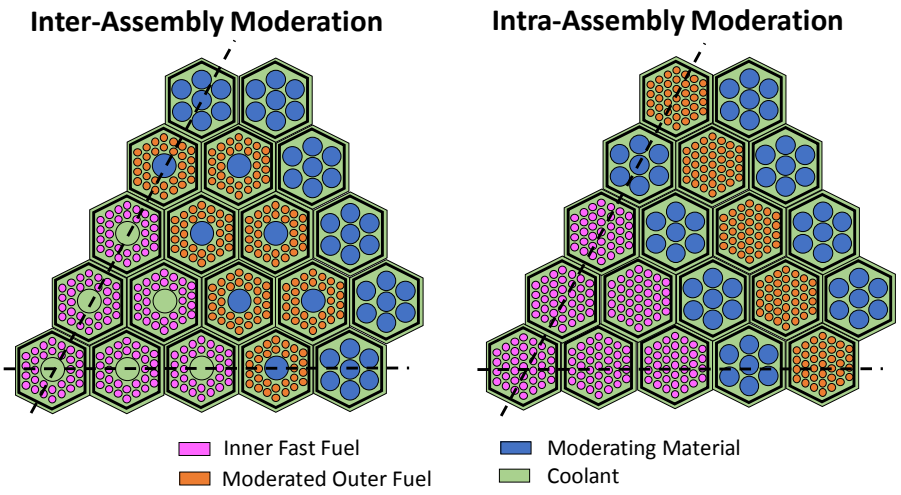

Figure 5.1: Illustration of the inter and intra-assembly layouts for a $1/6^{th}$ core model. Inner and outer fuel assemblies are shuffled after a specific burnup is reached, with the moderating material remaining in the same arrangement.

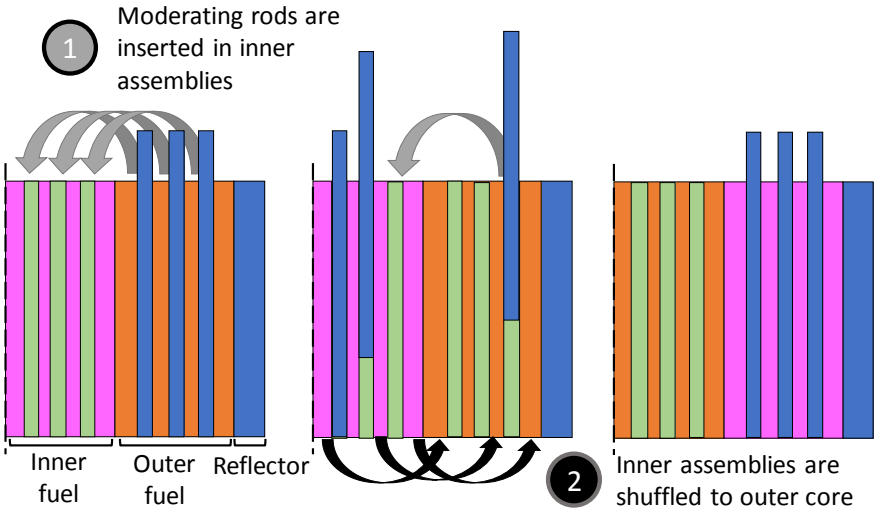

Figure 5.2: Illustration of the shuffling mechanism for inter-assembly configurations in r-z core cross-section. Moderating rods (blue) are taken out of the outer assemblies (orange) and fitted within coolant channels (green) in the inner assemblies (pink). Inner and outer assembly are then shuffled in this two stage process.

trated in Figure 5.3. The 'inter' case had a fuel volume of 2.12 m^3, and an internal moderator volume 0.18 m^3. The 'intra' case on the other hand, had 2.60 m^3 of fuel and 0.83 m^3 of internal moderator volumes. Despite the much larger moderator content in the intra layout (3.48 times higher), the resulting neutron spectrum in the outer assemblies was harder

than in the inter case, as seen in Figure 5.4. A substantially lower fraction of thermalized neutrons is present in the outer fuel region. The harder spectrum led to a higher plutonium quality, as highlighted in Figure 5.5(a). Additionally, while the intra-assembly configuration held a much higher fuel fraction (23.9% increase), its k_{eff} curve saw a substantial penalty relative to the inter-case (Figure 5.5(b)). The results appear to indicate that the inter-assembly layouts should be preferred moving forward. These configurations showed reduced plutonium quality and higher eigenvalue evolution for a reduced total core volume.

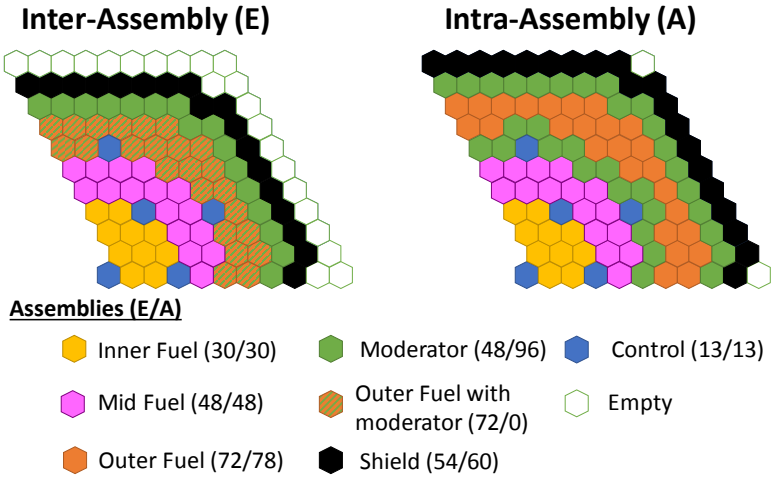

Figure 5.3: Diagram of the inter and intra-assembly layout considered with the REBUS code. A 1/3 core symmetry is assumed by the code.

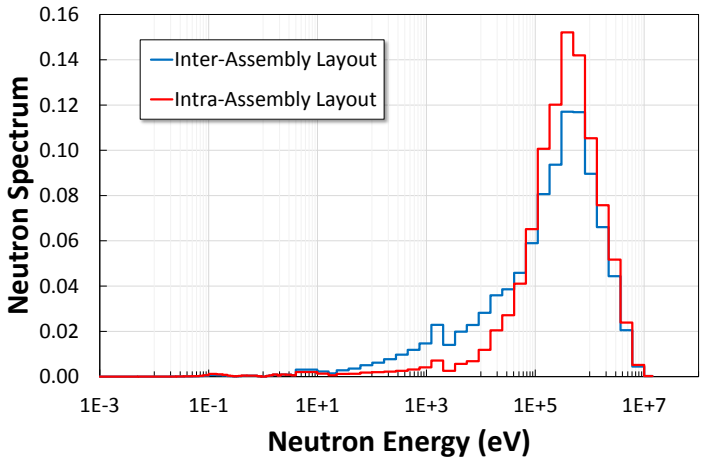

Figure 5.4: Comparison of the outer core neutron spectrum for the inter and intra-assembly moderation configurations. Results obtained using the *REBUXS* script.

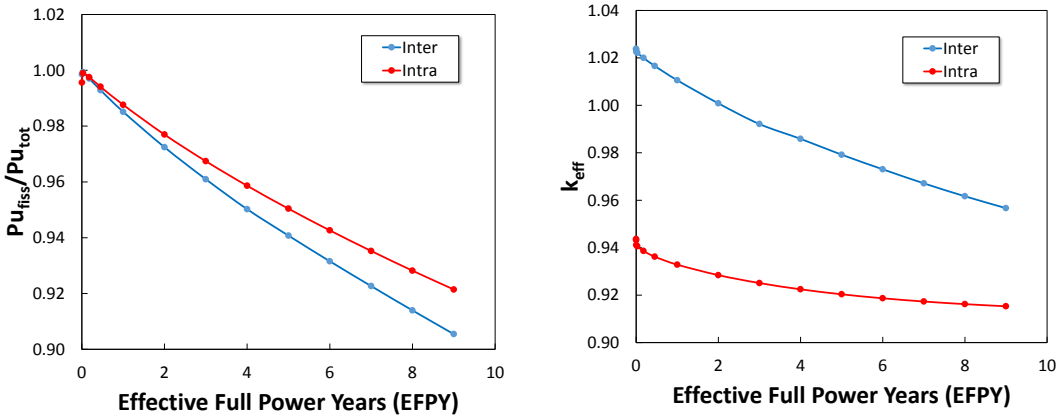

(a) Plutonium quality evolution.

(b) k_{eff} evolution.

Figure 5.5: Eigenvalue and plutonium ratio evolution in the inter and intra-assembly configurations.

The main underlying phenomena that explains the difference in spectrum between the two cases, is the variation in the neutron mean free path. As neutrons become more thermalized, the distance they can travel before interacting with a nucleus is drastically reduced. Equation 5.1 shows a good estimate for evaluating this value at different energy. ^{238}U dominates interaction in fuel assemblies, and its $1/\Sigma_t$ is indicative of the evolution of the neutron mean free path per energy group. As highlighted in Figure 5.6, at high energy groups, a neutron has a mean free path larger than half an assembly pitch (typically around 8 cm). This means that a neutron born within the center of an assembly is more likely to interact in a nearby assembly then the one it is born in. As the neutron is thermalized, the distance it can travel without ^{238}U absorption becomes smaller. At epithermal energies seen in the MXR (0.1 to 10 keV), neutrons tend to travel much shorter distances. As such, in an intra-assembly layout, a neutron that is thermalized in a moderating assembly, is much less likely to travel back to a fuel assembly. In inter-assembly configurations however, a neutron is thermalized within the assembly volume and needs to travel a mere few cm in order to reach a fuel rod. The end result is the more thermalized spectrum for inter-assembly

layouts shown in Figure 5.4.

$$\bar{l} = \Sigma_t \int_0^\infty dx x e^{-\Sigma_t x} = \frac{1}{\Sigma_t} \tag{5.1}$$

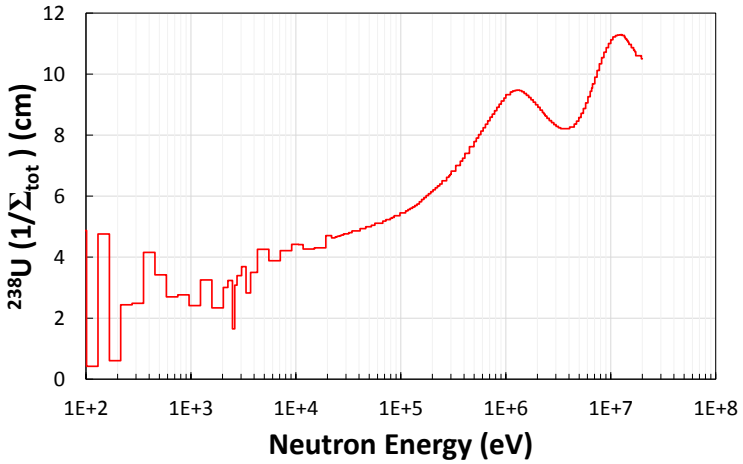

Figure 5.6: Evolution of the value for $1/\Sigma_t$ in ^{238}U with incident neutron energy. The value is a proxy for mean free path of neutrons traveling in a ^{238}U filled medium at a given energy. A typical atomic density for ^{238}U in a Sodium-cooled Fast Reactor assembly was used (1.5×10^{-2} at/b-cm). The 200 Group-collapsed Σ_t values were obtained using SCALE 6.1.[64]

5.1.2 Inter-assembly moderator parametric study

Since the previous analysis concluded that inter-assembly moderation is more effective at reducing plutonium quality, it will be the main focus of further analysis. This section will evaluate ideal moderator configurations in inter-assembly designs. Because the analysis only requires assembly-level simulations and needs to account for assembly heterogeneities, MCNP6 is employed. A first step is comparing different moderator types against each other. Five materials are considered: $ZrH_{1.6}$, graphite (C), BeO, MgO and $ZrD_{1.6}$ (i.e. ZrH with deuterium instead of tritium). The most common moderator, H_2O, is not considered due to problematic chemical reactions with the sodium coolant. Figure 5.7 highlights the effect of different moderators on the plutonium quality and their subsequent effect on k_∞. The moderating rod to fuel rod ratio is maintained constant in each of the 5 cases. With

the most thermalized spectrum, $ZrH_{1.6}$ is the most effective at reducing plutonium quality (due to an increase in ^{239}Pu σ_a/σ_f ratio). A more thermal spectrum induces an increase in the fissile cross-sections, and decrease in the breeding ratio. Hence k_∞ for an assembly with $ZrH_{1.6}$ starts at the highest relative value, but the drops the fastest out of the cases considered.

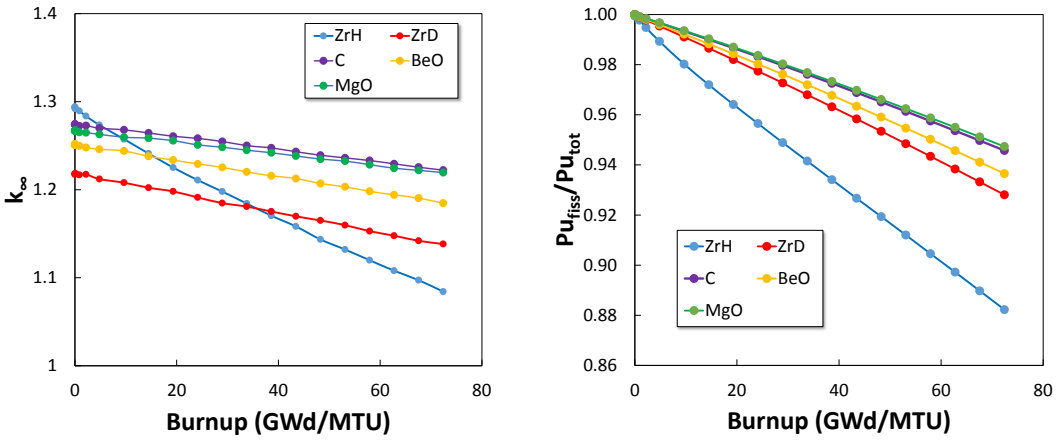

(a) Moderator type effect on k_∞ evolution. ($\overline{sd}$ = 60 pcm)

(b) Moderator type effect on Pu quality.

Figure 5.7: Effect of moderator types on k_∞ evolution and plutonium quality in assembly-level MNCP6 simulations. Each data point corresponds to the linear slope value of the corresponding parameter against burnup (e.g. With 15% moderating rod k_∞ with burnup slope is -0.0028 $(GWd/MTU)^{-1}$).

Understanding the underlying difference between moderator types requires a deeper look into nuclear scattering characteristics. A single neutron collision with a smaller nuclei (such as ^{1}H) results in a substantially greater loss of energy than a collision with a larger nuclei. The parameter quantifying this is the mean lethargy gain per collision, ξ. The parameter is a function of nuclear weight. Combined with the scattering cross-section, the moderating power ($\xi\Sigma_s$) of each moderator type can be inferred. Similarly, the ratio $\xi\Sigma_s/\Sigma_a$, is defined as the moderating ratio, and provides insight as to how effective a nucleus is at slowing down neutrons versus parasitically absorbing them. These parameters are tabulated in Table 5.1, along with the number of collision required for a neutron born at 2 MeV to reach 100 eV (epithermal bound) estimated using Equation 5.2. The values are

Table 5.1: Moderating power, ratio and number of collisions needed for a neutron to scatter down from 2 MeV to 100 eV. 2200 m/s cross-sectional data obtained from Duderstadt and Hamilton.[65]

	$\xi\Sigma_s$	$\xi\Sigma_s/\Sigma_a$	# coll.
H in $ZrH_{1.6}$	2.213	6.705	9.903
D in $ZrD_{1.6}$	0.191	574.108	13.660
Be in BeO	0.087	8.675	57.915
C in graphite	0.061	1.522	62.680
Mg in MgO	0.016	0.226	122.115

approximative, but are indicative of the neutron behaviour in each of these elements. Even though $ZrD_{1.6}$ has the highest moderating ratio, its moderating power is several times lower than that of $ZrH_{1.6}$. Assemblies containing $ZrH_{1.6}$ have the most thermalized spectrum and lowest plutonium quality, at the other end is MgO with the lowest moderating power. Since the primary objective of the optimization is to reduce plutonium quality, $ZrH_{1.6}$ was chosen as the main moderator type in further core optimization.

$$\#coll. = \frac{\ln\left(\frac{E_1}{E_2}\right)}{\xi} \tag{5.2}$$

The next step is to estimate a suitable fraction of moderator in the inter-assembly configuration using $ZrH_{1.6}$. A sensitivity analysis on the fraction of rods replaced with moderating material was conducted. The four cases considered are highlighted in Figure 5.8. Arrangements with good dispersion of moderating rods is favored; further analysis of moderator arrangement within assembly will be conducted in Section 5.3. The cases considered here had respectively, 5%, 15%, 25%, and 35% of their fuel rods replaced with moderating ones. The analysis is also conducted in MCNP6 since assembly-level simulations are less computationally taxing. Figure 5.9 shows the relative effects on the slopes of k_∞ and the Pu_{fiss}/Pu_{tot} ratio. The slopes against burnup are a good indicator of 'how fast' the plutonium quality drops and the eigenvalue drops with burnup. An asymptotic behavior in both

cases is observed, with increases in moderator volume fractions contributing to relatively less pronounced effects to the slopes. In other words, increasing the rod fraction from 5 to 15% results in a 50% faster drop in plutonium quality; passed a 25% moderator fraction, only minor variations in slopes are recorded. It should be noted that changes in the k_∞ slope were proportional to that of the plutonium quality. A compromise at 15% rod fraction was selected to be the main focus of the whole-core optimization conducted in the next section. Fractions above this were still considered, but to a lesser extent.

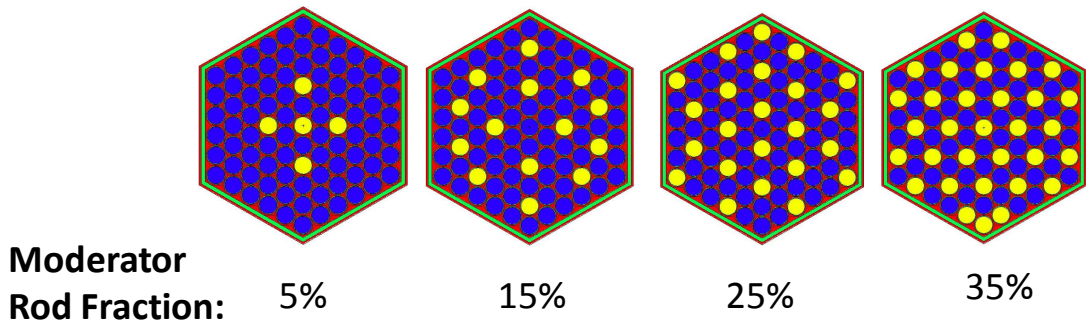

Figure 5.8: Diagram of the different moderator rod fraction considered in the parametric study. Visualization using the VISED tool. Fuel rods are highlighted in blue, and moderator rods in yellow.

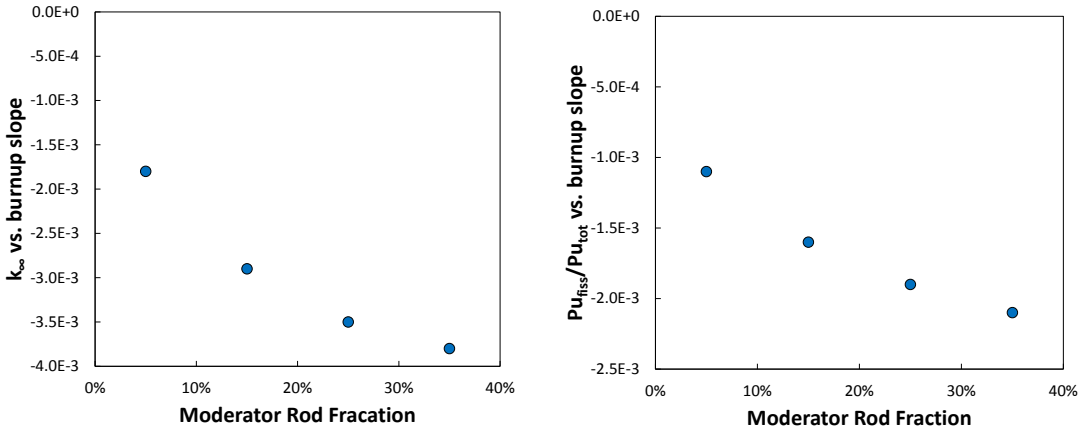

(a) k_∞ versus burnup slope.

(b) Pu quality ratio versus burnup slope.

Figure 5.9: Effect of increasing moderator rod fraction inside assembly model on k_∞ evolution and plutonium quality.

5.2 Core-Level Optimization

With the main aspects of the moderator arrangement within the core established, the analysis can now proceed to core-level optimization. The *REBUXS* script with REBUS is used here to screen through different options at a faster pace than MCNP6. Once ideal configurations are identified, more in-depth performance evaluation will be conducted in Section 5.4. The main objective at this stage is to identify a core model that can simultaneously extend the time its eigenvalue is maintained above unity, and reduce the plutonium quality in the outer region. Shuffling is not considered at this stage. While many different core designs were evaluated, only the most relevant are summarized here for brevity.

5.2.1 Thermalization search

As previously explained, simultaneously improving core longevity and reducing plutonium quality are competing design objectives. As such, the challenge is subdivided into looking at plutonium quality firsthand (this subsection), then focusing on longevity in Section 5.2.2. While the inter-core arrangement was shown to be more efficient in reducing plutonium quality, other aspects of moderator insertion need to be vetted. Three cases are considered in this section, all of which are based on the geometry specified for the LLR model. In the first case, 15% of rods in the outer core region are replaced with moderating ones containing $ZrH_{1.6}$. The inner and mid core regions have 15% rods replaced with 'empty' coolant-filled channels. The second case increases the moderator rod content to 25% to further investigate the results of Section 5.1.2. Lastly, the third case is similar to the first, but moderating rods are inserted in the inner and mid region, while the outer core contains 15% empty rods, as shown in Figure 5.10. This is to evaluate the effect of the location of the thermalized zone within the core.

The results are highlighted in Figure 5.11. The plutonium quality drops substantially when the moderator content is increased to 25%, but this is at a substantial cost to the

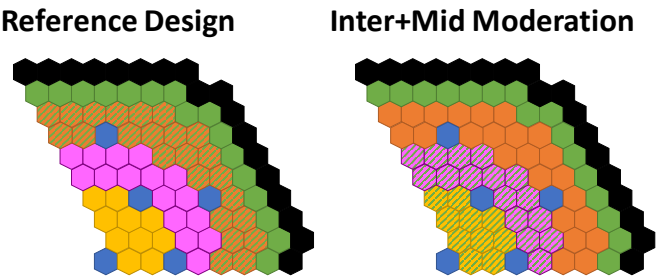

Figure 5.10: Diagram of the reference design with (15% or 25% $ZrH_{1.6}$ rod fraction) and the inner plus mid region moderation case. The hatched assemblies are the ones with moderator inserted (inter-configuration).

core eigenvalue. The higher moderator content case reaches k_{eff}=1.0 very quickly, and the slope is much more pronounced than the original case. No noticeable increase in the starting eigenvalue was observed despite the increase in moderator content. The 25% case was deemed to be an unfeasible starting point for a long-lived core design. Placing moderating material in the inner regions was similarly limited. No noticeable improvement in plutonium quality reduction is registered, while the k_{eff} drops as fast as the case with 25% moderating rods (albeit the starting eigenvalue is higher).

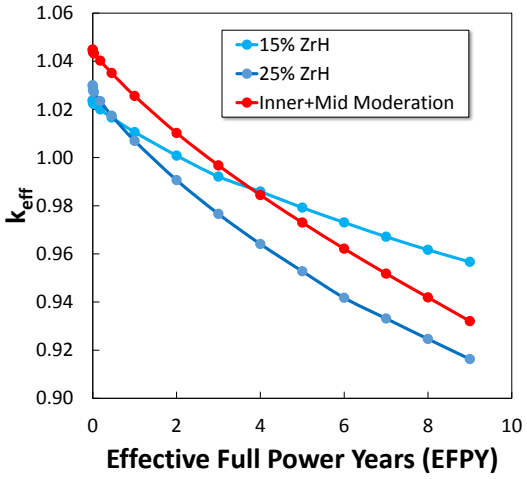

(a) k_{eff} evolution with burnup.

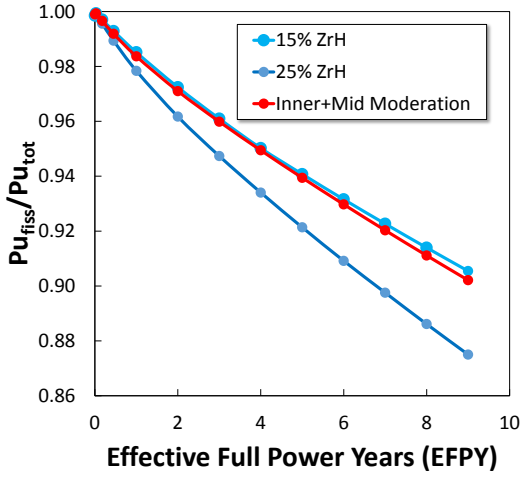

(b) Pu quality evolution with burnup (within zone with moderator inserted).

Figure 5.11: Comparison of k_{eff} and plutonium quality for 1/3 core model with 15% $ZrH_{1.6}$, 25% $ZrH_{1.6}$, and moderating rods inserted in the inner plus mid core region rather than the outer (with 15% $ZrH_{1.6}$).

From these three cases, it can be concluded that a 15% moderating rod fraction is still preferred; with moderated assemblies located in the outermost regions of the core. This configuration sees the slowest drop in eigenvalue, while still recording a significant reduction in plutonium quality. The next step will be to shift the k_{eff} curve upward by increasing fissile inventory.

5.2.2 Buckling search

This section will attempt to address the longevity of the selected core. Three competing effects are at play in the evolution of core eigenvalue: (1) the lower fissile inventory due to the reduced fuel volume fraction, (2) the drop in breeding ratio in the outer region due to spectrum softening, and (3) an increase in the initial eigenvalue due to the larger fission cross-sections in the moderated zones (because of the softer spectrum). This section will investigate different approaches for increasing the initial fissile inventory. Two options are available: increase core volume (axially or radially), or fuel enrichment.

Typically, fast reactors possess what is termed a 'pancake' layout, in light of their low height to diameter aspect ratio. A low active height is necessary due to two main reasons: it reduces the impact of coolant void positive feedback and the pressure drop accross the core. Reactivity feedback effects will be discussed in greater detail in Chapter 6; at this stage, increasing height is assumed to be acceptable in light of the results of Tsujimoto.[22] The researchers demonstrated that the addition of moderator to the outer core can reduce the coolant void coefficient. With regards to pressure drop, Equation 5.3 shows how this value is directly proportional to the fuel length. Where f is the friction factor, L the core length, and D_e the hydraulic diameter. Any increase in the active axial fuel region should result in a corresponding increase in Δp. Due to the low coolant velocity in the original LLR concept, pressure drop was estimated to be less than 10 psi.[13] Fractional increases in the

final design of the MXR are therefore assumed to be manageable.

$$\Delta p = f \frac{L}{D_e} \frac{\rho V^2}{2} \tag{5.3}$$

The reference design is the one highlighted in the previous section, with the LLR geometry and 15% moderating rod content (MXR-ref). Four other modified core geometries are considered in this section. One design variant has an increase in total core radius (MXR-rad), with one additional assembly ring at both the mid and outer regions (Figure 5.12(a)). Another variant has a 20% increased active core height (MXR-ax), with a fuel height of 132 cm (non-expanded). A third model, has an increased enrichment distribution (MXR-enrich) highlighted in Figure 5.12(b). Relative to the LLR base model, the lower and upper outer assembly enrichment was increased from 15% to 18%, and the central mid region enrichment was increased from 10.5% to 14.5%. Lastly, a final case combined all of these modifications together in one design (MXR-combine). The resulting fissile inventory and heavy metal volume for each of the four cases is highlighted in Table 5.2.

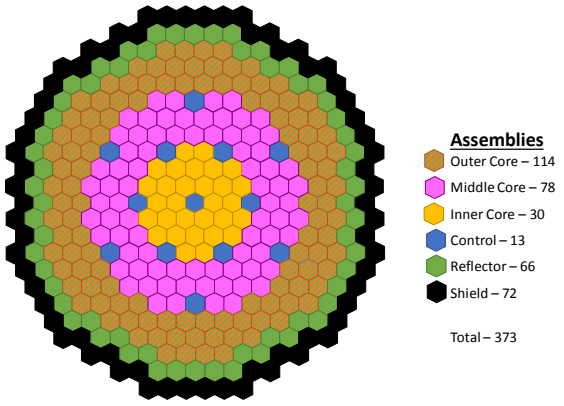

(a) Modified assembly configuration (MXR-rad).

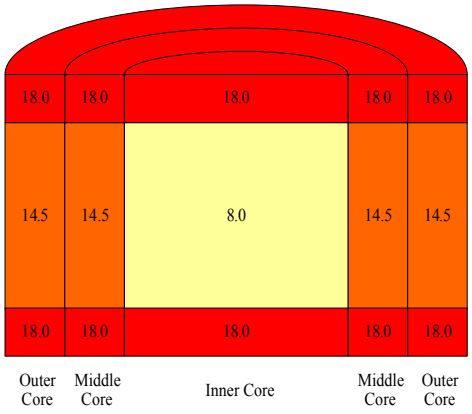

(b) Modified enrichment (w%) in zones (MXR-enrich).

Figure 5.12: Diagrams of the modified core layout and enrichment zones of the MXR models.

In all of the cases, the total power per assembly value was held constant. As a result, the power output in MXR-rad and MXR-combine was increased from 250 to 370 MW_{th}.

Table 5.2: Heavy metal (HM) volume and fissile inventory in the different geometries considered.

Case Name	Description	HM vol.	Fissile inv.
LLR	original fast design	2.501 m^3	3.317 t
MXR-ref	15% ZrH rods	2.117 m^3	2.907 t
MXR-rad	MXR-ref with 9 assembly rings	3.133 m^3	4.363 t
MXR-ax	MXR-ref with 1.2×length	2.540 m^3	3.488 t
MXR-enrich	MXR-ref with higher enrichment	2.117 m^3	3.085 t
MXR-combine	combined MXR modifications	3.759 m^3	5.583 t

This was deemed to be a suitable assumption in terms of power density scaling, and will be revisited in Chapter 6. The four MXR cases highlighted in Table 5.2 were simulated using the *REBUXS* code. The resulting performances are shown in Figure 5.13. Each of the highlighted modifications contributes to increasing the eigenvalue evolution. It is interesting to note that most k_{eff} slope are parallel to one another, with the exception of the MXR-enrich case. This can be explained by the reduction in breeding ration due to the lower ^{238}U content. Control rod shut-down margins are not taken into consideration at this stage and will be investigated further in later design iterations (see Chapter 7). Combining all of the proposed modifications leads to a 10,421 pcm increase relative to the MXR-ref case. The increase is entirely driven by the 68% higher fissile inventory. Despite a slightly purer plutonium quality than the reference case, it is concluded that MXR-combine is the most attractive configuration evaluated. Its geometry and specifications will be the main focus of further optimization work in this section.

5.3 Effects of Inter-Assembly Arrangements

Design optimization thus far has not taken into account assembly heterogeneity effects. Previous results recommended that moderating material should be inserted within the assemblies, replace 15% of rods, and use $ZrH_{1.6}$. Different arrangements of these rods while preserving total fuel content can still have an effect on the resulting performance. Fig-

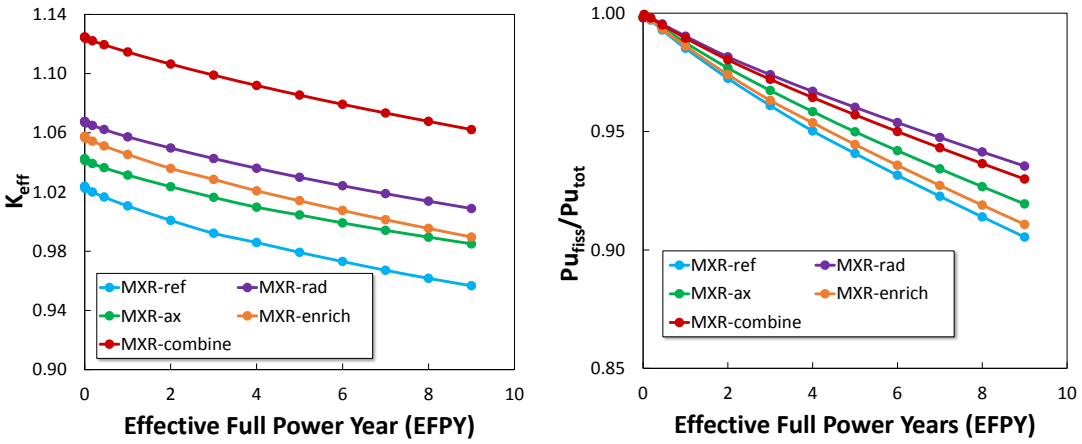

(a) k_{eff} evolution with burnup.

(b) Outer assembly Pu quality evolution with burnup.

Figure 5.13: Comparison of k_{eff} and plutonium quality for the four cases highlighted in Table 5.2.

ure 5.14 highlights different rod placements considered and their corresponding labels. MCNP6 assembly-level depletion simulations were conducted to analyze their effects on k_∞ and plutonium quality. The results are highlighted in Figure 5.15 for the corresponding cases. It appears that certain clustering of rods tends to simultaneously improve in eigenvalue evolution while reducing plutonium quality further. The most clustered arrangement, Inter5 shows the best performance on both fronts, followed by Inter3 and Inter4 respectively. This is despite the fact that Inter1 posses the most thermalized spectrum within the fuel rods as highlighted in Figure 5.16. Despite of its softer spectrum, the Pu_{fiss}/Pu_{tot} ratio evolution of Inter1 is the least steep, suggesting the two parameters are not completely correlated. The results seem to indicate that clustering of rods is desirable from the perspective of the two main design objectives. It should be noted that while deviance in the slope of the Pu_{fiss}/Pu_{tot} ratio are observed between the five cases, they are only of the order of several percentage points and are not substantial.

Clustering of fuel rods also presents another advantage; rather than using multiple small rods, a handful of larger moderating rods can be used within the assembly. This makes it possible to increase total moderating volume while maintaining the fuel rod content con-

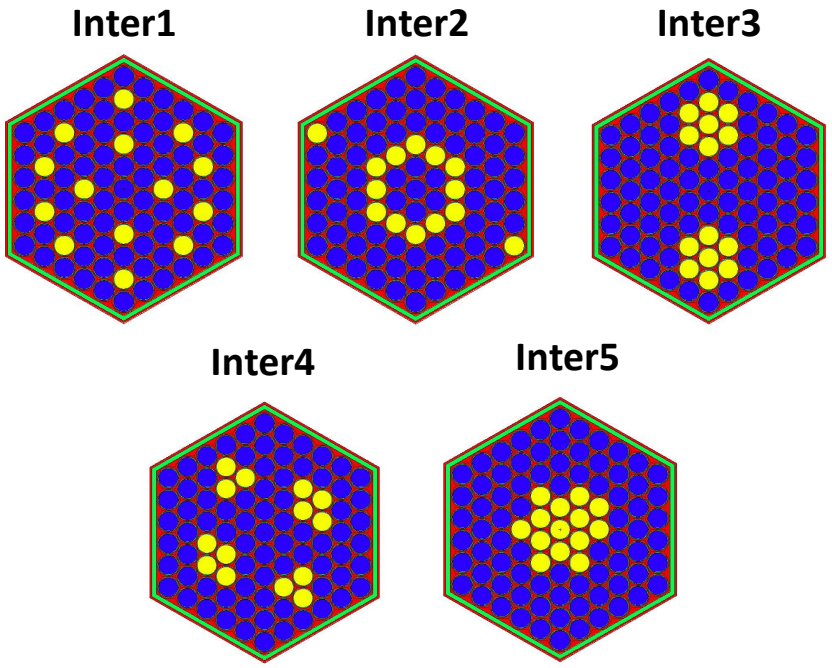

Figure 5.14: Different moderating rod arrangements with a maintained fuel rod fraction of 85%.

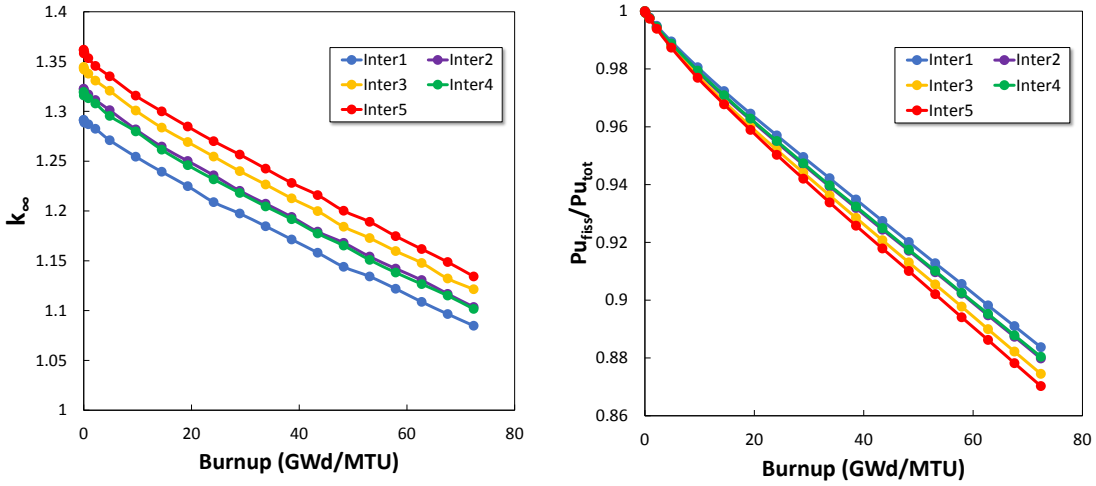

(a) Eigenvalue evolution.

(b) Plutonium quality ratio.

Figure 5.15: Effect of moderator rod arrangement within assembly on k_∞ and plutonium quality. Assembly-level simulations had an average standard deviation of 75 pcm.

stant. Lumped fuel rod arrangements for Inter3, 4 and 5 are shown in Figure 5.17. Having less moderating rods per assembly is also attractive from a shuffling standpoint since less

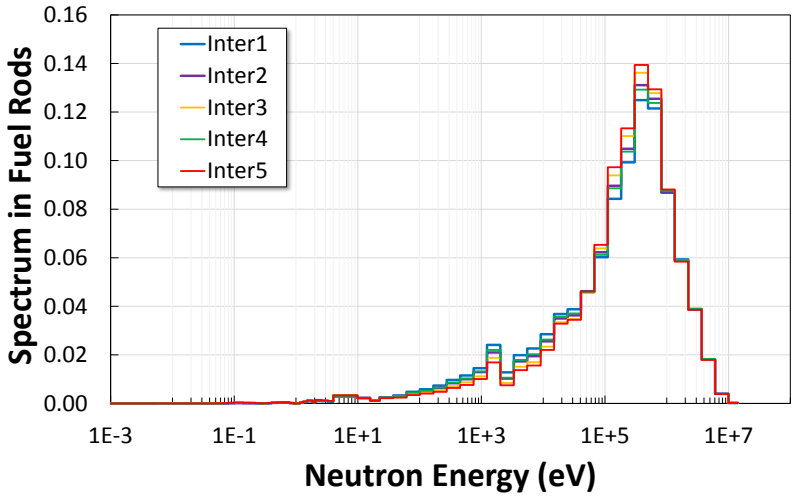

Figure 5.16: Neutron spectrum variations with different moderator arrangements within the assembly. Standard deviations for the total tallied flux were no more than 0.08%.

rods will need to be handled and taken in and out of assemblies. The resulting effects on k_∞ are not negligible as shown in Figure 5.18(a). The final k_∞ sees an improvement of 2054, 1885, and 3287 pcm for Inter3, 4 and 5 respectively. The Pu_{fiss}/Pu_{tot} sees small increase due to lumping for the most part, with the exception of Inter3 which sees a 1.1 percentage point reduction at the final timestep. It is interesting to note that while Inter3 shows indeed an increase in total moderator volume by 14.6%, Inter 4 and 5 see a net reduction in moderator volume of 16.5 and 15.1% respectively. This is due to the inefficient fitting of a single moderating rod in a hexagonal array as can be seen in Figure 5.14. From these results, it appears that Inter3-lump and Inter5-lump have the most improved k_∞ performance with slightly reduced plutonium quality over the original Inter1 case. Further analysis and optimization work will focus on these three cases.

Witnessing such large changes in performances, for seemingly small modifications to the assembly layout, can be explained by spatial shielding effects at the resonance region. In an epithermal spectrum, uranium and plutonium resonances have a much more prevalent effect on the overall system. As spatial self-shielding becomes more overriding, small changes in geometry can yield relatively large increases to absorption and fission reactions at specific energy groups. Figure 5.19 highlights the variation in flux distribution in the rel-

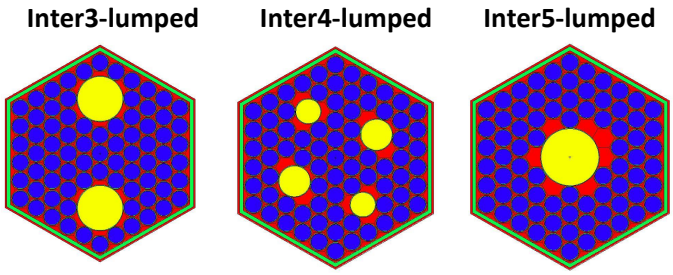

Figure 5.17: Illustration of the three lumped moderating rods cases with larger diameter rods.

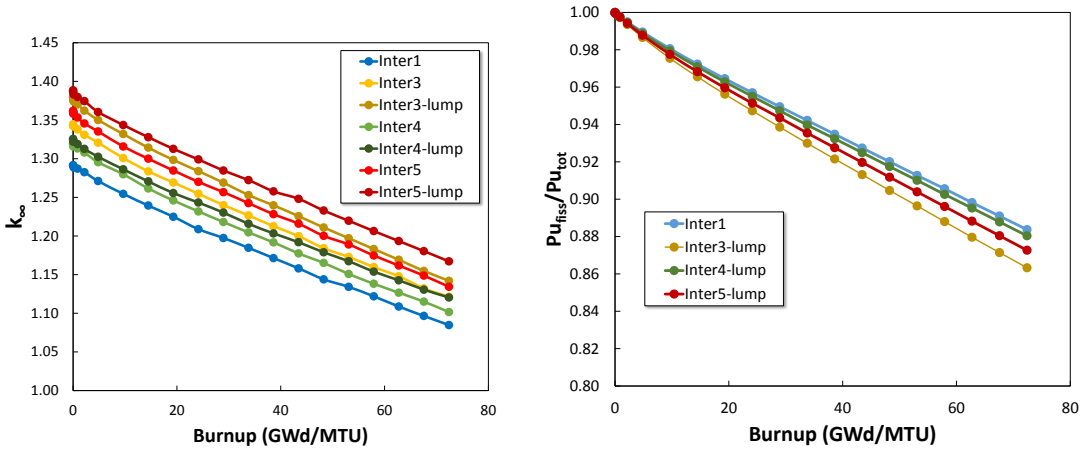

(a) Eigenvalue evolution.

(b) Plutonium quality ratio.

Figure 5.18: Effect of lumping moderating rod into larger rod. Assembly-level simulations had an average standard deviation of 77 pcm.

evant resonance region for three cases. These different contour maps explain the variations in the group-collapsed cross-sections shown in Table 5.3 for each case. As highlighted, Inter3-lump and Inter5-lump see a large increase in their fission cross-section, which can explain the higher initial k_∞ value. Inter5-lump has the edge over all other cases however, due to its reduced ^{238}U capture cross-section, which results in a breeding penalty, as discussed later. The ratio of the ^{239}Pu σ_c to σ_f is correlated to final plutonium quality after depletion. The case with the highest ratio sees the steepest Pu_{fiss}/Pu_{tot} curve. Leveraging these spatial shielding effects at core-level will be analyzed further in Section 5.4.

In a typical fast reactor, increasing core lifetime revolves around increasing the breeding

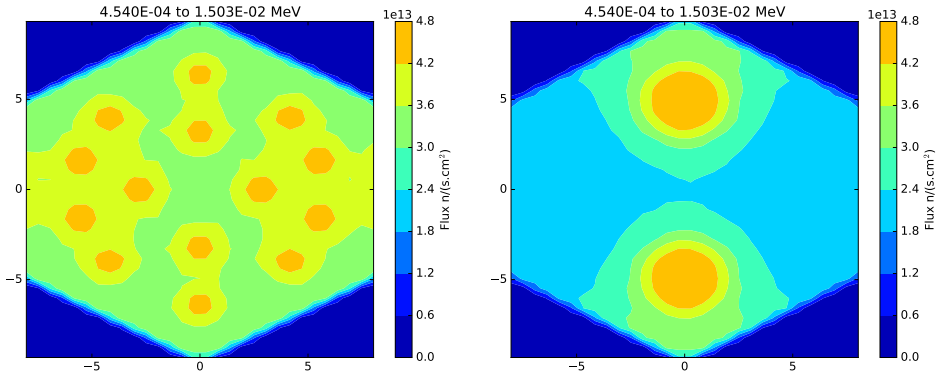

(a) Inter1.

(b) Inter3-lump.

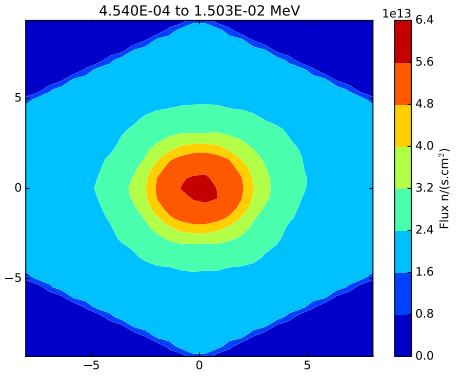

(c) Inter5-lump.

Figure 5.19: Neutron flux distribution at the epithermal energy group of interest in this analysis. All three contour plots are scaled to the same limits. FMESH tally errors at this energy group averaged 0.73%. Mesh tally sizes were 0.55×0.55×20.0 cm.

ratio achievable to ensure sufficient fissile material is generated as some is burned. In the MXR however, reaching this goal is essentially a tradeoff between starting at higher criticality and slowing the k_∞ drop with burnup. Adding moderator increases the initial k_{eff}, but this tends to have a negative impact on the breeding ratio, thus rendered the slope steeper. To highlight this effect, Figure 5.20 shows the evolution of the breeding ration, BR in the three main Inter cases. Because MCNP6 is unable to systematically output the BR value for a configuration, this must be calculated externally using Equation 5.4 using the reaction rates, R_X, for each relevant isotope. Only the main ^{238}U production chain is considered, since other transuranic production chains only play a minor role in fissile breeding. Breeding ratios are estimated at the corrector step of each depletion timestep

Table 5.3: Tallied microscopic cross-sections in barns for each of the main three Inter cases considered.

	Inter1	**Inter3-lump**	**Inter5-lump**
^{238}U σ_c (b)	0.3230 ± 0.0003	0.2836 ± 0.0003	0.2530 ± 0.0002
^{235}U σ_f (b)	3.1158 ± 0.0029	3.4499 ± 0.0030	2.9851 ± 0.0023
^{235}U σ_c (b)	1.0916 ± 0.0012	1.0685 ± 0.0010	0.8796 ± 0.0008
^{239}Pu σ_f (b)	4.3354 ± 0.0080	6.2005 ± 0.0116	5.1601 ± 0.0096
^{239}Pu σ_c (b)	2.1767 ± 0.0054	3.1665 ± 0.0078	2.4796 ± 0.0063
^{239}Pu σ_c/σ_f	0.5021 ± 0.0016	0.5107 ± 0.0016	0.4805 ± 0.0015

in MCNP6 (Note that MCNP6 does not output reaction rates at the final timestep). It can be clearly seen from Figures 5.20 and 5.18(a), that while Inter1 has the highest BR value, this does not outweigh its lower starting k_∞. Inter5 shows the longest lifetime, despite displaying the lowest BR value. It should be noted that the upward trend of the BR curve is due to the higher η value of ^{239}Pu relative to ^{235}U.

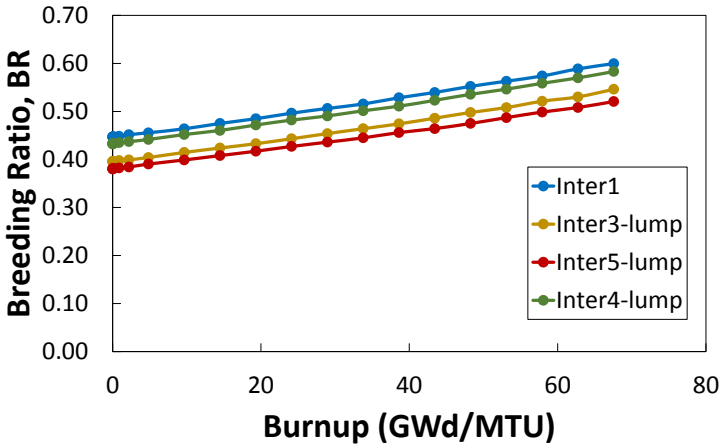

Figure 5.20: Evolution of the breeding ratio for different Inter arrangements.

$$BR = \frac{[R_a(^{238}U) + R_a(^{238}Pu) + R_a(^{240}Pu)] - [R_a(^{239}Np)]}{R_t(^{235}U) + R_t(^{239}Pu) + R_t(^{241}Pu)} \tag{5.4}$$

where

$$R_y(X) = \phi\Sigma_y(X) \tag{5.5}$$

Another pertinent observation is how few neutrons travel further than the periphery of the moderating ring at low-energies. This illustrates the point made in Section 5.1.1 about the reduced mean free path of slower neutrons which makes intra-assembly moderation ineffective. It can be clearly seen from Figure 5.21(b) that neutrons that have scattered down to near-thermal energies at the central moderator region, cannot even make it to the outer edges of the assembly. This illustrates the advantage of placing moderating material within the assembly geometry, in order to ensure low energy neutrons can still reach fuel rods.

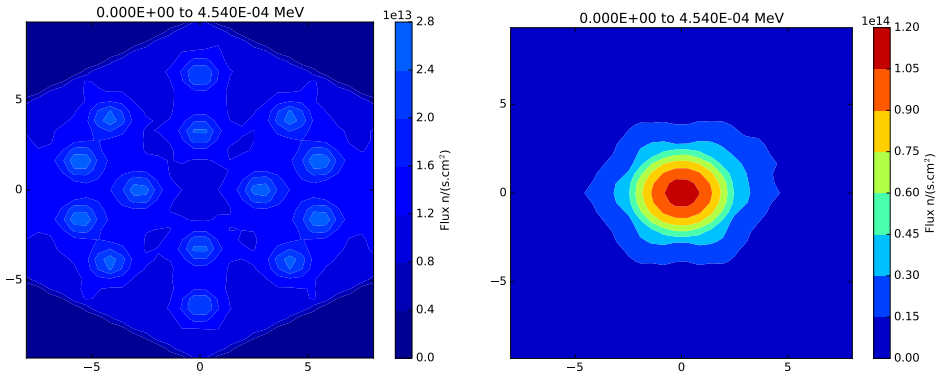

(a) Inter1. (b) Inter5-lump.

Figure 5.21: Thermal neutron flux distribution with identical color plot scaling. FMESH tally errors at this energy group averaged 1.17%.

5.4 Optimal Core Characteristics

With the moderator arrangement finalized, and the core geometry settled, full-core MNCP6 depletion analyses were conducted. Taking on the lessons from Sections 5.2 and 5.3, three main core configurations were arrived upon. The overall core geometry relies and enrichment of MXR-combine (see Table 5.2) was used. The inter-assembly moderating rod

Table 5.4: Comparison of the specifications of the optimal MXR core versus the original LLR layout. Note that highlighted dimensions are not thermally expanded, but values such as power density are estimated for the expanded condition.

	MXR-inter1	**LLR**
Thermal Power	370 MW_{th}	250 MW_{th}
Coolant T_{in}/T_{out}	395/550°C	395/550°C
Active core height	132 cm	110 cm
Core equivalent radius	171.7 cm	149.7 cm
Assembly pitch	16.5 cm	16.5 cm
Rod diameter	0.745 cm	0.745 cm
Fuel assemblies	222	150
Fuel/Moderating rods	77/14	91/0
Heavy metal inventory	37.0 t	24.6 t
Average enrichment	15.1%	13.5%
Average power density	48.6 kW/l	58.3 kW/l
Average specific power	10.0 MW/t-HM	10.1 MW/t-HM
Fuel enrichment:	upper-central-lower	upper-central-lower
- Inner region	- 18.0- 8.0-18.0%	- 18.0- 8.0-18.0%
- Mid region	- 18.0-14.5-18.0%	- 18.0-10.5-18.0%
- Outer region	- 18.0-14.5-18.0%	- 15.0-14.5-15.0%

configuration leverages the conclusions of the previous sections. Three moderating rod arrangements, Inter1, Inter3-lump, and Inter5-lump, were selected for whole-core analysis. The resulting whole core MXR modeled are correspondingly labeled MXR-inter1, MXR-inter3, and MXR-inter5. It should be noted that the MXR-inter5 has one additional fuel rod compared to the other two (85.7% fuel rod fraction instead of 84.6%) that can fit in the North-Eastern corner of the diagram in Figure 5.17. Whole-core level analysis was performed using MCNP6 to accurately capture spatial self-shielding effects at this level. The design specifications of the MXR-inter1 are highlighted in Table 5.4. The main differences with the other MXR layouts are the number of moderating rods (two for MXR-inter3, 1 for MXR-inter5) and fuel rods (same for MXR-inter3, 78 for MXR-inter5).

The effect of neutron thermalization can be clearly seen in Figure 5.22, with two distinct spectra in each core region. This illustrates the dual-spectrum nature of the MXR. The

proportion of neutrons larger than 100 keV in the outer region is around 79%, noticeably lower than that of a typical fast reactor. More detail flux maps at beginning-of-life (BOL) are shown in in Figure 5.23 for different energy groups. The thermalized regions appear almost distinctly in Figure 5.23(b), at the energy group between 0.4 and 15.0 keV. These epithermal neutrons are localized to the outer core region, and do not leak substantially to the mid-core regions. The region at the fast-thermal interface sees the highest fast and total flux values. This is the zone of highest neutron importance, and will see the highest level of power peaking as discussed later in Chapter 6. Thermal neutrons only appear at the radial reflector assembly (they are filled with $ZrH_{1.6}$), power peaking effects there will require further investigating. Lastly, it is interesting to note that 'prompt'-energy flux peaks solely in the thermalized assembly rings (where the epithermal flux peaks as well). This is due to the sharp drop of the hydrogen scattering cross-section at these energy ranges, leading to a preferentially higher proportion of these neutron energies than in other regions (the same phenomena is observed in the high energy range of Figure 5.22).

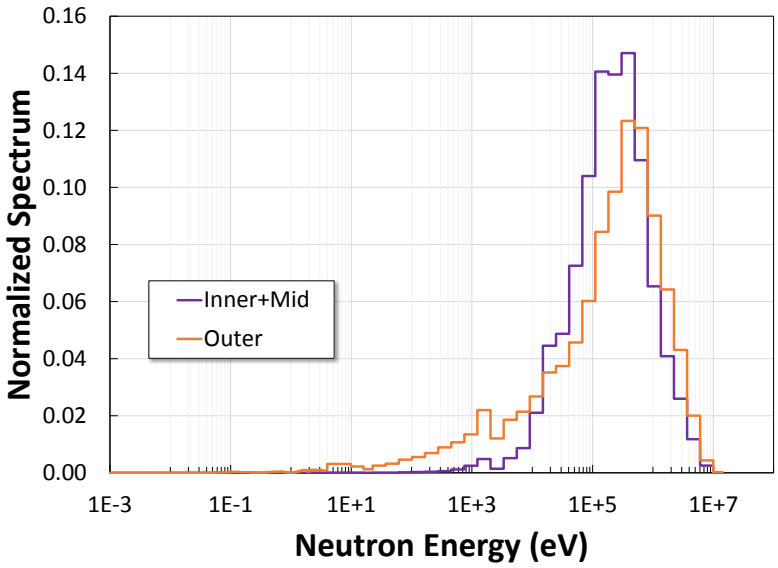

Figure 5.22: Variations in the neutron spectrum of the MXR-inter1 core design between the fast (inner+mid) and thermalized (outer) regions. Standard deviations of the total tallied fluxes were less than 0.1%.

With a core geometry finalized, shuffling can be taken into consideration. The main

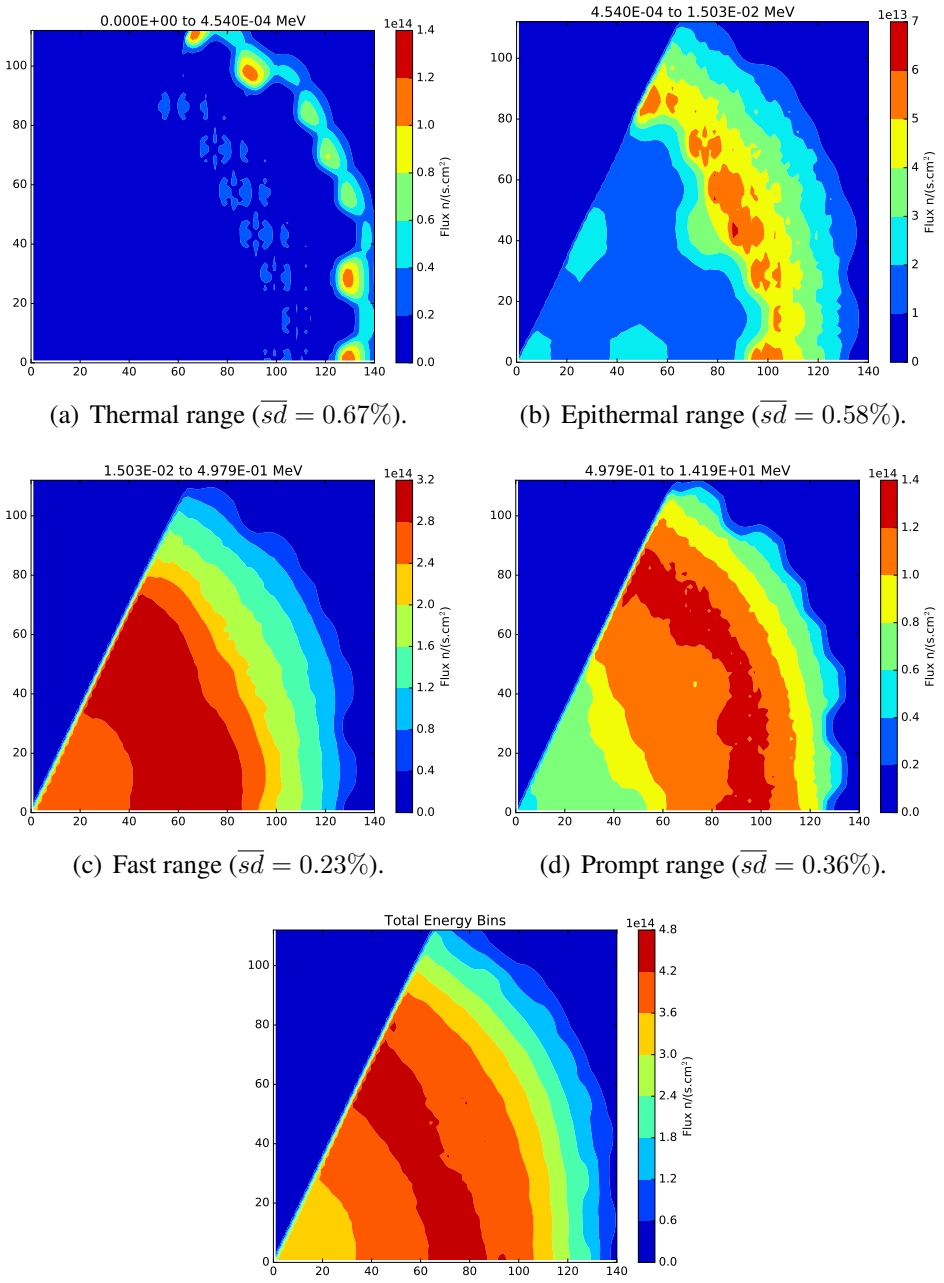

(a) Thermal range ($\overline{sd} = 0.67\%$).

(b) Epithermal range ($\overline{sd} = 0.58\%$).

(c) Fast range ($\overline{sd} = 0.23\%$).

(d) Prompt range ($\overline{sd} = 0.36\%$).

(e) Total range ($\overline{sd} = 0.20\%$).

Figure 5.23: Neutron flux distribution for different energy groups for a 1/6 model of the MXR-Inter1 design. For clarity purposes, the color gradients are not normalized to the same value. Mesh size was $1.85 \times 1.6 \times 143$ cm.

objective is to ensure that all fuel assemblies are exposed to a thermalized spectrum and therefore see a reduction in their plutonium composition. Shuffling presents other advantages in reactor design such as alleviating material damage. Assemblies that reached high

burnup can be preferentially shuffled to zones of low neutron importance to reduce their contribution, and vice versa for assemblies that were not exposed to high fluxes before the shuffling. This is desirable to avoid reaching material damage limits that will be discussed in Chapter 6. Since it is an advantage from a nonproliferation standpoint to limit access to the core, shuffling is envisaged to take place only once. The material within the outer region must reach a sufficiently reduced plutonium quality by the middle-of-life (MOL), since it will be exposed to a thermalized spectrum only once. An initial shuffling strategy was designed using trial and error; it is displayed in Figure 5.24. The main objective is to move assemblies that have generated little power (Inner core region) to the inner limit of the outer region, near the fast/thermal interface, where energy generation is the highest. Middle assemblies that see elevated power production levels are preferentially moved to the outermost regions. It should be noted that since there are 6 more outer assemblies than the sum of inner and middle ones, one assembly location remains unchanged as highlighted in Table 5.5 (assembly no. O908). Alternative shuffling strategies will be investigated further in Chapter 7.

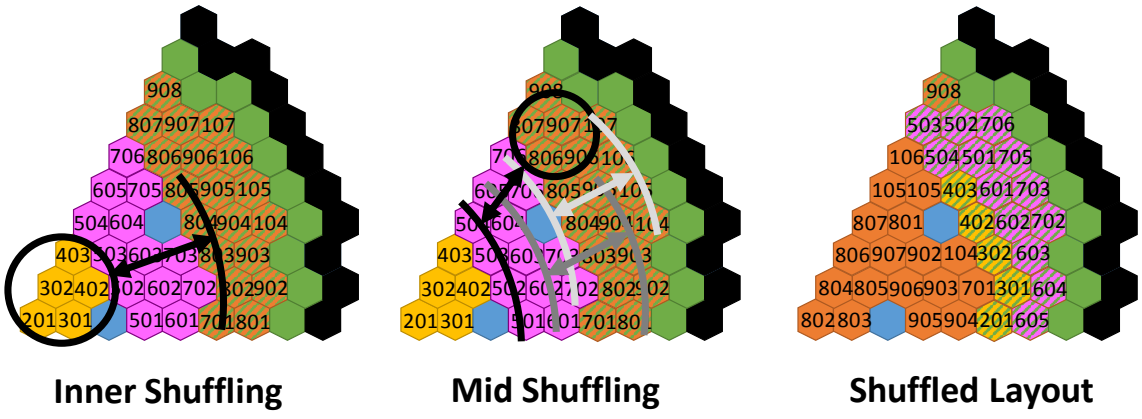

Figure 5.24: Assembly shuffling scheme with final layout illustrated. Hatched assemblies have moderating material inserted within them.

MCNP6 is unable to implicitly shuffle assemblies within a core configuration. An explicit Python script was built to extract the MOL composition form a MNCP depletion run, and build a new file with the depleted composition at the shuffled location. Test runs

Table 5.5: Listing of the original and shuffled assembly locations in a hexagonal grid.

Original		**Shuffled**
I201	→	O802
I301	→	O803
I302	→	O804
I402	→	O805
I403	→	O806
M501	→	O905
M502	→	O906
M503	→	O907
M504	→	O807
M601	→	O904
M602	→	O903
M603	→	O902
M604	→	O801
M605	→	O107
O701	→	I201
M702	→	O701
M703	→	O104
M705	→	O105
M706	→	O106
O801	→	M605
O802	→	I301
O803	→	I302
O804	→	I402
O805	→	I403
O806	→	M504
O807	→	M503
O902	→	M604
O903	→	M603
O904	→	M602
O905	→	M601
O906	→	M501
O907	→	M502
O908	→	O908
O104	→	M702
O105	→	M703
O106	→	M705
O107	→	M706

were conducted for an identical shuffling transformation (i.e. assemblies kept in the same location) to verify that results matched the original MOL eigenvalue. Because of initial deviance in fissile inventory between the outer region and the inner plus mid regions (only the mid and outer region have matching enrichment), sharp drops in eigenvalue are observed after shuffling. The drop in k_{eff} becomes more pronounced with increases in burnup before shuffling. Following multiple trials, shuffling after 13 years was concluded to be optimal. The resulting evolution in eigenvalues for each of the three cases are shown in Figure 5.25. Assemblies were shuffled in accordance with Table 5.5. The drop in k_{eff} is distinctly noticeable, and can be of the order of 3737 pcm at the extreme (MXR-inter5). Variations in the reactivity drop between each case can be attributed to a higher rate of fissile material depletion in the outer region (inner and mid concentration see little change). MXR-inter1 saw the highest outer fissile inventory at MOL, in line with the observation that the Inter1 assembly model had the highest breeding ratio. The outer fissile content is 5 and 3% lower at MOL for MXR-inter3 and MXR-inter5. This is balanced to some extent by the higher initial k_{eff} value. Ultimately, the core lifetime (defined as the year at which k_{eff} reaches 1.0) was approximately 25, 24, and 27 years for MXR-inter1, 3, and 5 respectively. MXR-inter3 has the shortest lifetime, despite having an initial k_{eff} above that of MXR-inter1.

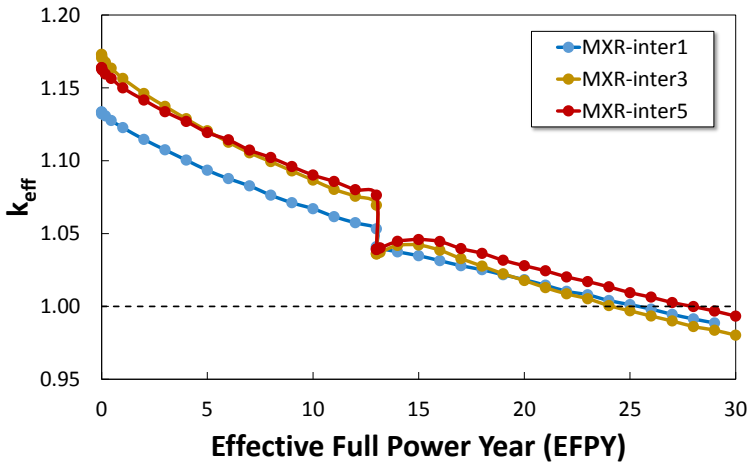

Figure 5.25: Core eigenvalue evolution for the different designs. Error bars are too small to appear on the plot. They averaged 26 pcm.

Ensuring a long-core lifetime is a primary objective alongside reducing plutonium quality. The isotopic evolution for each of the three cases are highlighted in Figure 5.26. The trends clearly demonstrate the design philosophy of the MXR. Outer assembly plutonium quality decreases rapidly and crosses the weapons grade limit prior to shuffling. The inner and mid assemblies are subjected to a fast spectrum before MOL, and their plutonium quality is maintained above the weapon-grade limit until shuffling occurs. After being exposed to the thermalized spectrum, the inner and mid-assembly plutonium drops below the weapon-grade limit. Note that at this point, inner and mid assemblies are placed in the 'outer' region, but are still referred to by the same name, for clarity. At the end-of-life (EOL), all assemblies are below the weapon grade limit, but do not cross the reactor-grade limit (reached in typical PWR). The advantage of this relative to the LLR plutonium quality will be evaluated further in Chapter 7. At this stage, it can be at least stated that the MXR composition constitutes an improvement relative to the LLR in terms of proliferation resistance. The final outer assembly plutonium composition does not differ substantially between the three cases, the isotopics appear to converge when exposed to a fast spectrum. The inner regions (that are in the thermalized zones at EOL) see a few percentage point improvements relative to MXR-inter1. All cases see substantial improvement relative to the LLR. Notably at the outer region, where the LLR quality remains above the weapon-grade limit throughout its lifetime.

Another important nonproliferation metric is the total amount of plutonium bred per assembly. Ensuring each assembly contains less than 1 SQ of material is desirable and in line with current PWR. Figure 5.27 shows the evolution of the plutonium quality for the reference LLR case, and the other three MXR models. While nearly all assemblies in the LLR reach 1 SQ by the EOL, almost none do so in the MXR cases. The only exception are the inner assemblies of MXR-inter1. The drop in production per assembly is attributed to the lower fuel volume fraction in the assemblies (to account for moderator rod insertion), and the higher fissile cross-sections leading to a reduced breeding ratio in the thermalized

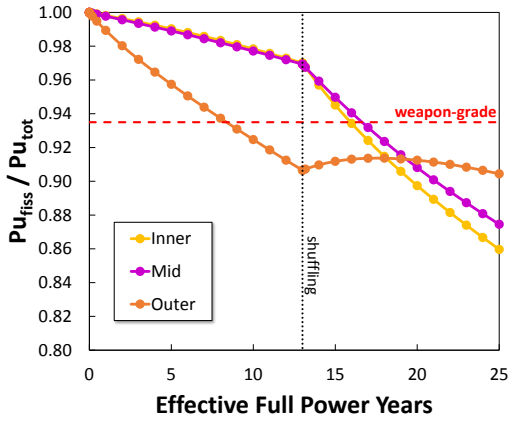

(a) MXR-inter1 regional Pu quality.

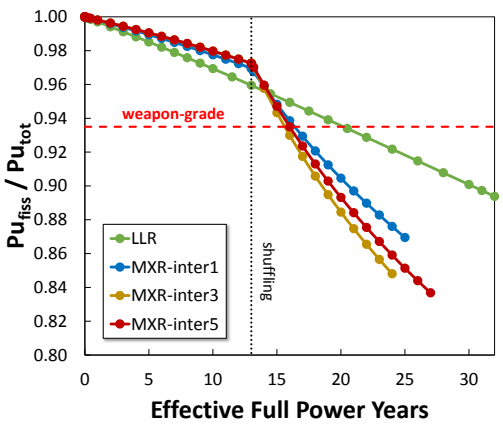

(b) Inner and mid-assembly Pu quality.

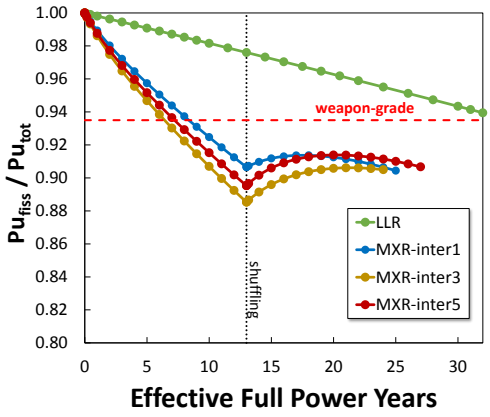

(c) Outer assembly Pu quality.

Figure 5.26: Evaluation of the plutonium quality for different MXR arrangements and in different regions. Although MXR assemblies are shuffled, the naming convention is maintained.

zone. In the case of MXR-inter3 and MXR-inter4, a potential proliferator would need to divert at least two assemblies to acquire sufficient material for a weapon. Reducing the plutonium quality even further is investigated in Section 5.5.

While the MXR designs are able to reduce plutonium quality and quantity relative to the original LLR core arrangement, some tradeoffs were necessary. To compensate for the reduction in fuel volume fraction (to make room for moderating material) and achieve buckling, the total core volume was increased as discussed in Section 5.2.2. This allowed an overall increase of 50.3% in total heavy metal inventory. The new core radius is 22 cm larger, 14.7% more than the original LLR design. The core height was also increased by

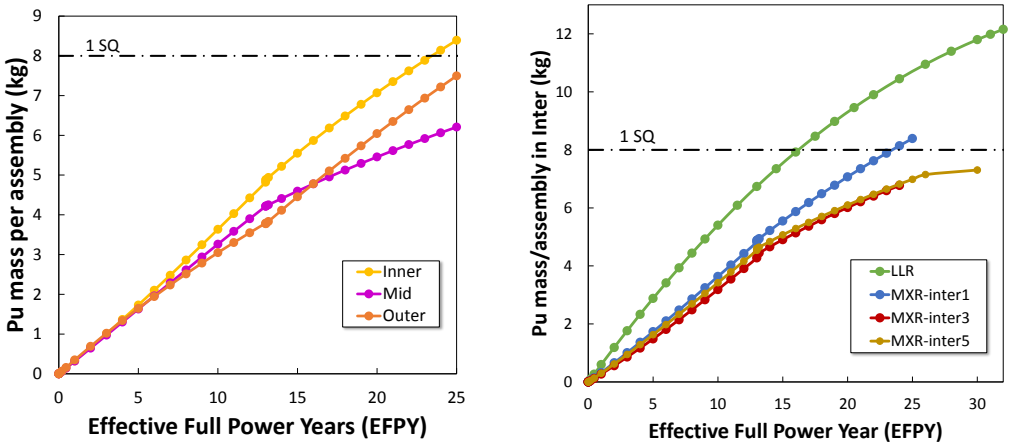

(a) MXR-inter1 Pu mass per assembly.

(b) Inner Pu mass per assembly.

Figure 5.27: Plutonium mass per assembly in the different MXR arrangements. Although MXR assemblies are shuffled, the naming convention is maintained.

20% as perviously stated. This is expected to minimally impact the transportability of the reactor. The average enrichment of the core was similarly increased to 15%, 1.5 percentage points above the original LLR value. In addition to the slightly increased size and resource requirements, the core lifetime was around 20% shorter than the base model (varied by inter arrangement). Lastly, the added complexity of shuffling the assemblies once in the core is expected to minimally impact the overall capacity factor of the reactor. On the other hand, in light of the increase in the total amount of assemblies within the core, the thermal power produced by the reactor was increased by 48% which brings a notable advantage over the LLR. Lastly, both the MXR-inter1 and MXR-inter5 arrangements stand out in the analysis. They both achieve higher reactor lifetimes, with the MXR-inter5 reaching higher levels of proliferation resistance as well. They will be subject to further analysis in Chapter 6.

5.5 Mixed U-Th and Mixed-Spectra Core

The design optimization thus far has mainly focused on plutonium quality. One of the original criticism of long-lived cores was also the large quantity of plutonium produced

per assembly.[15] This is one of the main advantages of using thorium as a substitute for ^{238}U for breeding fissile material as discussed in Section 3.2. Because the ^{233}U bread by ^{232}Th is equally attractive to a potential proliferator as ^{239}Pu, it must be denatured within a uranium mixture. As such, only mixed thorium-uranium (U-Th) mixtures will be analyzed. This section will begin by investigating the benefits of employing mixed U-Th fuel in the fast spectrum, then how to leverage the advantages of thorium in a mixed-spectrum configuration.

5.5.1 Fast U-Th core

Mixing uranium and thorium in fast reactors has been heavily investigated in the available literature.[66] Little research has been conducted on employing U-Th in a long-lived core configuration however. The uranium cycle is more efficient than the thorium cycle at producing fissile material in the fast spectrum as previously discussed. The performance advantages of doping the fuel with thorium metal mainly revolves around reducing uranium resource utilization, the amount of plutonium generated, and the overall radiotoxicity of the resulting waste. While REBUS is capable of accurately modeling thorium doped fuels in the fast spectrum, simulations were conducted with MCNP6 for consistency.

The original LLR layout was modified to dope the fuel with Thorium. While the same core geometry was used, the fuel enrichment was held constant at 20% (below the nonproliferation limit) throughout the different zones. The weight percent of thorium (relative to U-Zr, with the proportion of Zr to U maintained) in each zone was altered proportionally to originally enrichment grading in the LLR. Figure 5.28 shows the thorium weight fraction in each core region. The modified core is referred to as the LLR-Th. The initial fissile inventory was increased by 5% relative to the LLR in order to ensure the core reached criticality at BOL. This is due to the lower η value of ^{233}U relative to other fissile isotopes. Additionally, thorium has a lower heavy metal density than U-Zr (14.4 g-HM/cc against 11.7 g-HM/cc), this leads to an overall reduction in breeding ratio relative to the original

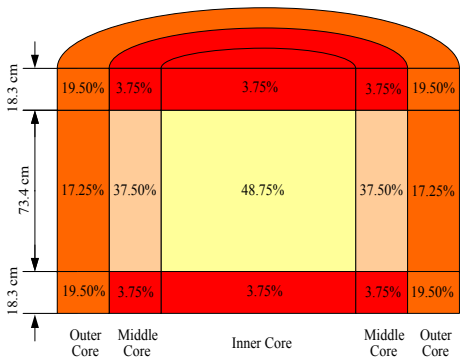

Figure 5.28: Wight fraction of thorium inside each fuel zone (relative to U-Zr). The fuel enrichment in all zones is maintained at 20%.

LLR.

The performance of the LLR-Th is highlighted in Figure 5.29. As anticipated, the core became subcritical earlier than the original LLR design. The overall lifetime of the core is decreased by around 14 years (20 years total). This is mostly attributed to the reduction in breeding ratio, highlighted in Figure 5.29(b), coupled with the lower initial heavy metal inventory. A significant drop in the inner region BR is observed relative to the original design. It corresponds to the region with the highest thorium fraction. The explicit breeding ratio script was updated here to account for fertile and fissile isotopes in the thorium cycle. For simplicity, not all reactions are taken into account as highlighted in Equation 5.6.

$$BR = \frac{[R_a(^{238}U) + R_a(^{238}Pu) + R_a(^{240}Pu) + R_a(^{232}Th)] - [R_a(^{239}Np) + R_a(^{233}Pa)]}{R_t(^{235}U) + R_t(^{239}Pu) + R_t(^{241}Pu) + R_t(^{233}U)} \tag{5.6}$$

From a nonproliferation standpoint, the LLR-Th shows little improvement in plutonium quality (relative to Figure 5.30(a)) for the outermost region (the most limiting case), which is expected. The core does breed a significantly lower quantity of plutonium per assembly as shown in Figure 5.30(b). The resulting reduction ensures no assembly reaches the 1 SQ limit defined by the IAEA, improving the proliferation resistance of the core. The ^{233}U bread in the LLR-Th is also maintained below the nonproliferation limit highlighted in

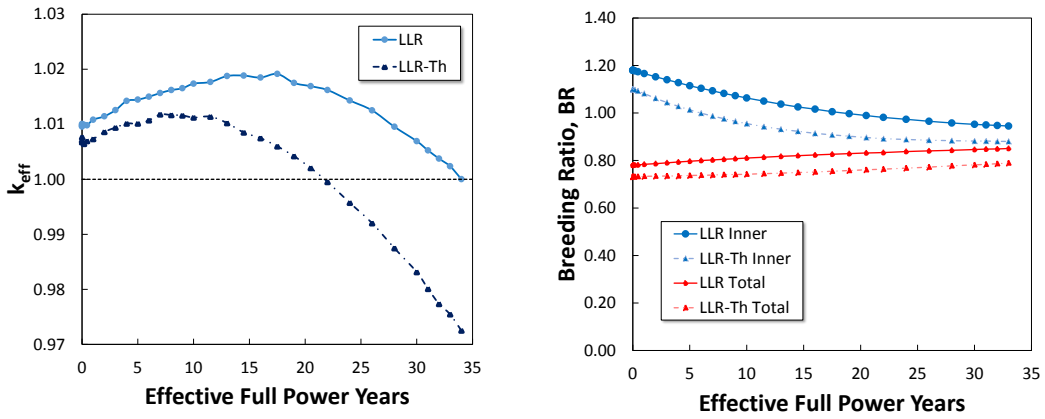

(a) Eigenvalue comparison.

(b) Breeding ratio comparison.

Figure 5.29: Performance of the LLR-Th core design versus the original LLR.

Table 5.6: Comparison of plutonium production in the LLR, LLR-Th and MXR-inter1 designs at EOL.

	LLR	**LLR-Th**	**MXR**
total m_{Pu} in 1/6 core (kg)	244.3	107.3	265.1
average m_{Pu}/assembly (kg)	9.8	4.3	7.2
max m_{Pu}/assembly (kg)	12.8	5.0	9.3

Section 3.2. The uranium denaturation ratio for the core, $(0.6m_{235} + m_{233})/m_t$, is shown in Figure 5.30(c) to be below the 12% limit defined by Forsberg et al.[46]

Plutonium breeding metrics are summarized in Table 5.6. The core as a whole sees a 56% reduction in total plutonium generated, and the maximum plutonium produced in a single assembly is 5.0 kg as opposed to 12.8 kg in the original LLR design. By comparison to the MXR, the LLR-Th sees some improvement in the average plutonium mass per assembly metrics. The main advantage is that no assembly in the LLR-Th reaches 1 SQ at EOL, while 11 do so for the MXR-inter1, and 18 reach 1 SQ in the original LLR. The MXR-inter5 is slightly more proliferation resistant than the MXR alternative, with 6 assemblies containing 1 SQ. This highlights the main benefit from a nonproliferation standpoint of doping fuel with thorium.

In addition to the shorter core lifespan than the MXR, the main design tradeoff of the

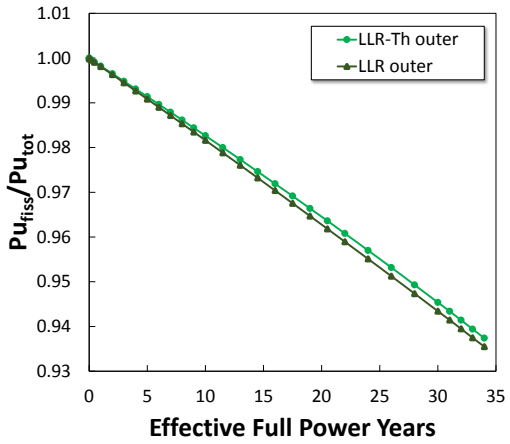

(a) Plutonium quality in the outer region.

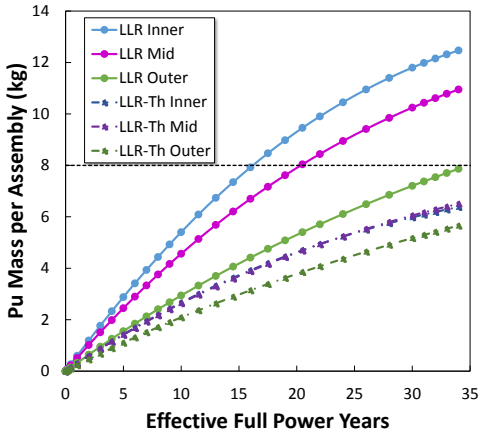

(b) Average plutonium mass per assembly.

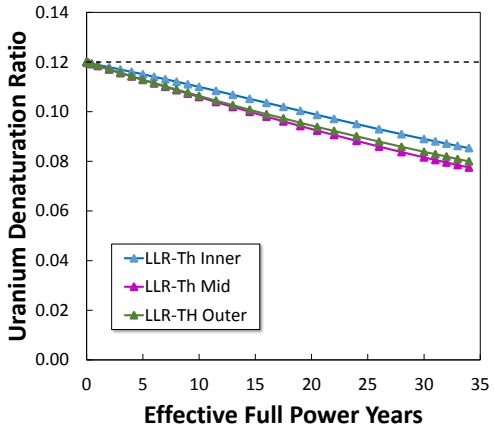

(c) Uranium denaturation ratio.

Figure 5.30: Comparison of nonproliferation metrics in the LLR-Th core design and the original LLR.

LLR-Th core is its feasibility. Less experience has been acquired with thorium fuels than their uranium counterparts. Even less data is available on mixed Th-U-Zr hybrids. The original LLR already pushes the boundaries of cladding maturity, with a fast fluence limit of 6×10^{23} n/cm^2, beyond the typical limit of 4×10^{23} n/cm^2 in metal-fueled sodium fast reactors. Little is known about fuel and clad damage beyond those points. The resulting technological readiness of the LLR-Th is expected to be lower than the LLR or MXR.

5.5.2 Mixed spectrum U-Th core

While the thorium production chain does not hold an advantage over the uranium chain in fast spectra, it does so in more thermalized ones. Table 5.7 highlights the changes in the η value ($\nu\sigma_f/\sigma_a$) for ^{233}U and ^{239}Pu in different spectra. The value for ^{233}U was 9% lower than that of ^{239}Pu in the fast spectrum, but is approximately 11% higher in the epithermal spectrum considered in this thesis (15% moderating rod fraction). The epithermal results were obtained from an assembly lattice model for the three inter layouts derived in Section 5.3. The higher ^{233}U η values make the thorium production chain better suited to breed fissile material in the epithermal regime.

Table 5.7: Reproduction factor η ($\nu\sigma_f/\sigma_a$) for different fissile isotopes at different neutron spectra. Epithermal values were obtained using MCNP simulations, while Fast and thermal ratio were reproduced from Table 3.1.

			Epithermal Spectrum		
	Thermal	**Fast**	**Inter1**	**Inter3-lump**	**Inter5-lump**
^{239}Pu	2.110	2.700	1.959 ± 0.004	1.929 ± 0.004	1.975 ± 0.005
^{233}U	2.300	2.450	2.184 ± 0.004	2.171 ± 0.005	2.182 ± 0.005

The cross-sectional ratios do not vary significantly for different moderator arrangements in Table 5.7, but the microscopic cross-sections themselves see notable changes. Comparing Inter3lump to Inter1, the $\nu\sigma_f$ value increases by 22% for ^{233}U and by 44% for ^{239}Pu. Spatial self-shielding effects are therefore still important. Depletion simulations were conducted for each of the three main assembly arrangement with a 20w% thorium doping content (i.e. fuel is 72U-8Zr-20Th). Figure 5.31 shows the effects on both k_∞ and the breeding ratio. Only 15% moderating rod fraction was considered in light of conclusions in previous sections. While the relative trends among the different arrangements are the same as for the original lattice models without thorium doping, difference between the two fuel types do emerge. The initial eigenvalues are lower for the thorium cases relative to their U-Zr counterparts, but the final eigenvalues (at burnup of 72 GWd/MTU) is slightly higher. This is because the lower heavy metal density of thorium-based fuels results in

a lower initial enrichment, but higher breeding outweighs this over time. The Inter1-Th configuration sees the largest improvement with a average BR value for the considered burnup, seeing an 8% increase over its U-Zr fuel counterpart. The uranium denaturation ratio drops below the 12% similarly to what was observed previously in Figure 5.30(c), and no substantial change in the plutonium quality reduction is observed from the previous model with U-Zr fuel.

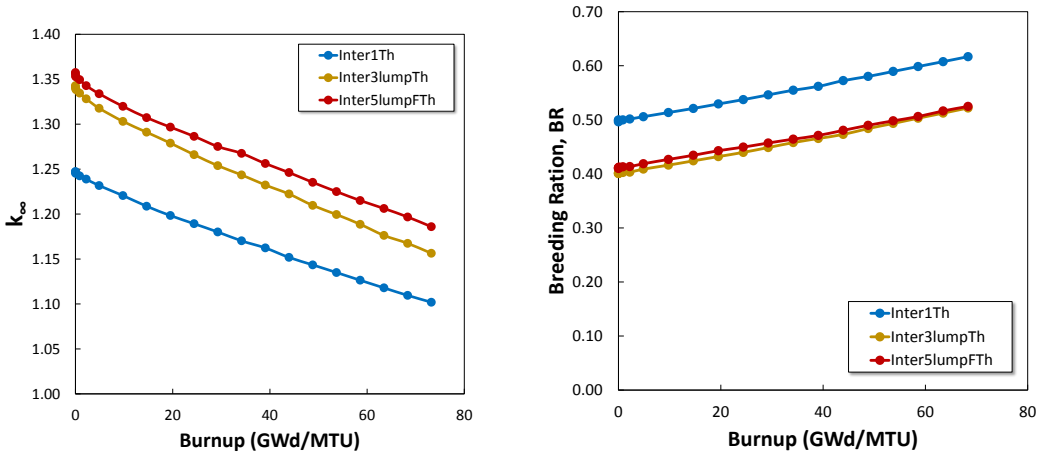

(a) k_∞ evolution.

(b) Breeding ratio evolution.

Figure 5.31: Comparison of the moderator arrangement in thorium-doped assembly lattice models. Simulations are obtained with MCNP6. Average standard deviation was of 75 pcm.

In order to investigate further the breeding benefit of thorium in the epithermal spectrum, assembly lattice depletion was conducted with varying thorium contents. The Inter1 arrangement was selected for the case study, in light of its highest BR curve. A sensitivity analysis was done for this arrangement with thorium weight contents of 20.3, 34.8, 44.2 and 57.5 w%. Figure 5.32 highlights the results, which are also summarized in Table 5.8. As expected, increasing the thorium content decreases the initial k_∞, but substantially increases the breeding ratio. At 57% thorium content, BR approaches unity. Such elevated breeding ratios could not be reached in comparable uranium models. However, the closer BR is to unity, the more likely its uranium denaturation ratio is to exceed the 12% limit. Care must be taken to ensure that limit is not reached in whole assemblies (since assem-

blies have different axial thorium content at the lower and upper bounds). If the criteria is not met in a core model, the starting ^{235}U enrichment in regions with high thorium content will need to be reduced from the 20% value. Interestingly, the plutonium quality ratio sees notable variations relative to the thorium content. A full 8 percentage point decrease in the ratio value is observed when shifting from a 20w% to 57w% thorium content. This can be explained by the differences in resonance absorption between ^{238}U and ^{232}Th, leading to small variations in spectrum, and resulting in changes in plutonium cross-section. The case with 57w% thorium content sees a 10.7% increase in the σ_a/σ_f ratio for ^{239}Pu relative to the U-Zr model (with the same moderator arrangement). It appears that increasing thorium content requires a balancing act; on the one hand, BR is increased at the cost of a lower starting k_∞, and plutonium quality is decreased while uranium attractiveness is increased. Reaching final conclusions regarding thorium fuel doping requires core-level depletion modeling.

Table 5.8: The effects of thorium content on key performance and nonproliferation parameters. The average standard deviation for the initial and final eigenvalue (k^i_∞ and k^f_∞) was 72 and 67 pcm respectively.

Th w%	**BR**^{av}	$\mathbf{k}^i_\infty$	$\mathbf{k}^f_\infty$	**(Pu**$_{fiss}$**/Pu**$_{tot}$**)**^{f}	**(U ratio)**^{f}
20.35%	0.541	1.247	1.102	89.10%	8.52%
34.82%	0.672	1.134	1.026	86.33%	9.25%
44.25%	0.767	1.060	0.989	84.45%	10.21%
57.52%	0.920	0.945	0.945	81.22%	12.63%

The analysis proceeded to evaluate a 1/6 core model with mixed spectrum and mixed U-Th fuel. The same thorium grading as in Figure 5.28 was used, but with the geometry of the MXR-combine case highlighted in Figure 5.12(a). The resulting model is referred to as the MXR-Th. The core had to be shuffled after 9 years, in light of the lower initial inventory. The total lifetime of the core was estimated to be 21 years, as shown in Figure 5.33(a). The results demonstrate that the MXR-Th is able to successfully reduce plutonium quality

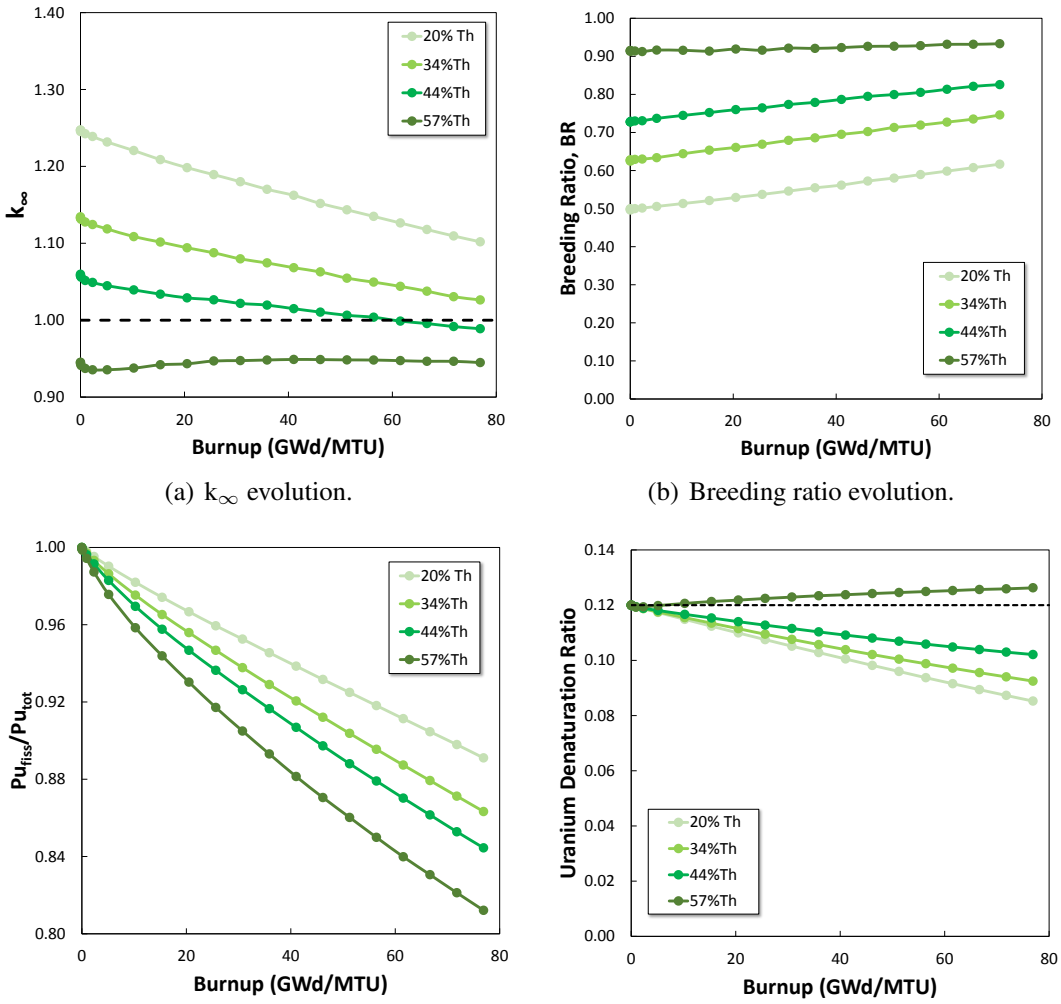

(a) k_∞ evolution.

(b) Breeding ratio evolution.

(c) Pu quality evolution.

(d) U denaturation evolution.

Figure 5.32: Evaluation of thorium weight content on the eigenvalue, breeding ratio, plutonium quality and uranium denaturation ratio in assembly lattice models. The moderator arrangement was the same as Inter1. MCNP eigenvalue standard deviation were of the order of 70 pcm.

below the weapon-grade limit at EOL while maintaining the uranium denaturation ratio in each assembly below 12%. The plutonium quantity per assembly is also significantly reduced as was seen with the LLR-Th.

Interestingly, the MXR-Th results highlight that at shuffling, an increase in reactivity is observed rather than a decrease as was seen with the other MXR configurations. This is mostly due to the higher fissile inventory in the outer region due to its higher breeding ratio. Despite of this, the lifespan of the core is reduced by 4 years relative to the MXR-

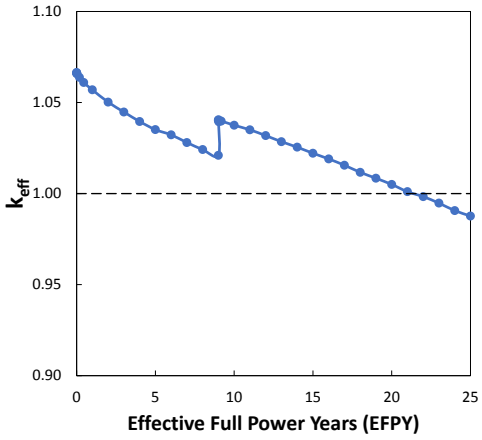

(a) Eigenvalue evolution in the MXR-Th.

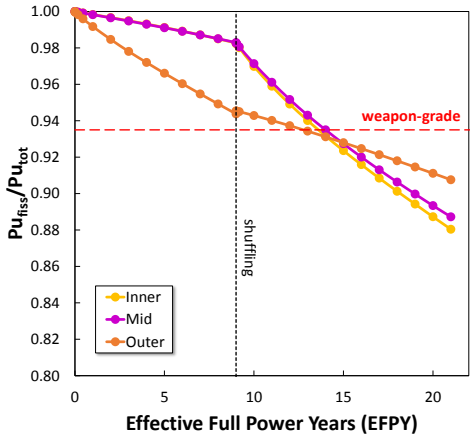

(b) Plutonium quality in the different core regions.

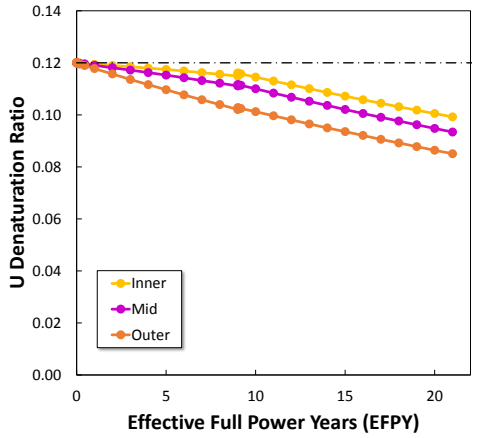

(c) Uranium denaturation ratio.

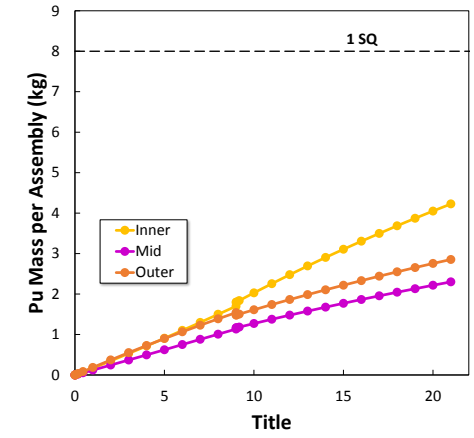

(d) Average plutonium mass per assembly.

Figure 5.33: Performance evaluation of the proposed MXR-Th core design.

inter1. This is mostly attributed to the lower initial heavy metal inventory as previously discussed. An additional disadvantage of the design relates to the main drawbacks of using thorium fuels, and their lack maturity and experimental validation. The main advantages of the MXR-Th stem from a proliferation resistance standpoint. Table 5.9 highlights the main nonproliferation metrics of the LLR, the MXR-inter1, and the MXR-Th. The benefit of doping the fuel with thorium can be directly seen with the plutonium mass metrics. No assembly reaches 1 SQ at the end of life (EOL), and the total production in the core is more than halved despite the higher initial heavy metal inventory. On the other hand, the plutonium quality is generally less proliferation resistant than the MXR-inter1, but by only

Table 5.9: Plutonium production characteristics in the MXR-Th versus other core designs. The results are for the specific end-of-life (EOL) of each case.

	MXR-Th	**MXR**	**LLR**
tot. m_{Pu} in core	631.8 kg	1540.2 kg	1465.8 kg
av(m_{Pu}/assembly)	4.3 kg	7.2 kg	9.7 kg
max(m_{Pu}/assembly)	5.8 kg	9.2 kg	12.8 kg
assemblies with > 1 SQ	0	66	108
av(Pu_{fiss}/Pu_{tot})	89.6%	88.0%	90.6%
max(Pu_{fiss}/Pu_{tot})	94.0%	93.1%	95.2%

few percentage points. As a whole, it is concluded that thorium-fueled MXR can improve their proliferation resistance but at cost to performance and feasibility of the concept.

5.6 Chapter Conclusion: A Base Model for the Mixed Spectrum Reactor

A wide range of findings were identified during the design optimization process. Inter-assembly moderation was found to be more effective that intra-assembly configuration, despite the added complexity when shuffling the fuel. Zirconium hydride ($ZrH_{1.6}$) was selected as moderating material, and 15% of fuel rods were replaced with the material to moderate a specific reactor zone. Introducing moderating material at the outermost core region was concluded to be more effective than placing it in the inner regions. Optimization using the *REBUXS* script found a suitable core geometry with a 20% expanded core height, 15% average enrichment value (1.5 percentage point higher than the original design) and two additional fuel assembly rings. A suitable shuffling strategy was outlined and the resulting MXR model was able to reach a core lifetime of around 25-27 years. The plutonium quality at EOL was below the weapon grade limit, and the quantity per assembly was reduced relative to the original LLR (but inner assemblies still generated more than 1 SQ of plutonium during the operating lifetime). Heterogeneity effects were also investigated and shown to be of high importance. Seemingly small changes in the moderator layout in the assembly contributed to large variations in cross-sections, and subsequently

to core performance. The MXR-inter1 and MXR-inter5 configurations were identified as the most attractive core layouts. Lastly, mixed U-Th fuels were also investigated and found to lead to an overall reduction in core lifetime. Plutonium quantity per assembly is reduced in such models, but the purity is slightly higher. Future analysis will focus primarily on the non-Th arrangements as they are believed to be more feasible. Special emphasis will be given to the MXR-inter1 due to power peaking issues arising with the MXR-inter5 that will be discussed in the next chapter. Additional modifications and improvements to the identified designs will be considered in Chapter 7.

CHAPTER 6

ASSESSMENT OF INHERENT SAFETY IN MIXED SPECTRUM DESIGN

The optimization in Chapter 5 focused on two main parameters: core lifetime until sub-critical, and plutonium breeding quality. The addition of moderating material to a reactor concept has the potential to introduce safety-related design challenges. These must be carefully evaluated in order to ensure the feasibility of the proposed design. The main objective of this chapter will be to assess important aspects of the MXR configuration. The study will not be an in-depth safety analysis with probabilistic risk assessment, rather an evaluation of important metrics in core designs at the conceptual level that can infer inherent safety. Final assessments will rely heavily on comparison with values in the original LLR design and typical sodium fast reactors. Factors that will be considered include reactivity feedback mechanisms, fluence limits and power peaking effects.

6.1 Neutronic Safety Analysis

The first part of the safety analysis will concentrate on neutronics-based metrics. This includes reactivity feedback coefficients, zone coupling within the core, fast fluence limits both inside and outside the core, as well as quasi-static feedback analysis. MCNP6 is used exclusively in this section to reach the level of accuracy needed for perturbation studies, and to adequately model assembly heterogeneity.

6.1.1 Reactivity coefficients

At its essence, evaluating reactivity feedback mechanisms in a nuclear core consists of perturbing the system and estimating the resulting change in eigenvalue. The perturbations incurred are all based on modification to the core temperature and its effects on core characteristics such as its geometry, material cross-sections, and the coolant density. Individual

parameters, or feedback coefficients, are considered individually in order to understand the underlying phenomena dictating core behavior in transient conditions. The modeling approach assumes the core can be approximated as a point source, this assumption will be investigated further in Section 6.1.2.

Perturbation analysis with MCNP requires manually changing specific core parameters, running an eigenvalue calculation, and computing the resulting change in reactivity according to Equation 6.1. Where k_p is the perturbed eigenvalue at temperature T_p, relative to the original eigenvalue k_0 at temperature T_0. The resulting stochastic uncertainty is estimated according to the previously described Equation 4.8. In order to reach adequate conclusions regarding small reactivity, the number of simulated particles was quadrupled to sufficiently minimize Monte Carlo standard deviations. Reactivity coefficients are reported in ¢/K, and are approximated using the relation in Equation 6.2, with the exception of cross-section related coefficients (estimated with Equation 6.3). The effective delayed neutron fraction, β_{eff} can be estimated using the 'kopts' setting in MCNP, and ΔT is the difference in temperature between T_p and T_0.

$$\rho = \frac{k_p - k_0}{k_p k_0} \tag{6.1}$$

$$\alpha = \frac{\rho}{\beta_{eff} \Delta T} \tag{6.2}$$

Reactivity coefficients can segregated roughly into three groups, depending on whether they are geometry-related, Doppler-feedback related, or coolant related. The first category includes the radial expansion coefficient, α_{rad}, the axial expansion coefficient, α_{ax}, as well as the control rod insertion coefficient, α_{ctrl}. At a given perturbed temperature, core dimensions can be modified using the HT9 steel thermal expansion coefficient highlighted in Appendix A. Radial and axial expansion are accounted for separately, with the corresponding fuel densities modified to ensure conservation of mass. During axial expansion

simulations, the control rod is maintained at the original level of the fuel top. For the control rod coefficient evaluation, the axial height of the core is maintained the same as in T_0 and the control rod position is lowered proportionally to thermal expansion rates above the core.

In order to account for logarithmic effects in cross-sectional temperature dependencies, Doppler coefficients are calculated using Equation 6.3. Cross-sectional libraries are perturbed separately for the fuel, the clad and the moderator. Their respective reactivity coefficients are labeled α_{fuel}, α_{clad}, and α_{mod}. In the case of the moderator, the S(α,β) card is also modified. Lastly, the coolant voiding coefficient is estimated by perturbing the sodium density at and above the fuel axial levels. Two values are estimated, the first, α_{void}, by perturbing the coolant temperature and modifying its density using the sodium volumetric expansion rate (see Appendix A for more information). The sodium void worth, α_{worth} is the coefficient resulting from completely voiding the sodium at and above the fuel level. The resulting coefficients are computed with Equation 6.2 as before. All the different coefficients considered are summarized in Table 6.1.

$$\alpha_D = \frac{\rho}{\ln\left(\frac{T_p}{T_0}\right)} \times \ln\left(\frac{T_0+1}{T_0}\right) \tag{6.3}$$

Following the aforementioned methodology, the eight reactivity coefficients are computed for both the original LLR and the MXR. Only the MXR-Inter1 assembly arrangement case is considered here as it is considered representative of the other configurations, with little variation expected in the other cases. Analyses were performed both at begining and end of life (BOL and EOL). The results are summarized in Table 6.2. Two trends with MXR values are immediately apparent; the first is that geometric coefficients are reduced relative to the LLR, the second is that Doppler and void coefficients are improved. The β_{eff} sees little variation between the two LEU-fueled models as expected. However, the axial and control rod coefficients are all 'less negative' for the MXR. This can be attributed

Table 6.1: Symbols and definition of the reactivity feedback coefficients considered in this thesis.

	Symbol
Effective delayed neutron fraction	β_{eff}
Radial expansion (¢/K)	α_{rad}
Axial expansion (¢/K)	α_{ax}
Control rod expansion (¢/K)	α_{ctrl}
Fuel Doppler (¢/K)	α_{fuel}
Clad Temperature (¢/K)	α_{clad}
Moderator Temperature (¢/K)	α_{mod}
Coolant void (¢/K)	α_{void}
Coolant void worth ($)	α_{worth}

to the increase in core volume, leading to a higher surface to volume ratio. With leakage already higher in the MXR model, further expansion induces proportionally less out of core leakage, which reduces effect on reactivity. The lower values can also be explained by the higher presence of thermalized neutrons in peripheral core regions, which are less likely to leak out of the core. Improvements in the Doppler coefficients however, are more substantial, especially at the fuel level. An epithermal spectrum has a higher proportion of neutrons near the resonance region. This is where the full extent of Doppler broadening of resonance peaks is observed, resulting in large changes in equivalent collapsed cross-sections. The phenomena is more pronounced with ^{238}U σ_c; its resonance region start at higher energies than ^{235}U σ_f. More neutrons are therefore lost to absorption than fission than is the case at T_0. The moderator reactivity value was estimated for the MXR as it is important in thermal reactors. In this case however, there appeared to be no statistically significant effect on reactivity with changes to moderator temperature. Lastly, the coolant void coefficients see some notable improvements as well in the MXR. Sodium scattering in the outer core region now increases reactivity in the epithermal spectrum by further softening the spectrum; it therefore increases fission cross-sections and reactivity.

The results appear to validate the assumption in Chapter 5 that increasing the core

Table 6.2: Reactivity feedback coefficients in the LLR and MXR-Inter1, at beginning and end-of-life (BOL and EOL).

	BOL		**EOL**	
	LLR	**MXR**	**LLR**	**MXR**
β_{eff}	0.007 $\pm$ 0.000	0.007 $\pm$ 0.000	0.005 $\pm$ 0.000	0.005 $\pm$ 0.000
α_{rad} (¢/K)	-0.086 $\pm$ 0.004	-0.055 $\pm$ 0.004	-0.149 $\pm$ 0.008	-0.109 $\pm$ 0.006
α_{ax} (¢/K)	-0.002 $\pm$ 0.003	-0.022 $\pm$ 0.003	-0.035 $\pm$ 0.005	-0.036 $\pm$ 0.005
α_{ctrl} (¢/K)	-0.014 $\pm$ 0.007	-0.006 $\pm$ 0.007	-0.015 $\pm$ 0.010	-0.018 $\pm$ 0.010
α_{fuel}(¢/K)	-0.047 $\pm$ 0.007	-0.124 $\pm$ 0.008	-0.054 $\pm$ 0.011	-0.115 $\pm$ 0.010
α_{clad} (¢/K)	0.001 $\pm$ 0.017	0.008 $\pm$ 0.016	0.003 $\pm$ 0.013	-0.015 $\pm$ 0.024
α_{mod} (¢/K)	N/A	0.001 $\pm$ 0.016	N/A	0.034 $\pm$ 0.024
α_{void} (¢/K)	0.027 $\pm$ 0.001	0.029 $\pm$ 0.001	0.040 $\pm$ 0.002	0.043 $\pm$ 0.002
α_{worth} ($)	0.050 $\pm$ 0.021	0.037 $\pm$ 0.022	2.674 $\pm$ 0.090	1.695 $\pm$ 0.064

height of the MXR (an uncommon design choice in sodium fast reactors) does not hinder core safety too drastically. While all the reactivity coefficients are within the norm of what is typically observed in fast reactors, it is still important to estimate whether their collective variations can negatively impact performance in transient conditions. A suitable approach for evaluating the performance of the MXR concept is to undertake quasi-static integral feedback analysis, and ensure safety criteria are still met. In order to ensure that this type of approximate analysis is applicable to the MXR, it must be first established that the core can be represented using point kinetics. Once this is established in Section 6.1.2, the integral feedback parameters will be evaluated in Section 6.1.3.

6.1.2 Core coupling

Introducing large distortions within a reactor core runs the risk of decoupling different zones. In extremes, this can essentially lead to two nearly-independent sub-cores within the same reactor. A dangerous consequence of this would be core tilting during transient or shutdown conditions. The reactor runs the risk of overcorrecting a decrease in reactivity

in one region, with a spike in the other. As such, evaluating the extent of core coupling is very important in the MXR. It can also lend insight into how accurate point kinetics model approximations are for the given model.

Avery first developed the theory for evaluating core coupling in 1958.[67] Coincidentally, these models were first applied to his original mixed-spectrum reactor concept, and are therefore very pertinent to the analysis in this thesis. He defined parameters, referred to as k_{ij} to measure the coupling between two core regions are. The integral parameter, k_{ij}, essentially evaluates the likelihood that a fission neutron from region j generates a next generation fission neutron in region i. To estimate this value, neutron sources must be calculated. S_i is defined as the total fission neutron source in region i, while S_{ij} is define as the total fission source from region i cause by neutrons originating in region j. Using the relations in Equation 6.4, the different k_{ij} parameters can be evaluated for a two region core.

$$\begin{aligned} k_{12} &= \frac{S_{12}}{S_2} & \qquad k_{11} &= \frac{S_{11}}{S_1} \\ k_{21} &= \frac{S_{21}}{S_1} & \qquad k_{22} &= \frac{S_{22}}{S_2} \end{aligned} \tag{6.4}$$

where

$$\begin{aligned} S_1 &= S_{12} + S_{11} \\ S_2 &= S_{21} + S_{22} \end{aligned} \tag{6.5}$$

MCNP6 is unable to implicitly calculate the different source terms. Doing so requires setting up the problem in a way that forces the solution. Instead of solving an eigenvalue problem, a source definition is specified. The main objective is to simulate the fission source in only one reactor zone to study its effect on the other zone. In other words, a virtual particle distribution is placed in the fast zone, and resulting neutron interactions in the thermalized zone are tallied. The simulation is then repeated with the fission source

placed in the thermal zone and the results tallied in the fast zone. To set up the problem, a detailed fission distribution needs to be acquired. Fission rates were tallied inside the fuel rods at three axial positions in each individual assembly in the 1/6 core model. The three axial locations correspond to the upper, central and lower enrichment regions within the assemblies (Figure 4.2(b)). The fission rates are separated for each zone and normalized to unity. In order to position the weighted source distribution in each individual assembly, the sources were approximated as cylinders within the assemblies, due to limitations with operating MCNP6. This assumption is valid since the neutron source consists solely of prompt neutrons (following a Watt distribution), with a large mean free path. The assumption was still verified by comparison with a single hexagon-shaped source term in an individual assembly. Comparing tallies at surrounding assemblies yielded an average fission tally error of 2%. The cylindrical source approximations were concluded to be valid. Figure 6.1 shows a representation of the source distribution for the simulated cases.

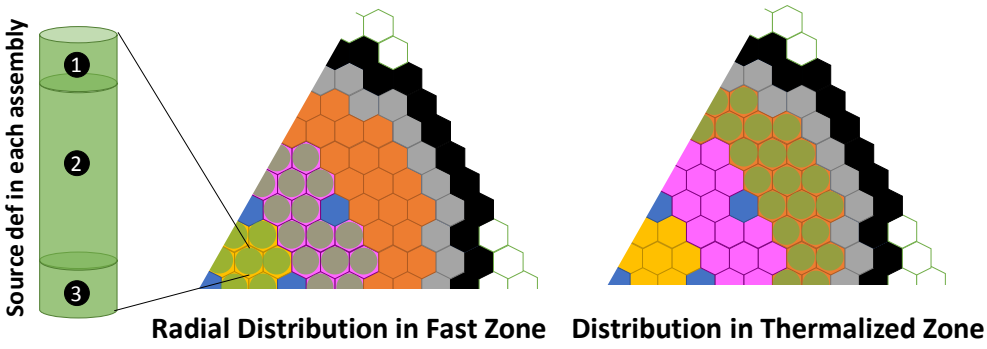

Figure 6.1: Illustration of the source distribution for the fast-to-thermal and thermal-to-fast simulations. The source term in each cylinder is weighted by the fission proportion in that assembly section.

After setting up a source definition in one zone, the fission neutron generation rate, $\nu\sigma_f\phi$, is tallied in every single assembly. The S_{ij} source terms can then be estimated by summing up the tally results in every assembly at a given zone. The relations are shown in Equation 6.6 for a fission source in the fast zone (f), with the labels t and f replacing the 1&2 labels in Equation 6.4. The same process can be followed to compute the thermal-to-

fast source terms by placing the source particles in the thermalized region (t) and inverting Equation 6.6. The terms n and m account for the number of assemblies in the thermalized and fast regions respectively. Simulations were performed to evaluate all of S_{ij} terms the for both the LLR and the MXR geometries (only Inter1 was considered for the MXR model, as it was deemed representative of other cases). A total of 5×10^6 virtual particles were simulated to ensure adequate statistical accuracy levels are reached. Figure 6.2 shows the S_{ft} and S_{tf} distribution in the MXR model.

$$
\begin{aligned}
S_{tf} &= \sum_{n}^{N_t} (\nu\Sigma_f)_n \phi_n \\
S_{ff} &= \sum_{m}^{N_f} (\nu\Sigma_f)_m \phi_m
\end{aligned}
\tag{6.6}
$$

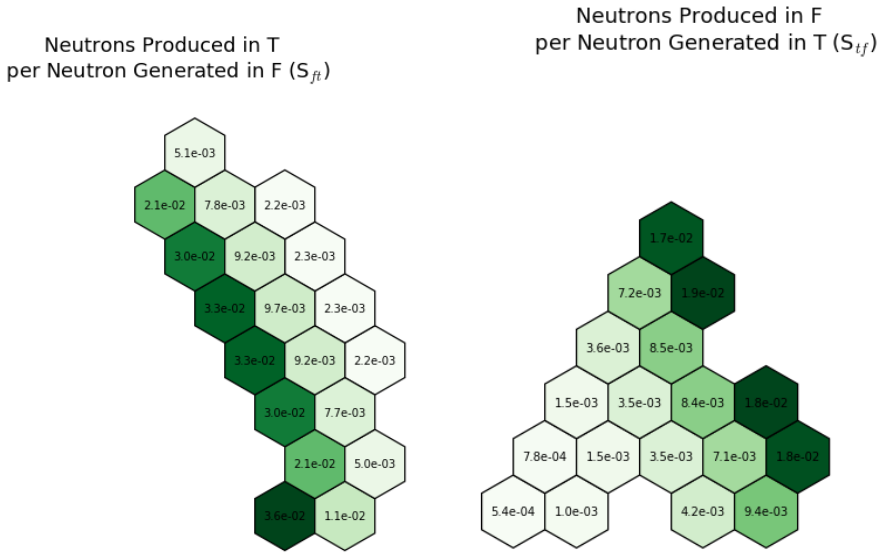

(a) Coupling from the fast to thermalized region, T ($sd_t = 0.054\%$).

(b) Coupling from the thermalized to the fast region, F ($sd_t = 0.053\%$).

Figure 6.2: Fission neutron source from region (T/F) generated from neutron in region (F/T). This provides the measure of the coupling in reactor zones. The results displayed are for the MXR-Inter1 configuration and are normalized per source particle.

Following the previously outlined methodology, the coupling parameters, k_{ft} and k_{tf} can be computed for a given configuration. The resulting values for the LLR and the MXR

Table 6.3: The coupling parameter values for the LLR and the MXR.

	LLR	**MXR**
k_{tf}	0.19999 ± 0.00008	0.24554 ± 0.00014
k_{ft}	0.24058 ± 0.00010	0.12645 ± 0.00008
k_{ff}	0.80001 ± 0.00020	0.75446 ± 0.00020
k_{tt}	0.75942 ± 0.00022	0.87355 ± 0.00037

are summarized in Table 6.3. Note that while there is no 'thermalized' zone in the original LLR, the t subscript is still use for comparative purposes. In that reactor, t simply denotes the outer core region, while f denotes the inner and mid regions. It is interesting to note that while k_{ft} is lower for the MXR (thermal causing fission in fast), its k_{tf} (fast causing fission in thermal) is higher. This can be linked to the addition of moderating material. On the one hand, thermalized neutrons have shorter mean free paths and are less likely to leak out of the thermalized region into the fast one. On the other hand, the epithermal causes an increase in fission cross-section, increasing the chance that a neutron originating in the fast zone would cause fission. The k_{tt} parameter also sees a large increase in the MXR due to the much higher proportion of fissions occurring in the outer (thermalized) core region relative to the inner and mid ones. In conclusion, it appears that the coupling parameters are in-line with what is observed in a well coupled reactor (the LLR). While the MXR k_{tf} is smaller by 4555 pcm, this is more than made up for with the 11413 pcm increase in k_{ft}. No dangerous decoupling phenomena is anticipated during transient scenarios, and the core can be adequately approximated by point kinetics model. This provides the basis for conducting quasi-static feedback analysis on the MXR.

6.1.3 Quasi-static integral feedback

Wade and Hill derived a simplified approach to evaluating the 'inherent safety' of sodium-cooled fast reactors.[53] The starting point is the quasi-static reactivity balance equation.

The relation assumes that transient scenarios are slow relative to reactor characteristics (such as delayed neuron constants and temperature induced geometry changes). The quasi-static reactivity and energy balance relations can be written as:

$$0 = \Delta\rho = (P-1)A + \left(\frac{P}{F} - 1\right) B + \delta T_i C - \Delta\rho_{ext} \tag{6.7}$$

$$\delta T_o = \delta T_i + \Delta T_c \left(\frac{P}{F} - 1\right) \tag{6.8}$$

where

$P\&F\ (\%) =$ power and coolant flow, normalized to operating conditions

$\delta T_i\ (K) =$ inltet temperature change from operating condition

$\delta T_o\ (K) =$ outlet temperature change from operating condition

$\Delta T_c\ (K) =$ difference between inlet and outlet coolant temperatures at operating conditions

$\Delta\rho_{ext}\ (¢) =$ externally-imposed reactivity change

$A\ (¢) =$ net power-flow reactivy decrement

$B\ (¢) =$ power/flow coefficient relative to operating conditions

$C\ (¢/K) =$ inlet temperature coefficient of reactivity

$(A+B)\ (¢) =$ reactivity decrement due to shift to zero-power conditions

The integral reactivity parameters, A,B, and C, dictate the behavior of the core after a giving perturbation. It is therefore crucial that these values are within acceptable bounds to ensure passive safety of the core during accident scenarios. Wade and Hill considered the four main accident scenarios: unprotected loss of flow (ULOF), unprotected loss of heat sink (ULOHS), unprotected over power (UTOP), and chilled inlet overcooling. Analysis of ULOHS concluded that $(A + B)$ should be minimized and C maximized, while the opposite proved true for the chilled inlet scenario. A balancing of these variables must therefore be reached. UTOP condition require a maximized $(A + B)$, and depend on the

external reactivity insertion (as well as the pump flow coastdown and the delayed neutron time constant, but these are assumed to be similar for the considered reactors). In the end, the following criteria needed to be met to ensure the core could be passively regulated:

$$A, B\&C < 0 \tag{6.9}$$

$$\frac{A}{B} \leq 1 \tag{6.10}$$

$$1 \leq \frac{C\Delta T_c}{B/2} \leq 2 \tag{6.11}$$

$$\frac{\Delta\rho_{ext}}{|B|} \leq 1 \tag{6.12}$$

More recently, Fiorina et al. introduced more conservative criteria, imposing the condition that δT_o be maintained lower than ΔT_c.[68] The ULOHS and the chilled inlet accident scenario, lead to the imposition of the first constraint below, while UTOP lead to the formulation of the second constraint:

$$\frac{2}{3} < \frac{A+B}{C\Delta T_c} < 2 \tag{6.13}$$

$$\Delta\rho_{ext} < |B| \left(A + \frac{A}{B}\right) \tag{6.14}$$

To evaluate the MXR design and assess if it falls within the aforementioned criteria, the integral parameters must first be estimated. Each parameter can be calculated by summing reactivity feedback coefficients from Section 6.1.1, depending on their specific timescales. For metal-fueled slugs assumed to be bounded to the clad, the integrals components can be estimated as follows:

$$A\ (\text{¢}) = \alpha_{fuel} \times \delta T_{fuel} + \alpha_{clad} \times \delta T_{clad} + \alpha_{mod} \times \delta T_{mod} \tag{6.15}$$

$$B\ (\text{¢}) = (\alpha_{fuel} + \alpha_{clad} + \alpha_{mod} + \alpha_{void} + \alpha_{ax} + \alpha_{rad} + \alpha_{ctrl}) \times \Delta T_c \tag{6.16}$$

$$C\ (\text{¢}/K) = \alpha_{fuel} + \alpha_{clad} + \alpha_{mod} + \alpha_{void} + \alpha_{ax} + \alpha_{rad} \tag{6.17}$$

Where each coefficient α has the same definition as in Table 6.1, and δT_{fuel}, δT_{clad} are the difference with coolant temperature between the clad and the fuel. For the purpose of

Table 6.4: Integral quasi-static feedback parameters and their corresponding criteria for the LLR and MXR designs. A ✓means a criterion is reached, a $\sim$ means the upper bound of the confidence interval does not meet the criteria, and a $\bigotimes$ infers that the given criteria is not met.

	BOL		**EOL**	
	LLR	**MXR**	**LLR**	**MXR**
A (¢)	-4.24 $\pm$ 0.65	-6.96 $\pm$ 0.56	-4.81 $\pm$ 0.98	-6.32 $\pm$ 0.74
B (¢)	-19.01 $\pm$ 0.25	-26.14 $\pm$ 0.31	-32.54 $\pm$ 0.27	-33.61 $\pm$ 0.47
C (¢/K)	-0.11 $\pm$ 0.02	-0.16 $\pm$ 0.02	-0.19 $\pm$ 0.02	-0.20 $\pm$ 0.04
$\Delta\rho_{ext}$ (¢)	13.79 $\pm$ 0.44	132.80 $\pm$ 4.18	11.59 $\pm$ 0.50	6.09 $\pm$ 0.29
A/B	0.22 $\pm$ 0.03 ✓	0.27 $\pm$ 0.02 ✓	0.15 $\pm$ 0.03 ✓	0.19 $\pm$ 0.02 ✓
$(C\Delta T_c)/(B/2)$	1.78 $\pm$ 0.31 $\sim$	1.93 $\pm$ 0.29 $\sim$	1.85 $\pm$ 0.19 $\sim$	1.83 $\pm$ 0.34 $\sim$
$\Delta\rho_{ext}/\lvert B\rvert$	0.73 $\pm$ 0.03 ✓	5.08 $\pm$ 0.17 $\bigotimes$	0.36 $\pm$ 0.02 ✓	0.18 $\pm$ 0.01 ✓
$(A+B)/(C\Delta T_c)$	1.38 $\pm$ 0.24 ✓	1.31 $\pm$ 0.20 ✓	1.24 $\pm$ 0.13 ✓	1.30 $\pm$ 0.24 ✓
$\lvert B\rvert(A + A/B)$ (¢)	23.25 $\pm$ 0.70 ✓	33.10 $\pm$ 0.64 $\bigotimes$	37.35 $\pm$ 1.02 ✓	39.94 $\pm$ 0.88 ✓

this analysis, δT_{mod} is assumed to be equal to δT_{clad}, this is deemed conservative in light of the very minimal heat generation within the moderator (see Section 6.2.5). Using these definitions, the A,B, and C integral parameters can be evaluated for both the LLR and the MXR models. The results are shown in Table 6.4. For the purpose of this analysis, $\Delta\rho_{ext}$ is taken to be the reactivity drop (relative to 1.0 at BOL and EOL) with an added margin (300 pcm), divided by the number of control rod (13):

$$\Delta\rho_{ext}\ (\text{pcm}) = \left(\frac{k - 1.0}{k} \times 10^5 + 300\right) / \ 13 \tag{6.18}$$

Overall, the performance of the MXR appears to match that of the LLR, with the vast majority of inherent safety criteria being met. The only exception is the UTOP related criteria at BOL, but this is expected to be manageable. It is due to the very elevated initial k_{eff} of the MXR, resulting in a $\Delta\rho_{ext}$ value of 132 ¢. With its high breeding ratio, the LLR design can maintain its 'excess reactivity' (k_{eff} - 1.0) at a low value throughout its lifetime.

Extending the MXR lifetime relies on maximizing the BOL excess reactivity. Reconciling the two objectives can involve insertion of control rods, or use of burnable absorbers. Potential solutions will be discussed further in Chapter 7. Despite of this setback, the integral parameters of the MXR are adequate and in-line with the LLR, even in the case of the $|B|(A + {}^{A}/_{B})$ criteria (which is below the $\Delta\rho_{ext}$ due to the excess reactivity). While the analysis shows adequate performance during transients at a core-level, further analysis at the assembly-level is also important. Localized power peaking effects will be investigated further in Section 6.2. Prior to that, estimation of fast fluence limitations are discussed in the next section.

6.1.4 Fast fluence

The operation of both PWR and fast reactors is limited by the total fuel burnup that can be sustained in their reactors. In addition to damage in the fuel, fast reactors designers must also account for cladding damage due to neutron bombardment. The high neutron energies present in a core can be harmful to both internal and external systems. Outside the core, a constant high fast flux can be problematic at the heat exchanger level and the reactor vessel. Internally, sustained atomic displacements in the clad can lead to creeping and even failure. These design limitations must therefore be carefully assessed for the MXR.

Since the LLR operates at a lower power density, it does not emit as many fast neutrons as a typical sodium-cooled fast reactor. This allowed the original design to rely on only a single reflector assembly ring and a single shielding ring (normally two reflector rings are used). While the MXR design has a larger core radius and a higher power output, its outer region neutrons are more thermalized, leading to a potential tradeoff. In order to compare the two cases, MCNP6 simulations at BOL and EOL were performed. The fast flux, taken to be neutrons at E $>$ 100 keV energies, at an external circular boundary is tallied. The circular plane is at a distance of 173 cm from the core center. Its upper and lower bound are the same as those of the fuel region in each case (i.e. a height of 143.3 cm for the

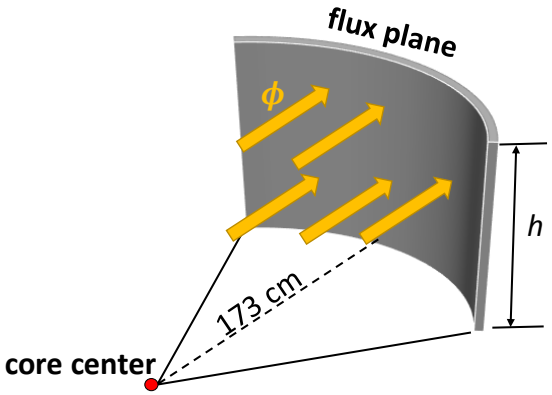

Figure 6.3: Illustration of the plane to tally the external neutron flux from the core. h= 143.3 cm for the MXR and h= 119.5 cm for the LLR.

Table 6.5: Comparison of the external fast flux, $\phi(> 100\text{keV})$ in the LLR and MXR.

	BOL	**EOL**
LLR (n/cm^2.s)	$(6.34 \pm 0.06) \times 10^{10}$	$(5.96 \pm 0.07) \times 10^{10}$
MXR (n/cm^2.s)	$(3.82 \pm 0.06) \times 10^{10}$	$(3.15 \pm 0.06) \times 10^{10}$

LLR and 119.5 cm for the MXR). Figure 6.3 illustrate the flux plane position and Table 6.6 summarizes the resulting values.

Despite the higher core power, the MXR sees a 40% reduction in external fast flux, ϕ(E >100 keV), at BOL, and a 47% reduction at EOL. The effect of neutron thermalization therefore outweighs the higher core power. This is an important finding since the core radius of the MXR was 22 cm larger than that of the LLR. The findings show that it is, in theory, possible to maintain the same distance of the Intermediate Heat Exchanger (IHX) from the core while seeing reduced fast neutron damage in the MXR. Doing so will ensure that the reactor vessel remains compact and transportable.

The second step is to consider fast flux damage at the internal level. Here the accumulation of damage over time must be taken into consideration at the cladding level. Equation 6.19 highlights how the fast fluence at EOL is estimated for a given clad outer diameter surface S. Fast reactors typically see fluences of the order of 2×10^{23} n/cm^2, but experi-

mental data for fluences as high as 4×10^{23} n/cm^2 without failure is available.[14] Advanced fast reactor designs, such as the LLR and other Breed & Burn concepts tout the ability to reach peak fast fluence of 6×10^{23} n/cm^2,[13, 66] assuming advanced clad material becomes available at the time of deployment. To evaluate peak clad fast fluence within the proposed MXR concepts, the axial region seeing the highest power level must be first determined. Figure 6.4 highlights this region for the MXR and the LLR. The dashed lines indicate the axial zones of interest. Interestingly, two peaks appear with the LLR, near the rod center and at the edge of the lower high enrichment regions. These sections are used to tally the clad surface flux using MCNP6 at each timestep. In order to gain better spatial resolution, the central peak is subdivided into 4 sections, with the additional lower section of the LLR divided into 2 small sections. This allows more detailed insight into the fast flux evolution with burnup.

$$\Psi_{EOL} = \sum_{t=0}^{T_{EOL}} \phi_t|_S \, (E > 100keV)\Delta t \tag{6.19}$$

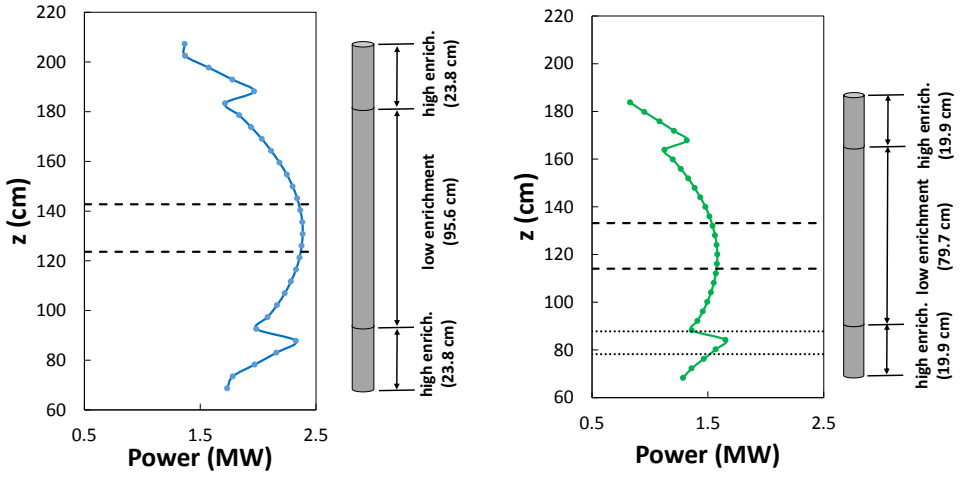

(a) MXR-inter1 axial power profile.

(b) LLR axial power profile.

Figure 6.4: Cycle averaged axial power profile for the whole cores. Values are summed in all radial directions and averaged between BOL, MOL and EOL. Dashed lines indicate the regions that see the highest peaks in power production.

As the values are tallied at each timesteps, a post-processing script extracted the result-

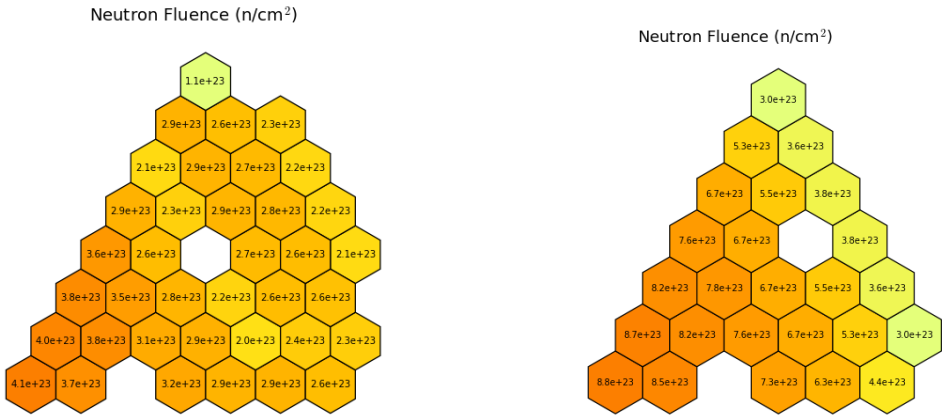

(a) MXR-inter1 fast fluence after 25 years.

(b) LLR fast fluence after 34 years.

Figure 6.5: Map of the peak axial fluence in each fuel assembly at the end-of-cycle (EOL) for the MXR and the LLR. The MXR final locations accounts for shuffling.

ing values at each 'predictor' step. This obtains the temporal flux profile that is used to deplete material compositions. The EOL fast fluence is estimated at each interval, with the highest value out of each interval highlighted in Figure 6.5 (this is to account for small axial deviance within different assemblies). The results are shown for the LLR and the MXR-inter1 layout (it is considered to be representative of the other layouts). Note that individual rods are not tallied, due to computational constraints; rather, the radial average across the assembly is obtained. This was deemed to be sufficiently representative of the models. Shuffling is taken into consideration in Figure 6.5(a), with the assemblies corresponding to their final locations.

The results clearly illustrate the benefit of using the MXR, with its assemblies witnessing substantially less incident fast neutron bombardment than the LLR. This is due to the thermalization in the outer region, reducing the overall proportion of fast neutrons in the spectrum, but also a benefit of shuffling assemblies and moving assemblies that see high rates to lower fluence regions. While k_{eff} does not reach 1.0 until 34 years, the fast fluence limit of 6×10^{23} n/cm^2 is reached after 25 years as shown in Figure 6.6(a). As a result, the LLR has a lifetime that is essentially equal to that of MXR-inter1 when accounting for material limits. In addition, if the same material damage limit (4×10^{23} n/cm^2) is used for

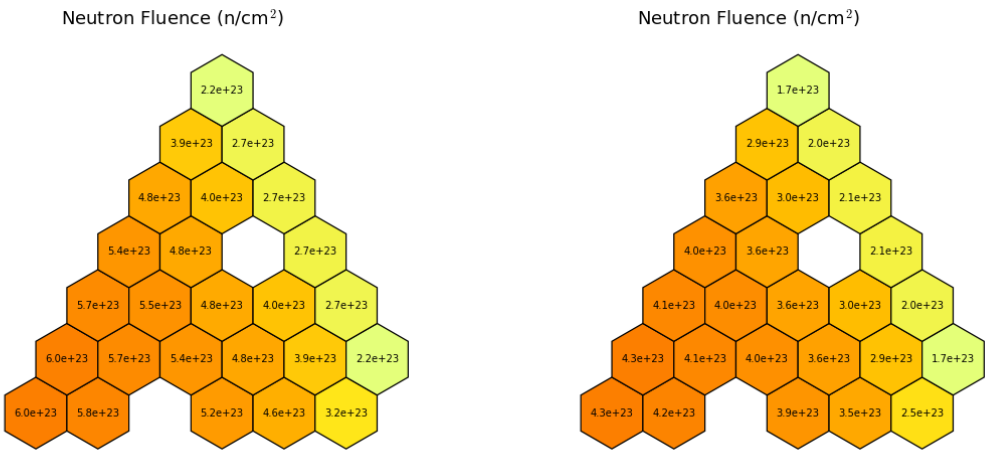

(a) LLR fast fluence after 25 years.

(b) LLR fast fluence after 19 years.

Figure 6.6: Operating years after which the LLR reaches the peak fast fluence limit of 6×10^{23} and 4.3×10^{23} n/cm^2.

both designs, the LLR lifetime would be reduced to 19 years as shown in Figure 6.6(b).

The resulting fast fluence milestones are summarized in Table 6.6. Values are estimated via linear interpolation between timesteps (peak fluence increases linearly with burnup). The LLR crosses the 4×10^{23} n/cm^2 limit after around 18 years, and the 6×10^{23} n/cm^2 limit after around 25 years. The MXR on the other hand, never crosses the latter limit, and sees a peak fluence of 4.1×10^{23} n/cm^2 at around EOL (when k_{eff} = 1.0). This is the range where experimental data is available, rendering the model more feasible than the LLR. Therefore, when using currently available material, the MXR design can outperform the LLR by approximately 8 years. If material becomes available that can withstand a 6×10^{23} n/cm^2 fast fluence, the LLR would only match the MXR lifetime. It can be therefore concluded that the MXR is a more feasible long-lived core design, despite the shorter time at which k_{eff} reaches 1.0 (25-27 years versus 34 years for the LLR). The design can be more readily deployed with current clad material (such as HT9 steel) without exceeding the cladding dpa (displacement per atom) limits that have been observed experimentally.

Table 6.6: Effective full power years at which different fast fluence thersholds are reached for the LLR and the MXR-inter1.

	LLR	**MXR**
EFPY at 4×10^{23} n/cm^2	17.9 years	24.5 years
EFPY at 6×10^{23} n/cm^2	25.0 years	-
EFPY at k_{eff} = 1.0	34.0 years	25.0 years

6.2 Thermal Analysis

After assessing reactivity feedbacks, core coupling, and neutron-induced damage; heat production rates in the MXR must be examined. The general goal of this section is to identify weaknesses from a thermal standpoint. Table 5.4 highlighted averaged power density and specific power for the whole core in the LLR and MXR. What is required here is to peer inside the core, even lower than the assembly level, to ensure no localized over-heating occurs. MCNP6 will be used to assess heat generation in different regions and compare the resulting values to typical fast reactor norms.

6.2.1 Radial power peaking

One of the main concerns with mixed-spectrum configuration is the potentially large radial power peaking at the fast/thermal interface. Large incident fast fluxes from the inner regions, meet thermalized assemblies with relatively high fission cross-sections. This can result in localized power peaking in assemblies. Average power within each assembly are extracted from MCNP6, and divided by the core assembly-average to obtain radial peaking ratios (P_i/P_{av}). Figure 6.7 highlights the resulting values observed in the MXR-inter1. The maximal ratios, 1.493 & 1.491 were both observed at BOL, and located at the fast/thermal interface as expected. These values are in-line with the LLR which sees the highest radial peaking value of 1.479 at EOL in the core center. Similar trends are observed for MXR-inter5, with the highest values seen at the same locations as MXR-inter1. Different

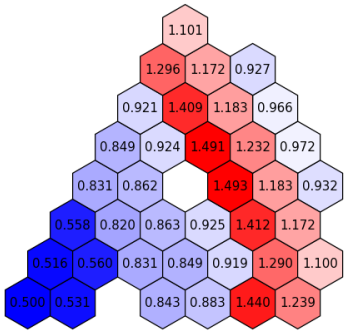

(a) Radial power peaking at BOL.

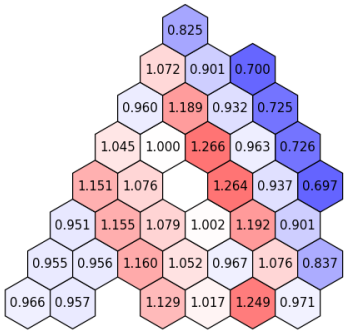

(b) Radial peaking at MOL1 prior to shuffling (13 years).

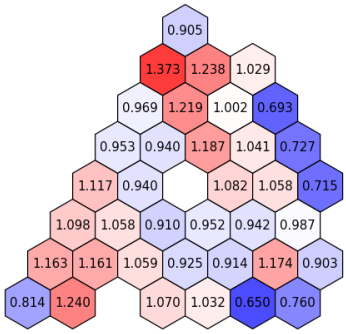

(c) Radial peaking at MOL2 after shuffling (13 years).

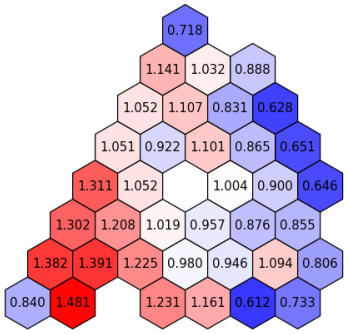

(d) Radial peaking at EOL (25 years).

Figure 6.7: Radial power peaking map of the MXR-inter1 layout at different timesteps. Assemblies shown in (c) and (d) were shuffled according to the previously outlined shuffling strategy. The colorbar ranges are the same in each plot. Values are obtained by dividing the power in each assembly by the core average.

approaches are applicable here, to further flatten the power profile of the MXR if deemed necessary. Enrichment levels can be lowered, neutron poison can be added or the control rod can be partially inserted. Alternatively, managing the symptom is an another option; this can be done by increasing the orifice diameter of specific assemblies to ensure a greater mass flow rate.

The next step is to peer more closely within the assembly to ensure no individual fuel rods see elevated heat production rates. The assemblies with the most pronounced radial peaking factors of Figure 6.7(a), number O804 & O805, were selected for further analysis.

Figure 6.8 shows the resulting values for MXR-inter and Figure 6.9 shows the linear heat rates in MXR-inter5. The empty space between the rods highlights where the moderating rods are located. The maximum recorded linear heat rate was 26.5 kW/m for MXR-inter1 and 47.8 kW/m for MXR-inter5. The MXR-inter1 peak rod values fall within the norm of what is encountered for typical sodium fast reactor designs such as the ABTR (average of 21.1 kW/m and peak of 38.5 kW/m).[69] The MXR-inter5 on the other hand, sees spikes above the norm, and is therefore not considered for further analysis. Substantial gradients are observed within the moderated assemblies; power can vary by as much as 65% within the same assembly (assembly pitch is only 16.5 cm). With a large volume of moderator concentrated in the center of the assembly, low energy neutrons have very short mean free paths and can only interact with adjacent fuel rods, raising their fission cross-sections and their power production as a result. These large inter-assembly power gradients make the inter5 arrangement less attractive from a safety standpoint. These peak linear heat rates will be used in sub-channel analysis in Section 6.2.3 to evaluate fuel melting margins. Chapter 7 will also investigate design modifications that can help alleviate power peaking, such as doping the fuel with burnable absorbers.

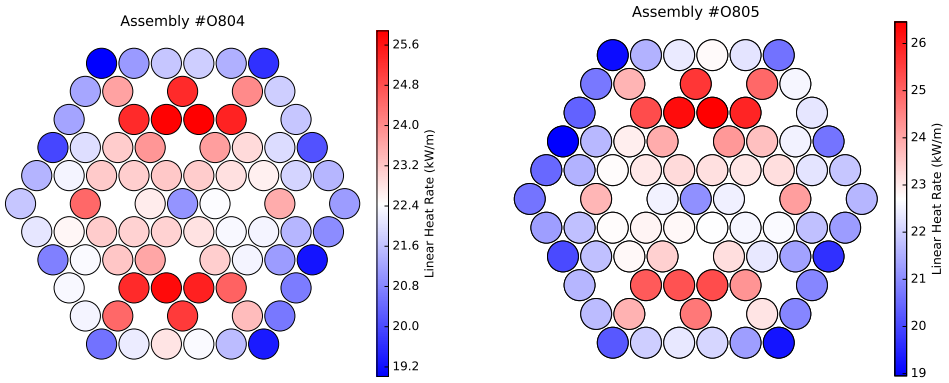

(a) Linear heat rate within Assembly O804. ($\overline{sd} = 0.33\%$)

(b) Linear heat rate within Assembly O805. ($\overline{sd} = 0.33\%$)

Figure 6.8: Linear heat rate (kW/m) in fuel rods within MXR-inter1 assemblies. The fuel assemblies shown are at the fast/thermal interface and experience the highest radial power peaking.

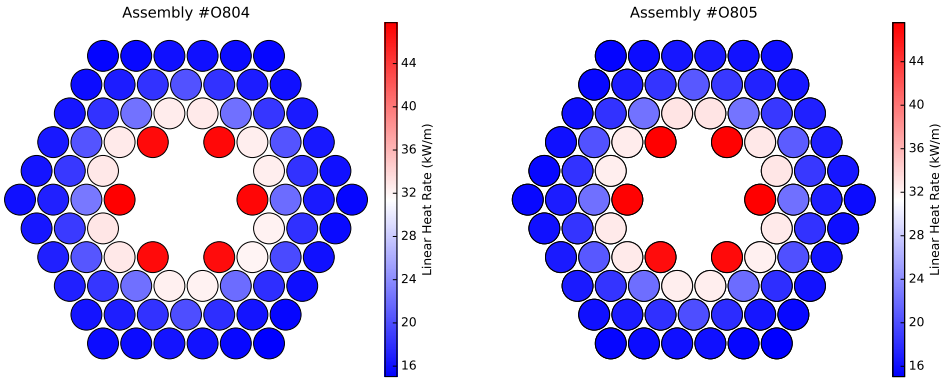

(a) Linear heat rate for Assembly O804 in MXR-inter5.. ($\overline{sd} = 0.34\%$)

(b) Linear heat rate for Assembly O805 in MXR-inter5.($\overline{sd} = 0.34\%$)

Figure 6.9: Linear heat rate (kW/m) in fuel rods within MXR-inter5 assemblies. The fuel assemblies shown are at the fast/thermal interface and experience the highest radial power peaking.

The rod-based results highlight the limitations of only relying on assembly-level analysis. This further illustrates the limitations of nodal-transport tools such as DIF3D (with future codes such as PROTEUS, potentially alleviating these limitations). In effort to ensure no additional inter-assembly power peaking is occurring, a very fine 'fmesh' was tallied across the core. Each mesh had dimensions of $1.9 \times 1.6 \times 143.3$ cm (the height of the fuel rod). Figure 6.10 displays the high-fidelity results. The high spatial resolution makes it possible to identify assembly boundaries and observe power variations within them. The elevated radial peaking at the fast/thermal interface from Figure 6.7(a) is observed here as well. Upon closer inspection however, it is apparent that the highest power peaking is in fact at the reflector/core interface, despite the relatively low assembly power ratio. This core region sees very thermalized neutrons being reflected (in light of the $ZrH_{1.6}$ contained within reflector assemblies). The very short mean free path of these neutrons results in them only interacting with the outermost fuel rods. Additionally, their low energy increases the fission cross-section, resulting in relatively large spike in power production at these far edges. Alternative reflector material will be considered in Chapter 7.

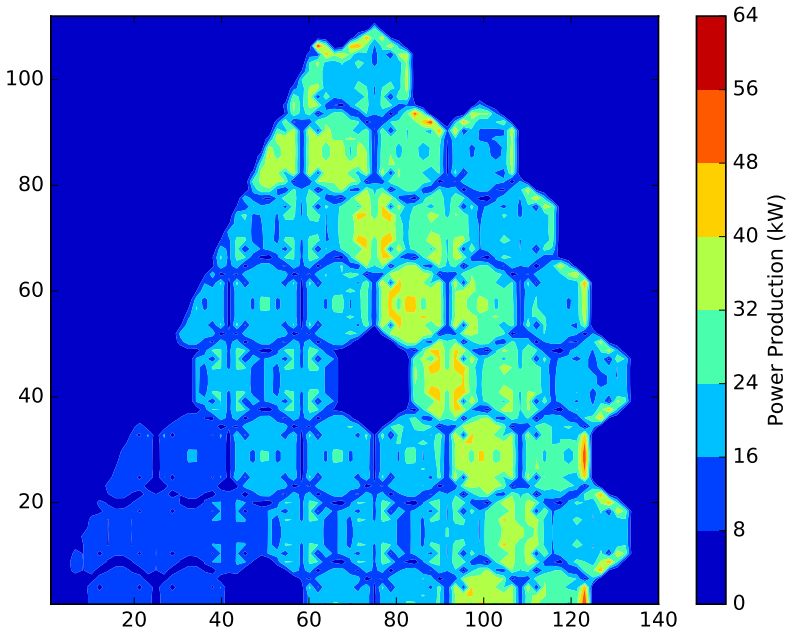

Figure 6.10: Radial power distribution in the MXR core. ($\overline{sd} = 0.39\%$)

6.2.2 Axial power peaking

The previous analysis did not account for axial variations within assemblies. As Figure 6.4(a) previously showed, the axial power profile in both the LLR or the MXR is not flat. It is therefore important to consider axial effects within assemblies. A mesh tally with cell sizes of $4.2 \times 4.8 \times 4.8$ cm was used to model the core. The grid is not as fine as that of Figure 6.10 due to computational limits, since 30 axial slices were considered, as opposed to 1 in the radial peaking evaluation. Nevertheless, the radial area is still smaller than the assembly pitch, and inter-assembly variations can be captured to some extent. Initially, cell power ratios were considered as shown in Equation 6.20. P_{core}^{xy} estimates the peaking within each cell column (xy), relative to the whole core average in each cell. P_{loc}^{xy} evaluates the localized peaking in each xy cell column relative to the average value within that column. The subscript i denotes any of the 30 z-meshes in a given xy cell column. The results for normalization each case are shown in Figure 6.11.

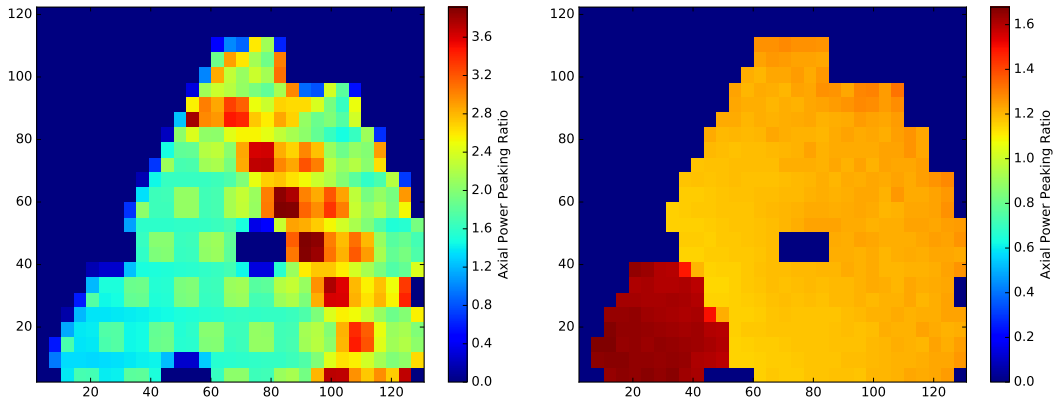

(a) Core averaged axial power peaking. (b) Locally averaged axial power peaking.

Figure 6.11: Axial power peaking of MXR-inter1 at BOL. Average Monte Carlo standard deviation for the mesh tally was 1.06%.

$$P^{xy}_{core} = \frac{\max(P^{xy}_i)}{\text{av}(P_i)} \qquad P^{xy}_{loc} = \frac{\max(P^{xy}_i)}{\text{av}(P^{xy}_i)} \tag{6.20}$$

The plots highlight how the most pronounced peaking effects are mostly radially driven. Figure 6.11(a) is near-proportional to the radial peaking plots, while Figure 6.11(b) shows that very little variation in axial peaking is observed within cases. Nevertheless, it is still important to verify that power production coinciding at axial peaks of radially hot zones are within the norms for a typical fast reactor. The maximum axial power density is therefore plotted in Figure 6.12 for BOL, MOL, and EOL in MXR-inter1. MOL was taken to be after 13 years of operation, immediately prior to when shuffling takes place. As expected, the highest values still coincide with the radial peaks. The most elevated power density value is of 105 kW/l and appears at BOL. This is notably lower than the peak value of 137.8 kw/l observed for the LLR. Axial peaking effects are therefore deemed to be manageable in the MXR. These results are not expected to be drastically different for alternative core configurations such as the MXR-inter5.

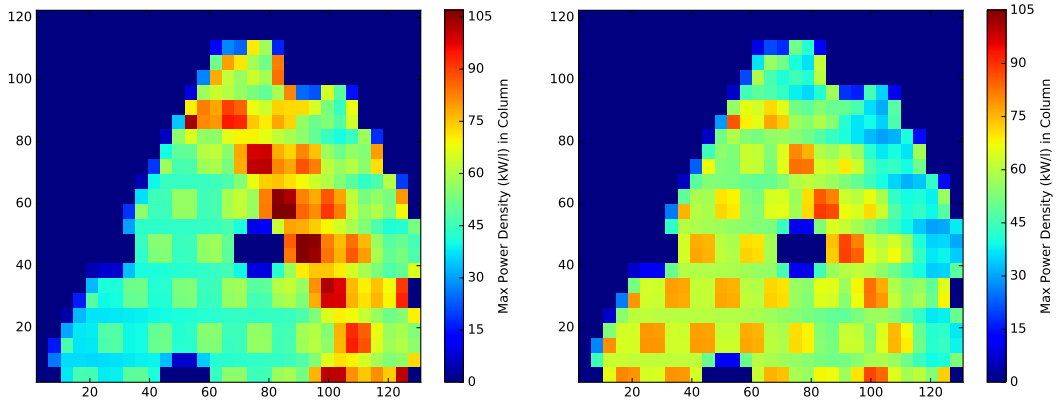

(a) Max power density at BOL. ($\overline{sd} = 1.06\%$) (b) Max power density at MOL. ($\overline{sd} = 1.10\%$)

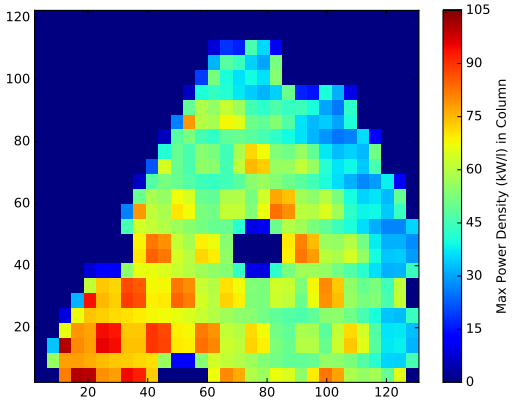

(c) Max power density at EOL. ($\overline{sd} = 1.15\%$)

Figure 6.12: Maximum power density in each cell column for the MXR-inter1 model at different timesteps.

6.2.3 Sub-channel thermal analysis

While, the previously evaluated power-related parameters were shown to be within the range of typical fast reactor values, it still important to consider their collective effects on material limits. The main concern is the maximum coolant and fuel temperatures. A channel-level thermal analysis was therefore conducted for the most limiting case identified in Section 6.2.1. The main objective is to estimate the coolant outlet, peak clad temperatures, and peak fuel centerline temperatures. An analytic approach was selected to estimate parameters. A diagram of the channel is shown in Figure 6.13. The model assumes that the linear heat rate follows a cosine-shaped axial distribution and that material properties

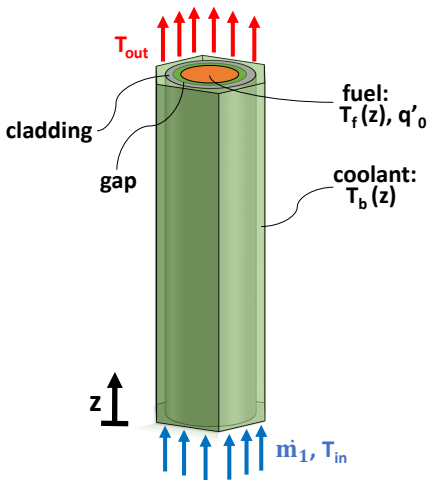

Figure 6.13: Illustration of the channel used in the analytic thermal analysis. The variables $\dot{m}_1$, T_{in} and q'_0 are fed as inputs to compute the temperature distributions T_b and T_f.

do not vary significantly within the channel. The peak linear heat rate is corrected from the average axial value using the relation in Equation 6.21. Where, L is the thermally expanded fuel height, and L_e accounts for the extrapolation length (typical sodium-fast reactor values were used for the diffusion coefficient).

$$q'_0 = \frac{L \times \pi}{2L_e \sin\left(\frac{\pi L}{2L_e}\right)} q'_{av} \tag{6.21}$$

The bulk coolant temperature at any point z can then be evaluated using the relation:

$$T_b(z) = T_{in} + \frac{q'_0}{\dot{m}C_p}\frac{L_e}{\pi}\left(\sin\frac{\pi z}{L_e} + \sin\frac{\pi L}{2L_e}\right) \tag{6.22}$$

C_p values were obtained for the average coolant temperature (472.5°C), using standard correlations.[70] The original mass flow rate for the average LLR channel was determined using the relation:

$$\dot{m} = \frac{2q'_0 L}{\pi(T_{out} - T_{in})C_p} \tag{6.23}$$

The bulk coolant temperature could then be employed to determine the axial tempera-

ture profile at the clad inner-level and fuel centerline:

$$T_c(z) = T_b(z) + q_0' \left[\frac{1}{2\pi R_{co} h} + \frac{1}{2\pi k_{cld}} \ln\left(\frac{R_{co}}{R_{ci}}\right) \right] \cos\frac{\pi z}{L_e} \tag{6.24}$$

$$T_f(z) = T_b(z) + q_0' \left[\frac{1}{2\pi R_{co} h} + \frac{1}{2\pi k_{cld}} \ln\left(\frac{R_{co}}{R_{ci}}\right) + \frac{1}{2\pi k_{Na}} \ln\left(\frac{R_{ci}}{R_f}\right) + \frac{1}{4\pi k_f} \right] \cos\frac{\pi z}{L_e} \tag{6.25}$$

Since the peak linear heat rating corresponds to BOL, the sodium bond between the fuel and the clad inner wall is still present. The smear density is taken to be 75%. R_f corresponds to the fuel-gap radius, while R_{co} and R_{ci} are in the outer and inner clad radii. The cladding thermal conductivity, k_{cld}, was assumed to be similar to that of martensitic steel 20Kh13.[70] In light of the small size of the gap, convection effects are ignored and heat transfer is assumed to occur via conduction primarily. The thermal conductivity value was derived using standard temperature correlations.[70] The fuel thermal conductivity, k_f was estimated using the Argonne AAA Handbook correlation shown in Equation 6.26, that accounts for the zirconium weight fraction, x_{Zr} (k_{alloy} is the thermal conductivity correction due to alloying effects).[71] Lastly, the heat transfer coefficient, $h = Nu \times k/De$, is determined using the CRBRP modified Schad correlations (corresponding to $1.05 \leq P/D \leq 1.15$) shown in Equation 6.27.[72] The main parameter values employed in the analysis are summarized in Table 6.7.

$$k_f = \left(1 - \sqrt{1 - x_{Zr}}\right) k_{Zr} + \sqrt{1 - x_{Zr}} \left[x_{Zr} k_{alloy} + (1 - x_{Zr}) k_U \right] \tag{6.26}$$

$$Nu = 4.496[-16.15 + 24.96(P/D) - 8.55(P/D)^2] \tag{6.27}$$

These were then used in the resulting temperature profiles shown in Figure 6.14. The fist two plots correspond to the average conditions in a LLR and MXR channel. With linear

Table 6.7: Main material parameters used in the thermal analysis.

Parameter	Value
k_{clad}	27.1 W/mK
k_f	25.2 W/mK
k_{Na}	70.3 W/mK
C_p	1.3 kJ/kgK
h	65.4 kW/m^{2}K

power rating values of approximately 15 kW/m in each (axial cosine peak q'_0 of 23 kW/m). The MXR case assumes a 20% increase in mass flow rate to account for the proportionally elongated length of the active region. The third plot highlights the most limiting case: the peak MXR-inter1 channel identified in Section 6.2.1 (26.5 kW/m) at overpower conditions (15% increase in nominal power). To ensure adequate margins, the mass flow rate in this model was increased by 60% relative to the nominal MXR channel. It should be noted that the close proximity of the three axial curves in average conditions is due to relatively low power density within these long-lived core designs. In typical sodium-cooled reactors operating under higher densities (of the order of 40 kW/m), the fuel centerline temperature profile would be substantially more elevated.

The limiting conditions for the three temperature profiles are the coolant boiling, clad eutectic point, and fuel melting temperatures. The three values were taken to be respectively 882, 650, and 1250°C. In the original AFR-100 design, it was assumed that future clad material would allow to reach a clad eutectic of 700°C.[13] In the peak channel for the MXR-inter1 (without overpower conditions) at the nominal flow rate, boiling margins are 217°C, clad eutectic margins are -17°C, and fuel melt margins are 512°C. A 7% increase in mass flow rate is sufficient to ensure the fuel-clad eutectic limit is not reached. However, to allow sufficient margins mass flow rate should be increased further. A parametric evaluation was performed in Table 6.8 to assess the increase mass flow rate requirements for the most limiting channel. Overpower condition were applied (115% of nominal power) in

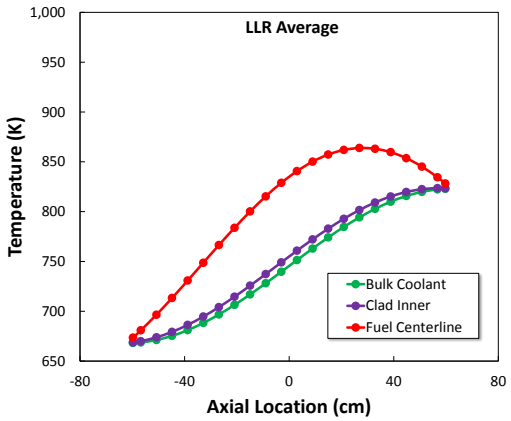

(a) LLR average channel profiles.

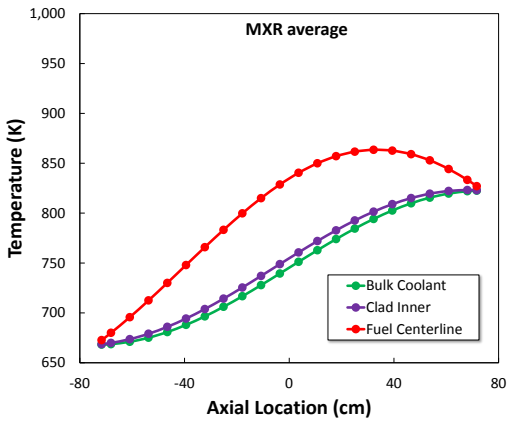

(b) MXR-inter1 average channel profile (with 20% increase in mass flow rate relative to LLR).

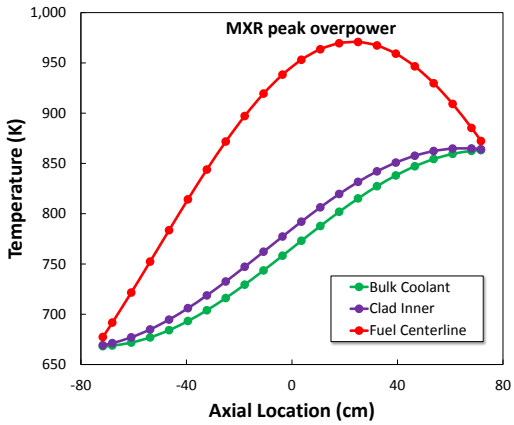

(c) MXR-inter1 peak channel profile at overpower condition (with 60% increase in mass flow rate relative to MXR-inter1 average).

Figure 6.14: Bulk coolant, clad inner, and fuel centerline axial temperature profiles in the different LLR and MXR-inter1 channels.

order to provide conservative margins. The analysis showed that the fuel-clad eutectic is the most limiting criteria in the design. Sensitivity analysis found that a 23.5% in mass flow rate relative to the nominal MXR channel ensured clad eutectic temperatures were reached. To ensure adequate margins, an increase in nominal mass flow rate between 40 and 60% is recommended. This can be done by altering the assembly inlet orifice diameter for limiting assemblies. Under such conditions, fuel melting margins are of the order of 530-550°C. Such high margins can be reached in this type of reactors due to the derated power density within the core. The proposed increases in mass flow rate are not expected to be too pe-

nalizing. Sodium designs do not have a limiting flow rate value (lead-cooled designs are limited by the clad erosion), and typical fast reactors have nominal flow rates 2-3 times higher than that of the original LLR design. More in depth analysis is required with more sophisticated thermal hydraulics model to accurately predict thermal characteristics. At this stage, it can still be deemed that the MXR-inter1 is feasible from a thermal standpoint, without any notable limitations. Chapter 7 will investigate MXR core configurations that can alleviate some of the constraints further still.

Table 6.8: Temperature margins to coolant boiling and fuel melting under overpower conditions (115% of nominal power values). Mass flow rates considered are relative to the nominal MXR-inter1 channel conditions.

	ΔT_{boil}	$\Delta T_{eutectic}$	ΔT_{melt}
$\dot{m}_{MXR} \times 100\%$	176.4°C	-57.9°C	460.8°C
$\dot{m}_{MXR} \times 120\%$	228.3°C	-6.1°C	503.2°C
$\dot{m}_{MXR} \times 140\%$	265.4°C	30.8°C	531.6°C
$\dot{m}_{MXR} \times 160\%$	292.9°C	58.3°C	552.4°C

6.2.4 Power evolution with burnup

Previous sections only briefly investigated the evolution of power generation with time. The analysis was limited to snapshots at different timesteps. This section will study in further detail the temporal profile of the power production within assemblies. As a first step, the accumulated power production in each assembly, is assessed. This is in effect, the burnup reached at EOL for reactor designs. Figure 6.15 displays a burnup map of the LLR, the MXR-inter1 and the MXR-inter5. The results do not account for peaking within assemblies, and the maximum value was determined to be 172 GWd/MTU for the case of the LLR. This is still below the maximum level tested experimentally, 200 GWd/MTU, even when accounting for a 1.16 axial peaking factor (obtained from Figure 6.4(b)).[14] As such, peak fast fluence is deemed a more limiting factor than maximum burnup.

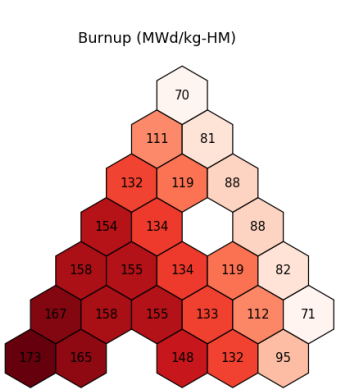

(a) LLR burnup at EOL (34 years).

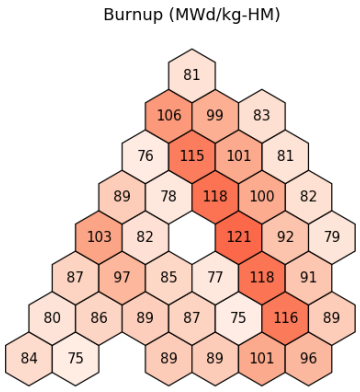

(b) MXR-inter1 burnup at EOL (25 years).

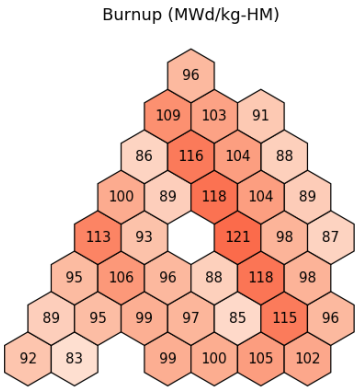

(c) MXR-inter5 burnup at EOL (27 years).

Figure 6.15: The discharge burnup in each assembly of the LLR, MXR-inter1, MXR-inter5. Shuffling is accounted for in the MXR locations; the locations in the diagrams correspond to the initial core layout. The colorscale for all three plots have the same range. Note that the values shown are for the average within the assembly.

Table 6.9 summarizes the main findings for each of the tree cases. The peak and average burnup are evidently higher for the LLR in light of its longer operating lifetime and lower heavy-metal inventory. The temporal power profile variation between assemblies appears much flatter for the MXR designs. The margin between the highest and lowest assembly burnup level reached is as high as 102 GWd/MTU for the LLR. It is only 46.7 and 37.7 GWd/MTU for the MXR-inter1 and MXR-inter5 respectively. This highlights the benefit of performing core shuffling and spreading out the contribution of each assemblies over time.

Table 6.9: Assembly burnup (BU) parameters in GWd/MTU for the three core designs at EOL. Note that peak(BU) corresponds to the maximum burnup value averaged over the whole assembly.

	LLR	**MXR-inter1**	**MXR-inter5**
peak(BU)	173.2	121.9	121.1
av(BU)	125.9	92.3	99.6
max(BU)-min(BU)	102.6	46.7	37.7

The next step is to evaluate variations at each time interval, to ensure no unexpected spikes occur. The power fraction (normalized to whole core output) evolution for assemblies in each of the three zones in MXR-inter1 is shown in Figure 6.16. The highest power fraction (4.0%) ever reached during the lifetime occurs in the outer region at BOL. This corresponds to the two assemblies previously identified in Section 6.2.1, O804 and O805. Since the linear heat rate in these assemblies was concluded to be within acceptable safety margins, all other assemblies are considered to be within acceptable margins. While some assemblies do see high power fractions at times, at its worst, this is no more than a 1.34 percentage point above the core average (2.7%). Alternative shuffling strategies will be investigated in Chapter 7 to optimize the overall power production in each assembly.

Lastly, it is important to assess the contribution of the fast versus thermalized zones to the overall power production in the reactor. Figure 6.17 plots the evolution of the relative contribution of each zone to the total power output. The results are for MXR-inter1 and account for shuffling. The core composition was designed to converge at MOL, and this can be clearly seen in the results. Both regions generate 50% of the power at that point. Nevertheless, the outer assemblies (which shift from the thermal to fast zone in Figure 6.17) tend to be responsible for the majority of the power generated throughout the core lifetime. This is due to the higher initial fissile inventory in those assemblies relative to the innermost ones. Further optimization of the enrichment at each zone can potentially help flatten the contribution from each zone.

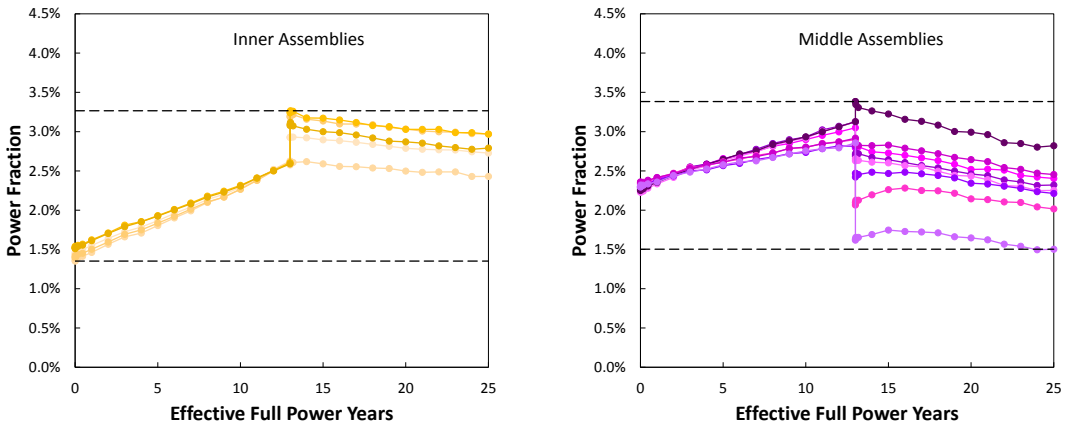

(a) Evolution in inner assemblies.

(b) Evolution in middle assemblies.

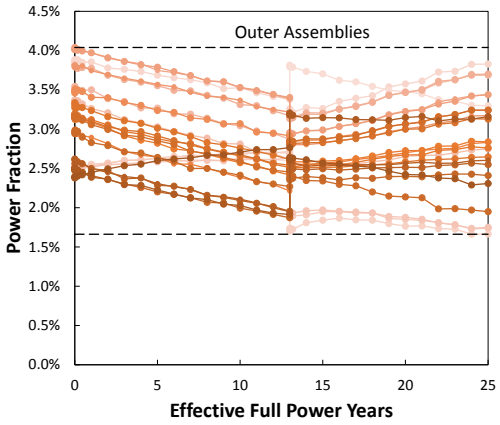

(c) Evolution in outer assemblies.

Figure 6.16: Assembly power fraction evolution in each of the three main regions throughout the MXR-inter1 lifetime (accounting for shuffling). Dashed lines show the upper and lower limits in power fraction of each case. While assemblies are shuffled after 13 years, their naming convention stays the same (even though outer assemblies are placed in the inner and mid region).

6.2.5 Moderator heating

In addition to power peaking effects, the insertion of moderating material within a sodium-cooled reactor can introduce other hazards. Zirconium hydride can disassociate at very high temperature causing a buildup of hydrogen within the rods. Hydrogen leaking from the moderating rod is very problematic in a sodium-cooled reactor as the two elements can react violently. It is therefore important to remain below the chemical limit of the material

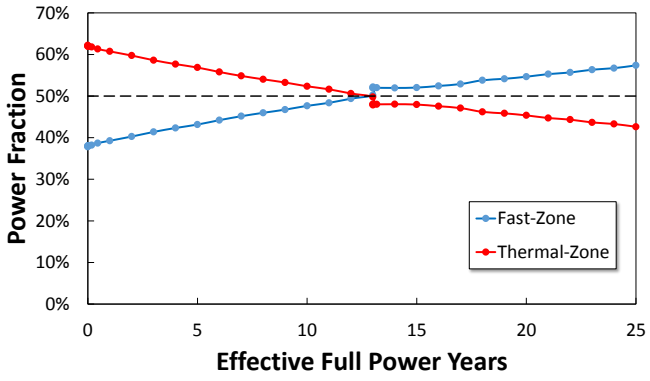

Figure 6.17: Proportion of the power generated in the fast versus thermalized zone before and after shuffling in MXR-inter1.

during operations. Zirconium hydrides have been extensively used in TRIGA reactors. Previous studies have determined that the molecule remains chemically stable up to 750°C during operating conditions, and can sustain temperatures as high as 1200°C during short transient pulses.[73]

Since the fuel and moderating material are separate, most heating in the $ZrH_{1.6}$ rods occurs from coolant convection as well as photon and neutron collision heating. Estimating the collision heating rate, requires coupled photon-neutron transport simulations using MCNP6. This can be very computationally expensive at a core level. A suitable approximation is to evaluate it at a reflected lattice assembly model. By normalizing the assembly power to the correspondingly highest radial power within the core, the peak zirconium rod heat generation can be estimated. Figure 6.18(a) shows the results for an MXR-inter1 type lattice. To assess the most conservative heat generation values, the lattice model values were denormalized using the highest fuel peaking values (linear heat rate of 26.5 kW/m multiplied by the axial peaking factor of 1.16, as obtained from Figure 6.4(a)). In most rods, around 60% of the energy released originates from neutron-based reactions, and 40% from photon collisions.

As shown in Figure 6.18(a), the peak linear power rating within a moderating rod was estimated to be 17 W/m, several orders of magnitude lower than that of a fuel rod. This

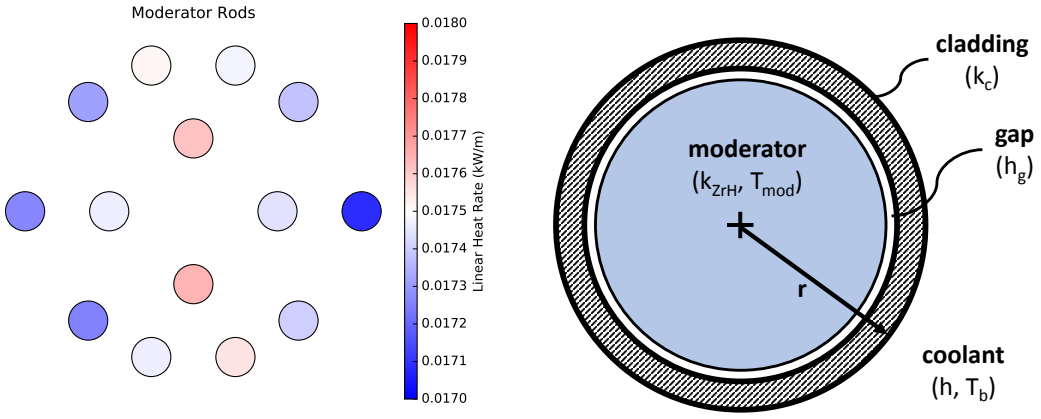

(a) Linear heat generation in moderator rods within assembly. (b) Radial diagram of heat transfer in individual rod.

Figure 6.18: Linear heat rate within moderating rods in a reflected assembly, and diagram of radial heat transfer system (with corresponding material properties within brackets).

peak value was then used to evaluate the radial heat conduction analytically, similarly to the computation in Section 6.2.3. Equation 6.28 is used to evaluate the maximum difference in temperature between the moderator and the surrounding coolant. Standard material property values were used,[70] alongside the typical gap conductivity value in an oxide fuel pellet (5.7 kW/m^{2}K). ΔT_{mod} was estimated to be in the order of just 0.052°C. This is expected since the peak linear heat rate value is small, and $ZrH_{1.6}$ has a relatively high thermal conductivity. As such, heat generation can be assumed to be negligible in the moderating material. The moderating material does however add an additional constraint during transient scenarios. Since its temperature closely follows that of the coolant, care must be taken to ensure the peak outlet temperature stays within $ZrH_{1.6}$ chemical stability limits as well as sodium boiling limits. While sodium does not reach its boiling point until around 880°C, zirconium hydride is stable up to 750°C under steady state conditions. The moderating material is known to be able to withstand temperatures above the sodium boiling point, during short transients in TRIGA pulses. Further research is needed to determine its chemical stability at high temperatures during longer transients that are within the design

basis of the reactor.

$$\Delta T_{mod} = T_{mod} - T_b = q'_0 \left[\frac{1}{2\pi R_{co} h} + \frac{1}{2\pi k_{cld}} \ln\left(\frac{R_{co}}{R_{ci}}\right) + \frac{1}{2\pi R_g h_g} + \frac{1}{4\pi k_{ZrH}} \right] \quad (6.28)$$

6.3 Chapter Conclusion: Validation of Inherent Safety Metrics in the MXR

Most safety-related metrics evaluated in this chapter, were deemed to be met by the MXR-inter1 design. The main parameters are summarized in Table 6.10. The design was shown to have a reduced peak fast fluence within the core, and a lower fast neutron flux outside the core. The fast and thermal zones are neutronically coupled, reducing the risks of power tilting. Doppler and void reactivity coefficients were improved, while expansion coefficients were slightly decreased relative to the original LLR. Most integral feedback parameters, used for quasi-static feedback analysis, were in-line with the LLR design. Similarly, power peaking effects were deemed manageable relative to typical sodium-cooled reactors (mostly due to the low power density of the core). Additionally, moderator and fuel temperature failure margins were relatively high, ensuring sufficient leeway during transients. Further research is needed to evaluate all the aforementioned parameters in more detail. Ideally, coupled neutronic-thermal analysis would be conducted in the future, to obtain a more thorough evaluation. Nevertheless, most of the analysis thus far validates the MXR design. The main concerns were the high initial starting k_{eff} which lead to one passive-safety criteria not being met, as well as the relatively 'unflattened' power profile within the core. The next chapter will investigate design modification that can help alleviate these and other concerns. It will also conduct a resource and nonproliferation evaluation of the final designs. While the analysis mostly focused on the MXR-inter1 variant, power peaking in the MXR-inter5 was evaluated and shown to be very pronounced in rods adjacent to the central moderator. As a result, the MXR-inter1 was selected as the main design basis for further analysis.

Table 6.10: Summary of main performance metrics of the LLR and MXR-inter1.

	LLR	**MXR-inter1**
peak(Ψ_{fast}) (n/cm^2)	8.8×10^{23}	4.3×10^{23}
peak(BU) (GWd/MTU)	173.22	121.87
A/B	0.22	0.27
$(A+B)/(C\Delta T_c)$	1.38	1.31
$\|B\|(A + A/B)$ (¢)	23.25	33.10
k_{tf} (BOL)	0.20	0.25
k_{ft} (BOL)	0.24	0.13
peak(P_{assem}/P_{av})	1.48	1.49
peak(q') (kW/m)	22.97	26.50
peak(q''') (kW/l)	137.8	106.91

CHAPTER 7
DESIGN IMPROVEMENTS AND PERFORMANCE EVALUATION

Previous reactor optimization work focused only on reactor lifetime and regional plutonium quality. The previous chapter identified some potential advantages and weaknesses of the MXR from a safety standpoint. The lessons will be incorporated into alternative designs in this chapter. Additional parameters will also be taken into consideration, such as resource requirements. These will be investigated in this chapter alongside a more in-depth review of the proliferation resistance of the finalized MXR design configurations. A final verdict on the characteristics of the MXR relative to the original LLR and typical LWR will be discussed at the end of the chapter.

7.1 Safety-Related Design Improvements

Overall MXR safety parameters were along the lines of those of the LLR. Some parameters however, showed room for further improvement. This section will investigate three main design modifications to that end. First, the shuffling strategy will be revisited, with more systematic approaches considered. Then, radial power peaking at the reflector/core interface will be discussed further, and alternative reflector compositions simulated. Lastly, design modifications that mitigate power peaking at the fast/thermal interface will be examined.

7.1.1 Alternative shuffling schemes

Chapter 6 highlighted some disparities in EOL burnup within assemblies of the MXR-inter1 configuration. While substantially lower than what is observed for the LLR, power is not evenly spread out within individual assemblies in the concept. In addition, a sharp reactivity drop is observed following shuffling in the MXR. These factors indicate that the

shuffling strategy for the core may be further improved upon. As previously explained, the original shuffling scheme was agreed upon through trial and error. This section will investigate more mechanistic approaches, and evaluate potential added benefits that they may bring.

The first approach investigated relies on flattening the total power contribution of different assemblies. At MOL, the burnup accrued in each assembly is estimated and assemblies are shuffled based on their respective contributions. Assemblies with high burnup were preferentially shuffled to locations where low burnup was observed. The shuffling methodology is illustrated in Figure 7.1. Essentially, fast assemblies are arranged in a list of ascending burnup order, and thermalized assemblies are arranged in descending order. The positions can then be correspondingly flipped between the two regions. Since there is one more outer assembly than there are fast ones, the thermalized assembly with the highest burnup is moved to the outer location that saw the lowest burnup. All remaining assemblies are switched as highlighted in Figure 7.1.

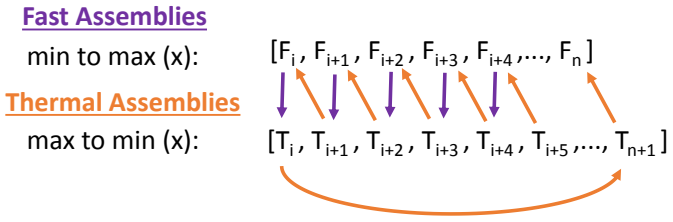

Figure 7.1: Diagram of the shuffling strategy pursued. Assemblies in each zone are listed in ascending and descending order of their x value (e.g. burnup, or fissile mass content), and the locations are flipped according to the arrows.

The second shuffling strategy relied on a similar methodology, but matched fissile inventory within each assembly, rather than burnup. The summed mass of ^{233}U, ^{235}U, ^{239}Pu, and ^{241}Pu in each assembly at MOL was evaluated, then used to guide the shuffling scheme following the schematic in Figure 7.1. The assemblies with the highest fissile inventory in the thermalized zone, were placed in locations that had low fissile inventory in the fast zone. This allows the shuffling strategy to account for breeding as well as fissile depletion

within assemblies. The resulting assembly arrangements for the burnup-based approach and the fissile content-based approach are shown in Table 7.1.

MCNP6 depletion simulations were then performed for each of these cases at the same MOL point as the original MXR-inter1 (13 years). Figure 7.2 highlights the effect on the evolution of core reactivity. The fissile-based scheme seems to have an advantage over the other two schemes with a total operating lifetime of 26 years. It also displayed the smallest drop in reactivity after shuffling, at 377 pcm (relative to 1290 pcm for the original shuffling scheme). The burnup-based strategy was the least effective from a longevity perspective, increasing the reactivity drop after shuffling and reducing the overall lifetime of the core by around 1 year. The burnup-based approach led to the shortest lifetime, at 24 years.

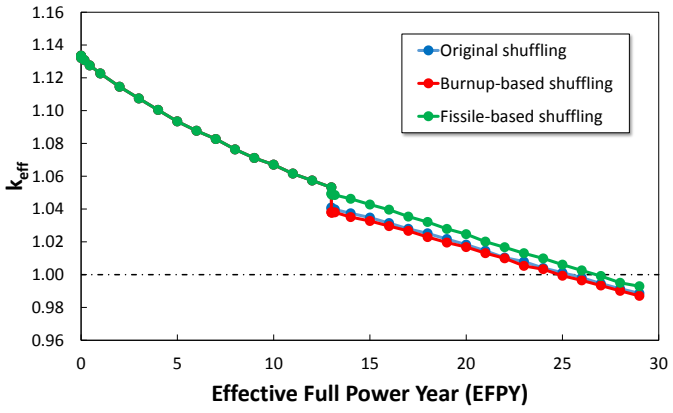

Figure 7.2: Eigenvalue evolution following the different shuffling schemes. The average Monte Carlo standard deviation was of 25 pcm.

Effective shuffling strategies can ensure a more balanced power production in each assemblies. Moving assemblies from regions of high importance to some with lower importance can converge the overall power contribution of each assembly. The assembly burnup for each three case, are compared in Figure 7.3. Analysis was conducted after 24 years since that was the maximum estimated lifetime of the burnup-based case. Usually, strategies that have the lowest max to min margin in burnup tend to also have the lowest peak burnup value, as power contribution is shared between assemblies. The fissile-based shuffling scheme breaks that trend. It saw the highest burnup margin of the three cases at 49

Table 7.1: Shuffled assembly locations in each scheme.

		assembly shuffling strategy				
		original		**burnup-based**		**fissile-based**
I201	→	O802		O804		O906
I301	→	O803		O701		O107
I302	→	O804		O805		O104
I402	→	O805		O806		O105
I403	→	O806		O803		O106
M501	→	O905		O105		O801
M502	→	O906		O104		O902
M503	→	O907		O908		O803
M504	→	O807		O106		O806
M601	→	O904		O904		O807
M602	→	O903		O905		O701
M603	→	O902		O902		O802
M604	→	O801		O907		O908
M605	→	O107		O801		O805
O701	→	I201		O807		O907
M702	→	O701		O906		O904
M703	→	O104		O903		O905
M705	→	O105		O802		O903
M706	→	O106	or	I302	or	M503
O801	→	M605		I702		M604
O802	→	I301		M402		M601
O803	→	I302		I301		M504
O804	→	I402		O107		M605
O805	→	I403		I201		M602
O806	→	M504		I403		M501
O807	→	M503		M706		M706
O902	→	M604		M604		M603
O903	→	M603		M703		M702
O904	→	M602		M602		I201
O905	→	M601		M605		M703
O906	→	M501		M601		I301
O907	→	M502		M705		M705
O908	→	O908		M603		M502
O104	→	M702		M504		I403
O105	→	M703		M503		O804
O106	→	M705		M501		I402
O107	→	M706		M502		I302

GWd/MTU, but the lowest peak burnup at 107 GWd/MTU. While there is a large disparity with the burnup of the innermost assemblies, all remaining assemblies have burnup values much closer to each other. The average burnup margin between different assemblies (as defined by Equation 7.1) are relatively. The drop in peak burnup is so significant, that it takes two additional years for the fissile-based case to reach the same value as the original shuffling case. These different values are summarized in Table 7.2. Further improvement to the fissile-based shuffling schemes requires fine-tuning of the enrichment levels, especially at the inner regions. Ultimately, advanced tools such as Genetic Algorithms need to be relied on to find more optimal schemes.[74]

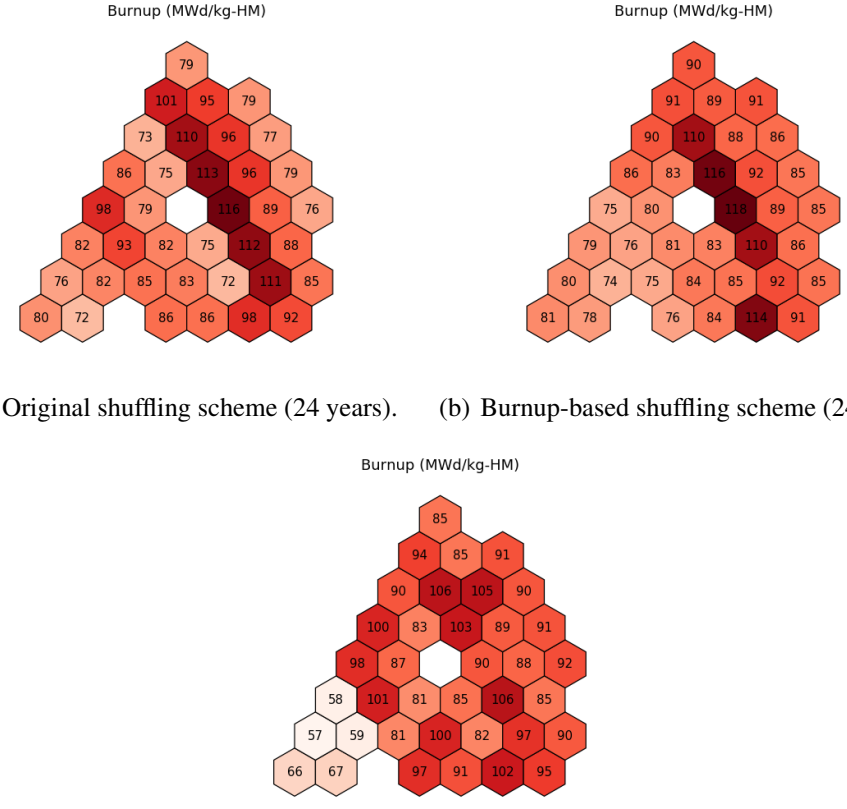

(a) Original shuffling scheme (24 years). (b) Burnup-based shuffling scheme (24 years).

(c) Fissile-based shuffling scheme (24 years).

Figure 7.3: Burnup comparison after 24 years for the three shuffling schemes in MXR-inter1. Note that the displayed assembly locations correspond to the original configuration before shuffling.

$$\overline{M} = \frac{\sum_{i}^{N} |BU_i - \overline{BU}|}{N} \tag{7.1}$$

Table 7.2: Burnup metrics (GWd/MTU) for each shuffling scheme. Results are for the MXR-inter1 configuration. The EOL for each case is 25, 24 and 26 years respectively. Peak burnup margins refer to the difference between max(BU) and min(BU), while average margins are estimated using Equation 7.1.

	original	**burnup-based**	**fissile-based**
24 years:			
peak(BU)	116.8	118.4	106.5
av(BU)	88.5	88.5	88.8
peak margin	44.3	44.2	48.8
average margin	10.1	8.1	9.4
EOL:			
peak(BU)	121.9	-	116.9
av(BU)	92.3	-	96.3
peak margin	46.7	-	55.1
average margin	10.7	-	10.8

The main disadvantage of the fissile-base shuffling scheme is with regards to radial power peaking. As shown in Figure 7.4, peaking values are more pronounced at both MOL2 (right after shuffling) and EOL. The previous peak in the original shuffling strategy (1.493 at BOL) is exceeded, with a max peak of 1.531 at EOL in the new shuffling scheme. This highlights the limitation of using fissile composition as the basis for assembly shuffling; assemblies with high contents tend to be placed in regions of high importance. Care must be taken when using such a scheme to ensure power peaking values are not exacerbated. For the case of the MXR-inter1 configuration, the results in this section appear to validate the original assumptions when devising the shuffling strategy. The original scheme balances out the advantages and disadvantages of the burnup and fissile-based approaches and is preferred for this type of layout.

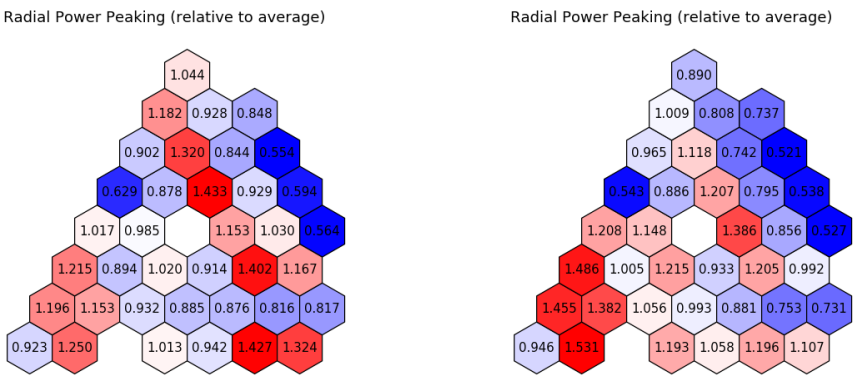

(a) At MOL2, right after fissile-based shuffling.

(b) At EOL (26 years), 13 years after fissile-based shuffling.

Figure 7.4: Radial power peaking of the MXR-inter1 after the fissile-based shuffling scheme. The assembly locations in the plot correspond to their final locations after shuffling.

7.1.2 Reflector material

The reflector/core region was identified in Chapter 6 to be potentially problematic. In light of the high volume of $ZrH_{1.6}$ inside reflected assemblies, very thermalized neutrons can travel back to the outer edges of the core and cause a high rate of fission reactions at the nearest fuel rods. Maximizing neutron thermalization is desirable within the outer region of the core, but not very useful at the very edge. As a result, an alternative reflector material was considered. In light of the results in Section 5.1.2, BeO was considered the next ideal moderator after $ZrH_{1.6}$ (ZrD is not a readily available material). It is also a commonly used reflector material in research reactors. As an added benefit, the reduction in absorption cross-section should result in some gain in reactivity. Figure 7.5 shows the resulting radial power distribution. The modified case will be referred to as MXR-BeO.

Comparing to the profiles in Section 6.2.1, a notable reduction in power peaking at the very edge of the core is observed in Figure 7.5(a). The maximum power reached within an individual mesh cell is approximately 25% lower than that of the original MXR-inter1. The slightly reduced neutron moderation at the reflector level eliminates the most pronounced peaks at the reflector/core interface. Conversely, the power fraction in the outermost as-

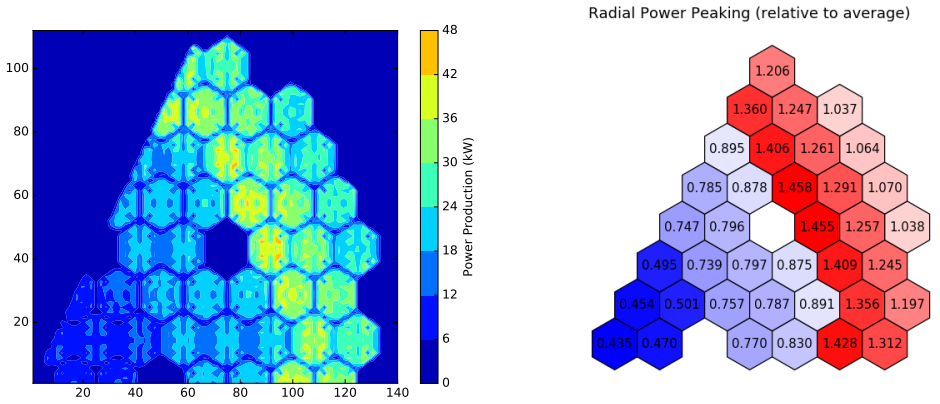

(a) Radial power distribution. ($\overline{sd} = 0.37\%$) (b) Radial power peaking per assembly.

Figure 7.5: Radial power production in the modified MXR core with BeO reflector. Results are shown for BOL. Values in (b) are relative to the assembly average.

sembly is increased as shown in Figure 7.5(b). The outer core now generates a higher proportion of the power than previously the case. The inner and mid radial power ratios are depressed relative to MXR-inter1. A notable advantage of using a reflector, is that it reduced the maximum assembly peaking value at the fast/thermal interface. The highest value is 1.458 versus 1.493 in the MXR-inter1. An additional benefit is that the core lifetime was also extended by one year (to 26 years) as shown in Figure 7.6(a) (note that the assemblies are now shuffled after 15 years). The lower absorption rate in the reflector is clearly beneficial from a neutronic buckling standpoint. These advantages do not come at a noticeable cost to plutonium quality within assemblies. Figure 7.6(b) illustrates how average assembly values drop below the weapon grade limit before EOL.

Another area where the reflector material can have an impact is the outer core fast flux. It must be ensured that the resulting value stays within bounds seen in the LLR. Following the same methodology as outlined in Section 6.1.4, the flux at E $>$ 100 keV was tallied at a radial plane 173 cm from the center of the core. The resulting values are shown in Figure 7.3. While the fast flux increases relative to the MXR-inter1, it is still within the bounds of what was observed for the LLR (slightly higher at BOL, but lower at EOL). This highlights the tradeoff with using BeO as a reflector material. The lower absorption rate results in

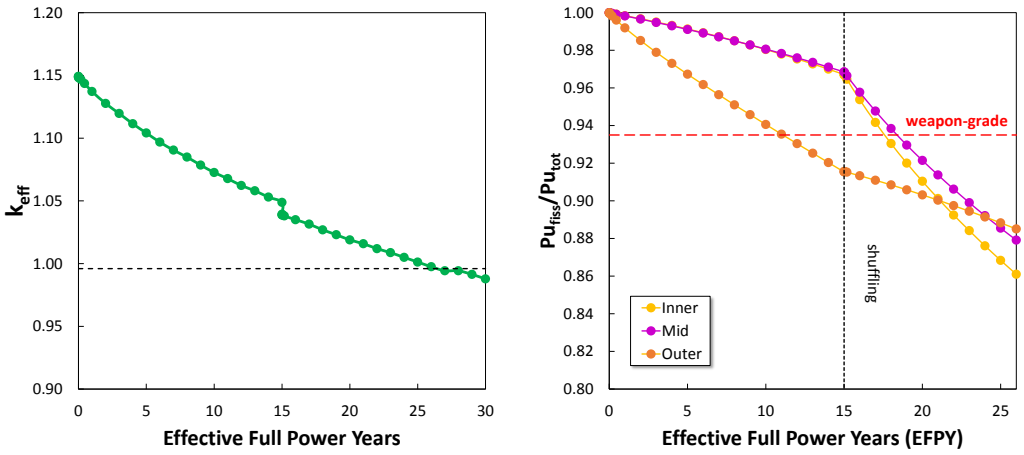

(a) Eigenvalue evolution of MXR-BeO. Average standard deviation of 25 pcm.

(b) Plutonium quality in MXR-BeO.

Figure 7.6: Performance evaluation of the MXR-BeO model, showing the eigenvalue and plutonium quality evolution.

overall improvements in reactivity, coupled with an increase in fast neutrons escaping the core (relative to MXR-inter1). Nevertheless, the benefits are concluded to outweigh the external flux related issue. The BeO reflector is deemed a desirable core modification. Another issue that arose from the modified reflector is a higher overall power contribution from outer assemblies (65-35% at BOL). This will be addressed in the next section.

Table 7.3: External fast flux of MXR-BeO at 173 cm from the center of the core.

	Fast Flux	**Diff. with LLR**
BOL	$(6.77 \pm 0.07) \times 10^{10}$ n/cm^2.s	6.72%
EOL	$(5.67 \pm 0.07) \times 10^{10}$ n/cm^2.s	-4.85%

7.1.3 Burnable poison in fuel

The MXR sees notable power peaking at the fast/thermal interface. This is the region with the highest neutron importance at BOL. Neutron poison can be employed in this region to reduce the peaks, similarly to what is done in thermal reactors. This is an effective approach for the MXR since the outer region is thermalized. Additionally, the MXR has

a high initial k_{eff} with a relatively large reactivity swing from BOL to EOL. Employing burnable neutron absorbers such as gadolinium can help alleviate this.

A sensitivity analysis was conducted at the assembly-level, in order to determine the best approach for introducing burnable absorbers. Doping both the fuel and the moderator material with gadolinium of different weight fraction is investigated. The model used is based on the inter1 assembly configuration (14 moderating rods). Figure 7.7 shows the effect of the addition of different fractions of gadolinium. The results show how the reactivity swing is decreased for different levels of doping. The burnable absorbers also contribute to a slight increase in the plutonium fissile ratio. The final plutonium quality (at 72.4 GWd/MTU) and the reactivity swing values are summarized in Table 7.4 for each case.

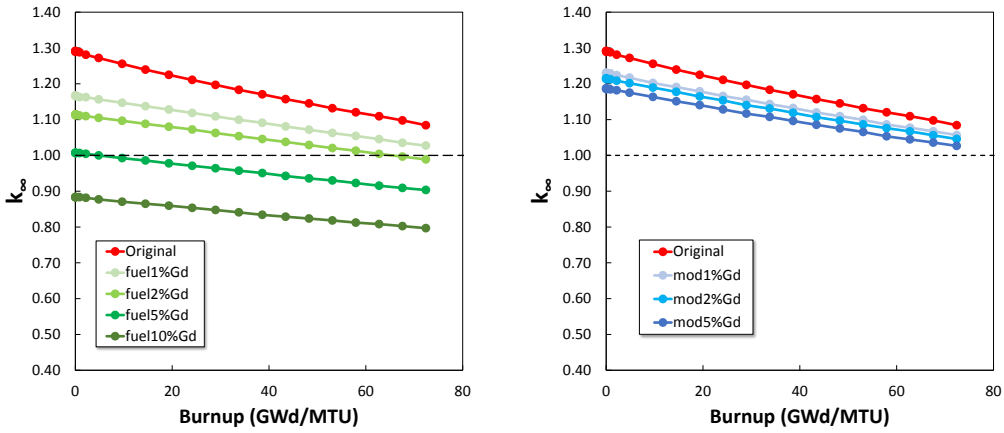

(a) Doping the fuel with Gd.

(b) Doping the moderator with Gd.

Figure 7.7: Eigenvalue evolution with burnup in an assembly lattice model, with additional burnable absorbers. The neutron poisons were added at the fuel and moderator level.

The results illustrate how the reactivity swing in the fuel can be alleviated, at a small penalty in final plutonium quality. The addition of burnable absorber does not appear to be as effective as is typically the case in thermal reactors. While the MXR operates in the epithermal spectrum, the majority of neutrons remain fast and are not strongly affected by the presence of the neutron poison (Gd cross-section is substantially lower at higher energies). As such, a small fraction of gadolinium doping was deemed sufficient to help

Table 7.4: Reacitvity swing (Δk = k_i-k_f) and final plutonium ratio (72 Gwd/MTU burnup) for different levels of Gd doping.

	Δ**k**	$(\mathbf{Pu}_{fiss}/\mathbf{Pu}_{tot})^f$
original	20718 pcm	0.883
fuel 1% Gd	14007 pcm	0.890
fuel 2% Gd	12566 pcm	0.893
fuel 5% Gd	10347 pcm	0.895
fuel 10% Gd	8675 pcm	0.894
mod 1% Gd	17223 pcm	0.890
mod 2% Gd	16785 pcm	0.893
mod 5% Gd	15943 pcm	0.896

address power peaking effects. Even 1w% doped fuel sees a 32% reduction in the reactivity swing, and maintains a relatively elevated final k_{eff} value. The analysis also concluded that moderator doping is less effective than doping the fuel. It increased plutonium quality at a faster rate than it reduces the reactivity swing.

A whole core model was then considered, with the outer assemblies highlighted in Figure 7.8(a) doped with 1w% Gd. Despite the neutron poison, six additional control rod assemblies were found to be needed in order to ensure adequate shutdown margins. All control rods are 90% ^{10}B enriched. The inter-assembly moderator configuration is similar to that of MXR-inter1. The shuffling strategy is based on the original approach (Table 5.5), with the added difference that there are now equal number of inner/mid and outer assemblies (no assembly was left in place as was previously the case). In light of the findings in Section 7.1.2, BeO was used as the reflector material instead of $ZrH_{1.6}$. The eigenvalue evolution in Figure 7.8(b) shows that the proposed design can reach a lifetime of 25 years with shuffling occurring at year 13 (similarly to previous designs). Reactivity sees a net increase of 560 pcm following shuffling (rather than a drop as in MXR-inter1) in light of the reduced fissile depletion in the outer region. Thanks to the addition of burnable

absorber, the reactivity swings across the cycle is reduced by 3225 pcm while maintaining the same core lifetime. The plutonium isotopic ratio of the core follows a similar trend to that of MXR-inter1, with a composition at EOL of 85.8%, 87.7% and 91.0% for each of the inner, mid and outer assemblies.

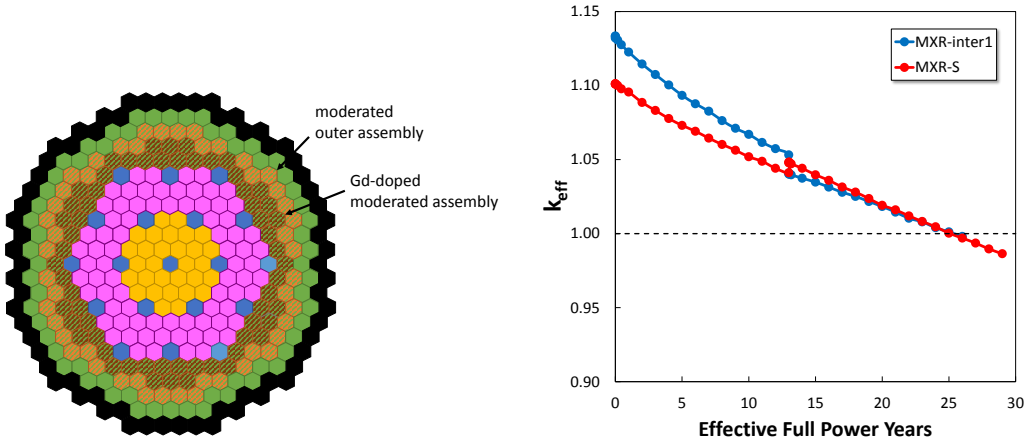

(a) MXR-S core layout.

(b) Eigenvalue evolution of MXR-S. ($\overline{sd} = 24$ pcm)

Figure 7.8: Layout and performance of the MXR-S core configuration. Gd-doped assemblies have 1w% Gd in the U-Zr fuel composition. Six additional control rod assemblies were added to the new design to ensure adequate shutdown margins..

Power peaking analyses was then conducted for the new design, referred to as MXR-S. Assembly radial peaking at different steps in the life-cycle are shown in Figure 7.9. The benefit of doping the fuel with burnable absorber becomes apparent for the BOL case in Figure 7.9(a). The maximum value at this point in time, is reduced from 1.493 (MXR-inter1) to 1.332. The highest value reached throughout the operating lifetime was 1.377 at MOL2 (when the reactor is restarted after assembly shuffling), which is still lower than the peak value in the original LLR model (1.479). These initial results appear to validate the design philosophy of the MXR-S.

In order to verify that peak linear power rating is reduced, rod-level power generation was tallied using MCNP6 similarly to what was conducted in Chapter 6. From Figure 7.9, it is apparent that the highest assembly peaking is observed within assemblies O804 and

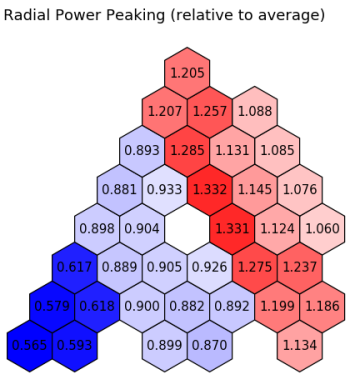

(a) Peaking at BOL.

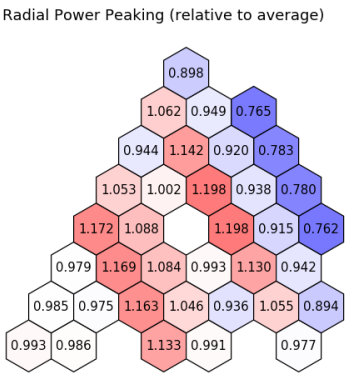

(b) Peaking at MOL1 before shuffling (13 years).

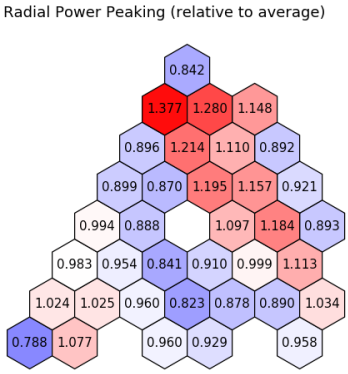

(c) Peaking at MOL2 after shuffling (13 years).

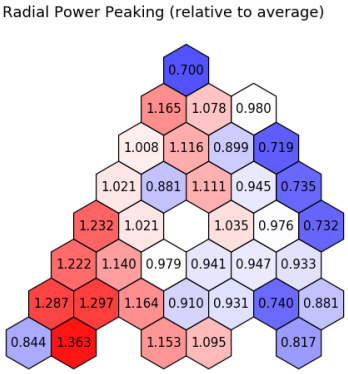

(d) Peaking at EOL (25 years).

Figure 7.9: Radial power peaking per assembly in the MXR-S. Assembly locations in (c) and (d) corresponds to the positions after shuffling.

O805 at BOL, as well as with assembly O807 at MOL2 (MOL after shuffling). Rod-level power generation is plotted in Figure 7.10 with the same colorbar range that was used in Figure 6.8. A peak value of 23.1 kW/m was observed, and corresponds to assembly O805 at BOL. The results are very close to the peak value for the original LLR (23.0 kW/m) and much lower than maximum values that occur in typical fast reactors. Since the peak fuel and coolant temperatures were validated for the MXR-inter1 for a higher linear rating, they are deemed to be within acceptable ranges for the MXR-S.

The inter-assembly power levels were then investigated in Figure 7.11 at BOL and EOL (the two points where the highest peaks were observed). As can be seen, the power

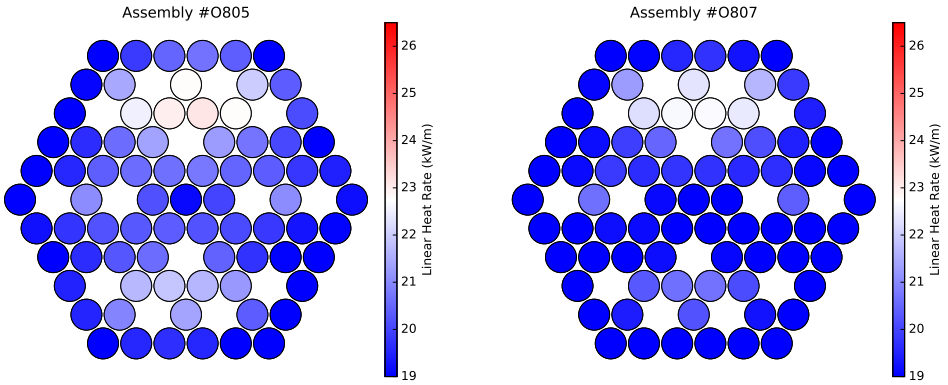

(a) Linear heat rate within Assembly O805 at BOL. ($\overline{sd} = 0.29\%$)

(b) [Linear heat rate within Assembly O807 at MOL2. ($\overline{sd} = 0.34\%$)

Figure 7.10: Linear heat rate (kW/m) within assembly fuel rods of the MXR-S design. Values are normalized to the range of Figure 6.8 (19 to 26.5 kW/m) for comparative purposes. The highest value observed was 23.1 kW/m.

generation is considerably flatter than for the previous MXR-inter1 and MXR-BeO (shown in Figures 6.10 & 7.5(a)). A reduction in power production in the thermal region shifts some of generation to the mid-assemblies thus contributing to a flatter profile. The power analysis results validate the utility of using gadolinium doping to reduce power peaking effects. More sophisticated optimization of Gd doping location and quantity is expected to improve results even further.

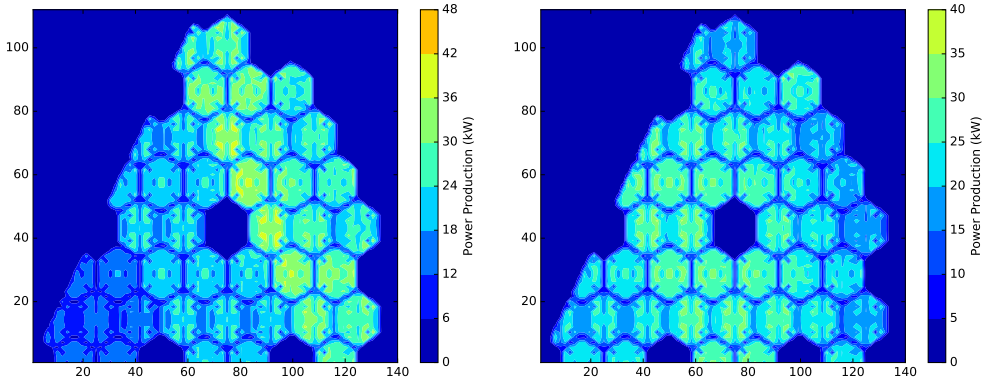

(a) Radial power distribution at BOL. ($\overline{sd} = 0.34\%$)

(b) Radial power distribution at EOL. ($\overline{sd} = 0.53\%$)

Figure 7.11: Power generation within the MXR-S 1/6 core model at BOL and EOL (25 years). The color-ranges are normalized to the range in Figure 6.10.

The peak fast fluence for the MXR-S was also evaluated, with the resulting value in each assembly shown in Figure 7.12. After the same operating lifetime (25 years), the peak fast fluence is 3.76×10^{23} n/cm^2 in the MXR-S, versus 4.13×10^{23} n/cm^2 in the MXR-inter1. This constitutes a 9% reduction relative to the original design; bringing the maximum value even closer to where experimental data has already been observed ($3.9\text{-}4.0\times10^{23}$ n/cm^2).[14] The spread between assemblies is also slightly less pronounced of the previous design iteration of the MXR. The results highlight the benefit of flattening the core power distribution within the core. Further parametric optimization can be expected to improve upon these results further.

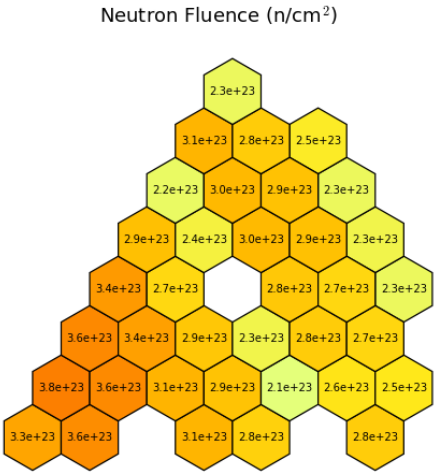

Figure 7.12: Peak fast fluence in each assembly of the MXR-S design. A peak value of 4.13×10^{23} n/cm^2 was reached in assembly no. 302.

Another concern that was highlighted in Chapter 6, was feedback mechanisms at BOL. While the MXR-inter1 had comparable integral feedback parameter values to the LLR, it was unable to ensure unprotected shutdown in light of the high initial k_{eff}. The reduction of the reactivity swing in the MXR-S and the additional control rods can alleviate this limitation. Reactivity coefficients are calculated at BOL with 35% control rod insertion into the core. This brought down the initial k_{eff} to 1.00947. Table 7.5 shows the resulting reactivity coefficients, and integral feedback parameter values. With the reduced initial

$\Delta\rho$ margin, all inherent safety criteria are now met; demonstrating that the MXR can be expected to reach the same level of passive safety as the original LLR design.

Table 7.5: Reactivity feedback parameters for the MXR-inter1 and the MXR-S at BOL and EOL. Checkmarks (✓) indicated that passive safety criteria are met for the integral quasi-static parameter considered.

	BOL		**EOL**	
	MXR-inter1	**MXR-S**	**MXR-inter1**	**MXR-S**
β_{eff}	0.007 ± 0.000	0.007 ± 0.000	0.005 ± 0.000	0.005 ± 0.000
α_{rad} (¢/K)	-0.055 ± 0.004	-0.088 ± 0.005	-0.109 ± 0.006	-0.102 ± 0.006
α_{ax} (¢/K)	-0.022 ± 0.003	-0.024 ± 0.004	-0.036 ± 0.005	-0.030 ± 0.005
α_{ctrl} (¢/K)	-0.006 ± 0.007	-0.081 ± 0.008	-0.018 ± 0.010	-0.020 ± 0.009
α_{fuel}(¢/K)	-0.124 ± 0.008	-0.154 ± 0.009	-0.115 ± 0.010	-0.136 ± 0.010
α_{clad} (¢/K)	0.008 ± 0.016	-0.011 ± 0.019	-0.015 ± 0.024	0.017 ± 0.022
α_{mod} (¢/K)	0.001 ± 0.016	0.036 ± 0.018	0.034 ± 0.024	0.004 ± 0.022
α_{void} (¢/K)	0.029 ± 0.001	-0.283 ± 0.009	0.043 ± 0.002	0.050 ± 0.002
α_{worth} ($)	0.037 ± 0.022	-0.031 ± 0.026	1.695 ± 0.064	1.796 ± 0.064
A (¢)	-6.96 ± 0.56	-8.49 ± 0.64	-6.32 ± 0.74	-7.52 ± 0.72
B (¢)	-26.14 ± 0.31	-93.88 ± 0.39	-33.61 ± 0.47	-33.61 ± 0.43
C (¢/K)	-0.16 ± 0.02	-0.52 ± 0.03	-0.20 ± 0.04	-0.20 ± 0.03
$\Delta\rho_{ext}$ (¢)	132.80 ± 4.18	9.77 ± 0.32	6.09 ± 0.29	4.03 ± 0.18
A/B	0.27 ± 0.03 ✓	0.09 ± 0.01 ✓	0.19 ± 0.02 ✓	0.22 ± 0.02 ✓
$(C\Delta T_c)/(B/2)$	1.93 ± 0.29 ∼	1.73 ± 0.10 ✓	1.83 ± 0.34 ∼	1.81 ± 0.31 ∼
$\Delta\rho_{ext}/\lvert B\rvert$	5.08 ± 0.17 ⊗	0.14 ± 0.00 ✓	0.18 ± 0.01 ✓	0.17 ± 0.01 ✓
$(A+B)/(C\Delta T_c)$	1.31 ± 0.20 ✓	1.26 ± 0.07 ✓	1.30 ± 0.24 ✓	1.35 ± 0.23 ✓
$\lvert B\rvert(A + A/B)$ (¢)	33.10 ± 0.64 ⊗	102.37 ± 0.75 ✓	39.94 ± 0.88 ✓	41.13 ± 0.84 ✓

7.2 Proliferation Resistance and Safeguards

One of the main objectives of the MXR is to improve the proliferation resistance of long-lived cores. The analysis thus far has mostly focused on averaged metrics such as plutonium quality in a core zone. This section will undertake more in-depth analysis at the assembly level to better ascertain the risks associated with the proposed configurations. Numerous

methodologies have been proposed in the literature to assess proliferation resistance of systems. The analysis in this section relies mostly on the Sandia National Lab method,[28] which was previously outlined in Table 2.1. This provides a more holistic evaluation of important metrics both at the broad and localized level. In addition, while the fissile-to-total plutonium is a useful parameter to measure plutonium quality during the design optimization, more advanced tools are available. The Bathke Figure of Merit (FOM) is a useful tool for quantifying the attractiveness of fuel material for a potential proliferator and comparing it to alternative designs.[52]

7.2.1 Assembly diversion risks

Previous analyses averaged the plutonium metrics for the three core regions. This is limiting, since a potential proliferator may only need to steel one single assembly. It is therefore important to look at each assembly individually and identify the weakest ones from a non-proliferation standpoint. Figure 7.13 shows both the plutonium quality and quantity in each assembly at EOL for different cases considered. Note that the EOL for the LLR was taken to be 25 years in light of the fast fluence limit. The advantages of the MXR designs are evident; a much smaller proportion of assemblies reach 1 SQ of plutonium at EOL, and assemblies have much lower plutonium quality on average. Slight differences can also be observed between the two MXR designs considered here. No assembly in the MXR-S remains at the weapon-grade limit (93% fissile) at EOL.

A more thorough comparison is conducted in Table 7.6. The most relevant plutonium parameters at EOL are compared for the different models. It is interesting to note that even the average composition of the LLR is above desired limits. On average, assemblies contain more than 1 SQ of plutonium, and the quality is above the weapon-grade (WG) limit. While the MXR designs do reduce the total amount of assemblies containing 1 SQ in the core, the main advantage is in plutonium quality. All assemblies apart from one (in the 1/6 model, therefore six in total) are below the WG limit in the MXR-inter1; and none

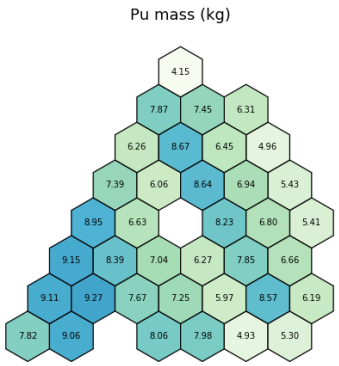

(a) MXR-inter1 Pu mass per assembly at EOL (25 years).

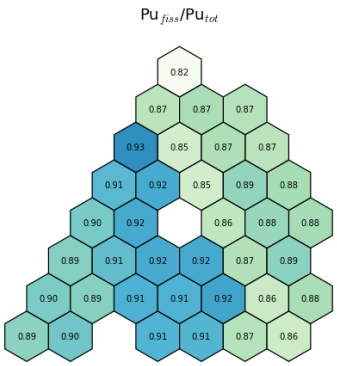

(b) MXR-inter1 Pu quality at EOL (25 years).

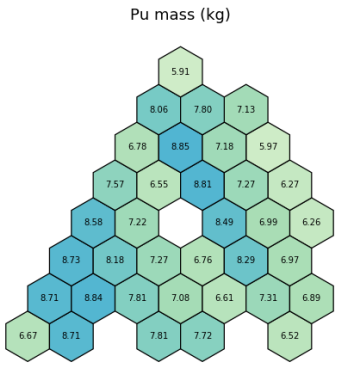

(c) MXR-S Pu mass per assembly at EOL (25 years).

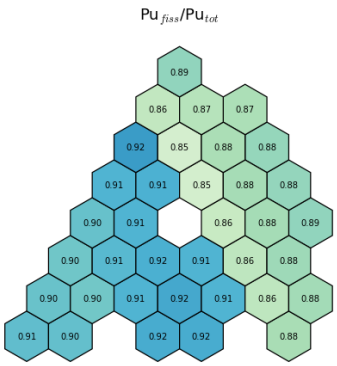

(d) MXR-S Pu quality at EOL (25 years).

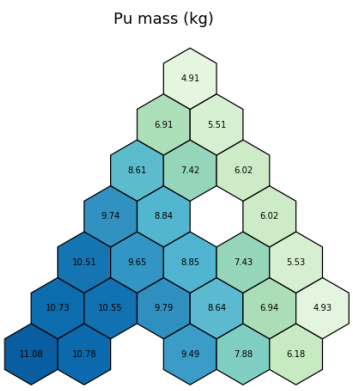

(e) LLR Pu mass per assembly at EOL (25 years).

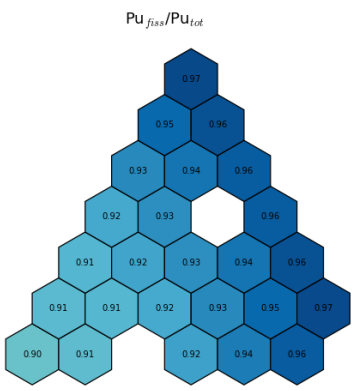

(f) LLR Pu quality at EOL (25 years).

Figure 7.13: Plutonium quantity and quality per assembly at EOL for different core configurations considered.

is above that threshold for the MXR-S. In contrast, a total of 96 assemblies are weapon-grade in the LLR (16 in the 1/6 model). More importantly, the LLR has four assemblies at EOL that are both weapon-grade and contain more than 1 SQ. These would be the most attractive to a potential proliferator. On the other hand, no assembly in the MXR models reaches both limits simultaneously.

Table 7.6: Plutonium breeding metrics at EOL (25 years) for the different reactor designs.

	LLR	**MXR-inter1**	**MXR-S**
tot. m_{Pu} in core (kg)	1,217.6	1,590.9	1611.5
av(m_{Pu}/assembly) (kg)	8.1	7.2	7.5
max(m_{Pu}/assembly) (kg)	11.1	9.3	8.9
assemblies with $>$ 1 SQ	78	66	66
av(Pu_{fiss}/Pu_{tot})	93.6%	88.7%	89.2%
max(Pu_{fiss}/Pu_{tot})	96.6%	93.1%	92.5%
assemblies with $>$ WG	96	6	0
assemblies with $>$ 1 SQ & $>$ WG	24	0	0

One weakness of the MXR design relative to the LLR, from a safeguardability standpoint, is that the core needs to be shut down twice throughout its lifetime, rather than only once. It is therefore important to assess the nonproliferation metrics at MOL before assemblies are handled and shuffled inside the core. Table 7.6 summarizes the main criteria. The plutonium quality is higher than at EOL since half of the assemblies have not been exposed to a thermalized spectrum yet. It is worth noting that while the average plutonium ratio is above the WG limit, there is a large disparity between the fast and thermalized region as shown in Figure 7.14. A potential proliferator would need to divert at least two assemblies in order to obtain 1 SQ worth of WG material. This is not as proliferation resistant as a PWR (where all plutonium is below WG limit and 2 assemblies are also needed for 1 SQ), but is an inherent limitation to the design. By virtue of operating on a mixed-spectrum, assemblies will need to be accessed and shuffled in order to expose all of them to the ther-

malized spectrum. The only workaround is to revert to a fully thermal configuration. This type of core will be considered in Section 7.2.3.

Table 7.7: Plutonium breeding metrics for the MXR-inter1 and MXR-S at MOL (13 years), before shuffling occurs.

	MXR-inter1	**MXR-S**
tot. m_{Pu} in core (kg)	905.4	935.0
av(m_{Pu}/assembly) (kg)	4.1	4.3
max(m_{Pu}/assembly) (kg)	5.3	5.2
assemblies with $>$ 1 SQ	0	0
av(Pu_{fiss}/Pu_{tot})	93.7%	94.3%
max(Pu_{fiss}/Pu_{tot})	97.4%	97.3%
assemblies with $>$ WG	108	108
assemblies with $>$ 1 SQ & $>$ WG	0	0
no. of WG assemblies needed for 1 SQ	2	2

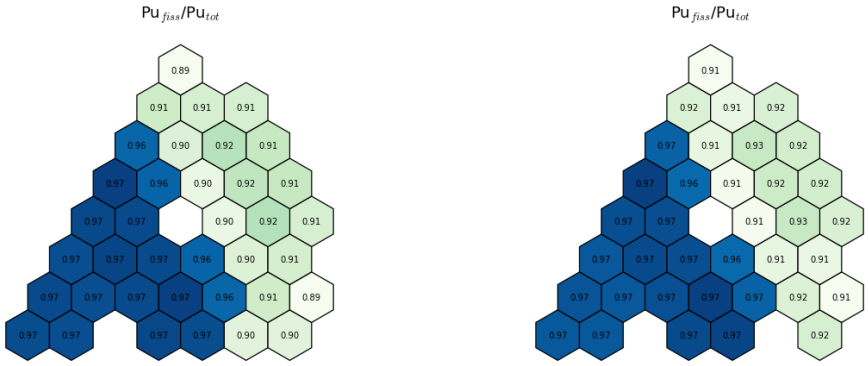

(a) MXR-inter1 Pu quality at MOL (13 years). (b) MXR-S Pu quality at MOL (13 years).

Figure 7.14: Plutonium quality of MXR models at MOL, prior to shuffling.

In theory, a potential proliferator could divert material at times other than MOL and EOL. Unanticipated shutdown for maintenance could provide an opportunity to divert an assembly undetected, or in a 'breakout' scenario, a state actor could force an interruption of operation and extract plutonium bearing material. It is therefore important to assess how long assemblies remain attractive for use in a weapon. These 'windows' are displayed in

Figure 7.15, and summarized in Table 7.8. As shown, the windows at which a state can divert two assemblies to reach 1 SQ of plutonium are substantially narrower for the MXR cases. These two-assembly diversions windows are 14 years for the MXR-inter1, just 7 years for the MXR-S, and 18 year for the LLR. Additionally, at no point in either MXR concepts can a state acquire 1 SQ worth of weapon-grade material in a single assembly, while that window is 9 years long for the LLR. Herein lies the main benefit of the MXR designs, they reduce the perceived benefits of assembly diversions. It is noteworthy that the MXR-S performs better that the MXR-inter1 across all of these metrics considered. Flattening the power distribution appears to go hand in hand with improving the plutonium metrics. Additional 'diversion window' plots for the different models considered are shown in Appendix C.

Table 7.8: Assembly attractiveness windows for each design. Both reactors are assumed to operate for a total of 25 years.

	LLR	**MXR-inter1**	**MXR-S**
1 SQ window	9 years	4 years	2 years
WG window	25 years	25 year	17 years
1 SQ & WG window	9 years	0 years	0 years
$2\times$(0.5 SQ & WG) window	18 years	14 years	7 years

From a nonproliferation standpoint, despite the reduction in material attractiveness, safeguarding the core remains an imperative. The core is accessed twice rather than once, increasing the potential risks. It should be noted that despite of this limitation, the material in the MXR is less attractive at each time the core is accessed, than is the case when the LLR core is accessed at EOL. Adequate safeguarding measures must be derived to minimize the risk of potentially undetected diversions, especially at MOL where plutonium-bearing material is being handled. Figure 7.16 illustrates the different checks and balances that can ensure vigilant monitoring of the core. To minimize proliferation risks, the fuel handling mechanism could either be present within the reactor vessel, or located off-site, and only

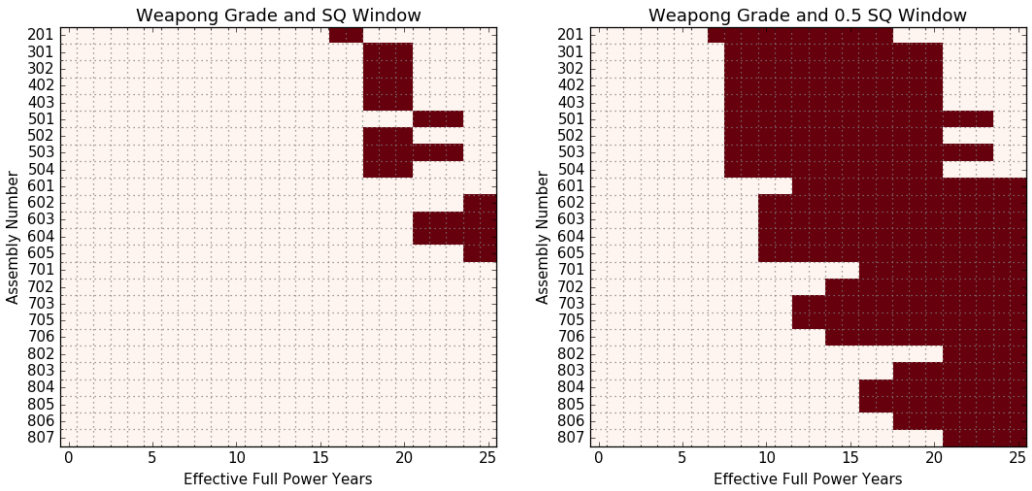

(a) Points in time where assemblies contain 1 SQ of WG Pu window for the LLR.

(b) Points in time where assemblies contain 1/2 SQ of WG Pu window for the LLR.

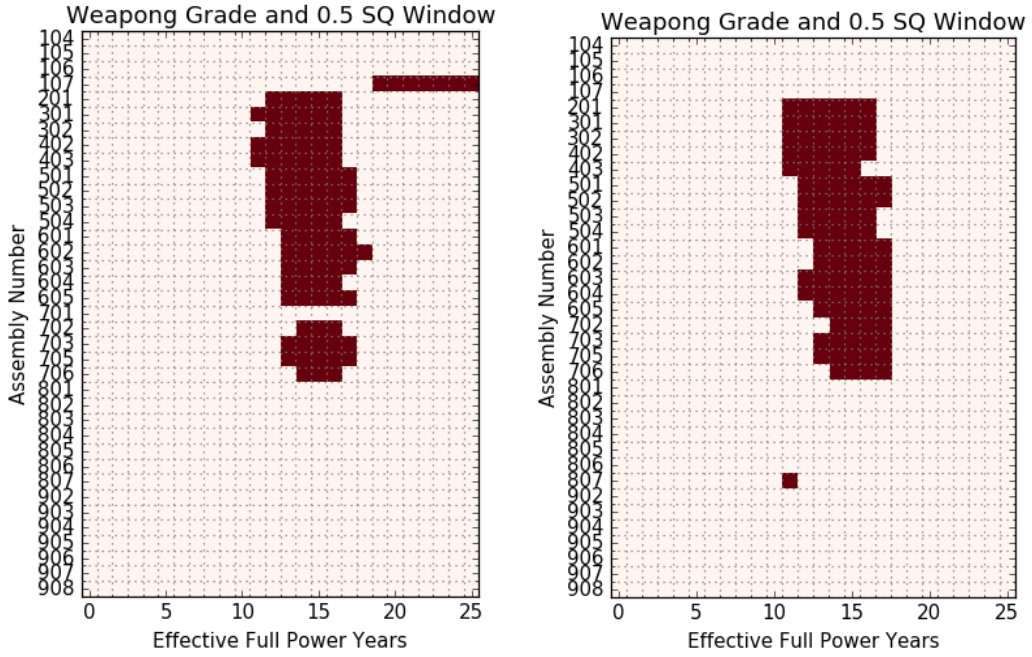

(c) Points in time where assemblies contain 1/2 SQ of WG Pu window for the MXR-inter1.

(d) Points in time where assemblies contain 1/2 SQ of WG Pu window for the MXR-S.

Figure 7.15: Windows of opportunity where a proliferator can divert weapon-grade (WG) plutonium for a single or two-assembly diversion. The colored bins indicate that given plutonium composition is above the sated limits above the plot. MXR-inter1 and MXR-S plots where assemblies contain over 1 SQ of weapon-grade plutonium are not shown as at no instance during their lifetime is this threshold met.

brought to the host nation during MOL. The first approach has been proposed by design such as the Terrapower Traveling Wave Reactor, as a way to ensure the core remains sealed while shuffling takes place; ensuring the host nation does not have access to weapon-grade material.[75] In the second approach, the assembly handling mechanism would be provided by the hub nation that originally manufactured the core, and transported on-site. Following its use, it would be returned to the hub to ensure it cannot be repurposed for diverting irradiated fuel material. An IAEA inspector will need to be present on-site throughout the time the core is exposed at MOL, similarly to what is currently the case for a typical PWR. Alternatively, the IAEA could even be tasked with operating the shuffling equipment if dependence on the hub-country raises energy security concerns to the host nation. A transported off-site shuffling infrastructure was deemed more feasible, and secure than shuffling without opening the core vessel. Since the operation only need take place once after 13 years, this was not deemed to be overly burdensome, with minimal capacity factor penalty.

The shuffling mechanism itself would have to proceed in three stages: (1) moderator rods are inserted into the inner and mid assemblies, (2) moderating rods are removed from the outer assemblies, and (3) assemblies are displaced in accordance with the set shuffling scheme. Starting with the first step would ensure no inner assemblies are shuffled without adequate thermalization that reduces their material attractiveness. The insertion of moderating material is envisaged to take place while assemblies are stationary in the core, in a similar way to what is done with the control rod spider in a PWR assembly. Shutdown margins were assessed for the core in this state at MOL, with all moderating rods inserted. Analysis for the MXR-S with all control rods inserted found that k_{eff} can be maintained at 0.89672 ± 0.00014, ensuring sufficient margins to avoid re-criticality accidents when moderator material is inserted within all assemblies. It remains possible however, that state decides not to proceed with shuffling of assemblies for one reason or another. This scenario is investigated in greater detail in Appendix D. The main finding was that the core could operate up to 23 years before the peak fluence of 4×10^{23} n/cm^2 was reached. If that limit

is lifted, the core can operate up to 27 years. Power peaking effects also appear to exceed the original peak for the MXR-S, compromising the safety of such a decision. In addition, even though inner and mid assemblies would not be exposed to a thermalized spectrum, only a limited number of assemblies remain above the WG limit at EOL. This is due to the fact that these assemblies see a relatively higher burnup than peripheral ones in the original LLR. As such, this scenario does not constitute a major risk from a proliferation standpoint.

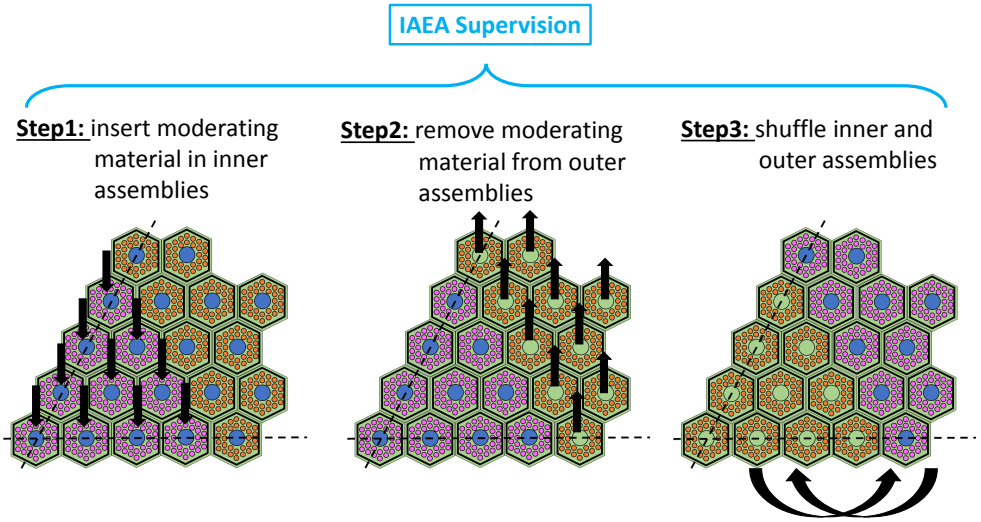

Figure 7.16: Illustration of the different steps for the MXR shuffling at MOL. The shuffling rig is not present on-site during operation and is only provided by the hub for shuffling procedure. Note that this is only an illustration of the MXR, the number of assemblies is not conserved.

Further improvements to nonproliferation metrics of the MXR are still possible. A multi-objective optimization could simultaneously address burnup, core lifetime and plutonium production. Plutonium breeding metrics tend to be correlated with high burnup; ensuring both are more evenly distributed in a core design is expected to be feasible. This was highlighted to some extent in the MXR-S core as previously discussed. Another potentially interesting case-study, from a nonproliferation standpoint, would be to evaluate the monitoring capabilities of an antineutrino detector on the MXR. These detectors are being actively researched as a way to passively and continuously probe the material composition

in a reactor core to potentially detect an assembly diversion. Previous studies have evaluate the deployment of these detectors alongside long-lived core designs;[76] this can be extended to the mixed-spectrum variants. In summary, it appears that the MXR sees some improvement relative to the LLR from a nonproliferation standpoint, but is unable to reach the characteristics a typical LWR. Quantifying the attractiveness level of the MXR is the subject of the next section. This would allow to compare the material between the LLR, MXR, and LWR.

7.2.2 Fuel attractiveness evaluation

As highlighted in Chapter 3, the different plutonium grades are not exactly hard limits. To more accurately quantify and compare the attractiveness of irradiated nuclear fuel, Bathke introduced figures of merit (FOM).[52] These unclassified formulae were designed so that they could not be reverse-engineered to gain insight into weapon design specifics. They were reviewed by weapon experts at U.S. National Laboratories, and determined to sufficiently capture the dominant factors in nuclear weapon design considerations. Equations 7.2 & 7.3 show the two figures that were derived. FOM_1 quantifies the material attractiveness while ignoring the risk of pre-ignition (or fizzling) due to spontaneous neutron fissions. The reasoning is that even a pre-mature detonation would still reach devastating yields. Nevertheless, provided a choice, a potential proliferator would preferentially divert material with a lower risk of fizzling. As such, FOM_2 is also considered in this section. Material attractivness is dependent on the bare critical mass of the acitinide (M), their equivalent heat generation (h), their dose rate evaluated a 1 m from surface (D), and the rate of neutron emission (S).

$$FOM_1 = 1 - \log_{10}\left(\frac{M}{800} + \frac{M \times h}{4500} + \frac{M}{50}\left[\frac{D}{500}\right]^{3.322}\right) \tag{7.2}$$

$$FOM_2 = 1 - \log_{10}\left(\frac{M}{800} + \frac{M \times h}{4500} + \frac{M \times S}{6.8 \times 10^6} + \frac{M}{50}\left[\frac{D}{500}\right]^{3.322}\right) \tag{7.3}$$

Evaluating the FOM requires processing the results from MCNP6 and extracting the actinide vector of the irradiated fuel. The corresponding heat production rate, emitted dose, and neutron source for each isotope in the fuel is obtained using the tables provided by Bathke.[52, 77] The last step is evaluating the critical bare mass, M, of the given actinide vector. Iterative runs are conducted in MCNP6 for a simple spherical geometry with different radii, and containing the isotopic vector. Linear interpolation is used to find the approximate radius corresponding to k_{eff} = 1.0, and an additional simulation is conducted to verify the value. These parameters are then used to estimate the main components of Equations 7.2 & 7.3. Once an FOM value is derived, its relative meaning can be inferred using Table 7.9. Again, these ranges are not intended to be hard cut-offs; they are more indicative of the material worth.

Table 7.9: Meaning of FOM values. Taken from [52].

FOM	**Weapons Utility**	**Attractiveness**
> 2	Preferred	High
1 to 2	Attractive	Medium
0 to 1	Unattractive	Low
<0	Unattractive	Very Low

The FOM_1 values for the LLR and MXR-inter1 were evaluated in Table 7.10. MXR-S values were expected to match very closely those of MXR-inter1 and are not shown here. Both the average and 'worst' compositions were evaluated. The max values corresponded to assemblies with the highest Pu_{fiss}/Pu_{tot} ratio. The actinide vector considered accounted for the isotopes of U, Np, Pu, Am and Cm. This gives a holistic evaluation of diverting a whole fuel assembly. Results show a 29% reduction in overall material attractiveness in the MXR core. An improvement relative to the original design. Values for a PWR could not be estimated since it is theoretically impossible for very low-enriched fuel to reach a bare critical configuration, due to logarithmic behavior.[45] It should be noted that all of

the cases considered fell within the 'low attractiveness' range.

Table 7.10: FOM_1 values for different spent fuels. The 'max' cases for LLR and MXR-inter1 were taken to be assembly nos. O802 and O107 respectively.

	LLR	**MXR-inter1**
av(FOM_1)	0.75	0.53
max(FOM_1)	0.77	0.62

Limiting the analysis to whole actinide vector can be incomplete. A potential proliferator would perceptibly intend to separate pure plutonium out of the mixture. Comparing the plutonium quality using the FOM is therefore a useful exercise. It will provide a more valuable comparative tool instead of the Pu_{fiss}/Pu_{tot} ratio. Table 7.11 shows the FOM results when only plutonium is accounted for. A PWR spent fuel vector is obtained from a typical Westinghouse core design. Unsurprisingly, all FOM_1 are in the high attractiveness range. Since this formula ignores neutron emissions (^{240}Pu is a strong neutron emitter and the second most dominant isotope bred after ^{239}Pu), nearly any plutonium composition is weapon-usable to an advanced weapon state or a proliferation with little concern regarding fizzling. On the other hand, when accounting for neutron emissions, both the PWR and all MXR assemblies are in the medium attractiveness range. The only case that is within the high attractiveness range, is the outer LLR assembly. This again highlights the advantage of the MXR in terms of reducing plutonium quality, as no assembly reaches that threshold. It is estimated that for the worst cases in each design, the MXR sees a 14% reduction in plutonium attractiveness. This case is even lower than the average LLR quality. Overall, the MXR sees a 12% improvement relative to the LLR, but is 50% worse than the PWR vector. While the same attractiveness as conventional reactors could not be reached with the MXR, it is still a notable improvement relative to the original LLR design.

Since the MXR core is accessed twice, at MOL and EOL, the composition before shuffling is also examined. The results are highlighted in Table 7.12. The overall FOM_1 is

Table 7.11: FOM_1 and FOM_2 values for the plutonium vectors in spent fuels of the LLR, the MXR-inter1 and a typical PWR composition after 3 cycles.

	PWR	**LLR**	**MXR-inter1**
av(FOM_1[Pu])	2.21	2.60	2.48
max(FOM_1[Pu])	-	2.70	2.57
av(FOM_2[Pu])	1.07	1.83	1.61
max(FOM_2[Pu])	-	2.11	1.82

between the LLR and MXR values in Table 7.10. The reduced total plutonium content balances out the higher isotopic quality. At the extreme, the plutonium vector itself reaches the FOM levels of the LLR at EOL. The added risk is somewhat alleviated by the fact that no single assembly contains 1 SQ; two would need to be diverted to obtain enough material for a weapon. Assuming adequate safeguarding is provided, this is expected to be of relatively lower risk to go undetected.

Table 7.12: FOM values for the MXR-inter1 design at MOL, when the core is accessed.

	MXR-inter1 (MOL)
FOM_1	0.69
av(FOM_1[Pu])	2.62
max(FOM_1[Pu])	2.71
av(FOM_2[Pu])	1.89
max(FOM_2[Pu])	2.19

7.2.3 Further proliferation resistance improvements

Core designs that are able to further improve upon the proliferation resistance of the MXR were considered. As previously mentioned, the biggest weakness of the MXR from a proliferation standpoint, is the attractiveness of its material at MOL when shuffling occurs.

Two design variants are investigated in this section. The first builds on the MXR-Th of Chapter 5, and addresses how to elongate its lifetime. The second considers the benefits of adding moderating material inside all core regions. The core would not operate in a 'mixed' configuration, but simply as an epithermal reactor.

The improved thorium-based design, referred to as MXR-Th2, uses the core configuration shown in Figure 7.17(a). The concept employs four different types of assemblies: two driver regions, and two blanket regions. Since thorium can breed more effectively in the epithermal range, one of the blanket region can be placed within the moderated outer zone. The central fuel in both blanket regions contains 48w% thorium, while the driver regions have 17w% thorium content. All upper and lower fuel regions contain 4w% Th, and all ^{235}U enrichment was to the 20% limit. Assemblies are shuffled using the original scheme in Chapter 5, and the core lifetime was estimated to be 25 years as shown in Figure 7.17(b). Further optimization of the thorium and uranium content, as well as the shuffling strategy, can be expected to improve results further. For instance, the ^{238}U quantity in the fast region can be increased since it is a better breeder than ^{232}Th in that regime.

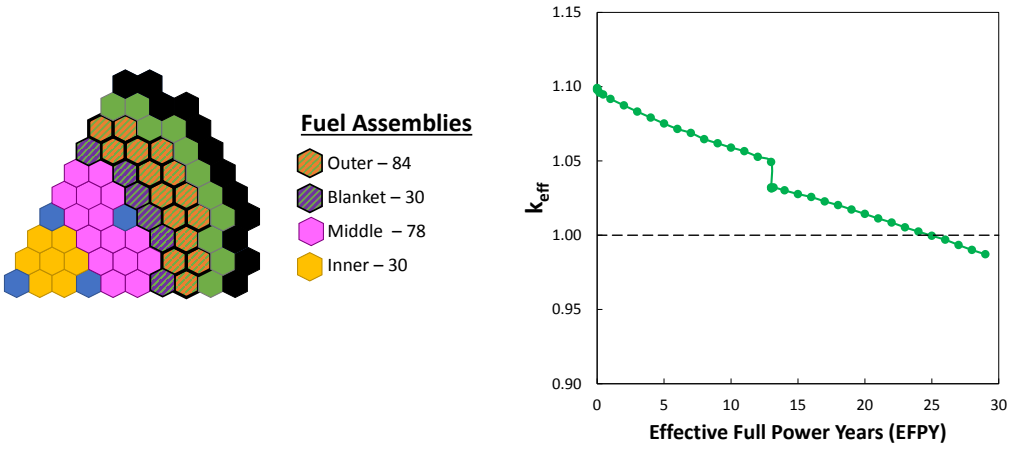

(a) Diagram of 1/6 MXR-Th2 core model.

(b) Eigenvalue evolution of MXR-Th2. ($\overline{sd} = 25$ pcm)

Figure 7.17: Outlined and performance of the proposed MXR-Th2 core.

Maps of plutonium breeding metrics are shown in Figure 7.18 at MOL and EOL. While the plutonium quality remains relatively high at MOL, the total amount of plutonium per as-

sembly is substantially reduced. A total of 3 assemblies would need to be diverted at MOL to obtain 1 SQ of plutonium. Additionally, no single assembly generates 1 SQ throughout the core lifetime. While two assemblies (in the 1/6 model, 12 in whole core) remain above the weapon-grade limit at EOL, the denaturation ratio of uranium is maintained below the 12% limit throughout operation.

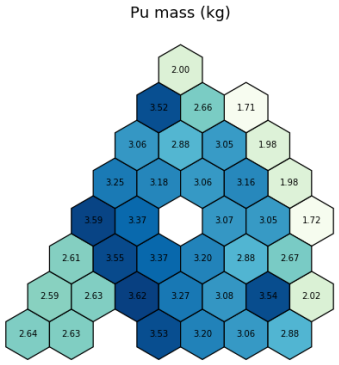

(a) Map of plutonium mass per assembly at MOL.

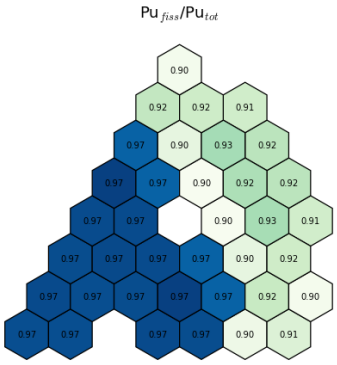

(b) Map of plutonium quality at MOL.

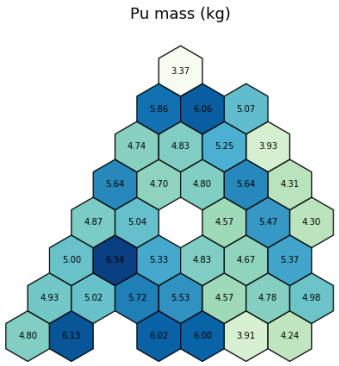

(c) Map of plutonium mass per assembly at EOL.

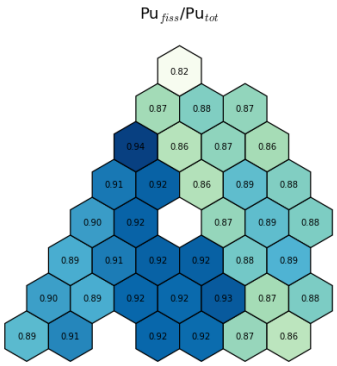

(d) Map of plutonium quality at EOL.

Figure 7.18: Plutonium breeding metrics in the MXR-Th2 at MOL (13 years) and EOL (25 years).

The second design used U-Zr fuel and moderating material inserted in all fuel assemblies. The design will be referred to as the Long-lived Epithermal Reactor (LER). It was deemed useful to consider this variant for comparative purposes. The LER has the same configuration as the MXR-S, without any Gd doping. Figure 7.19(a) shows the resulting eigenvalue and plutonium quality evolution. No shuffling is undertaken in the core since

all assemblies are exposed to a thermalized spectrum. The core lifetime is reduced relative to the MXR-S; k_{eff} can be maintained above 1.0 for only 16 years. On the other hand, the plutonium quality in all assemblies drops relatively quickly (Figure 7.19(b)). They all reach below the weapon-grade limit after approximately 10 years. The case highlights the tradeoff in the MXR: having a fast region allows better fissile material breeding and an extension of core lifetime, but at some cost to proliferation resistance.

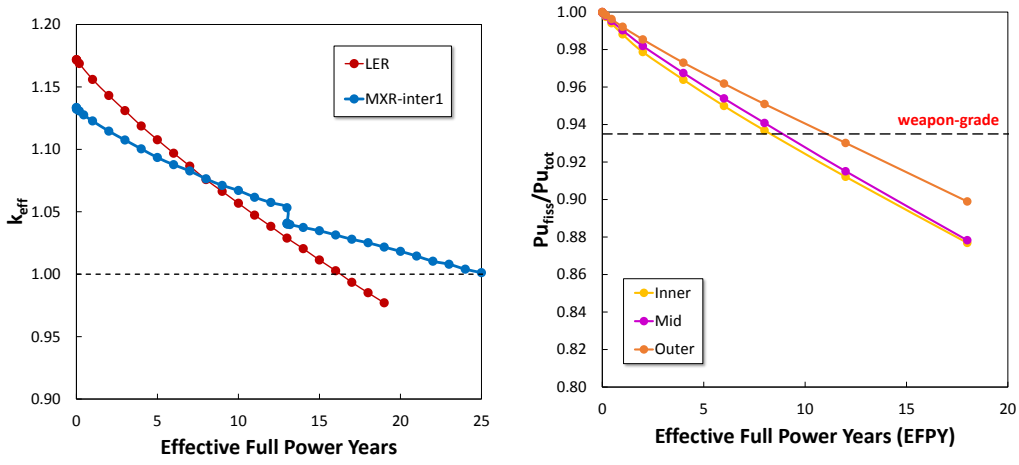

(a) Eigenvalue evolution of LER.

(b) Plutonium quality in LER.

Figure 7.19: Main performance metrics of the Long-lived Epithermal Reactor (LER).

The main nonproliferation parameters are highlighted in Table 7.13 for the two newly proposed core configurations. Further information on the MXR-Th2 metrics can be found in Appendix C. Both the MXR-Th2 and the LER do not reach 1 SQ of plutonium within their assemblies. In light of its low burnup, at no point in the LER lifetime can two assemblies be diverted to obtain 1 SQ of weapon-grade plutonium, at least three are needed. For the MXR-Th2, that window is of only two years. The latter reactor also does not see substantial improvement in FOM values at MOL or EOL for its actinide vectors. It should be noted that while the FOM accounts for the overall attractiveness of the material, a hypothetical proliferator would normally separate out fissile plutonium or uranium isotopes from the fuel. The difficulty in separating ^{233}U from the fuel (enrichment is essentially required since it is a mixed U-Th fuel lattice) is unaccounted for in the formula. The pluto-

nium metrics are also slightly higher than the MXR-inter1, but it should be noted that the overall quantity per assembly is reduced. Ultimately, it can be concluded that the MXR-Th2 does address the main proliferation weakness of the MXR-inter1 at MOL. While the plutonium is more attractive than that of a PWR, a total of at least 3 assemblies would need to be diverted undetected to obtain sufficient material for a weapon. In light of this trade-off, the MXR-Th2 could be deemed to closely match the proliferation resistance of a PWR, and would not place an 'added burden/risk' to the nonproliferation regime. The LER on the other hand, is found to be the most proliferation resistant design considered, but only by a small margin (attractiveness is similar to MXR-Th2, but main advantage is no need to shuffle at MOL). The improvements also come at an unacceptable cost to core lifetime, which is almost halved.

Table 7.13: Nonproliferation metrics for the LER and the MXR-Th2. The max cases for the MXR-Th2 at MOL and EOL corresponded to assemblies number O605 and O107 respectively, while the max case for the LER at EOL was O106.

	MXR-Th2	**LER**
1 SQ window (years)	0	0
WG window (years)	25	12
1 SQ & WG window (years)	0	0
2×(0.5 SQ & WG) window (years)	8	0
MOL		
av(FOM_1)	0.64	-
av(FOM_2[Pu])	1.90	-
max(FOM_2[Pu])	2.20	-
EOL		
av(FOM_1)	0.52	0.52
av(FOM_2[Pu])	1.64	1.60
max(FOM_2[Pu])	1.84	1.70

7.3 Fuel Cycle Evaluation

Having taken a more in-depth look at the proliferation resistance of the MXR, the last step in the study is to evaluate it in the broader context of the nuclear fuel cycle. Since a PWR can reach better proliferation resistance than the MXR, it is important to evaluate whether fuel consumption or waste generation see any notable improvement in the proposed designs. The first part of the section will deal with overall fuel requirements, including front-end metrics, such as enrichment and natural uranium mining. The second part will then consider waste and environmental aspects of the MXR. The main focus will be on comparing the performance of the different MXR designs to the LLR and a typical PWR. Most of the analysis in this section will be guided by the Fuel Cycle Evaluation Campaign metrics.[78]

7.3.1 Fuel requirements

Previous sections have looked into overall heavy metal and ^{235}U initial loading in the MXR concepts; this section will take a closer look at resource requirements. Additionally to different fuel consumption metrics, separative work units (SWU) will need to be assessed. The value can be calculated by solving Equations 7.4 and 7.5. The letters and subscript F, P, and W relate to the feed, product and waste steam respectively. x refers to the weight fraction of ^{235}U in the uranium, i.e. the enrichment level. Knowing that $F = P + W$, the ratio F/P can be evaluated to estimate how many kg of natural uranium feed are required to obtain 1 kg of uranium, at a specified enrichment, x_p. The optimum tails assay, x_w, was estimated using the online URENCO SWU Calculator,[79] and found to be 0.227w% ^{235}U.

$$x_f F = x_p P + x_w W \tag{7.4}$$

$$SWU = P \times V(x_p) + W \times V(x_w) - F \times V(x_f) \tag{7.5}$$

where $V(x)$ is the value function, defined as:

$$V(x) = (1 - 2x) \ln \left[\frac{(1-x)}{x} \right] \tag{7.6}$$

The above set of equations can be used both to determine the total quantity of natural uranium needed for the MXR as well as the SWU requirements. These values, alongside relevant fuel consumption metrics are summarized in Table 7.14. The values are approximate and are compared to those of a conventional PWR design with optimized fuel cycle characteristics.[80] The PWR is assumed to be a standard Westinghouse design, with 17×17 fuel assembly, an 18-month cycle, and 92 assembly feed. In order to account for the different power rating, thermal efficiency, and operating lifetimes of the different designs, values are normalized by the total useful energy produced throughout the life-cycle (i.e. normalized by GWe-yr). The MXR results were nearly identical for the MXR-S and MXR-inter1, as such, only the latter values are used.

Table 7.14: Fuel consumption evaluation metrics for the different reactors.

	PWR	**LLR**	**MXR**	**MXR-Th2**	**LER**
Thermal power (MW_{th})	3565	250	370	370	360
Efficiency	33%	40%	40%	40%	40%
Average enrichment	4.5%	13.5%	15.1%	20%	15.1%
Fissile Inventory (t-^{235}U/GW_e-yr)	1.0	1.3	1.5	1.5	2.4
HM consump. (MTU/GW_e-yr)	22.4	9.9	10.0	9.5	15.6
Natural U consump. (MTU/GW_e-yr)	200.0	269.5	307.1	183.4	479.3
Natural Th consump. (MTTh/GW_e-yr)	-	-	-	1.8	-
SWU (t-SWU/GW_e-yr)	164.3	274.6	316.9	199.6	494.5
Av. discharge burnup (GWd/MTU)	49.1	92.6	91.2	96.2	58.4
Development cost	A	B	B	C	B
Development time	A	B	B	B	B
Infrastructure compatibility	A	A	A	C	A
Familiarity of licensing	A	B	B	D	B
Barriers to implementation	A	C	B	C	B

The results show an increased in fuel requirements for most of the proposed designs, in light of their higher initial fuel enrichment. The only exception is the thorium-based design that sees a net reduction in natural uranium consumption. The higher natural uranium consumption for the MXR is somewhat alleviated by the higher discharge burnup, but is still noticeably higher than a PWR. A rough calculation of the PWR resource requirements using LLR specifications (13.5% enrichment and 92.6 GWd/MTU discharge burnup) yields similar outputs to those of the MXR. Compared to the LLR, the MXR has slightly higher natural uranium and SWU requirement than the LLR, despite similar total fuel consumption (this is the case since power produced was normalized per assembly). SWU costs are increased by 15% to account for the higher average enrichment in the MXR relative to the LLR. The LER (epithermal design) achieves the worst values in light of its reduced operating lifetime (16 years).

The development metrics shown in Table 7.14 were obtained from the Appendix C of the Fuel Cycle Evaluation and Screening Study.[81] The quoted bins for the LLR correspond to those of the fuel cycle case 'EG02' in the screening study. Its description, "Once-through using enriched-U fuel to high burnup in thermal or fast critical reactors", was deemed to best fit that of a long-lived reactor design. The bins are ranked alphabetically in the order of their attractiveness (A is best). Development and licensing requirements are ranked lower for the thorium-based design due to the lack of maturity of that type of fuel. It should be noted that while development costs of the LLR and MXR are in the same bin, the MXR has an upper hand relative to the original. As previously mentioned, since the MXR clad and fuel operate within the bounds of known experimental data, less R&D efforts are required to validate an advanced type of fuel cladding that can withstand the high dpa of the LLR. This also contributes to a higher score in the barrier to implementation metric.

7.3.2 Waste and environmental impacts

The final design evaluation metrics account for environmental issues, the primary of which is waste generation. By virtue of operating with a higher discharge burnup, the MXR concept is expected to fare better than a typical PWR. This section will quantify the metrics using the guidelines provided by the Fuel Cycle Evaluation and Screening study.[81] The generation of low-level waste (LLW) is not considered in the analysis, as it deemed to be similar in all the different reactor designs considered. The evolution of the activity of spent fuel within the different core designs is shown in Figure 7.20(a). Values after 100 and 100,000 years are tabulated in Table 7.15. The results are obtained by generating a MCNP6 input at EOL and depleting the isotopic composition at zero power. Due to strong agreement between the MXR-S and MXR-inter1, only the latter results are analyzed here.

Table 7.15: Waste generation evaluation metrics for the different reactors. Spent Nuclear Fuel (SNF) mass is assumed to vary little from the original composition.

	PWR	**LLR**	**MXR**	**MXR-Th2**
Mass of SNF (t/GW_e-yr)	25.5	11.0	11.1	10.3
Mass of depleted U (t/GW_e-yr)	117.5	259.7	297.1	178.9
100 yr SNF Activity (kCi/GW_e-yr)	497.34	172.68	201.58	183.54
100,000 yr SNF Activity (kCi/GW_e-yr)	0.88	0.56	0.56	1.62

The discrepancies observed in the normalized activity after 10 years of cooling between the PWR and the other fast-based models, is mostly driven by fission products (FP). These isotopes are responsible for the majority of the activity early on, but their activity quickly drops over time as they tend to have shorter lifetimes (see Figures 7.20(b) and 7.20(c)). At 10 years, the quantity of FP in reactors such as the LLR is lower than that of a PWR for two main reasons: (1) the higher thermal efficiency means less FP are produced for the same amount of electricity, (2) the long residence in the core (25 years) means that a lot of the FP have decayed before the reactor EOL. This last point is more clearly illustrated in Table 7.16, which shows how the most active radionuclides see sharp decreases depending

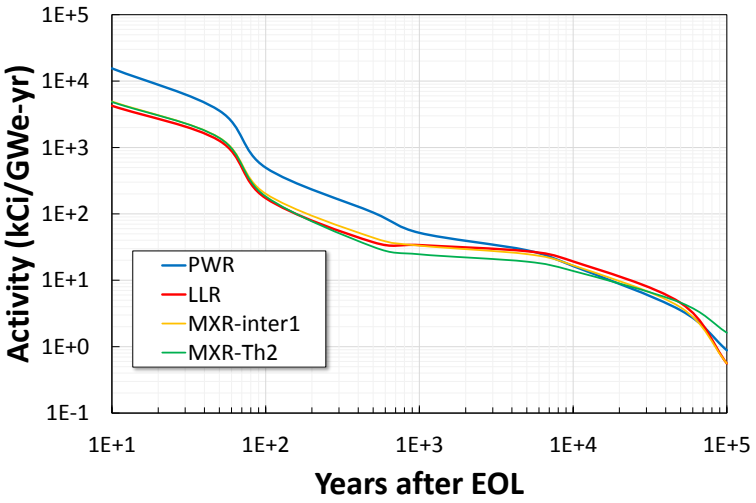

(a) Normalized activity evolution for the four designs considered.

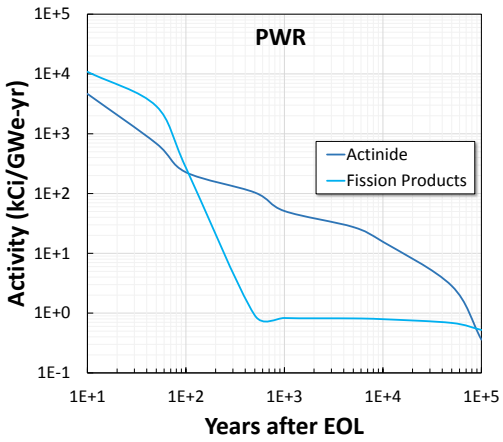

(b) Evolution of the actinide versus fission product activity in the PWR.

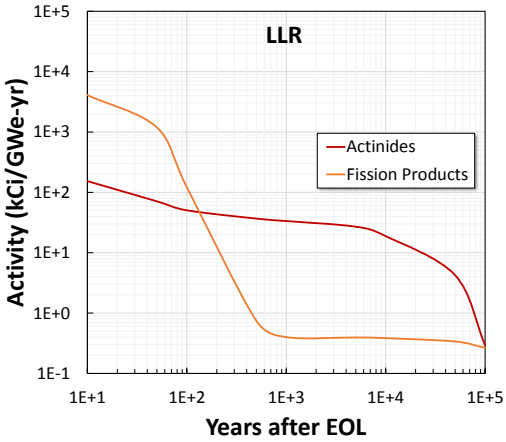

(c) Evolution of the actinide versus fission product activity in the LLR.

Figure 7.20: Main performance metrics of the Long-lived Epithermal Reactor (LER).

on how short their lifetime is. The most active two, ^{137}Cs and ^{90}Sr have a half-life close to that of the long-lived cores. In addition to a reduced FP activity, long-lived designs have a lower actinide activity after 10 years as well. This is mostly due to a lower ^{238}Pu and ^{241}Pu fraction within the fuel, that dominate activity levels at this stage. At around 100 years, a reduction of around 60% in normalized activity is observed between the long-lived designs and the PWR. The MXR sees a small increase relative to the LLR due to a larger proportion of actinides in the fuel at this point. After around 1000 years, all of the different curves start to converge, and very little benefit is gained by the long-lived designs. Small divergences

are still observed at around 100,000 years however. The MXR-Th2 sees a higher activity at this point due to three by-products of the thorium chain: ^{229}Th, ^{233}U, and ^{225}Ac. Around that same time range, the uranium based long-lived designs (LLR and MXR-inter1) have a reduced activity relative to the PWR in light of the higher rate of actinide burning in the fast and epithermal spectrum.

Table 7.16: Variation in the activity of the main fission products, 10 years after EOL.

	PWR	**LLR**	**diff.**	**half-life**
^{85}Kr (kCi/(GW$_e$-yr)	1.98×10^5	6.28×10^4	-68.3%	10.8 yr
^{90}Sr (kCi/(GW$_e$-yr)	2.44×10^6	1.11×10^6	-54.4%	28.8 yr
^{90}Y (kCi/(GW$_e$-yr)	2.44×10^6	1.11×10^6	-54.4%	64.1 h
^{134}Cs (kCi/(GW$_e$-yr)	3.10×10^5	5.10×10^4	-83.6%	2.1 yr
^{137}Cs (kCi/(GW$_e$-yr)	4.60×10^6	1.60×10^6	-65.2%	30.1 yr
^{147}Pm (kCi/(GW$_e$-yr)	6.95×10^5	9.20×10^4	-86.7%	2.6 yr
^{154}Eu (kCi/(GW$_e$-yr)	1.21×10^5	2.00×10^4	-83.4%	8.6 yr

In terms of waste volume, Table 7.15 illustrates some of the benefit of the long-lived core designs in regards to waste generation. Due to their increased fuel burnup and lower material loading per unit of energy, the total spent fuel mass of designs such as the LLR and MXR is reduced by approximately 57%. The main drawback of the MXR variants is the increase in depleted uranium fuel. To reach the much higher average enrichment for the long-lived cores, natural uranium feed and depleted uranium tails are subsequently increased. While this waste is not dangerously toxic, it still constitutes an environmental hazard.

Other environmental of the different designs were also considered and compared to the PWR. They are summarized in Table 7.17. Values were estimated using the multipliers from the Evaluation and Screening report.[81] The analysis focused on three main points: land usage, water consumption and carbon emissions. Requirements at both ends of the fuel cycle were included in the analysis. The fuel cycle stages taken into consideration were: mining, conversion, enrichment, conversion, fabrication, reactor construction, reactor op-

eration, interim waste storage and geological repository. Since LLW is not considered, land and water requirements for a shallow land burial are not accounted for in the analysis. The calculations also assume that multiplier values for UOX fabrication are representative enough to model U-Zr fuel fabrication.

Table 7.17: Waste generation evaluation metrics for the different reactors.

	PWR	**LLR**	**MXR**	**MXR-Th2**
Land use (km^2/GW_e-yr)	0.182	0.189	0.204	0.157
Water use (ML/GW_e-yr)	23,887	23,949	23,984	23,871
Carbon emitted ($t\text{-}CO_2/GW_e$-yr)	41.6	43.7	47.7	35.1

While the water consumption appears to increase for the MXR and LLR, it should be noted that the metrics used by the Fuel Cycle Evaluation Campaign do not account for varying thermal efficiency in the designs. A typical PWR efficiency, of around 33%, is assumed. The higher efficiency of the sodium-cooled long-lived reactors should decrease total water consumption in their respective cycle. Because the same water consumption factor is used for all four cases (2.37×10^4 ML/GWe-yr), overall variations between each case depend mostly on front-end requirements. With their higher enrichment requirements, the LLR and MXR water consumption may appear slightly larger than a PWR, but would be reduced in reality. Values are lower for the MXR-Th2 in light of the reduced natural uranium consumption. Land usage variations are mostly driven by front-end activities, most notably uranium mining. As a result, this metric is around 11% higher for the MXR relative to the PWR per unit of energy produced, but is reduced by 15% for the MXR-Th2. This is because thorium mining is less land-intensive, and front-end processing needs are reduced. Carbon emissions are slightly higher for the MXR and LLR, relative to a PWR, but this is not by substantial amounts. Emissions tend to be relatively low in the nuclear sector, and mostly driven by energy consumption in the front-end and during reactor construction. Reduction in back-end land requirements and carbon consumption in the

MXR are insufficient to alleviate the increases at the front-end due to the higher enrichment required. The results illustrate that resource requirements do not vary greatly between the MXR and the LLR. All the long-lived designs see improvements relative to typical PWRs in terms of waste generation, but consume more energy and uranium in the front-end. This leads to higher mining and processing costs. Nevertheless, the main advantage of long-lived designs over a typical PWR remains the fact that they can better cater to small markets needing decades-long continuous operation without refueling. Water-cooled reactors are less able to meet these criteria, due to cladding corrosion issues.

7.4 Chapter Conclusion: Discussion of the MXR Performance and Feasibility

Two main design recommendations were identified in this Chapter from a safety standpoint. The first is to replace the MXR reflector material with BeO, and the second is to dope some of the outer assembly fuel with small quantities of gadolinium. The two approaches resolve power peaking issues at the two most problematic interfaces: the fast/thermal one, and the core/reflector one. Reactivity feedback analysis showed that the resulting core model, referred to as MXR-S, was able to meet all of the passive safety criteria developed by Wade (the addition of 6 control assemblies proved crucial in this task).[53] From a nonproliferation standpoint, analysis showed how the MXR could substantially reduce windows of opportunity for a potential proliferator to divert 1 SQ of weapon-grade plutonium. While the design is not able to reach the same level of proliferation resistance as a typical PWR, it still constitutes a notable improvement over the original LLR model. The main design weakness of the MXR is the reliance on shuffling at MOL. This is not considered to be a large impediment, since it is likely the LLR itself would require access the core at least once before EOL, for maintenance purposes. Design improvements to the MXR were assessed to weigh the viability of more proliferation resistant design. An epithermal LER design, where all assemblies are moderated, was found to reduce plutonium attractiveness much more effectively than the MXR, but at an unacceptable cost to performance (oper-

ating lifetime reduced by nearly half). An alternative thorium-fueled concept, MXR-Th2, was also investigated. The core had four zones: two breeder and two driver. One of each was in the fast zone and in the moderated region. The design took advantage of the better breeding capabilities of thorium in the epithermal regime. MXR-Th2 was able to reach the nominal core lifetime (25 years), while improving many proliferation metrics. While plutonium quality remains relatively unchanged relative to the MXR, no single assembly ever reaches 1 SQ, and at least three would be needed to divert enough material for a weapon at MOL. The MXR-Th2 was concluded to be the most proliferation resistant of the designs considered. The final evaluation took into account resource and environmental requirements of the various concepts. Normalized uranium, land, and carbon consumption in the MXR were found to be very similar to those of the LLR. They both remain higher that that of a typical PWR. Despite their higher burnup, long-lived designs require increased initial enrichment leading to further strains in terms of resource requirements. The main advantage of the LLR and MXR was a net reduction in waste generated, in light of the lower actinide loading in the fuel and better transmutation. The MXR-Th2 was the only design that achieved improvements relative to the PWR in terms of resource consumption. This came at the cost of design feasibility however, due to the lack of experimental data on thorium-based material.

CHAPTER 8
CONCLUSION

8.1 Summary

A mixed-spectrum core configuration is proposed as a mean to improve the proliferation resistance of long-lived fast reactors. The MXR contains moderating rods in its outer core region to moderate neutrons to the epithermal regime, while the inner core region remains in the fast spectrum. This allowed the core to breed additional fissile material in one zone and extend its lifetime, while also reducing plutonium quality in another. At the middle-of-life (MOL), inner and outer assemblies are shuffled to ensure all of them are exposed to the thermalized spectrum. The final isotopic composition of the MXR was shown to be below the weapon-grade limit, a net advantage over the original fast reactor design it is based on (the LLR). The main design tradeoffs in achieving this, were a higher average fuel enrichment, a larger core volume, a slightly larger fuel consumption, and a reliance on accessing the core twice during its lifecycle. The larger volume did however allow for an increase in power production by 48%.

Screening of the design space was conducted to yield an optimal core model. A wide range of different configurations were considered and assessed. Due to inherent limitations of the REBUS deterministic code, improvements were required. These included explicit modeling of fission product decay chains and manually updating of the composition throughout depletion. Better cross-sectional treatment was needed to account for assembly heterogeneity and low-energy neutrons. The improved deterministic code was mainly relied on as a design scoping tool, with the MCNP6 stochastic code used more heavily for final evaluations. The optimization process found that the most effective approach to core thermalization was to rely on $ZrH_{1.6}$ as a moderating material, placed within outer

fuel assemblies (rather than using a mix of moderating and fuel assemblies), and using different rod arrangements. Small changes to the moderator placement had large spatial self-shielding effects that altered the overall core performance. The final core arrangement was able to match the 25 year LLR lifetime, with a similar average discharge burnup.

Safety analysis was conducted to evaluate the feasibility of the proposed layout. As expected, power peaking was observed to be mostly occurring at the fast/thermal interface, but also at the reflector/core boundary. Potential solutions included replacing the reflector material with BeO instead of $ZrH_{1.6}$ and doping the fuel with small amounts of gadolinium. The MXR reached a peak linear power rating of 26.5 kW/m, which is within the bounds of typical sodium-cooled reactors, and was estimated to still yield reasonable margins to melting during transients. Reactivity feedback mechanisms ensured adequate inherent passive safety of the core. The Doppler and void reactivity coefficients notably saw improvements in the MXR design. Another important advantage of the MXR relative to the LLR, is the notable reduction in the peak fast fluence in the clad. The peak value of approximately 4×10^{23}n/cm^2 is close to limits at which experimental material data has been obtained for a fast reactor.[14] As such, the design is deemed to be more feasible than the LLR, which cannot rely on currently available material in order to sustain the 6×10^{23}n/cm^2 peak fluence after 25 years of operation. Lastly, core coupling between the fast and thermal zones was ensured to be within the bounds of typical fast reactor, reducing the risks for core tilting effects.

Final parametric evaluations of the MXR concluded that while the design was unable to reach the same level of proliferation resistance as a typical LWR, it still constitutes a worthy improvement over the original LLR. Fine-tuning of the MXR can ensure no fuel assembly contains weapon-grade plutonium at end-of-life (EOL), and only a few contain 1 SQ. At no time during the operating lifetime of the reactor can a state obtain 1 SQ of weapon-grade material from a single assembly. There are only two years during which, an assembly could yield that quantity of plutonium at any purity level. These windows are substantially larger

for the LLR. Proliferation metrics can be improved upon further by relying on a mixed U-Th fuel in the MXR. Leveraging the breeding capabilities of thorium in the epithermal spectrum allows the modified design to maintain a 25 year lifetime, while simultaneously reducing the total quantity of plutonium produced per assembly. As a result, no assembly reaches 1 SQ of any plutonium grade in the MXR-Th2, and three assemblies would need to be diverted to obtain that amount at MOL. The main drawback of such a design is the relative lower maturity of thorium-based fuels.

Overall the MXR design sees notable improvements over the LLR while maintaining a similar operating lifetime. The concept is deemed more feasible due to its lower clad damage and reaches higher levels of proliferation resistance. These advantages are believed to outweigh the main challenges of the design: a slightly larger core volume, increases in resource consumption, and the reliance on shuffling halfway through the operating lifetime.

8.2 Contribution

The research work contributes to advances in four main areas: (1) improvement of proliferation resistance of long-lived reactors without substantial performance penalties, (2) emphasis on considering nonproliferation characteristics during conceptual design optimization, (3) extending the knowledge on the versatile mixed-spectrum reactors, and (4) improving modeling capabilities for thermalized systems using deterministic nodal codes. While the first contribution is the main objective of the thesis, the other three should still be noted. Nonproliferation aspects of a core are seldom considered in the design stage of a reactor, and should be given greater emphasis in light of the advanced, non-LWR concepts on the horizon. Mixed-spectrum reactors have been investigated for a wide variety of applications, but little work has been conducted thus far on a wide-range design screening, or an inter-assembly level safety evaluation. Improvements and benchmarks of the determinstic transport codes are expected to benefit a wide range of analysis for both mixed and thermal systems. Further research is required to ensure these tools are able to reach

stochastic-codes levels of accuracy.

8.3 Future Work

The proposed MXR configurations achieve the sated objective of improving proliferation metrics while maintaining adequate core lifetime. Further fine-tuning of the design can further the aforementioned advantages and alleviate some of the limitations. A multi-objective optimization using advanced algorithms (e.g. Genetic Algorithms) can more thoroughly screen the design space to identify more optimal core configurations. The main drive would be to reduce resource requirements, flatten the burnup profile within the core, and further improve on plutonium breeding metrics. More comprehensive scoping of shuffling strategies can also help achieve this goal.

The safety evaluations conducted thus far are at a high-level. More in-depth investigations will require the use of coupled neutronic-thermal transient simulations. This would provide more accurate modeling of transients scenarios without relying on point-kinetics approximations. Closer evaluation of the moderator insertion mechanism would also be beneficial. Stresses, flow distributions, and thermal expansion rates in the moderator channel tubes must be considered; alongside thermo-mechanical analysis of the moderating rods themselves.

Future work should also consider cross-sectional uncertainties and their impact on final isotopic composition. By virtue of operating in the epithermal spectrum, the inherently large errors in the resonance regions are expected to have notable effects on core performance. Lastly, assessing the viability of antineutrino monitoring technology on the proposed mixed-spectrum reactor can be invaluable. Optimizing the proliferation resistance of the design concurrently with detector capabilities can place bounds on the total quantity of plutonium that can be theoretically diverted without detection.

Appendices

APPENDIX A

FAST REACTOR CORE MODELING SPECIFICATIONS

The different long-lived design considered in the thesis were all based on the specifications of the AFR-100. Table 4.2 provided an overview of the design specifications. More information can be found in Table A.1 below. The values are for room temperature conditions and the operating conditions. Further explanation on how the latter values were derived, will be provided in this section.

Table A.1: Evolution of the LLR dimensions from room temperature and under operating conditions. Based on the AFR-100 model.[13]

	Room Temperature	**Operating Condition**
Assembly pitch (cm)	16.50	16.62
Duct thickness (cm)	0.30	0.30
Active height (cm)	110.00	119.45
Driver clad inner diameter (cm)	1.39	1.40
Driver clad outer diameter (cm)	1.49	1.50
Wire wrap diameter (cm)	0.107	0.108
Reflector inner clad diameter (cm)	1.51	1.52
Reflector outer clad diameter (cm)	1.61	1.62
Control inner clad diameter (cm)	4.87	4.90
Control outer clad diameter (cm)	5.01	5.04

In neutron transport simulations, geometric dimensions were modified to more closely mimic operating conditions. Changes in dimensions are primarily driven by thermal expansion rate and fuel irradiation swelling. With in an inlet/outlet temperatures of 395/550°C, an average temperature of 472.5°C was used to estimate the thermal expansion rates within the core. Equation A.1 was used to estimate the resulting HT9 steel expansion rates at different levels.[82] The ratios at inlet, core, and outlet levels were respectively 1.0045, 1.0055, and 1.0065. The average value of 1.0055 was used to expand most of the dimensions in Table A.1. The assembly pitch expansion is mainly driven by the grid plates below

that are made of SS-312. The expansion rate for the latter at inlet temperatures of 395°C was estimated to be 1.0074. Upon irradiation, the fuel radially swells to reach the clad inner wall. A 75% smear density is assumed, with the remainder of the inner clad volume filled with sodium before irradiation. Axial swelling is then taken to be of around 8%, based on experimental data.[83] Sodium density variations are estimated using Equation A.2.[43]

$$[\Delta L/L_0]_{HT9} = -0.2191 + 5.678 \times 10^{-4}T + 8.111 \times 10^{-7}T^2 - 2.576 \times 10^{-10}T^3 \quad \text{(A.1)}$$

$$[\rho]_{Na} = 1011.8 - 0.2205T - 1.9226 \times 10^{-5}T^2 + 5.6371 \times 10^{-9}T^3 \quad \text{(A.2)}$$

More intricate geometries needed to be accounted for as well. Fuel rods are wrapped around with a helix wire wrap to separate them from each other. This can be difficult to model accurately during simulations. Instead, the clad outer diameter was increased to 1.502 cm to incorporated the added HT9 mass of the wire-wrap. The helix area was estimated using Equation A.3, then used to compute the combined rod radius in Equation A.4. A helix ratio, h_w, of 1.0001087 was used. The radii r_{co}, r_{ci}, and r_w correspond to outer clad, inner clad, and wire respectively.

$$A_{comb} = A_{clad} + A_{wire} = \pi \times (r_{co}^2 - r_{ci}^2) + h_w \times \pi r_w^2 \quad \text{(A.3)}$$

$$r_{comb} = \sqrt{\frac{A_{comb}}{\pi} + r_{ci}^2} \quad \text{(A.4)}$$

As U-Zr swells in the radial direction when it is irradiated, it pushes the sodium bond upwards into the plenum. The displaced sodium bond height above the fuel must be accounted for as it affects neutron reflection back into the core. The displaced sodium bond height, l_{bnd} is estimated from Equation A.5, using the sodium mass m_{bnd} calculated in Equation A.6. Note that the initial mass is estimated under ambient temperature condi-

tions (ρ_{amb}), while the length is estimated for the outlet temperature condition (ρ_{out}). The resulting displaced sodium height was estimated to be approximately 31.35 cm. For simplicity, the core is modeled under the expanded condition throughout its lifetime, with the U-Zr fully expanded (both radially and axially), and the sodium bond displaced. This is assumed to be a valid assumption since the U-Zr fuel expands fairly quickly to reach these conditions.[83] The resulting axial bounderies of the different core regions are highlighted in Table A.2 under ambient and operating conditions.

$$l_{bnd} = \frac{V_{bnd}}{A_i} = \frac{\rho_{out} \times m_{bnd}}{\pi r_{ci}^2} \tag{A.5}$$

$$m_{bnd} = \rho_{amb} \times V_0 = \rho_{amb} \times (1 - 0.75) \times r_{ci}^2 l_{fuel} \tag{A.6}$$

Table A.2: Axial dimension of the LLR under ambient and operating conditions.

	Room Temperature	**Operating Condition**
lower shield (cm)	33.00	33.15
lower reflector (cm)	66.00	66.29
lower fuel (cm)	84.30	86.17
middle fuel (cm)	157.70	165.87
upper fuel (cm)	176.00	185.75
sodium bond (cm)	176.00	217.10
gas plenum (cm)	341.00	351.83

The majority of fuel densities were obtained from the PNNL compendium.[84]. The values were subsequently divided by the expansion rate factors in order to account for expansion effects and to conserve mass. In the case of HT9 steel within the core, the density is multiplied by a factor of (1/1.0055^3). In the case of the the U-Zr fuel, this factor is $[0.75 \times 1/(1.08 \times 1.005^3)]$. Variations in sodium density were simply computed using Equation A.2. Table A.3 highlights the different densities for each of the main material used within the core and their corresponding corrected values. Zirconium hydride was assumed to expand at the same rate as HT9 steel.

Table A.3: Material densities at ambient temperature and average core temperature. The corrected values account for thermal expansion and fuel swelling.

	Room Temperature	**Operating Condition**
U-10Zr (g/cc)	16.02	10.94
HT9 (g/cc)	7.76	7.63
Na (g/cc)	0.95	0.84
$ZrH_{1.6}$ (g/cc)	5.61	5.52

Isotopic vectors for the fuel are displayed in Table A.4 for completeness. The values are for the differing enrichment levels of the LLR. The HT9 steel and $ZrH_{1.6}$ are not shown here; standard atomic weight fraction values were used to compute them.

Table A.4: Isotopic vector for the U-Zr fuel at different enrichment levels.

enrichment:	**8.0%**	**10.5%**	**14.5%**	**15.0%**	**18.0%**
^{235}U (a/b-cm)	2.0189×10^{-3}	2.6498×10^{-3}	3.6592×10^{-3}	3.7854×10^{-3}	4.5425×10^{-3}
^{238}U (a/b-cm)	2.2924×10^{-2}	2.2301×10^{-2}	2.1304×10^{-2}	2.1180×10^{-2}	2.0432×10^{-2}
^{90}Zr (a/b-cm)	3.7171×10^{-3}	3.7171×10^{-3}	3.7171×10^{-3}	3.7171×10^{-3}	3.7171×10^{-3}
^{91}Zr (a/b-cm)	8.1061×10^{-4}	8.1061×10^{-4}	8.1061×10^{-4}	8.1061×10^{-4}	8.1061×10^{-4}
^{92}Zr (a/b-cm)	1.2390×10^{-3}	1.2390×10^{-3}	1.2390×10^{-3}	1.2390×10^{-3}	1.2390×10^{-3}
^{94}Zr (a/b-cm)	1.2556×10^{-3}	1.2556×10^{-3}	1.2556×10^{-3}	1.2556×10^{-3}	1.2556×10^{-3}
^{96}Zr (a/b-cm)	2.0229×10^{-4}	2.0229×10^{-4}	2.0229×10^{-4}	2.0229×10^{-4}	2.0229×10^{-4}

APPENDIX B

REBUS SIMULATION OPTIONS AND SETTINGS

Stochastic codes have few mathematical parameters to fine-tune apart from the number of virtual particles they simulate. The opposite is true for deterministic codes, with a wide range of variables and settings that need be considered for the simulation. A parametric study of different simulation settings was conducted in Section 4.3.3 in an effort to reduce the occurrence of negative flux values due to numerical convergence issues. This section goes into slightly more detail and provides an overview of the final settings settled upon for the optimization search using *REBUXS*.

As previously explained, the REBUS suite is formed of four main sub-codes. The first, MC^2, is a cross-section generation tool. In the developed models, a 'thermal' 894-group structure, referred to as 'THERM894', is used before flux weighting with TWODANT. The coarse group structure after flux weighting was a 73-group structure referred to as 'THERM73'. A third order angular scattering order setting was used for the code. In the 1-D CPM option, a reflective boundary was assumed for the model. The ^{242m}Am cross-section needed to be ignored due to software errors with generating 'THERM73' collapsed value. The 'PENDF' option was activated to account for resolved resonance self-shielding.

When using TWODANT, the 2-D discrete ordinates code, a third order scattering angle was also used, along with a second degree quadrature. A S_{12} angular order was employed by the code in r-z geometry. Mesh sizes were approximately 5 cm in the r-direction, and 8 cm in the z-direction. The TWODANT calculations were performed using broad-group cross-sections ('*c_twodant_group = BG*'). A mock-up of the input specifications for the core geometry is shown in Figure B.1. Each cell lattice represents a smeared, homogenized composition. Note that the different regions have varying lengths; i.e. each row and column do not necessarily have the same dimensions. Control rod assemblies (no. 16 and 17) were

accounted for as thin rings between different fuel regions.

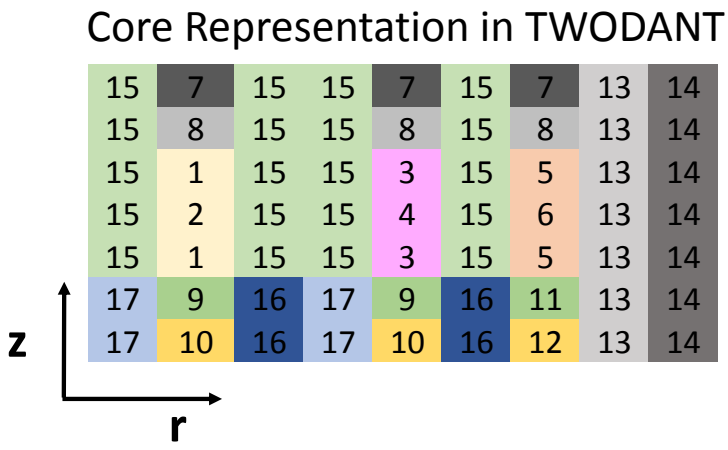

Figure B.1: Representation of the TWODANT input for a sample core geometry considered in the thesis. Each numbered region corresponds to a homogenized material region: inner fuel (1,2), mid fuel (3,4), outer fuel, sodium channel/bond (15,9), control rods (6,17), gas plenum (10,12), reflector material (8,13), and shield material (7,14) .

Once the ISOTXS, cross-sectional data was generated at each timestep in REBUXS, detailed flux distributions were computed using the DIF3D/VARIANT code. The core consisted of a 1/3 symmetric geometry with periodic boundary conditions applied. Hexagonal nodes were used to represent the assemblies, with their inner composition homogenized by the code. Axial boundaries varied between different regions, with 20 cm increments used for the fuel regions. Each of these fuel axial slices contained approximately 3 sub-meshes. Transport settings used for the majority of cases are summarized in Table B.1. In terms of the nodal spatial approximations for the source term, the flux term, and the leakage term (S-F-L), fourth, sixth, and first order polynomials were used respectively. A P_3 flux and leakage expansion were used by the code. Two xy-plane partial current sweeps (per group, per axial mesh sweep, and per outer iteration), and five in the axial direction. The eigenvalue convergence criteria was set to 10^{-5}. For the fission source convergence, both the average and pointwise criteria were set to 10^{-4}.

Standard settings were used for REBUS depletion using the non-equilibrium cycle options. The maximum number of region-density iterations and cyclic mode iterations were

Table B.1: Transport Settings used in the DIF3D simulations.

Parameter	**Setting Used**
S-F-L	40601
P_N	3
xy-sweeps	2
axial-sweeps	5
k_{eff} convergence	10^{-5}
source convergence	10^{-4}

set to 5. The burnup convergence criteria was set to 0.1. The main improvements in the *REBUXS* model, were in card '09', which specifies the neutron absorption and decay chains for individual isotopes. An exhaustive lists of different fission products reactions were accounted for. A total of 137 fission product isotopes were considered. They are listed in Table B.2 alongside the main actinides considered in the REBUXS models. Separate distributions were considered for each of the following isotopes: ^{234}U, ^{235}U, ^{236}U, ^{238}U, ^{237}Np, ^{236}Pu, ^{238}Pu, ^{239}Pu, ^{240}Pu, ^{241}Pu, ^{242}Pu, ^{241}Am, ^{242m}Am, ^{242}Am, ^{242}Cm, ^{243}Cm, ^{244}Cm, ^{245}Cm, ^{246}Cm. So-called 'DUMP' isotopes were used for more obscure reactions such as ^{244}U α decay reactions. This meant, that the resulting isotopes were essentially ignored. Individual isotopic reaction rates are also accounted for, mostly in the form of (n,γ) absorption, as well as β and α decays.

Table B.2: List of all the isotopes considered by REBUXS during depletion simulations.

Minor Actinides	^{234}U , ^{235}U , ^{236}U , ^{238}U , ^{237}Np , ^{236}Pu ,^{238}Pu , ^{239}Pu , ^{240}Pu, ^{241}Pu , ^{242}Pu , ^{241}Am , ^{42M}Am ,^{243}Am , ^{242}Cm ,^{243}Cm,^{244}Cm , ^{245}Cm , ^{246}Cm
Fission Products	^{73}Ge, ^{74}Ge, ^{76}Ge, ^{75}As, ^{76}Se, ^{77}Se, ^{78}Se, ^{80}Se, ^{82}Se, ^{79}BR, ^{80}Kr, ^{82}Kr, ^{86}Kr, ^{86}Rb, ^{86}Sr, ^{88}Sr, ^{94}Nb, ^{94}Mo, ^{108}Cd, ^{116}Cd, ^{116}Sn, ^{119}Sn, ^{120}Sn, ^{122}Sn, ^{124}Sn, ^{126}Sn, ^{126}Sb, ^{122}Te, ^{123}Te, ^{124}Te, ^{130}I , ^{128}Xe, ^{136}Xe, ^{136}Cs, ^{136}Ba, ^{142}Pr, ^{142}Nd, ^{152}Gd, ^{160}Gd, ^{160}Tb, ^{160}Dy, ^{161}Dy, ^{162}Dy, ^{163}Dy, ^{164}Dy, ^{165}Ho, ^{166}Er, ^{167}Er, ^{81}Br, ^{83}Kr, ^{84}Kr, ^{85}Rb, ^{87}Rb, ^{89}Y , ^{90}Sr, ^{90}Zr, ^{91}Zr, ^{92}Zr, ^{93}Zr, ^{94}Zr, ^{96}Zr, ^{95}Mo, ^{96}Mo, ^{97}Mo, ^{98}Mo, ^{100}Mo, ^{99}Tc, ^{100}Ru, ^{101}Ru, ^{102}Ru, ^{103}Ru, ^{104}Ru, ^{104}Pd, ^{105}Pd, ^{106}Ru, ^{106}Pd, ^{107}Pd, ^{108}Pd, ^{109}Ag, ^{110}Pd, ^{110}Cd, ^{111}Cd, ^{112}Cd, ^{113}Cd, ^{114}Cd, ^{115}In, ^{117}Sn, ^{118}Sn, ^{121}Sb, ^{123}Sb, ^{125}Sb, ^{125}Te, ^{127}I, ^{128}Te, ^{129}I, ^{130}Te, ^{130}Xe, ^{131}Xe, ^{132}Xe, ^{133}Cs, ^{134}Xe, ^{134}Cs, ^{134}Ba, ^{135}Xe, ^{135}Cs, ^{137}Cs, ^{137}Ba, ^{138}Ba, ^{139}La, ^{140}Ce, ^{141}Pr, ^{142}Ce, ^{143}Nd, ^{144}Nd, ^{145}Nd, ^{146}Nd, ^{147}Pm, ^{147}Sm, ^{148}Nd, ^{148}Sm, ^{149}Sm, ^{150}Nd, ^{150}Sm, ^{151}Sm, ^{151}Eu, ^{152}Sm, ^{152}Eu, ^{153}Eu, ^{154}Sm, ^{154}Eu, ^{154}Gd, ^{155}Eu, ^{155}Gd, ^{156}Gd, ^{157}Gd, ^{158}Gd, ^{159}Tb, ^{R87}S, ^{135}Ba, ^{126}Te

APPENDIX C
DIVERSION WINDOW PLOTS

Different diversion scenarios were considered in Chapter 7. For brevity, not all of the different windows of opportunities were included. They are displayed here for completeness. The windows consider the characteristics of plutonium in each assembly throughout their lifetime in the core. The results are displayed as bin-plots, with a red square indicating a plutonium criteria being met. Four main types of windows are considered: (1) if the plutonium is weapon-grade or above, (2) if the assembly contains 1 SQ of plutonium or higher, (3) if the assembly contains 1 SQ or more of plutonium that is above weapon-grade, and (4) whether the assembly contains more than 1/2 SQ above weapon-grade quality (to consider two-assembly diversion scenarios).

Figure C.1 highlights the proliferation windows for the original LLR design. As highlighted, plutonium remains weapon-grade in most assemblies, for the vast majority of their residence within the core. This leads to a substantial portion of time in which assemblies contain 1/2 SQ or more of weapon-grade material. The inner assemblies are among the first to reach 1 SQ of plutonium in the core. Another interesting observation is the fact that the more plutonium is bred in the core, the lower its quality tends to be. This provides an interesting relation when considering both the SQ and quality of plutonium; once assembly reach both criteria, they only do so for limited period of times. After a certain burnup is reached, the plutonium quality drops below the weapon-grade limit, despite still being over 1 SQ.

The windows for the MXR-inter1 are shown in Figure C.2. Here, it can be seen that at no point does one assembly contain 1 SQ of weapon-grade material. This is notably due to the fact that the weapon-grade window is much narrower for the MXR-inter1, in light of the thermalized spectrum. One interesting exception however, is assembly no. 107, which sees

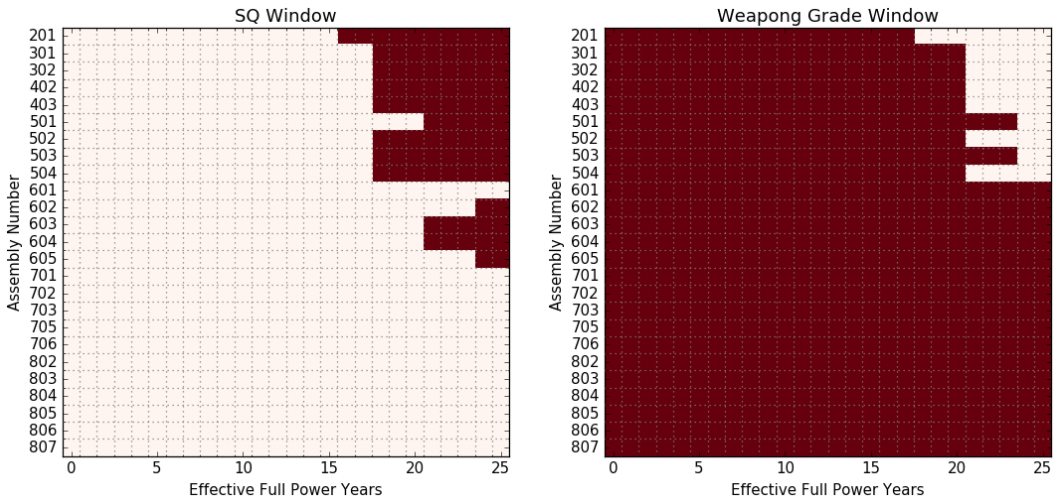

(a) Points in time when LLR assemblies contain at least 1 SQ of Pu.

(b) Points in time when LLR assemblies contain Pu above weapon-grade.

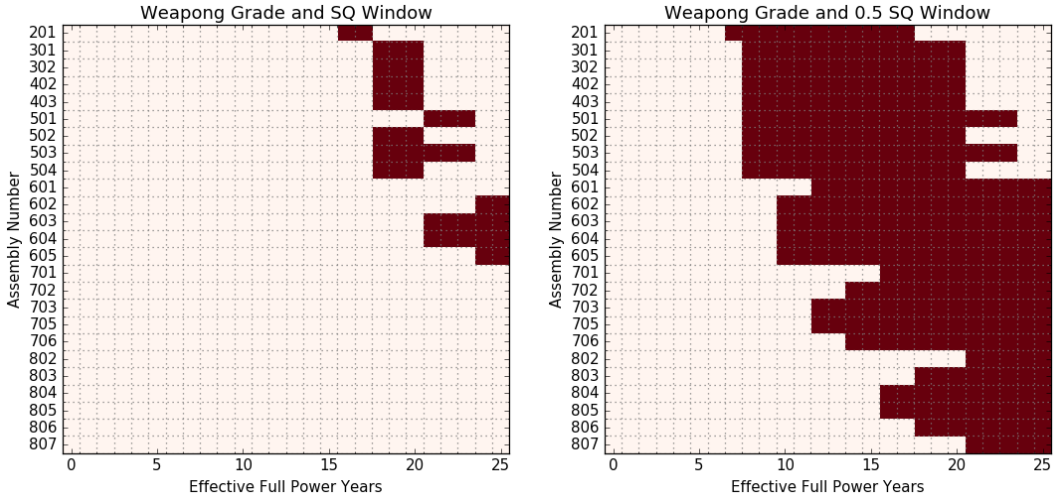

(c) Points in time when LLR assemblies contain at least 1 SQ of Pu.

(d) Points in time when LLR assemblies contain Pu above weapon-grade.

Figure C.1: Diversion windows for the LLR design. Red blocks indicates times at which an assembly meats the corresponding nonproliferation criteria.

its quality rise back above the weapon-grade limit after it is shuffled back into the fast zone of the core. This essentially prolongs some of the diversion windows as a result. Flatter power profiles can ensure this issue is avoided, as will be seen for the MXR-S design.

The MXR-S results, shown in Figure C.3, highlight some of the design improvements. The issue related to assembly no. 107 is avoided now, with diversion windows substantially reduced. There are also fewer clusters of instances were 1 SQ can be reached, contributing

to better metrics.

Lastly, the MXR-Th2 results in Figure C.4 show much improvement with regards to quantity of plutonium within the core. At not point does a single assembly reach 1 SQ throughout the reactor lifetime. The weapon-grade window is more 'patchy' however than in previous models. Assembly no. 107 behaves similarly to the case in MXR-inter1, and returns to weapon-grade after being shuffled to the fast zone. This can be expected to be improved upon with similar design modifications as those that were introduced for the MXR-S. Despite of this, the clustering of opportunities for two-assembly diversion scenarios is much reduced relative to other cases.

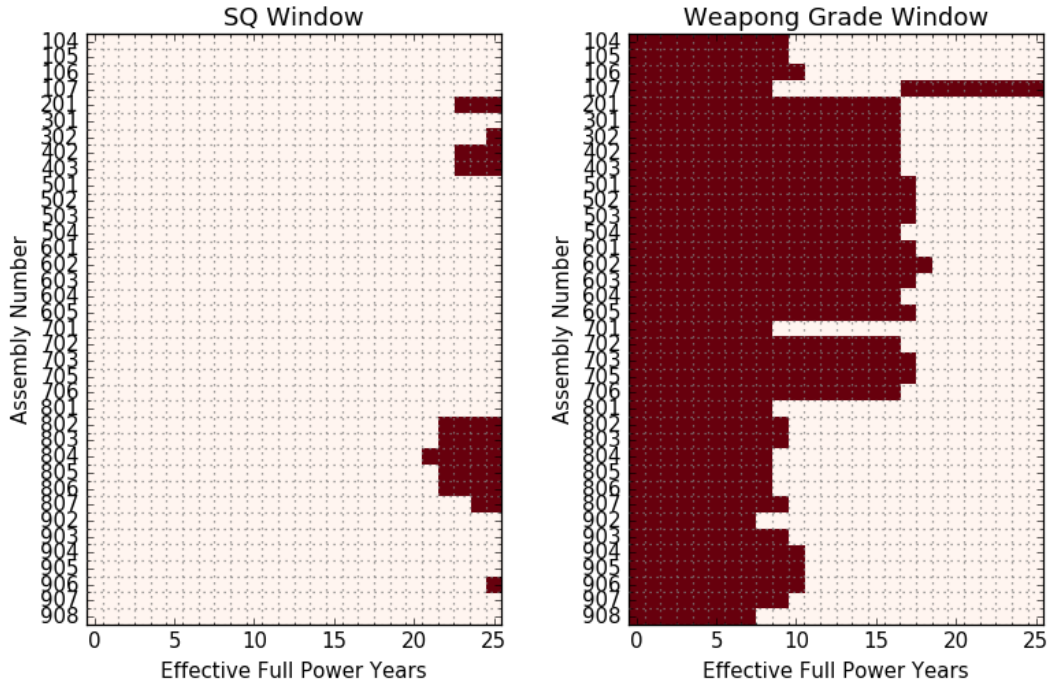

(a) Points in time when MXR-inter1 assemblies contain at least 1 SQ of Pu.

(b) Points in time when MXR-inter1 assemblies contain Pu above weapon-grade.

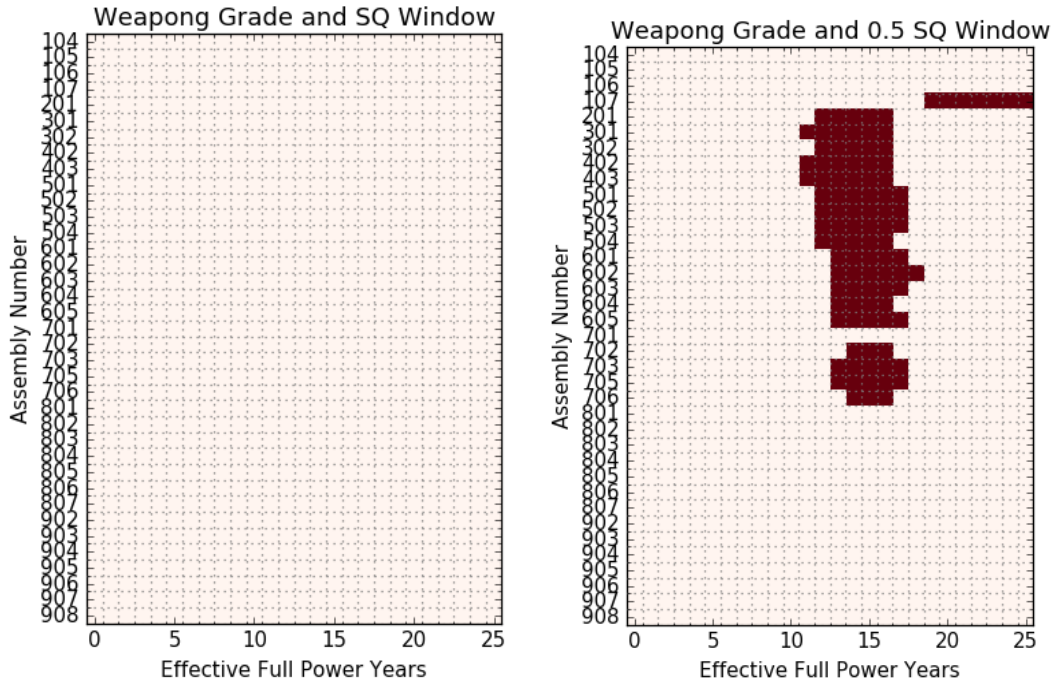

(c) Points in time when MXR-inter1 assemblies contain at least 1 SQ of Pu.

(d) Points in time when MXR-inter1 assemblies contain Pu above weapon-grade.

Figure C.2: Diversion windows for the MXR-inter1 design. Red blocks indicates times at which an assembly meats the corresponding nonproliferation criteria.

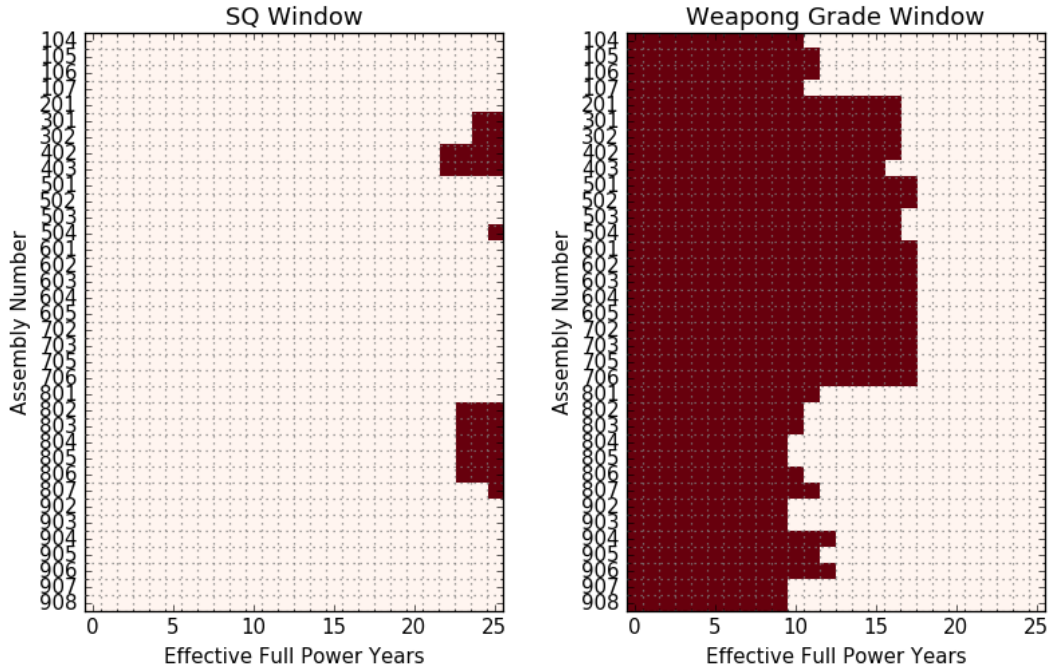

(a) Points in time when MXR-S assemblies contain at least 1 SQ of Pu.

(b) Points in time when MXR-S assemblies contain Pu above weapon-grade.

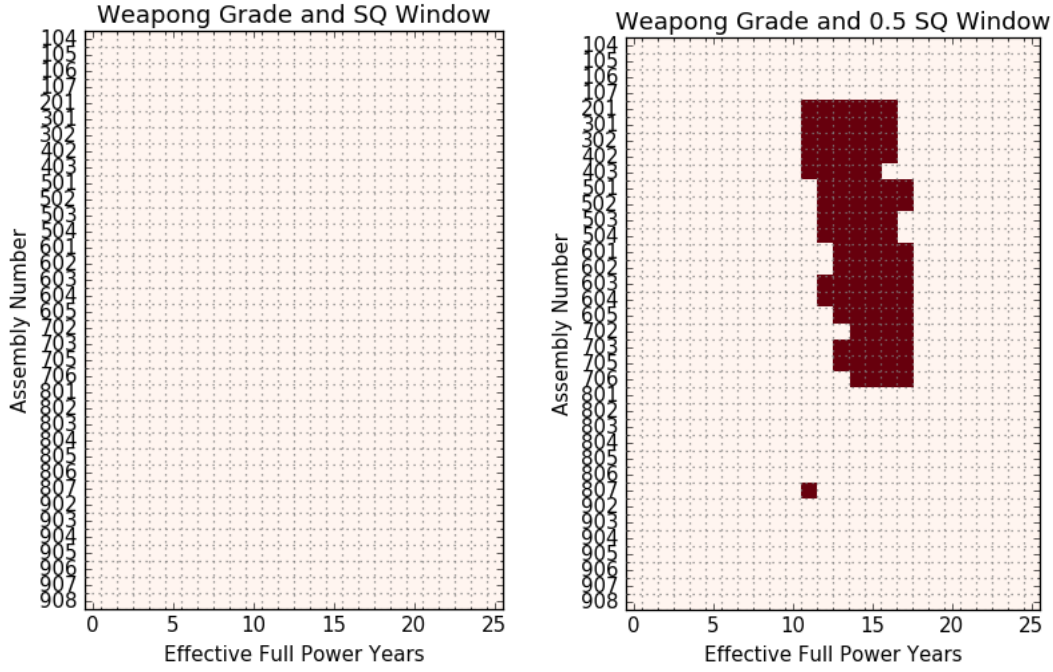

(c) Points in time when MXR-S assemblies contain at least 1 SQ of Pu.

(d) Points in time when MXR-S assemblies contain Pu above weapon-grade.

Figure C.3: Diversion windows for the MXR-S design. Red blocks indicates times at which an assembly meats the corresponding nonproliferation criteria.

(a) Points in time when MXR-Th2 assemblies contain at least 1 SQ of Pu.

(b) Points in time when MXR-Th2 assemblies contain Pu above weapon-grade.

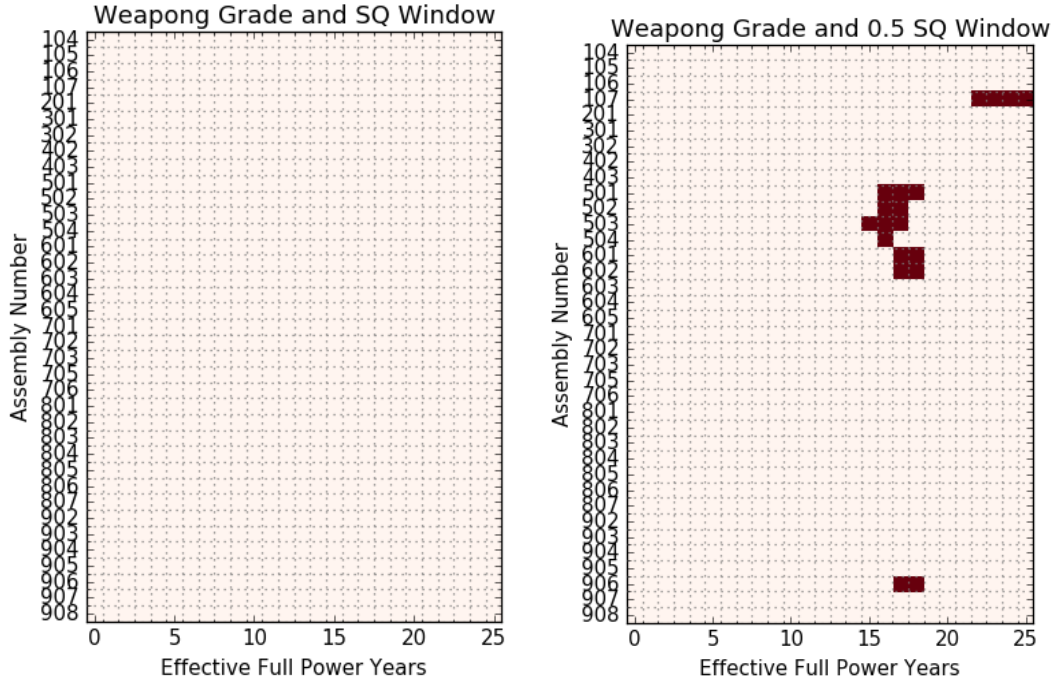

(c) Points in time when MXR-Th2 assemblies contain at least 1 SQ of Pu.

(d) Points in time when MXR-Th2 assemblies contain Pu above weapon-grade.

Figure C.4: Diversion windows for the MXR-Th2 design. Red blocks indicates times at which an assembly meats the corresponding nonproliferation criteria.

APPENDIX D

MXR NO SHUFFLING SCENARIO

This section considers a case whereby the host nation of the MXR refuses to perform the required shuffling operations. It should be note that such a case would be met with notable backlash from the international community, but is still important to take into consideration. MCNP6 simulations were run for the original MXR-S with an increase depletion timeline. Figure D.1(a) shows that k_{eff} can be maintained above unity for up to 27 year. This appears to potentially increase the core lifetime, but is in fact limited by an increase in peak fast fluence within the core. Figure D.1(b), shows that the peak fast fluence after 27 years is now 4.9^{23} n/cm^2. If the core is certified for a limit of 4.0^{23} n/cm^2, that threshold is crossed at approximately 23 years, thus shortening the total operating time of the core.

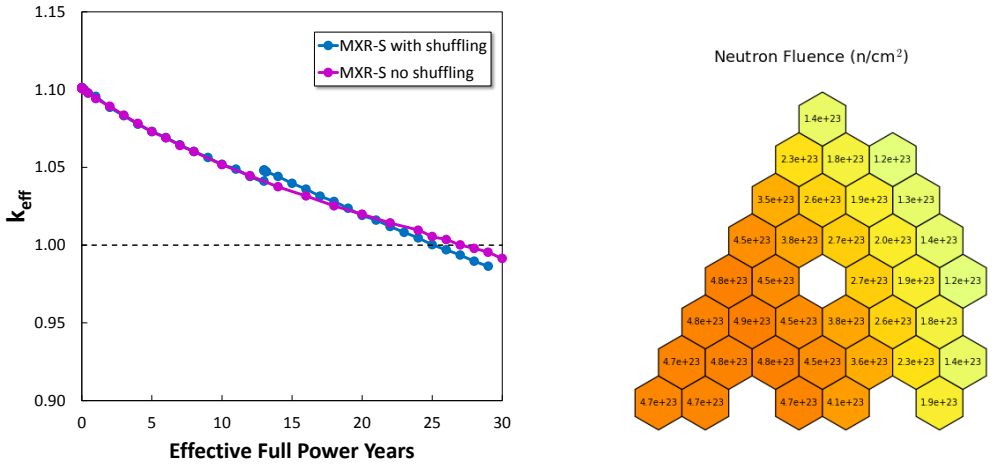

(a) Eigenvalue evolution for the MXR-S with and without shuffling.

(b) Assembly peak fast fluence after 27 years with no shuffling.

Figure D.1: MXR-S lifetime performance metrics without shuffling of the fast and thermalized assemblies.

In addition, avoiding shuffling exacerbates some of the power peaking within individual assemblies. As shown in Figure D.2, the power peaking ratio limit of 1.377 is surpassed. This could potentially lead to safety limitations and force even earlier the end of operation

of the reactor.

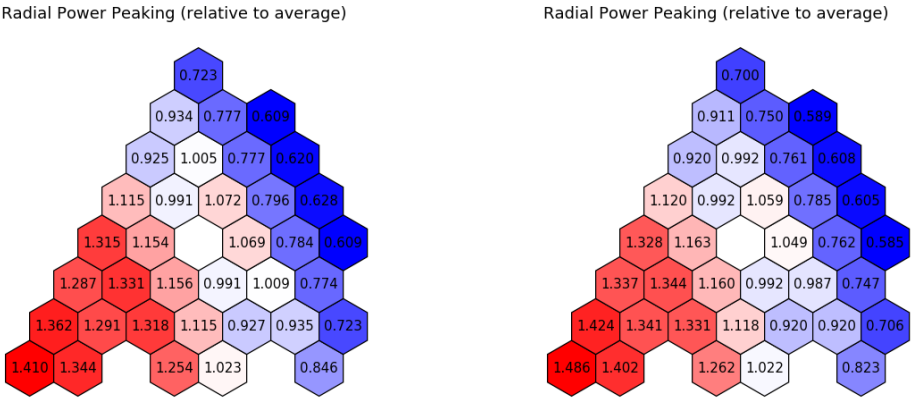

(a) Peaking factors after 22 years.

(b) Peaking factors after 27 years.

Figure D.2: Assembly power peaking factors in the MXR-S if no shuffling is conducted.

Lastly, proliferation metrics do not suffer substantially when no shuffling occurs, but are evidently still lower than in the original MXR-S design. Figure D.3 shows the plutonium quality and quantity in each assembly after 22 and 27 years of irradiation. Only a handful of assemblies are above the SQ and WG limits, but more than was originally the case in the original MXR-S design. A broader look at the diversion windows in Figure D.4, reveals that material remains attractive for longer within the core as a result. However, the windows still remain narrower than those of the LLR reactor.

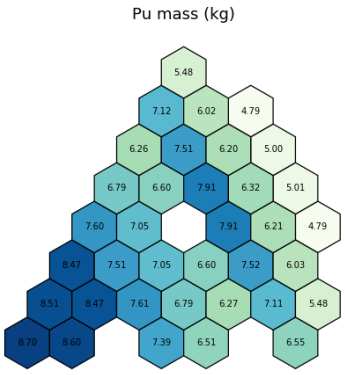

(a) Assembly Pu mass after 22 years.

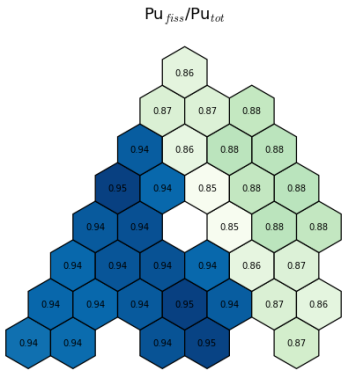

(b) Assembly Pu quality after 22 years.

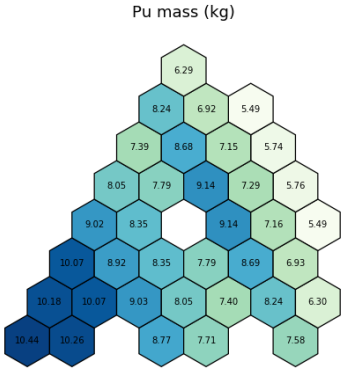

(c) Assembly Pu mass after 27 years.

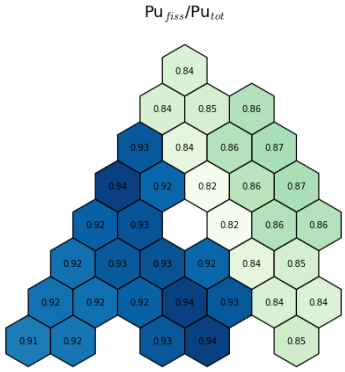

(d) Assembly Pu quality after 27 years.

Figure D.3: Assembly plutonium quality and mass in the MXR-S without shuffling after 22 and 27 years.

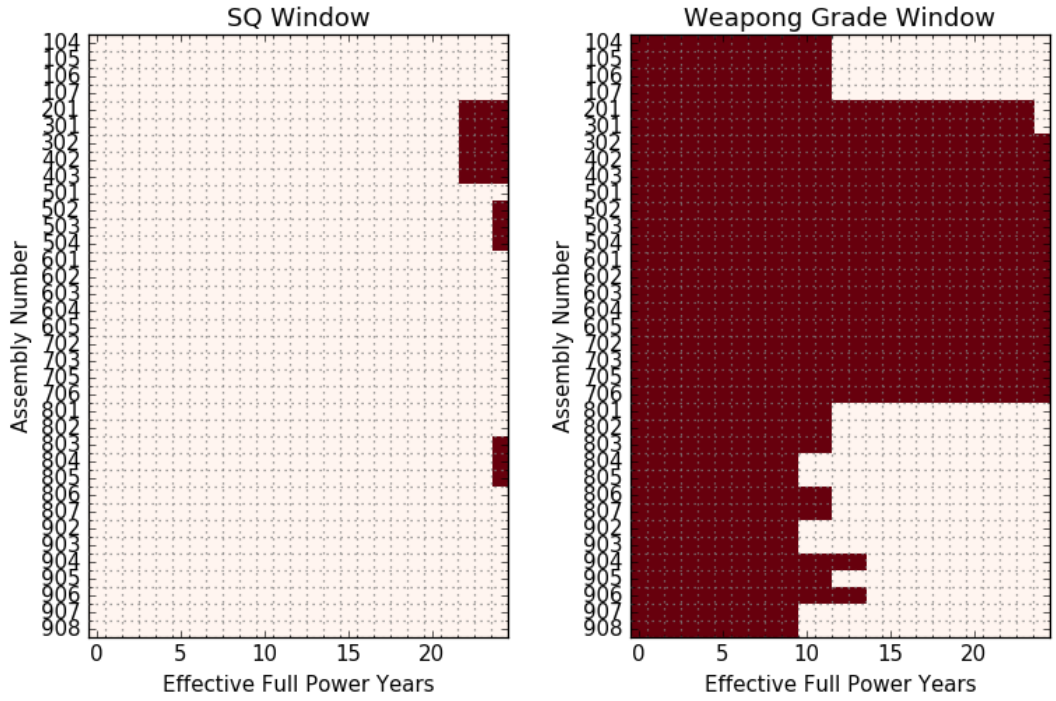

(a) MXR-S without shuffling: when assemblies contain at least 1 SQ of Pu.

(b) MXR-S without shuffling: when assemblies contain Pu above weapon-grade.

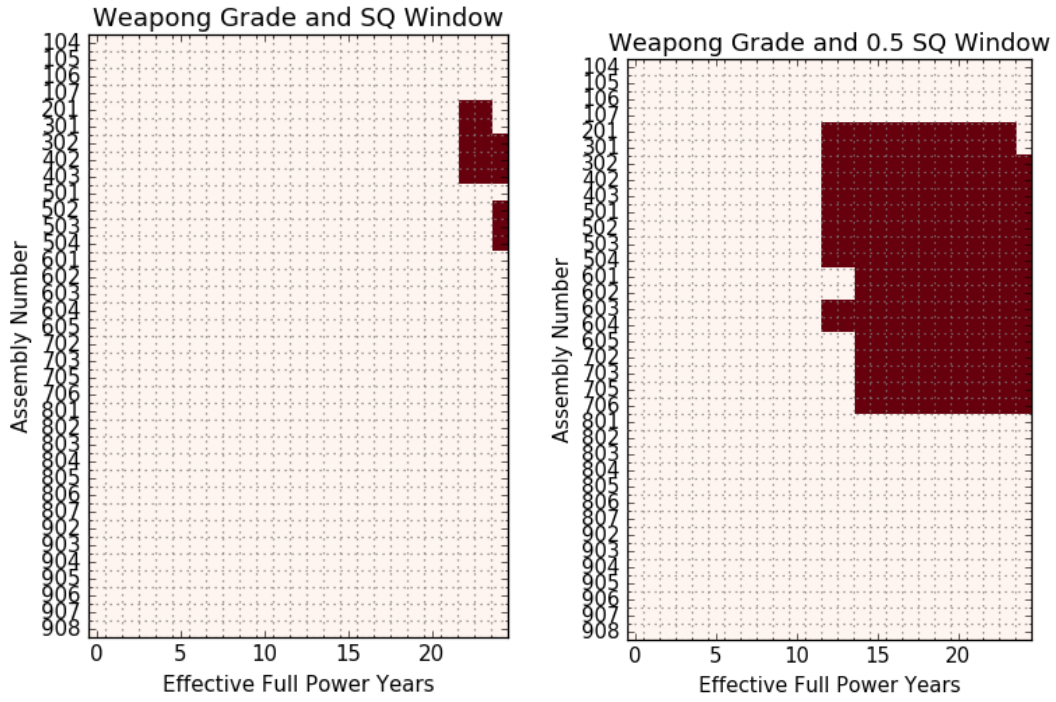

(c) MXR-S without shuffling: when assemblies contain at least 1 SQ of Pu.

(d) MXR-S without shuffling: when assemblies contain Pu above weapon-grade.

Figure D.4: Diversion windows for the MXR-S without any shuffling.

REFERENCES

[1] *Energy, Electricity and Nuclear Power Estimates for the Period up to 2050*. IAEA, 2016 Edition, ISBN: 978-92-0-106816-3.

[2] " A technology roadmap for Generation IV nuclear energy systems," U.S. DOE Nuclear Energy Research Advisory Committee, Tech. Rep., 2002, Generation IV International Forum Report No.: GIF-002-00.

[3] G. J. Youinou, "Powering sustainable low-carbon economies: Some facts and figures," *Renewable and Sustainable Energy Reviews*, vol. 53, pp. 1626–1633, 2016.

[4] *Fast Reactor Database: 2006 Update*. IAEA, 2006, IAEA-TECDOC-1531.

[5] T. B. Cochran *et al.*, *Fast Breeder Reactor Programs: History and Status*. International Pannel on Fissile Material, 2010, Princeton, NJ.

[6] S. M. Feinberg, "Discussion comment," in *ICPUAE*, Geneva, Switzerland, 1958.

[7] T. Taewooo, L. Deokjung, and T. K. Kim, "Design of ultralong-cycle fast reactor employing breed-and-burn strategy," *Nuclear Technology*, vol. 183, pp. 427–435, 2013.

[8] E. Greenspan and F. Heidet, "Energy sustainability and economic stability with breed and burn reactors," *Progress in Nuclear Energy*, vol. 53, pp. 794–799, 2011.

[9] *Plans for new reactors worldwide*, World Nuclear Association, www.world-nuclear.org, 2016.

[10] C. F. Smith, W. G. Halsey, N. W. Brown, J. J. Sienicki, A. Moisseytsev, and D. C. Wade, "SSTAR: The US lead-cooled fast reactor (LFR)," *Journal of Nuclear Material*, vol. 376, 3 2008.

[11] *Emerging nuclear energy countries*, World Nuclear Association, www.world-nuclear.org, 2017.

[12] J. J. Sienicki *et al.*, "Status Report on the Small Secure Transportable Autonomous Reactor (SSTAR) Lead-Cooled Fast Reactor (LFR) and Supporting Research and Development," Aronne National Laboratory, Tech. Rep., 2006, ANL-GenIV-089.

[13] T. Kim, C. Grandy, and R. Hill, "A 100 MWe Advanced Sodium-Cooled Fast Reactor Core Concept," in *PHYSOR 2012: Advances in Reactor Physics*, vol. 2, pp. 1458–1470.

[14] D. C. Crawford, D. L. Porters, and S. L. Hayes, "Fuels for sodium-cooled fast reactors: US perspective," *Journal of Nuclear Materials*, vol. 371, pp. 202–231, 2007.

[15] A. Glaser, L. B. Hopkins, and M. V. Ramana, "Resource Requirements and Proliferation Risks Associated with Small Modular Reactors," *Nuclear Technology*, vol. 184, no. 1, 2013.

[16] R. Avery, *Coupled fast-thermal power breeder reactor*, US Patent No. 2,9992,982, Jul 18, 1961 (filed Dec 10, 1957).

[17] G. J. Fischer and R. J. Cerbone, "The Fast-Mixed Spectrum Reactor Interim Report - Initial Feasibility Study," Brookhaven National Laboratory, Tech. Rep., 1979, BNL 50976.

[18] B. Atefi, "An Evaluation of the Breed/Burn Fast Reactor Concept," PhD thesis, MIT, 1979.

[19] N. E. Stauff, M. J. Driscoll, B. Forget, and P. Hejzlar, "Resolution of proliferation issues for a sodium fast reactor blanket," *Nuclear Technology*, vol. 170, pp. 371–382, 2010.

[20] S. E. Bays, "Heterogeneous Sodium Fast Reactor Designed for Transmuting Minor Actinide Waste Isotopes into Plutonium Fuel," PhD thesis, University of Florida, 2008.

[21] S. Sen *et al.*, "A versatile innovative coupled thermal-fast test reactor," in *PHYSOR 2016*, Sunn Valley, ID, 2016.

[22] K Tsujimoto, T Iwasaki, N Hirakawa, T Osugi, S Okajima, and M Andoh, "Improvement of reactivity coefficients of metallic fuel LMFBR by adding moderating material," *Annals of Nuclear Energy*, vol. 28, no. 9, pp. 831 –855, 2001.

[23] Arms Control Association, "Strengthening Congressional Oversight of 123 Agreements," *Issue Briefs*, vol. 7, no. 18, 2015.

[24] C. McCombie, T. Isaacs, N. B. Muslim, T. Rauf, A. Suzuki, F. von Hippel, and E. Tauscher, "Multinational Approaches to the Nuclear Fuel Cycle," *American Academy of Arts and Sciences*, 2010, ISBN 0-87724-084-1.

[25] E. Greenspan, "The encapsulated nuclear heat source reactor for low-waste proliferation-resistant nuclear energy," *Progress in Nuclear Energy*, vol. 40, no. 34, pp. 431 –439, 2002.

[26] V. Gilinski, M. Miller, and H. Hubbard, "A Fresh Examination of the Proliferation Dangers of Light Water Reactors," *The Nonproliferation Policy Education Center*, 2004.

[27] OECD, "2007 Annual Report," Generation IV International Forum (GIF), Tech. Rep., 2007, Paris, France.

[28] V. D. Cleary *et al.*, "Strengthening the Foundation of Proliferation Assessment tools," Sandia National Laboratory, Report No. SAND 2007-6158, Tech. Rep., 2007.

[29] Z. Mian *et al.*, "Fissile Materials in South Asia: The Implications of the US-India Nuclear Deal," *International Panel on Fissile Materials*, 2006.

[30] W. H. Hannum, D. C. Wade, H. F. McFarlane, and R. N. Hill, "Nonprolfieration and safeguards aspects of the IFR," *Progress in Nuclear Energy*, vol. 31, pp. 203–217, 1-2 1997.

[31] J. Kang and F. von Hippel, "Limited Reprocessing Benefits from Recycling Unseparated Transuranics and Lanthanides from Light-Water Reactor Spent Fuel," *Science and Global Security*, vol. 13, pp. 169–181, 2005.

[32] R. S. Kemp, "The Nonproliferation Emperor Has No Clothes," *International Security*, vol. 38, no. 4, pp. 39–78, 2014.

[33] S. M. Meyer, *The Dynamics of Nuclear Proliferation*. University of Chicago Press, 1984.

[34] M. R. Joseph Cirincione Jon B. Wolfsthal, *Deadly arsenals: Nuclear, biological, and chemical threats*, 2nd ed. Carnegie Endowment for International Peace, 2005.

[35] S. D. Sagan, "Why Do States Build Nuclear Weapons? Three Models in Search of a Bomb," *International Security*, vol. 21, no. 3, pp. 54–86, 1996.

[36] D. Albright and C. Gay, "Taiwan: Nuclear nightmare averted," *Bulletin Atomic Scientist*, vol. 54, no. 1, 1998.

[37] M. Braut-Hegghammer, "Revisiting Osirak: Preventive Attacks and Nuclear Proliferation Risks," *International Security*, vol. 36, no. 1, pp. 101–132, 2011.

[38] A. Ahmad, F. von Hippel, A. Glaser, and Z. Mian, "A Win-Win Solution for Iran's Arak reactor," *Arms Control Today*, 2014.

[39] T. Patton, "Combining Satellite Imagery and 3D Drawing Tools for Nonproliferation Analysis: A Case Study of Pakistan's Khushab Plutonium Production Reactors," *Science and Global Security*, vol. 20, no. 2-3, pp. 117–140, 2012.

[40] M. Fuhrman, *Atomic Assistance: How "Atoms for Peace Programs Cause Nuclear Insecurities*. Cornell University Press, 2012.

[41] M. Kroenig, *Exporting the Bomb: Technology Transfer and the Spread of Nuclear Weapons*. Cornell University Press, 2010.

[42] D. J. Jo and E. Gartzke, "Determinants of Nuclear Weapons Proliferation," *Journal of Conflict Resolution*, vol. 51, pp. 167–194, 1 2007.

[43] A. E. Waltar and A. B. Reynolds, *Fast Breeder Reactors*. Pergamon Press, 1981.

[44] "IAEA Safeguards Glossary - 2001 Edition," IAEA, Tech. Rep., 2001, International Nuclear Verification Series no. 3.

[45] A. Brown and A. Glaser, "On the Origins and Significance of the Limit Demarcating Low-Enriched Uranium from Highly Enriched Uranium," *Science and Global Security*, vol. 24, pp. 131–137, 2 2016.

[46] C. W. Forsberg *et al.*, "Definition of Weapon-Usable Uranium-233," Oak Ridge National Laboratory, Tech. Rep., 1998, ORNL/TM-13517.

[47] G. Kessler, C. Broeders, W. Hoebel, B. Goel, and D. Wilhelm, "A New Scientific Solution for Preventing the Misuse of Reactor-Grade Plutonium as Nuclear Explosive," *Nuclear Engineering and Design*, vol. 238, no. 12, pp. 3429 –3444, 2008.

[48] J. C. Mark, F. von Hippel, and E. Lyman, "Explosive Properties of Reactor-Grade Plutonium," *Science and Globale Security*, vol. 17, pp. 170–185, 2009.

[49] Office of the Press Secretary, "Additional Information Concerning Underground Nuclear Weapon Test of Reactor-Grade Plutonium," U.S. Department of Energy, Tech. Rep., 1994.

[50] B. Pellaud, "Proliferation aspects of plutonium recycling," *Comptes Rendus Physique*, vol. 3, no. 7, pp. 1067 –1079, 2002.

[51] P. A. Burns *et al.*, "Determination of the ratios of Pu-239 and Pu-240 to Am-241 for nuclear weapons test sites in Australia," *Health Physics*, vol. 67, pp. 226–232, 3 1994.

[52] C. G. Bathke *et al.*, "The Attractiveness of Materials in Advanced Nuclear Fuel Cycles for Various Proliferation and Theft Scenarios," *Nuclear Technology*, vol. 179, pp. 5–30, 1 2012.

[53] D. Wade and R. Hill, "The design rationale of the IFR," *Progress in Nuclear Energy*, vol. 31, no. 1, pp. 13 –42, 1997, The Technology of the Integral Fast Reactor and its Associated Fuel Cycle.

[54] L. Buiron *et al.*, "Minor actinide transmutation in SFR depleted uranium radial blanket: neutronics and thermal-hydraulics evaluation," in *Proceedings of GLOBAL 2007*, Boise, ID, 2007.

[55] G. Zhang *et al.*, "Comparison of Reduced-moderation Boiling Water Reactor and Sodium-cooled Fast Reactor Technologies," in *Proceedings of GLOBAL 2015*, Paris, France, 2015.

[56] "Neutronics Overview v 1.1," Transatomic Power Corporation, Tech. Rep., 2016, ORNL/TM-13517.

[57] J. T. Goorley *et al.*, *MCNP6 User's Manual*, 1st ed., LA-CP-13-00634, Los Alamos National Laboratory, 2013.

[58] W. S. Yang and B. J. Toppel, "REBUS-3 Code Enhancements for ADS Fuel Cycle Analyses," Argonne National Laboratory, Tech. Rep., 2002, ANL-AAA-016.

[59] A. E. Dubberley *et al.*, "SUPERPRISM oxide and metal fuel core designs," in *Proceedings of ICONE 8*, Baltimore, MD, 2000.

[60] I. I. Bondarenko, *Group Constants for Nuclear Reactor Calculations*. Consultants Bureau, 1964.

[61] C. H. Lee and W. S. Yang, *MC2-3: Multigroup Cross Section Generation Code for Fast Reactor Analysis*, ANL/NE-11-41, Argonne National Laboratory, 2011.

[62] C. H. Lee and N. E. Stauff, "Improved Reactivity Worth Estimation of MC2-3/DIF3D in Fast Reactor Analysis," in *Proceedings of ANS Sumer Meeting*, paper 14201, San Antonio, TX, 2015.

[63] Y. S. Jung, C. H. Lee, and M. A. Smith, "Verification of High-Fidelity Neutronics Code PROTEUS for C5G7 Benchmark Problems," in *Transactions of the American Nuclear Society*, San Fransisco, California, vol. 116, 2017.

[64] B. J. Ade, "SCALE/TRITON Primer: A Primer for Light Water Reactor Lattice Physics Calculations," Oak Ridge National Laboratory, Tech. Rep., 2012, NUREG/CR-7041 (ORNL/TM-2011/21).

[65] J. J. D. amd L. J. Hamilton, *Nuclear Reactor Analysis*. John Wiley & Sons, 1974.

[66] G. Zhang, "Advanced Burner Reactor with Breed-and-Burn Thorium Blankets for Improved Economics and Resource Utilization," PhD thesis, UC Berkeley, 2015.

[67] R. Avery, "Theory of coupled reactors," in *Second UN International Conference on the Peaceful Uses of Atomic Energy*, 1958.

[68] C. Fiorina, N. Stauff, F. Franceschini, M. Wenner, A. Stanculescu, T. Kim, A. Cammi, M. Ricotti, R. Hill, T. Taiwo, and M. Salvatores, "Comparative analysis of thorium and uranium fuel for transuranic recycle in a sodium cooled Fast Reactor," *Annals of Nuclear Energy*, vol. 62, no. Supplement C, pp. 26 –39, 2013.

[69] C. Y. I. *et al.*, *Advanced Burner Test Rector Design Description*, ANL-ABR-1, Argonne National Laboratory, 2006.

[70] "Thermophysical Properties of Materials for Nuclear Engineering: A Tutorial and Collection of Data," IAEA, Tech. Rep., 2008, IAEA-THPH.

[71] Y. S. Kim and G. L. Hofman, "AAA Fuels Handbook," Argonne National Laboratory, Tech. Rep., 2003, ANL-AAA-068.

[72] M. S. Kazimi and M. D. Carelli, "Heat Transfer Correlation for Analysis of CRBRP Assemblies," Oak Ridge National Laboratory, Tech. Rep., 1976, CRBRP-ARD-0034.

[73] M. T. Simnad, "The U-ZrHx Alloy: Its Properties and Use in TRIGA fuel," *Nuclear Engineering and Design*, vol. 64, pp. 403 –422, 1981.

[74] P. J. Turinsky, P. M. Keller, and A.-K. H. S., "Evolution of Nuclear Fuel Management and Reactor Operational Aid Tools," *Nuclear Engineering and Technology*, vol. 37, no. 1, pp. 80–90, 2005.

[75] E. Ellis *et al.*, "Traveling-Wave Reactors: A Truly Sustainable and Full-Scale Resource for Global Energy Needs," in *Proceedings of ICAP'10*, paper 10189, San Diego, CA, 2010.

[76] C. Stewart and A. Erickson, "Using Antineutrinos to Detect Single-assembly Diversion from a Long-life Fast Reactor with a Once-through Fuel Cycle," in *Proc. of the INMM 55th Annual Meeting*, Atlanta, Georgia, 2014.

[77] C. G. Bathke *et al.*, "The Attractiveness of Materials in Advanced Nuclear Fuel Cycles for Various Proliferation and Theft Scenarios," in *International Workshop for Users of Proliferation Assessment Tools*, College Station, Texas, 2010.

[78] R. Wigeland *et al.*, "Nuclear Fuel Cycle Evaluation and Screening - Final Report," Idaho Natioinal Laboratory, Tech. Rep., 2014, INL/EXT-14-31465.

[79] URENCO, *The URENCO SWU Calcaulator*, urenco.com/swu-calculator, 2017.

[80] J. R. Secker *et al.*, "Optimum Discharge Burnup and Cycle Length for PWRs," *Nuclear Technology*, vol. 151, pp. 109–119, 2 2005.

[81] R. Wigeland *et al.*, "Nuclear Fuel Cycle Evaluation and Screening - Appendix C: Evaluation Criteria and Metrics," Idaho Natioinal Laboratory, Tech. Rep., 2014, INL/EXT-14-31465.

[82] L. Leibowitz and R. A. Blomquist, "Thermal conductivity and thermal expansion of stainless steels D9 and HT9," *International Journal of Thermophysics*, vol. 9, no. 5, 873–883, 1988.

[83] G. L. Hofman, R. Pahl, C. Lahm, and D. Porter, "Swelling Behavior of U-Pu-Zr Fuel," *Metallurgical Transactions A*, vol. 21, no. (A), 517–528, 1990.

[84] R. J. McConn Jr. *et al.*, "Compendium of Material Composition Data for Radiation Transport Modeling," PNNL, Tech. Rep., 2011, PNNL-15870 Rev. 1.